Investigation of Novel Linker Technologies and Payloads for Use in Protein-Drug Conjugates

A thesis submitted to the University of Manchester for the degree of Doctor of Philosophy in the Faculty of Science and Engineering

2023

Ivan J Paul

School of Natural Sciences, Department of Chemistry

Blank page

Table of contents

Total word count: 64,240

List of figures

List of tables

List of abbreviations

°C – degrees Celsius

μ – micro

2D – two dimensional

Å – Angstrom

Ac – acyl

ADC – antibody-drug conjugate

an. – anhydrous

app. – apparent

aq. – aqueous

Ar – aryl

Bn – benzyl

Boc – *tert*-butyloxycarbonyl

br. – broad (spectral)

cat. – catalytic

Cbz, Z – carboxybenzyl

Chloroform-d – deuterated chloroform

cm^{-1} – wavenumber

conc. – concentrated

d – doublet

Da – Dalton

DCM – dichloromethane

DMAP – 4-dimethylaminopyridine

DMF – dimethylformamide

DMSO – dimethylsufoxide

E – entegen

e.g. – for example

eq – equivalents

ES – electrospray ionisation

Et – ethyl

et. al. – et alia

FACS – fluorescence-activated cell sorting

FGI – functional group interchange

fig. – figure

Fmoc – fluorenylmethoxycarbonyl

g – gram(s)

h – hour(s)

HPLC – high performance liquid chromatography

Hz – hertz

IAP – inhibitor of apoptosis protein

IC – inhibitory concentration

IR – infrared

J – coupling constant

K – Kelvin

k – kilo

L – generic ligand, litre

LCAP – liquid chromatography area percent

LCMS – liquid chromatography-mass spectrometry

LDA – lithium diisopropylamide

m – milli, multiplet

M – molar, parent mass

m/z – mass to charge ratio

Me – methyl

min – minute(s)

mmol – millimole(s)

mol – mole(s)

Ms – methylsulfonyl

MTG – microbial transglutaminase

n – nano

NAMPT – nicotinamide phosphoribosyltransferase

NMR – nuclear magnetic resonance

p – pentet

PBS – phosphate-buffered saline

PDC – peptide-drug conjugate

PEG – polyethylene glycol

PG – protecting group

Ph – phenyl

POI – protein of interest

PPI – protein-protein interactions

ppm – part(s) per million

PROTAC – proteolysis targeting chimera

q – quartet

quant. – quantitative

R – generic substituent

R_f – retention factor

rpm – revolutions per minute

RT – room temperature

s – singlet, second(s)

SAR – structure activity relationship

sat. – saturated

SCX – strong cationic exchange

S_N – nucleophilic substitution

T – temperature

t-Bu – *tert*-Butyl

TFA – trifluoroacetic acid

TGase – transglutaminase

THF – tetrahydrofuran

TLC – thin layer chromatography

t_R – retention time

Ts – toluenesulfonyl

UPLC – ultra performance liquid chromatography

v/v – volume per unit volume

VHL – von Hippel-Lindau

w – weak (spectral)

w/v – weight per unit volume

Z – zusammen

ZQG – carboxybenzyl protected glutamine-glycine

δ – chemical shift

Abstract

Antibody-drug conjugates (ADCs) are an emerging class of targeted chemotherapies. They consist of an antibody joined to a small molecule payload by a linker. Through the exquisite binding selectivity of the antibody for its specific antigen and subsequent internalisation of the conjugate, this class of therapeutics offers a way to selectively deliver a potent cytotoxin to cancerous cells. Developments in this field have culminated in multiple approved therapeutics that are used to treat a range of cancers.

Microbial transglutaminase (MTG) is an enzyme that has been investigated as a means by which to conjugate linker-payloads to antibodies. The native function of MTG is to crosslink proteins by condensing glutamine and lysine residues, which gives rise to one of the drawbacks with this conjugation strategy – under certain conditions MTG can crosslink antibodies, leading to reduced yields.

This challenge can be overcome by carrying out a two-step chemoenzymatic conjugation, or simply using the linker-payload in large excess (typically 50-80 equivalents). The extra purification step required for the former adds operational complexity and may reduce overall yield, whereas the latter represents a significant waste of often expensive or synthetically advanced payload. We aim to develop an alternative strategy that allows an efficient one-step conjugation, suppresses antibody crosslinking, and requires only a moderate excess of linker-payload.

In order to do this we expanded the known substrate scope of MTG, with the aim of finding a more active substrate than lysine. If a linker-payload uses the improved substrate as a conjugation handle, it may allow the conjugation to outcompete any crosslinking, even when the linker-payload is in moderate excess.

During the work we verified some of the few previous results reported in the literature and systematically explored the structure-activity relationship (SAR) by iterative substrate design. Alkyne-containing amines were found to be a promising motif, with some members of this class showing high reactivity. However further work is required to fully develop a general chemical motif that is both highly active and functionalisable.

23

This work also sought to design, synthesise, and test a series of proteolysis-targeting chimeras (PROTACs) targeting the enzyme nicotinamide phosphoribosyltransferase (NAMPT), with a view to develop these compounds as novel ADC payloads.

PROTACs are heterobifunctional molecules that induce degradation of a specific protein of interest, which can achieve superb degradation potencies due to their event-driven pharmacology. NAMPT is the rate-limiting enzyme in the NAD salvage pathway in mammals, making it essential for normal metabolism. Cancer cells are particularly sensitive to the suppression of NAMPT function, as they rely more heavily on NAD in their altered metabolic state.

PROTACs are an attractive potential payload class for ADCs partly because of the excellent potencies they can achieve, which may allow them to be used in the targeting of low-antigen expressing cells. Their unique mechanism of action also provides an opportunity to diversify the available classes of ADC payloads, expanding the technology's potential to treat a wide range of different conditions.

We synthesised a range of PROTACs based on the NAMPT inhibitor FK866 and ligands for both VHL and CRBN E3 ligases. Ultimately the compounds we produce did not induce any observable protein degradation despite engaging with and inhibiting NAMPT, however literature published during the course of this work suggests that screening an expanded collection of linkers and altering the FK866 exit vector may lead to effective PROTACs.

Declaration and copyright statement

No portion of the work referred to in the thesis has been submitted in support of an application for another degree or qualification of this or any other university or other institute of learning.

All work described herein was performed by myself, with the exception of the FP assay performed by Minghao Gao, and the WST-1 assays and Western blots, both performed by Lucy Li.

The author of this thesis (including any appendices and/or schedules to this thesis) owns certain copyright or related rights in it (the "Copyright") and they have given the University of Manchester certain rights to use such Copyright, including for administrative purposes.

Copies of this thesis, either in full or in extracts and whether in hard or electronic copy, may be made **only** in accordance with the Copyright, Designs and Patents Act 1988 (as amended) and regulations issued under it or, where appropriate, in accordance with licensing agreements which the University has from time to time. This page must form part of any such copies made.

The ownership of certain Copyright, patents, designs, trademarks and other intellectual property (the "Intellectual Property") and any reproductions of copyright works in the thesis, for example graphs and tables ("Reproductions"), which may be described in this thesis, may not be owned by the author and may be owned by third parties. Such Intellectual Property and Reproductions cannot and must not be made available for use without the prior written permission of the owner(s) of the relevant Intellectual Property and/or Reproductions.

Further information on the conditions under which disclosure, publication and commercialisation of this thesis, the Copyright and any Intellectual Property and/or Reproductions described in it may take place is available in the University IP Policy (see http://documents.manchester.ac.uk/DocuInfo.aspx?DocID=24420), in any relevant Thesis restriction declarations deposited in the University Library, the University

Library's regulations (see http://www.library.manchester.ac.uk/about/regulations/) and in the University's policy on Presentation of Theses.

Acknowledgements

A big thank you to Dr Sam Butterworth, without whom I would not have been able to produce this work. You have been a constant source of ideas and inspiration throughout my time in Manchester. The past four years have been a pleasure.

Thank you as well to Professor Michael Greaney for giving me the opportunity to pursue my doctoral studies on the iCAT CDT, and for supporting me and all of the other iCAT students along the way. And thank you to Paulina Hoyos, who looked after all of us on a day-to-day basis and kept everything running smoothly behind the scenes. I would also like to acknowledge the EPSRC, whose funding made this project possible.

To Aidan – you made my PhD what it was, for better or for worse. Endless afternoons filled with geography quizzes, crosswords, bike rides, and anything but work, really. I may have got much more work done without you, but I wouldn't have had nearly as much fun. I know that you'll go on to do great things, and hope you're making lots of new friends in London during all your free time. And maybe one day you can follow in my footsteps and submit your thesis too.

Andy – thanks for organising the best leaving do, and for 3D printing me a way to remember TGase forever… You've kept me sane during the long slog of writing up with coffee, bike chat, and virtual sports. I hope the next 18 months treats you kindly, and that your training for the Fred goes smoothly – I'll be there to cheer you on.

And thank you to the rest of the Butterworth Group: Minghao, May, Sergi, Yunsong, Emily, Jun, Tom, Alex, Lucy, James, Mohamed, Anna, Rachel, and Olly. You've all made it a pleasure to come into work, and have helped me along the way, both with chemistry and provision of snacks.

Thank you Mum and Dad. Your unwavering support and faith in me has given me the confidence to pursue this PhD in the first place, and get through it. Thanks for putting up with me being a perpetual student – I promise I'll get a real job one day.

And finally, thank you to my loving partner Georgia. I definitely couldn't have done this without you. Your patience has been endless, especially during these past few months

when I've been less than enjoyable to be around. You've picked me up when I've been down, and celebrated my successes with me. I can't wait to start the next chapter of my life with you.

1 Development of a microbial transglutaminase bioconjugation method for the production of antibody-drug conjugates

1.1 Antibody-drug conjugates

Antibody-drug conjugates (ADCs) have emerged as a promising class of therapeutics, particularly in the field of cancer treatment. ADCs are composed of an antibody linked to a cytotoxic small molecule payload through a chemical linker (figure 1.1). ADCs take advantage of the exquisite selectivity of monoclonal antibodies (mAbs) and allow the drug to be delivered specifically to cells that express the antigen targeted by the mAb. This paradigm is referred to as targeted delivery and reduces the toxic side effects of administering a cytotoxic anti-cancer agent. By doing this ADCs are often more effective with fewer toxic side effects over a larger range of concentrations than their small molecule analogues, which is known as having a larger therapeutic window.

Amongst the genetic faults of cancer cells, the expression of tumour-specific antigens or tumour-associated antigens (antigens that are found in healthy cells too, but are overexpressed in tumour cells) is observed. Several human cancers express unique tumour-specific or tumour-associated antigens, which represent promising targets for ADC therapy.[1]
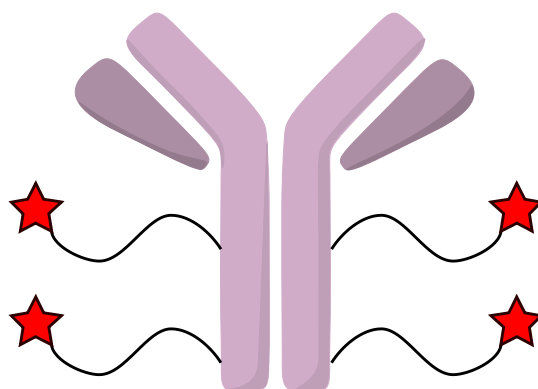
Figure 1.1 Cartoon schematic of an ADC. The antibody is represented in purple and the cytotoxic payloads are represented by red stars. The two components are joined by a linker, represented as a black line.

The concept of targeted drug delivery, known as the "magic bullet" theory, was initially proposed by Paul Ehrlich in the early 20th century. The idea was to deliver a cytotoxic drug specifically to a tumour by attaching it to a targeting agent.[2,3] The first proof-of-concept for this approach occurred in 1958 when methotrexate was conjugated to an antibody targeting leukaemia cells.[4] The subsequent development of ADCs was hampered by the availability of suitable targeting agents, with the process to produce specific murine mAbs only being discovered in 1975.[5] The early ADC systems encountered challenges such as immunogenicity issues when using murine mAbs in human patients, low drug potency, high antigen expression on healthy cells, and linker instability.[6] However, as research progressed, these issues were gradually overcome: for example, the development of humanised mAbs significantly reduced immunogenicity problems.[7] These efforts culminated in the first FDA approval of an ADC in 2000: Mylotarg, a treatment for acute myeloid leukaemia (AML). Although Mylotarg was temporarily withdrawn from the market in 2010 due to the lack of improvement in survival rates, it was reapproved in 2017 with a lower recommended dose, different treatment schedule, and for a different patient population.[8] Around 100 years after Ehrlich first proposed the idea of targeted drug delivery, Mylotarg showed us that it was a viable therapeutic strategy.

The mechanism of action for ADCs is relatively straightforward, although optimising the individual components and the overall system presents challenges (figure 1.2). ADCs are typically administered intravenously to overcome poor absorption and prevent degradation by gastric acid and proteolytic enzymes. Once in the bloodstream, they circulate until the mAb recognises and binds to the target antigen. Receptor-mediated endocytosis then occurs and the antigen-ADC complex is internalised within an early endosome. As the endosome becomes acidic, some receptors (including some bound to ADCs) are recycled and transported back to the cell surface – a process known as receptor recycling. The recycling of receptor-bound ADCs is typically minimal, but excessive recycling can negatively impact the potency of the ADC as less drug payload ends up in the cell. As such the extent of recycling should be investigated and quantified. The remaining conjugates within the endosome progress into a late endosome, initiating lysosomal degradation. The exact point at

which the payload is released depends on the nature of the linker, with cleavable linkers releasing their payload in the endosome stages, whilst non-cleavable linkers release their payload in the lysosome. The payload is then free to have its cytotoxic effect within the cell, for example interfering with microtubule formation or DNA structure, inducing cell cycle arrest or promoting apoptosis.[9]
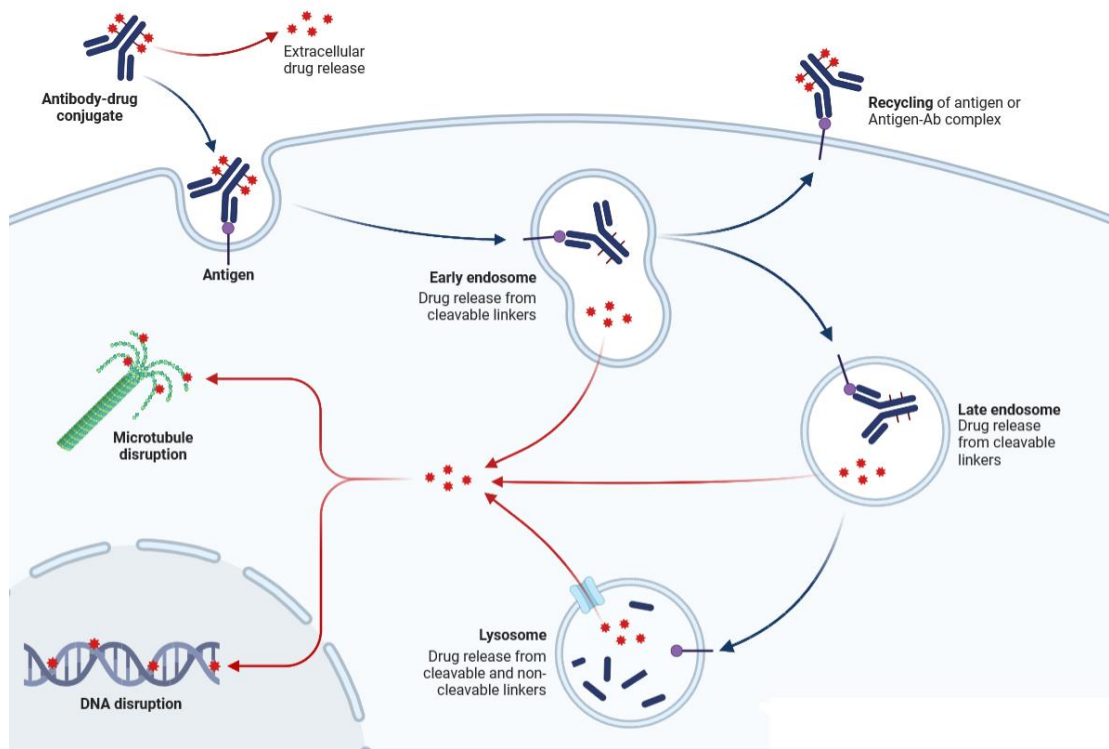
Figure 1.2 Schematic of ADC mechanism of action. Figure reproduced from a template from BioRender.com.[10]

This mechanism of action gives rise to a number of challenges. If the linker is not sufficiently stable in circulation, premature release of the cytotoxic payload may occur. This can lead to off-target toxicity, lowering the therapeutic window of the conjugate. Conversely if the linker can't be effectively broken down in the lysosome, the free, active payload may not be released, rendering the conjugate ineffective.[11] If the chosen antigen and antibody don't have a very high affinity, the binding efficiency of the ADC will suffer and less payload will enter the cell. Similarly if the target antigen isn't expressed very much on the surface of the target cells, it's possible the uptake of the ADC will be poor. The efficiency of receptor-ADC internalisation also affects the extent of internalisation, as does the rate of receptor recycling.[12] And finally, the

intrinsic activity of the cytotoxic payload will determine the effect the payload has once internalised.[9]

1.2 Antibody basics

Antibodies are large proteins that form part of the immune system. They recognise and bind to specific parts of pathogens, known as the antigen. Once bound to an antigen, the antibody can do several things, such as: neutralising the pathogen directly by blocking certain surface proteins, recruit other parts of the immune system by binding to effector cells, or binding pathogen entities together (agglutination or precipitation) to encourage phagocytosis.[13]

Human antibodies are Y shaped and are made up of four subunits: two identical heavy chains, and two identical light chains. The four chains are linked to one another by disulphide bonds. The structure is split into the two antigen-binding fragments (Fab) that represent the two prongs of the Y, and the crystallisable fragment (Fc) that makes up the trunk of the Y (figure 1.3).[14]
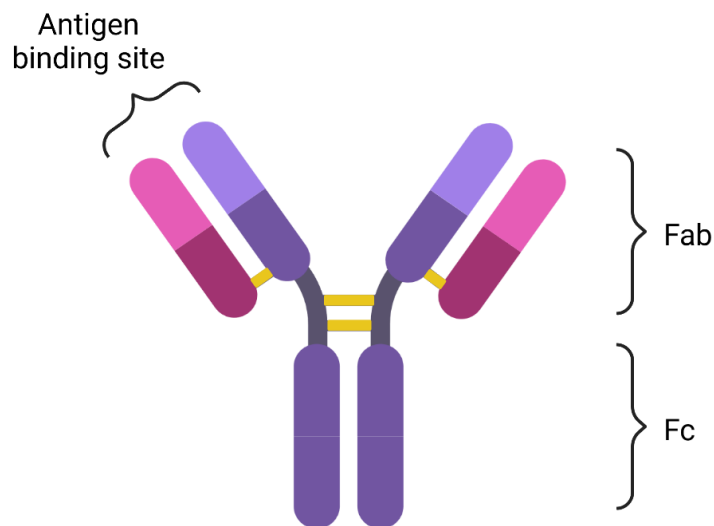
Figure 1.3 Cartoon representation of the IgG structure. The heavy chains are shown in purple, the light chains in pink and the 4 disulphide bridges in yellow. Figure made with BioRender.com

The tip of each Fab is where the antigen binds. This region is known as the variable domain, as the sequence varies vastly between different antibodies allowing them to

recognise different antigens. Having two identical antigen-binding sites gives the antibody the ability to bind strongly to pathogens with repeating antigen sites and allows the formation of larger antibody or antigen-antibody complexes. The part of the antigen that binds to the antibody is known as the epitope.

The Fc region governs binding to effector cells and determines the function and class of antibody. The class also determines where/when antibodies are secreted. Placental mammals have 5 classes of antibodies, of which IgG is the most common class and provides antibody-based immunity against pathogens.[15] "Ig" stands for immunoglobulin, another way of referring to antibodies. The classes are divided into subclasses, referred to as IgG1, etc. Effector cells bind to the Fc region with Fc receptors, known as FcRs.

Besides the two end regions that vary greatly, the sequence of the remainder of the antibody is conserved and hence known as the constant region. Antibodies are glycoproteins and have carbohydrate chains attached to the constant region, at locations that vary by class. The exact nature of the antibody glycosylation determines its function and interactions with other entities.[16] For example, IgG antibodies are glycosylated at Asn297 and the exact nature of the attached *N*-linked glycan has a large impact on the overall structure and function of the antibody.[17]

When certain antibodies bind to their cell-surface receptor antigens, they are internalised along with the receptor. This is the basis upon which ADCs are based and allows selective delivery of a conjugated payload to cells that express the appropriate receptor.[12]

Antibodies that are produced for research are usually monoclonal. This means they only bind to one specific antigen through one epitope and can be used to target specific cells or tissues that express their antigen receptor.[18] For this reason monoclonal antibodies are ideally suited to the generation of ADCs.[19]

1.3 Conjugation methodologies for the preparation of ADCs

When preparing ADCs, the way in which the payload is conjugated is of paramount significance. The method used determines the extent of conjugation (how many

payloads are attached to each mAb, known as drug-antibody ratio (DAR)), the range of DARs obtained in the product mixture, and the site of conjugation.

The DAR fundamentally affects the properties of the overall conjugate. As the number of small molecules on an antibody increases, the chances of conjugate aggregation increase, which can reduce the efficiency of payload delivery to target cells. The potency of the conjugate is also affected, with lower DARs leading to lower efficacy, but higher DARs potentially increasing the toxicity of the conjugate.[20] Additionally if a heterogeneous product mixture is obtained with a range of DARs, it becomes difficult to analyse the reactions and determine which species are actually responsible for the effects seen. If the conjugate is taken forward to clinical trials, processes producing heterogeneous mixtures are often less consistent and harder to implement quality control for.

In addition the site of conjugation has a large impact on ADC properties. This is explored in the work of Strop *et al.*[21] They designed and synthesised a series of ADCs that had various small molecule payloads, conjugated at different positions. This allowed them to investigate how the site of conjugation influences stability, toxicity and efficacy. They produced conjugates based on an anti-M1S1 antibody, C16, with one conjugate derivatised on the light chain (C16-LC) and one on the heavy chain (C16-HC). They compared these two ADCs with naked C16. Conjugation yielded similar DARs (averages of 1.8 for C16-LC and 1.9 for C16-HC) and intact and reduced LCMS analysis determined that the conjugations had been site-selective.

The potencies of both conjugates were similar *in vitro*, with EC_{50} values of 53 and 54 pM in the $M1S1^+$ pancreatic cancer cell line BxPC3. When they measured the pharmacokinetic (PK) properties of the conjugates, they found that in mice C16-LC showed a similar rate of clearance to the unconjugated C16, but C16-HC had an accelerated clearance. They then tested this in rats and found the C16-HC clearance was increased even further. Due to the site-selective nature of their conjugations, it's likely this difference was down to the location of the payload on the antibody and how this changes the interaction of the ADCs with surrounding tissues. Finally, they investigated the relative stability of the conjugates. Both conjugates showed similar

stability in mice, with the DAR 2 species being the only one observed. This suggests that the DAR 1 species, once produced, is rapidly cleaved such that it can't be observed. In contrast, rat models allowed the detection of both DAR 1 and DAR 2 species for C16-HC. In the rat model C16-LC appeared very stable, with no change in the concentration of the DAR 2 species.

As the ADCs contained the same (cleavable) linker chemistry, these differences can be attributed solely to the site of conjugation. These results demonstrate that site of conjugation can have effects on both the stability of the conjugates and the PK properties. Additionally their results show that ADCs can have significantly different effects between different animal models, highlighting the importance of model choice.

1.3.1   Chemical conjugation methods

Chemical conjugation involves the reaction between a reactive group on the linker and an accessible surface amino acid residue. Since there are typically multiple residues available on the surface, these methods result in a mixture of ADCs with different DARs. This heterogeneity introduces variations in the properties of the different ADC products, which can lead to challenges during quality control and impede the drug approval process.[22] Problems such as aggregation and reduced antibody binding affinity may arise when an excessive number of payloads are attached. As discussed above the specific site of conjugation also plays a crucial role and has been demonstrated to significantly impact the stability and PK properties of ADCs.[21] Despite these limitations, random conjugation approaches have been successfully employed to generate ADCs, provided the process has effective monitoring, control, and purification methods for the product mixture.

1.3.1.1   Lysine conjugation

The ε-NH$_2$ of surface lysine residues is commonly used as a reactive handle to form a peptide bond with an activated carboxylic acid group in the linker, usually an *N*-hydroxysuccinimide (NHS) ester (figure 1.4). While this chemistry is reliable and straightforward, the presence of multiple accessible lysine residues on a typical antibody (can be in the range of 30-40) results in a range of DARs and conjugation sites.[23] If the lysine residue involved in conjugation is crucial for antibody binding, it

may lead to a decrease in binding affinity. Despite these drawbacks, lysine conjugations have been successfully used to generate ADCs. For example the FDA-approved Kadcyla is produced via lysine conjugations, although the product mixture contains a range of species with DARs from 0-8.[24,25]

The use of NHS esters can also lead to challenges with hydrolysis and chemoselectivity, with the possibility of generating conjugates through histidine, serine, threonine, and tyrosine residues. Research is underway into other types of reagents that could address these issues, including sulphonyl halides, iminoboronates, diazonium salts, aldehydes, and isothiocyanates (figure 1.4). Although this represents an area of interest, few of these new strategies have reached the stage where they have been used to produce ADCs.[26]
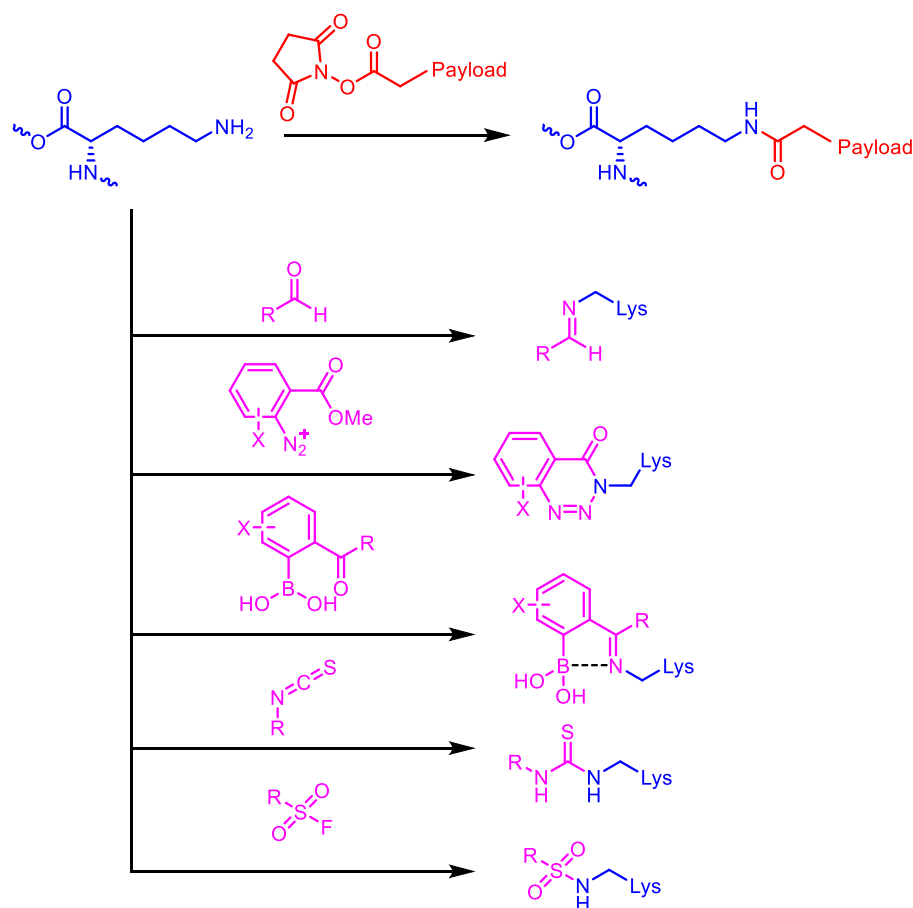
Figure 1.4 Overview of lysine (shown in blue) conjugation strategies. Above: classic NHS ester (shown in red) approach. Below: different approaches (shown in purple) developed to overcome the stability and chemoselectivity issues associated with the NHS method.

1.3.1.2 Cysteine conjugation

Conjugations can also be carried out using cysteine residues on the mAb and electrophiles on the linker. Before conjugation can occur, the naturally forming disulphide bonds must be reduced to release the free thiols on the cysteine residues. For example, human immunoglobulin G 1 (IgG1), a common type of antibody used in ADC research, contains 4 interchain and 12 intrachain disulphide bonds. Among these, the interchain disulphides are non-critical for structural stability. By selectively reducing the interchain disulphides under mild conditions, 2, 4, 6, or 8 free thiols can be generated, which can then react with suitable electrophiles.[25] The selective reduction of interchain disulphides is a well-established technique and can be achieved using tris(2-caboxyethyl) phosphine (TCEP, **1**) or dithiothreitol (DTT, **2**). Intrachain disulphides remain unaffected under these conditions, even when the reducing agents are present in excess.[27]
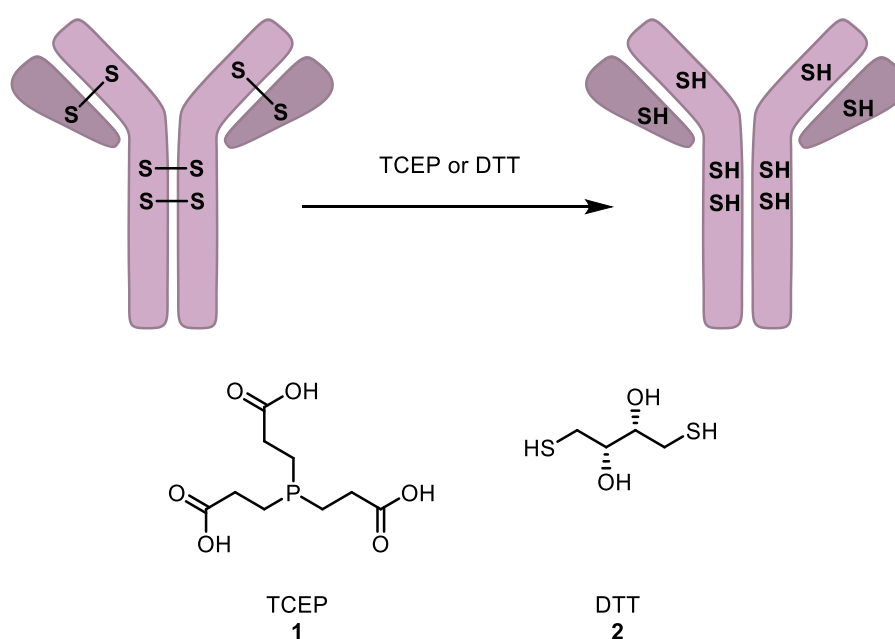
Figure 1.5 Above: Schematic representation of reducing the interchain disulphide bonds in a mAb to generate free, reactive cysteine residues. Below: Chemical structures of TCEP and DTT, both used to affect the disulphide bond reduction. Notably, they leave intrachain disulphides intact.

Maleimides are commonly used as the electrophile, as the resulting thio-Michael addition is extremely reliable. This is one of the most common conjugation strategies,

as it introduces a significant degree of control into a simple chemical conjugation process. Although this method has had great success, for example in the preparation of FDA-approved Adcetris, issues can arise with the limited plasma stability of the thiol-maleimide adducts.[28] The retro-Michael reaction can occur, prematurely releasing the payload. Maleimide exchange reactions can then occur with reactive thiols present in albumin, free cysteines, or glutathione.[29] This leads to toxic compounds entering general circulation which can lead to systemic toxicity. If the adducts are simply hydrolysed once they are formed, the resulting products cannot undergo retro-Michael reactions (figure 1.6).[29,30]

An alternative approach to overcome the instability issue was developed by Kolodych *et al.*[31] They developed a heterobifunctional reagent called 4-((4-(cyanoethynyl)benzoyl)oxy)-2,3,5,6-tetrafluorobenzenesulphonate (CBTF, **3**), which enables amine-to-thiol coupling while preventing the reverse reaction. The 3-arylpropionitrile group replaces the maleimide as the thiol-reactive electrophile, forming a vinyl cyanide which cannot undergo the reverse reaction. The other end of the molecule has an activated fluoroaryl ester that can react with an amine-functionalised drug payload to form a stable amide bond. To demonstrate their new reagent didn't produce any toxic by-products, they synthesised the product expected from the full proteolytic degradation of an ADC produced with CBTF, **4**. They assessed the toxicity of **4** in both HeLa and HuH-7 cells and observed no ill effects up to a concentration of 100 µM. They also demonstrated that CBTF can produce conjugates with excellent plasma stability compared to standard thiol-maleimide ADCs and accordingly CBTF is now available commercially.
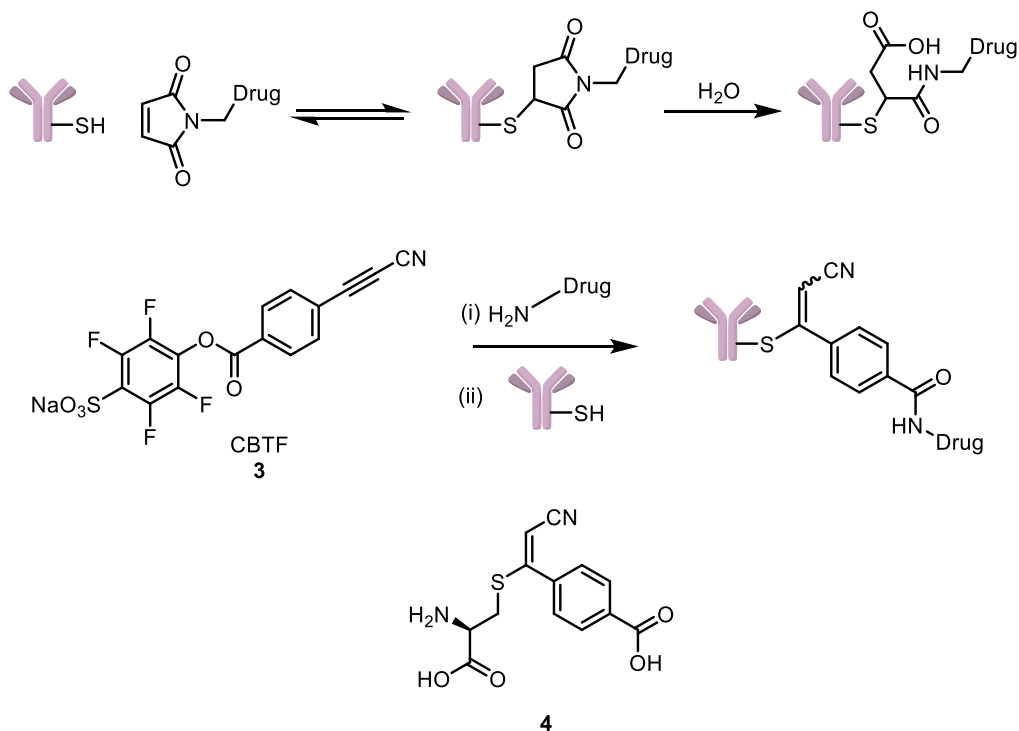
Figure 1.6 Above: The thio-Michael addition of cysteines into maleimides is facile, but the products can be unstable in plasma due to the retro-Michael possible. Hydrolysis of the adducts produces open chain conjugates, which are not susceptible to retro-Michael reactions. Middle: CBTF is a bifunctional cross-linking reagent that can conjugate an amine-containing payload to a free cysteine on a mAb. The adducts produced are more stable in circulation than the classic maleimide analogues, reducing the rates of premature payload release. Below: The expected by-product from complete proteolytic degradation of an ADC produced with CBTF. Kolodych et al. tested this for potential toxic effects and found it was tolerated by HeLa and HuH-7 cells up to 100 μM.

1.3.1.3 Cysteine rebridging

While the cleavage of certain disulphide bonds can be tolerated without significantly altering the tertiary protein structure, cysteine rebridging presents an alternative approach to control the DAR and heterogeneity of ADCs, potentially avoiding stability issues that may arise from removing structurally important disulphide bonds. The process involves selective reduction of interchain disulphides as described earlier, followed by bis-alkylation. This conjugation step repairs the interchain structure while facilitating the attachment of the payload. Electrophiles such as dibromomaleimides,[32] dibromopyridazinediones,[33] and 1,3-bis(p-toluenesulfonyl)propane-based cores[34] (figure 1.7) are used in these alkylating reactions. The alkylation mechanisms typically

involve a series of conjugate additions and eliminations. The rebridging agent can either contain a reactive handle for subsequent attachment of the payload, or can be pre-modified to include the payload. To streamline the process, Lee *et al.* advanced the development of these alkylating agents by creating a dithioaryl(TCEP)pyridazinedione reagent (**5**) capable of both reducing the interchain disulphides and alkylating the resulting thiols in a single step, enabling efficient rebridging (figure 1.7).[35]
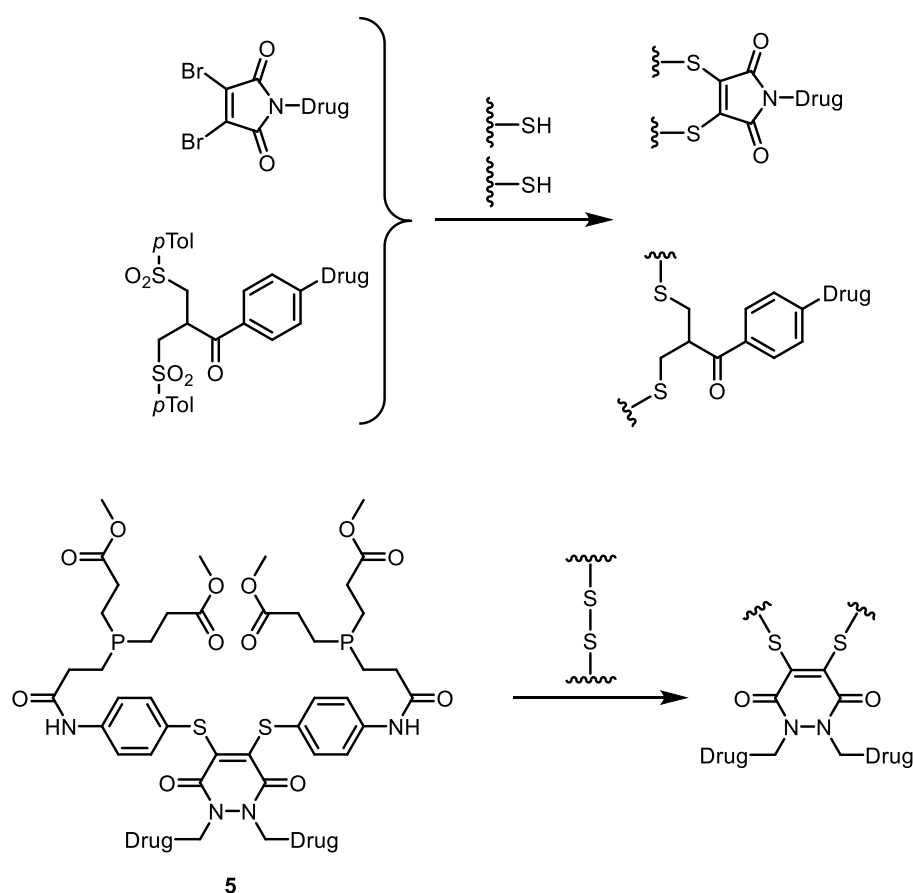
Figure 1.7 Cysteine rebridging strategies. This approach reforms disulphide bonds after functionalising them, reducing the risk of altering the tertiary structure of the antibody. Below: Lee et al. developed a dithioaryl(TCEP)pyridazinedione reagent that can accomplish the cysteine rebridging process all in one: the TCEP cores affect the disulphide reduction and the pyridazinedione part affects the rebridging.

Whilst cysteine rebridging offers a way to functionalise antibodies in an extremely site-selective manner, a drawback associated with the method is the production of "half antibodies" as impurities.[36] Half antibodies consist of just one heavy and light chain, and are the result of rebridging within the hinge region of a single heavy chain rather

than between the free thiols in the hinge regions of two different heavy chains. For example, Behrens *et al.* produced ADCs using a dibromomaleimide rebridging strategy to attach MMAF to trastuzamab and the anti-CD98 antibody IGNX, and observed through LCMS analysis that whilst around 70% of the product mixture was the desired full ADC, the remaining 30% was the half antibody formed through rebridging within the hinge region of a single heavy chain.[32] The production of half antibody by-products, which reduce yield and may necessitate additional purification steps, can be mitigated by affecting the *in situ* reduction and rebridging of antibodies. This requires either the use of specific, tuned rebridging agents alongside an appropriate reductant,[37] the use of an all-in-one reduction/rebridging agent such as dithioaryl(TCEP)pyridazinedione **5**,[35] or the use of a rebridging agent that can react with all eight cysteine residues and cause complete, all-in-one rebridging.[38]

1.3.1.4 Thiomabs and selenomabs

The development of cysteine conjugation strategies has not only enabled the creation of ADCs but has inspired the development of thiomabs, genetically modified mAbs with additional cysteine residues. This approach allows for even higher levels of homogeneity to be achieved, surpassing 90%. ADCs derived from thiomabs have demonstrated good efficacy and therapeutic windows *in vivo*.[39]

Thiomabs are produced by introducing engineered cysteines that form mixed disulfide links with either free cysteine or glutathione. To expose the reactive cysteines a reduction step is necessary, which can be accomplished using either TCEP or DTT. However, this reduction step also affects the interchain disulphides in the antibody. A re-oxidation step employing dehydroascorbic acid (DHAA) therefore becomes necessary to restore the engineered cysteines before they can be alkylated. Although the thiomab strategy offers precise control over the location and number of conjugation sites, the reduction and re-oxidation steps may reduce the overall yield of the conjugates obtained.[40]

Analogous to thiomabs are selenomabs, which are engineered mAbs with one or more selenocysteine residues incorporated during translation.[41] Selenocysteine possesses unique reactivity that is orthogonal to other amino acid residues, enabling site-

selective conjugation. The nucleophilic nature of selenocysteine allows for fast, single-step, and complete conjugation reactions under near physiological conditions, eliminating the need for reduction and subsequent re-oxidation steps. This characteristic may lead to improved yields compared to their sulphur analogues.

However, similar to cysteine-maleimide adducts, selenocysteine-maleimide adducts are prone to facile retro-Michael additions in plasma which can result in de-conjugation, premature toxin release, and increased off-target toxicity. To address this issue iodoacetamides can be used as electrophiles. When using cysteine residues as conjugation points, iodoacetamides cannot be used as they exhibit cross-reactivity with methionine, lysine, and histidine residues. The significantly increased nucleophilicity of selenocysteine, however, allows for fast and selective reaction of iodoacetamides with the selenol, even in the presence of other nucleophilic natural residues.[41]
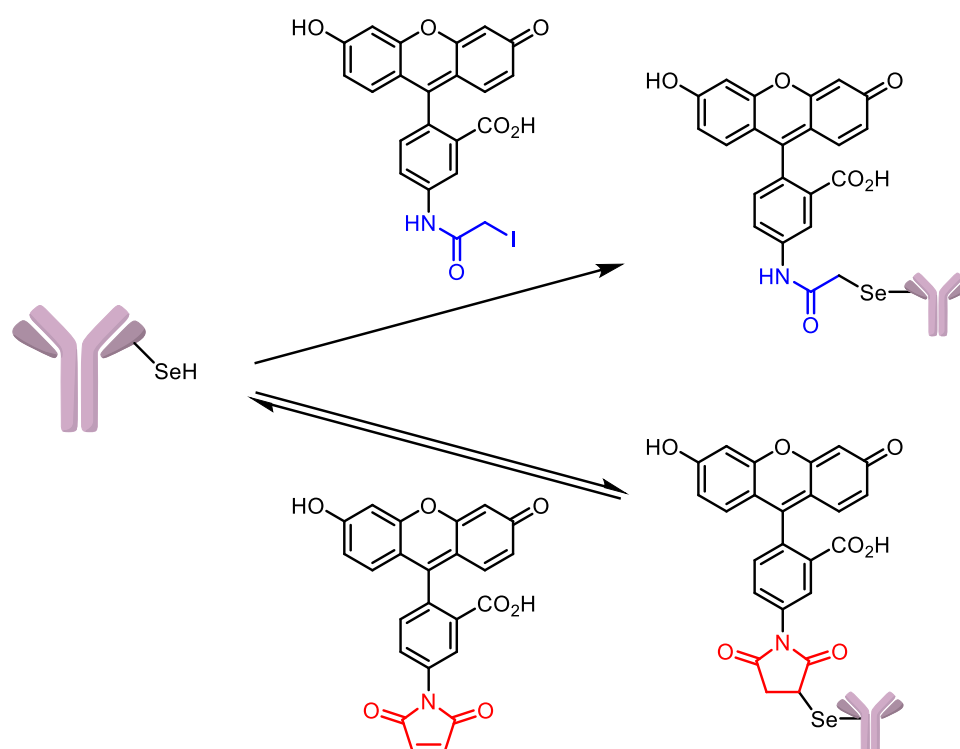
Figure 1.8 Schematic of selenocysteine conjugation of fluorescein via maleimides (reversible) and iodoacetamides (irreversible). The vastly increased nucleophilicty of selenols compared to other groups found in the natural amino acids allows the selective reaction of iodoacetamides with selenocysteine, even in the presence of groups such as methionine, cysteine, lysine, and histidine.

1.3.2 Enzymatic conjugation methods

Enzymatic conjugation methods offer two approaches: direct conjugation of the antibody with the linker or installation of a specific reaction handle on the antibody for subsequent chemical conjugation. Due to the inherent selectivity of enzymes, enzymatic conjugations occur site- and sequence-selectively. This allows precise control over the site and degree of conjugation, resulting in a homogeneous mixture of ADCs with similar DARs. Another advantage of enzymatic methods is the inherent biocompatibility of the reaction conditions, as they are already biological.

1.3.2.1 Formylglycine generating enzyme

Formylglycine generating enzyme (FGE) has been identified in both eukaryotes and prokaryotes and catalyses the oxidation of a cysteine residue to the aldehyde containing formylglycine residue. FGE recognises the amino acid sequence CXPXR, where X is usually serine, threonine, alanine, or glycine. Recognition is by primary structure only, suggesting that a short tag could be incorporated into a protein and FGE would install an aldehyde at the corresponding location. In 2007 Carrico *et al.* incorporated this tag into proteins and incubated these proteins with prokaryotic FGE from *Mycobacterium tuberculosis* and observed conversions to formylglycine of >90% in all but one of their proteins.[42,43]

The group then functionalised their aldehyde-containing proteins with aminooxy- or hydrazide-functionalised probes. Their proteins were robustly labelled, in contrast with their control panel (in which the modified cysteine had been mutated to an alanine) which was unaffected. Interestingly they showed that they could obtain sequential modifications of proteins: initial conjugation with a hydrazide probe gave the *N*-acylhydrazone conjugate **6**. By incubating this with an aminooxy functionalised probe, they could switch the attached probe. This was driven by the increased thermodynamic stability of the oxime conjugate **7**.
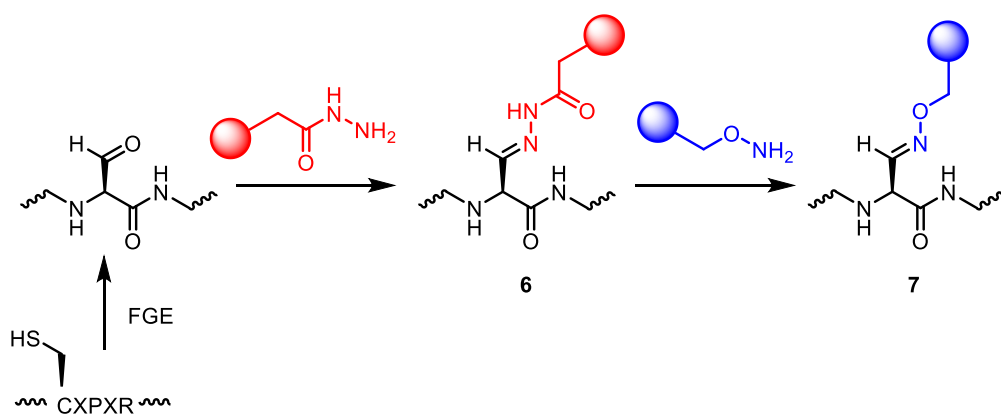
Figure 1.9 Carrico et al.'s FGE-based approach to sequential protein labelling. Initially a hydrazide-containing payload (shown in red) is attached, forming a hydrazone-linked conjugate (6). Subsequent addition of an aminooxy-containing payload (shown in blue) allows payload exchange, in favour of the more thermodynamically stable oxime-linked conjugate (7).

A drawback with the oxime- and hydrazine-producing conjugations above is that they generate C=N bonds, which can be hydrolytically unstable in biologically relevant conditions. An alternative way of conjugating the aldehyde-containing proteins generated with FGE has been developed and is based on the Pictet-Spengler (PS) reaction. Agarwal *et al.* developed a modified PS substrate, replacing the canonical aliphatic amine with a more nucleophilic aminooxy moiety.[44] This increases the rate of the partially rate-limiting iminium ion formation.

Formation of iminium
is partially rate-limiting

Aminooxy group
allows increased
rate of formation for
intermediate

Additionally they moved the aminooxy group to the 2 position of the indole, allowing the more nucleophilic 3 position to intercept the oxyiminium intermediate, further increasing the overall rate of reaction. Finally methylation of the nitrogen ensured rapid C-C bond formation through the intramolecular electrophilic substitution. They validated their methodology on a series of proteins, including human IgG antibody, by conjugating a series of payloads including fluorophores and biotin.

1.3.2.2 Sortase

Sortase A, derived from *Staphylococcus aureus*, exhibits transpeptidase activity *via* hydrolysis of the threonine-glycine bond within an LPxTG recognition sequence. A nucleophilic cysteine residue in the sortase active site cleaves the T-G bond, forming a reactive thioester intermediate. An oligoglycine-containing payload then attacks the thioester intermediate through the reactive terminal NH_2 of glycine. This attaches the oligoglycine-payload to the threonine of the protein substrate and releases sortase (figure 1.11).[45]

Sortase A can accommodate substrates comprising one to five glycines, displaying optimal efficiency with two or more glycines.[46,47] Sortase can accept a broad range of substrates on the threonine side, making it a generally applicable method of conjugation that has been used to attach fluorophores, photoaffinity probes, fatty acids, peptide nucleic acids, polymers, solid supports, and other polypeptides.[48]
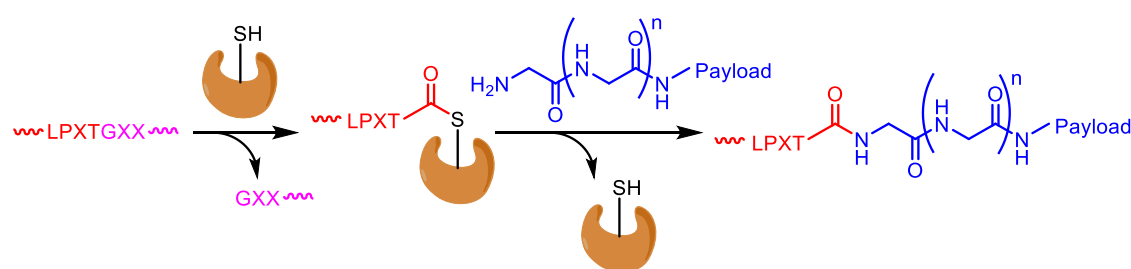
Figure 1.11 Sortase (represented in orange) mechanism of action.

Beerli *et al.* employed the sortase strategy specifically for ADCs by incorporating recognition tags (LPETG) at the *C*-termini of both heavy and light chains of antibodies.[49] They used MMAE and maytansine, appended with pentaglycine motifs as the payloads and conjugated them to anti-CD30 and anti-HER2 mAbs. This generated analogues of Adcetris and Kadcyla, respectively. The generated ADCs exhibited equivalent *in vitro* activity compared to their commercial counterparts and achieved complete tumour regression in a rodent xenograft model.

Sortase conjugation methodology requires a substantial excess of polyglycine nucleophile to drive the equilibrium towards the product.[50,51] Furthermore, the presence of competitive nucleophiles such as water and lysine residues can lead to the formation of various undesired by-products, complicating purification. Policarpo *et al.* have devised a flow-based process to overcome these obstacles.[52] Their approach involves immediate release of the product from the immobilised enzyme microreactor, minimising reverse reactions and reducing contact time with the enzyme to mitigate side reactions like hydrolysis and dimerisation. This was achieved by using an evolved version of sortase with faster reaction kinetics. The optimised process enabled the synthesis of the desired bioconjugate within 30 minutes, needed only low nucleophile concentrations and successfully minimised side reactions. This allowed them to synthesise a conjugate that had previously been inaccessible due to competing side reactions.

1.3.2.3 Tubulin tyrosine ligase

Tubulin tyrosine ligase (TTL) represents a promising approach for conjugation. Normally involved in regulating microtubule stability within cells, TTL recognises a 14-amino acid sequence (known as a tub-tag) at the *C*-terminus of α-tubulin and enzymatically attaches a tyrosine residue.[53] When this recognition sequence is engineered into an antibody, TTL becomes capable of attaching tyrosine derivatives with reactive functional groups such as azides, aldehydes, amines, and nitro groups.[54] This allows subsequent chemical modification by well-established bioorthogonal means to introduce linkers and payloads.
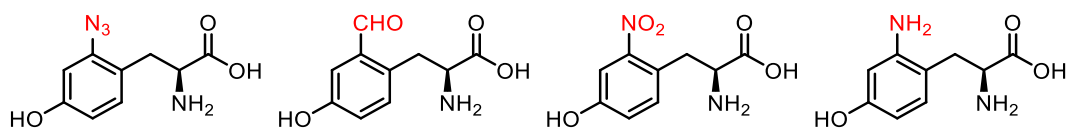
Figure 1.12 The tyrosine derivatives that Schumacher et al. could incorporate into proteins carrying a tub-tag.

Schumacher *et al.* demonstrated the versatility of this method by site-specifically modifying various proteins, including green fluorescent protein (GFP), ubiquitin, and two GFP-specific nanobodies (GBP1 and GBP4).[55] They introduced both azido-tyrosine and formyl-tyrosine, both of which can be further derivatised using established chemistry.

1.3.2.4 Glycoengineering

An alternative approach for appending reactive groups to antibodies involves modifying the sugar moieties present on mAbs rather than directly modifying the protein itself. In the case of IgG mAbs, each heavy chain carries a biantennary *N*-linked oligosaccharide at the conserved residue asparagine 297, which influences effector functions while maintaining binding affinity. Enzymatic modification of this sugar chain provides an opportunity to introduce reactive groups that can serve as conjugation handles. This method capitalises on the tolerance of glycosyltransferases towards chemical modifications of their sugar substrates, enabling the incorporation of groups such as ketones, alkynes, and azides.[56,57]

8
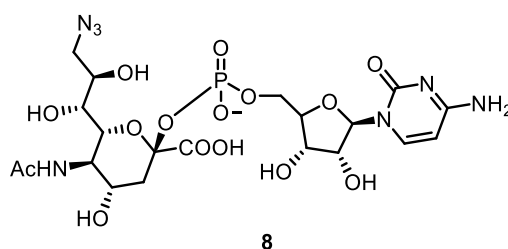
*Figure 1.13 Chemical structure of azide-functionalised sialic acid derivative **8** that Li et al. incorporated into the oligosaccharide chain of an antibody.*

Li *et al.* demonstrated the utility of this approach by remodelling the oligosaccharides of an anti-CD22 mAb using a cytidine monophosphate (CMP) sialic acid derivative with an azide group at C-9 (figures 1.13 and 1.14, compound **8**).[58] They subsequently

employed strain-promoted azide-alkyne cycloaddition (SPAAC) chemistry to attach a dibenzylcyclooctynol (DIBO) unit, which was further decorated with a linker and the cytotoxic agent doxorubicin, resulting in the synthesis of a well-defined ADC with a DAR of 3.5. As the effector properties of ADCs contribute to their anticancer activity, the impact of glycan glycoengineering and payload conjugation on the binding to Fcγ Receptor IIIA was investigated. Encouragingly, the conjugated antibodies exhibited no difference in binding compared to their unmodified counterparts. Zhu *et al.* also employed this methodology to introduce a keto-galactose moiety into the oligosaccharides of an anti-HER2 antibody, which was subsequently conjugated to aminooxy auristatin F, resulting in an ADC with a DAR of 4.[59]
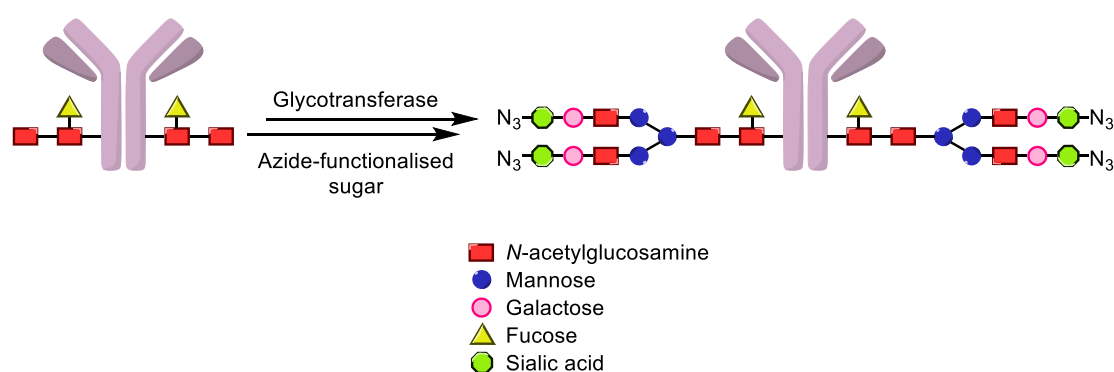
Figure 1.14 Schematic overview of the glycoengineering approach taken by Li et al. Using glycotransferase they attached an azide-functionalised sugar to the end of the natural oligosaccharide. Through a subsequent SPAAC they then attached a cytotoxin, completing the synthesis of their ADC.

1.4 Microbial transglutaminase

Transglutaminases are a class of enzymes that catalyse the reaction between a glutamine side chain and a lysine side chain, resulting in the formation of a peptide bond while releasing ammonia. The first transglutaminase was discovered in 1959 and was isolated from guinea-pig liver.[60] Clarke *et al.* observed that the enzyme incorporated amines into proteins and that a wide variety of amines were tolerated.[60] Subsequent research on the mechanism of blood clotting determined that the transglutaminase activity arose from an acyl-transfer reaction between the γ-carboxamide group of a peptide-bound glutamine residue and the ε-amino group of a peptide-bound lysine residue (figure 1.15).[61] In general transglutaminases either affect

protein cross-linking, or incorporate free amines into proteins. In both cases the products are often more resistant to mechanical and proteolytic degradation and are used by organisms in tissues where these properties are useful, for example hair, skin, blood clotting, and wound healing.[62]
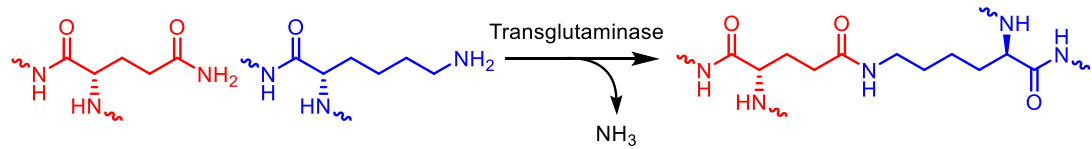
Figure 1.15 Overview of the reaction transglutaminases catalyse. Glutamine and lysine residues are condensed, releasing ammonia.

Since the original discovery of mammalian transglutaminase, many other members of the enzyme family have been found in microbes,[63] plants,[64] invertebrates,[65] amphibians,[66] fish,[67] and birds.[68] Of particular significance has been the enzyme derived from bacteria – microbial transglutaminase (MTG).

Transglutaminases are widely used in the food industry, and MTG was discovered in response to the need for a cheap, reliable source of transglutaminase. Through its crosslinking activity transglutaminase can alter the texture and structure of meat and act as a bonding agent. It is important in the production of sausages and reconstituted meat products. Transglutaminase is also widely used in the dairy industry to alter the texture, structure, and consistency of milk, ice cream, and cheese. The enzyme can also be used to improve dough elasticity and resilience in baking, as well as the texture of bread and pasta.[69] MTG is commonly extracted from *Streptomyces mobaraensis*, although it can be extracted from a number of other microbial sources.[70] Interestingly the native function of MTG in *Streptomyces mobaraensis* is not fully understood. It has been postulated, however, that MTG cross-links inhibitory host proteins, providing the organism with protection.[69]
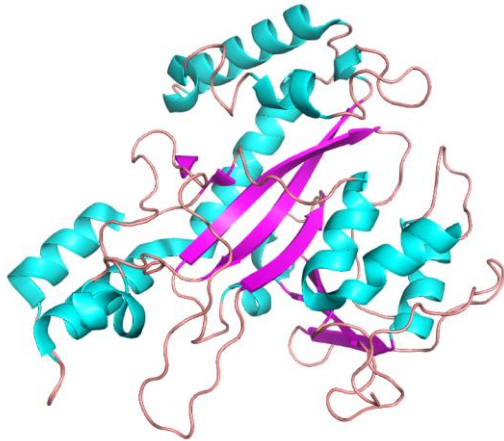
Figure 1.16 Left: crystal structure of MTG showing the enzyme's tertiary structure (PDB: 1IU4). Right: among other uses in the food industry, transglutaminase has been used by Gordon Ramsay and TikTok chef Nick DiGiovanni to create the world's largest beef Wellington, weighing as much as an 8 year old child.[71] Image: Nicole Wilson/Guinness World Records.

1.4.1 Active site and mechanism of action

Although human and microbial transglutaminases affect the same transformation, they share no sequence or structural homology. Additionally mammalian transglutaminases are calcium and guanosine-5'-triphosphate dependent, whereas MTG is not. MTG also demonstrates a larger substrate scope, which may be contributed to by the increased accessibility of the active site and the decreased steric hindrance of the MTG active site cleft.[72] Additionally MTG has a lower rate of deamidation.[73]

Despite these differences, both human and microbial transglutaminase contain a cysteine-histidine-asparagine catalytic triad, although the structural orientation of this triad differs – the position of the His and Asp residues is reversed relative to the cysteine.[69]
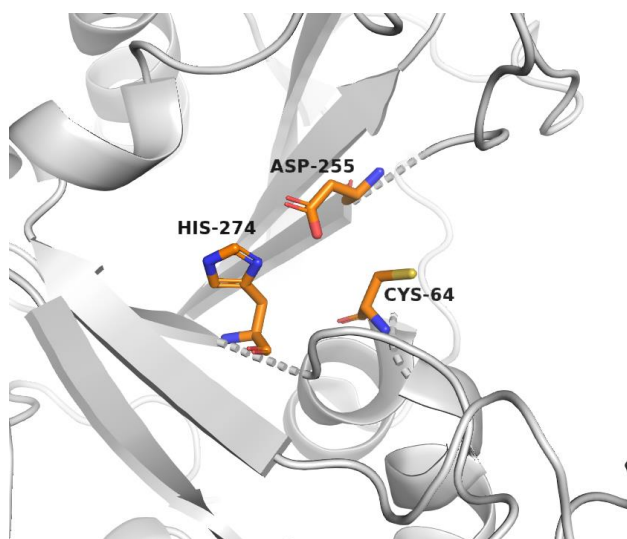
Figure 1.17 Crystal structure of the active site of MTG. The catalytic triad is shown: Cys64, Asp255, and His274. PDB = 1IU4

The active site of MTG comprises a catalytic triad composed of Cys64 and Asp255 serving as a nucleophilic catalyst and a proton acceptor/donor, respectively. The nearby His274 is thought to maintain a favourable conformation of Asp255 through a hydrogen bond interaction. Asp255 is critical to the enzymatic function of MTG and alanine mutagenesis to produce D255A reduced enzymatic function to background levels. Mutagenesis of His274 producing H274A only reduces enzymatic function by 50%, suggesting that whilst it helps activity to some extent, it isn't crucial for function.[72]

The mechanism of MTG is similar to a cysteine protease. Asp255 deprotonates Cys64, which attacks the γ-carboxamide of the glutamine substrate, displacing ammonia and forming a reactive thioester intermediate. The reactive lysine then attacks the thioester, reprotonating Asp255 in the process. The product leaves the active site, regenerating the deprotonated Cys64 to engage in further reactions (figure 1.18).[72]
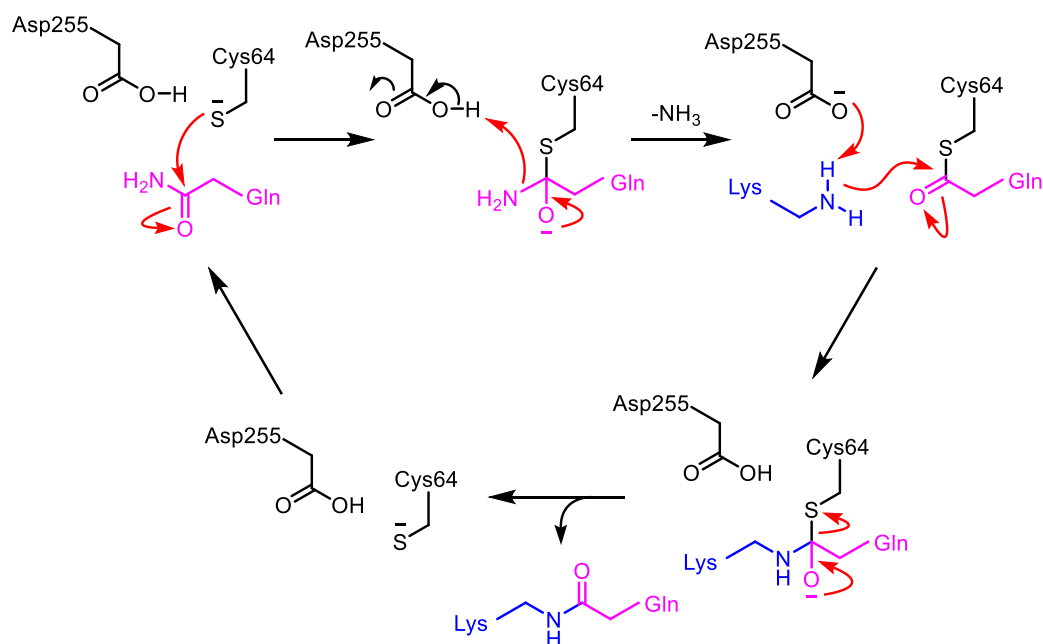
Figure 1.18 Mechanism of MTG catalysed reaction between lysine and glutamine. Key residues Cys64 and Asp255 are shown, but non-critical residue His274 is omitted for clarity.

1.4.2   MTG substrates

Generally MTG shows more substrate specificity for the acyl donor than it does for the acyl acceptor. The exact requirements for an acyl donor to be a preferential substrate remain unknown and research is ongoing into this area.[74] The crystal structure of MTG solved by Kashiwagi *et al.*, however, gives some insight into the relationship between MTG and its substrates.[72]

The surface charge of MTG is predominantly positive, but the area around the active site cleft is overall negative; there are many nearby acidic residues, such as Asp1, Asp3, Asp4, Glu249, Asp255, and Glu300. Glu249, Glu300, and Asp304 are positioned near the part of the active site the amine donor substrate is thought to bind in, giving this area a strongly negative charge. This encourages the binding of positively charged substrates over neutral ones, which perhaps explains the reduced rates of deamidation seen with MTG in comparison to mammalian transglutaminases.[73] There are also a number of aromatic and hydrophobic residues around the active site, including Trp59, Tyr62, Tyr75, Tyr278, Tyr291, and Tyr302, that could make the binding of more lipophilic substrates more favourable.

With regards to the broader substrate scope of MTG compared to mammalian transglutaminases, Kashiwagi *et al.* postulate that this could partly be explained by the increased flexibility in the walls of the MTG active site cleft, that may decrease the steric restrictions imposed on the enzyme-substrate complex, allowing a greater variety of substrate structures to be accommodated.
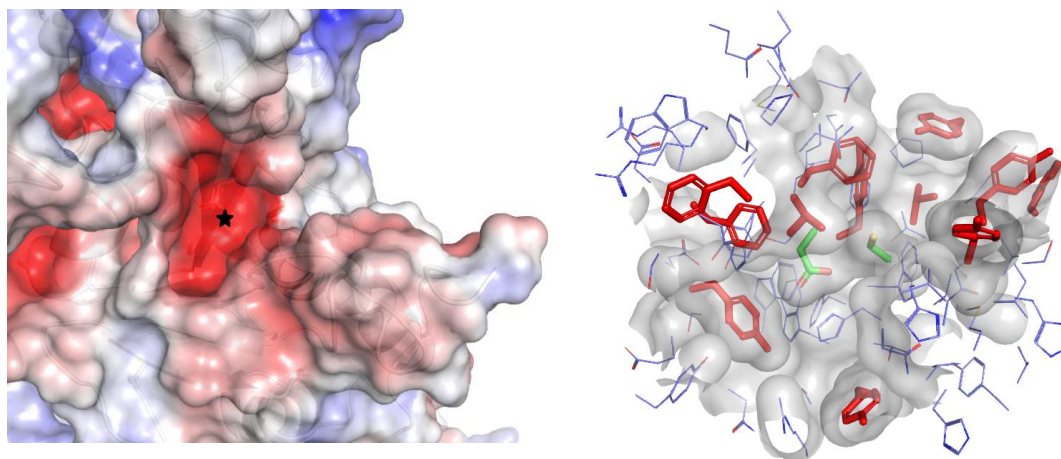
Figure 1.19 Left: active site of MTG shown with surface charges. Black star indicates the active site cleft, red represents negative charge and blue represents positive charge. Right: active site of MTG with nearby aromatic and lipophilic residues coloured in red. PDB = 1IU4.

Apart from some simple substrates tested by Ohtsuka *et al.*, the exact nature of amine donors tolerated by MTG was relatively unknown.[75] Gundersen *et al.* contributed to this question by investigating a number of unnatural amine-containing substrates.[76] They used the model peptide Z-protected glutamine-glycine, ZGQ (**9**), as the acyl donor. In brief their experiments were performed by incubating ZQG with 2.5 equivalents of amine donor and MTG at 37 °C for 72 h. Conversion was measured by quantifying the decrease in the UV signal of ZQG. This meant the UV absorption of the amine donors did not affect the measurement. Notably, though, the pH was not kept constant between different substrates and instead adjusted to the estimated pK_a of the amine donor being tested.
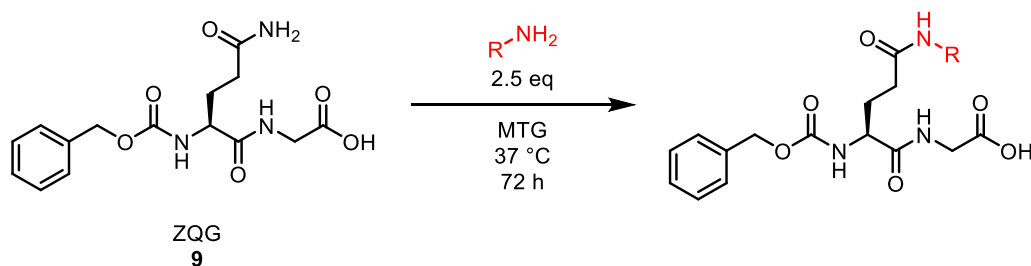
Figure 1.20 Schematic overview of the reaction Gundersen et al. *used to test the reactivity of various amine donors under MTG catalysed conditions.*

Initially they confirmed that negative charge in the form of a free carboxylic acid is poorly tolerated near the active site,[75] but increasingly tolerated as it is moved further along an alkyl chain away from the reactive amine. Masking this negative charge in the form of an ester recovers activity with glycine and can be rationalised by the predominantly negatively charged active site interacting unfavourably with negatively charged substrates.

A number of other natural amino acids were then tested. They were tested as esters to escape the poor reactivity of the free carboxylic acids. None showed any significant reaction. It's likely that as these were all alpha-branched amines, the increased steric bulk around the reactive amine prevented the intermediate thioester being formed, leading to lower conversions.

Next they tested some aromatic substrates, under the hypothesis that the aromatic residues surrounding the active site may contribute to binding. Benzylamine (**10**) showed a high conversion of 94% and aniline (**11**) a lower conversion of 19%, which could be a combination of the decreased nucleophilicity of the nitrogen lone pair and increased steric bulk around the amine. For both of these examples the non-aromatic analogues (**12** and **13**) showed decreased reactivity, though, suggesting that aromaticity in the substrate can help with binding to some degree. Substitution to generate electron-rich rings (*m*-anisidine, **14**) or electron-poor rings (3-chloro-4-fluorobenzylamine, **15**) decreased reactivity, to 11% and 23%, respectively.

Hydroxylamine (**16**) is a highly active MTG substrate and is used as the substrate in the standard MTG activity assay.[77] Gundersen *et al.* sought to combine this reactivity with

the reactivity of benzylamine and tested *O*-benzylhydroxylamine, **17**. Despite the good conversions of both of the constituent moieties, *O*-benzylhydroxylamine displayed a conversion of only 3%. The authors suggest that this is down to the increased bulk around the reactive NH_2 compared to hydroxylamine.

The small, π-electron rich substrates propargylamine (**18**) and aminoacetonitrile (**19**) were tested, both showing excellent conversions (>99% and 90%, respectively). Keen to explore the possibility of using MTG to install other click handles, they also measured the conversions of propylamine azide (**20**) and ethylamine azide (**21**), demonstrating that both of these substrates showed reactivity of >95%.
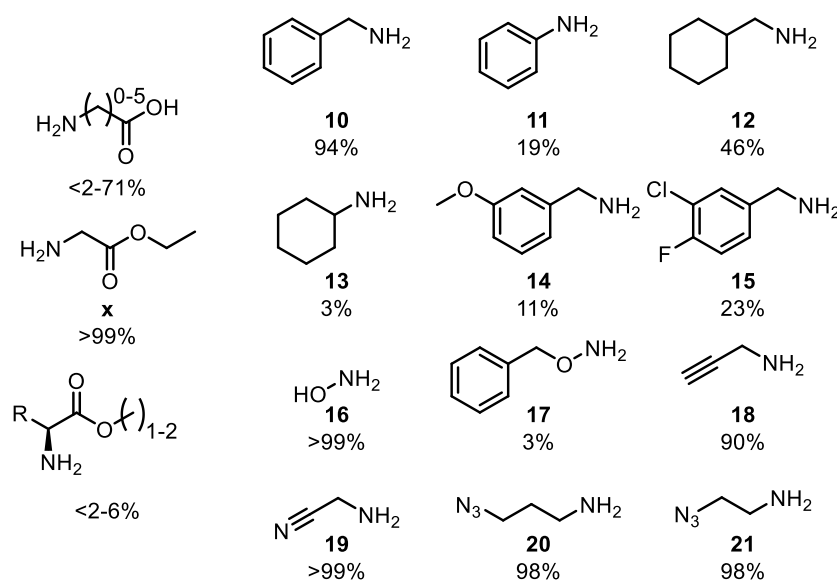
Figure 1.21 Selected examples of amine-donor substrates tested by Gundersen et al.

Their observations can be generalised as follows:

- Amines without alpha-branching are the most effective MTG substrates. Although a small amount conversion can be observed with alpha-branched amines, it's vastly decreased compared to the unbranched substrates. In general this is thought to be because of increased steric bulk around the reactive NH_2.
- Negatively charged groups near the reactive NH_2 decrease reactivity. As the distance between the reactive amine and the negative charge increases,

reactivity increases. If the negative charge is masked (for example with an ester), reactivity is recovered.

- Benzylamine is a good substrate, but substitution on the aromatic ring decreases reactivity in all the examples tested.

- Small, π-electron rich amines are extremely reactive, as are small azido alkylamines. This allows the installation of either click partner onto a protein using MTG.

The group then went on to develop chemoenzymatic conjugations strategies with MTG (discussed below), inspired by the fact the enzyme could effectively incorporate either an azide or an alkyne into a protein.

1.4.3 Use as a bioconjugation methodology

In addition to its use in the food industry, MTG has been widely and successfully used in the field of biotechnology as a bioconjugation methodology.[69] As MTG accepts a wide range of amine substrates besides its natural substrate lysine, amine-functionalised payloads can be readily incorporated into biomolecules. The higher substrate specificity for the glutamine coupling partner means excellent site selectivity can be achieved.

MTG has been used extensively for conjugation of antibodies to form ADCs. IgG antibodies have a reactive glutamine at position 295, but in the native form of the antibody this is blocked by the glycosylation at N297. To reveal the reactive glutamine the antibody first has to be deglycosylated, which is affected with peptide-*N*-glycosidase F, commonly known as PNGase F. This method gives rise to homogeneous mixtures of conjugates with well-defined DARs.[78] Alternatively the antibody can be engineered to include an MTG recognition tag, containing a reactive glutamine.[79] This method doesn't require deglycosylation of the antibody. As the nature of the oligosaccharides attached to the antibody has a profound effect on its function, this is an advantage.[80] Engineering an antibody to include a specific tag, however, adds an additional cost to the process and may affect the scalability of the route.

Key challenges in MTG-mediated bioconjugations are identifying MTG-reactive glutamine residues on the antibody in question and preventing cross-linking. Antibodies typically have a number of MTG reactive lysine residues on their surface, which can act as amine-donor substrates. This can lead to extensive protein-protein linking, hindering the approach.[69] A common solution to this problem is using the amine-functionalised payload in high excess, typically around 50-80 equivalents. Although this can successfully suppress the cross-linking, it is an extremely inefficient use of the payload, which is often a complex molecule that is either challenging to make or expensive to purchase. This issue becomes even more significant when the production of the conjugates is scaled up and represents a continuing challenge with MTG.

Another common way to overcome the cross-linking issue is to perform a two-step chemo-enzymatic bioconjugation. In short, MTG is used to install a reactive handle on the protein (usually either an azide or an alkyne so either a CuAAC or SPAAC can be used). The reactive handle is a small, simple molecule, so it can be used in excess without cost worries. Any unconjugated reactive handle is then removed and the actual payload can then be attached to the protein through a CuAAC or SPAAC. For the click step the payload can be used in only moderate excess, reducing the cost and waste of the overall process.

Dennler *et al.* used this approach to conjugate MMAE to trastuzamab.[81] Direct conjugation of MMAE to the antibody resulted in a DAR of 1.0-1.6, but it necessitated the use of 80 equivalents of toxin to prevent the formation of mAb-mAb linkages through the reaction of surface lysines on the antibody. They then used a two-step chemoenzymatic approach that offered a more precise DAR of 2.0 and proved to be more cost-effective, requiring only 2.5 equivalents of the expensive toxin for complete conjugation. MTG was used to attach an azide-functionalised linker to the deglycosylated mAb, which could then be connected to the alkyne-functionalised MMAE via a SPAAC reaction. Although this two-step method requires only a slight excess of toxin, a high excess of the linker lysine donor is still necessary. This prevents the entire process from being conducted in one pot since most of the toxin would react with the excess linker.
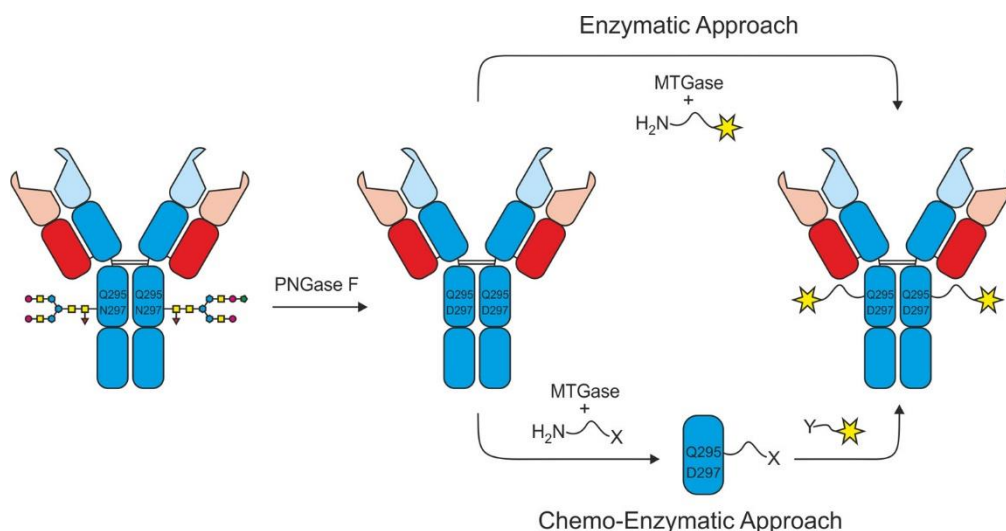
Figure 1.22 Schematic of the two approaches taken by Dennler et al. *The two-step chemoenzymatic approach wasted less payload overall and yielded more homogeneous conjugates, but required a purification step before the final reaction. Figure reproduced unmodified from Dennler et al. (2014).[81]*

Lhospice *et al.* also demonstrated this two-step approach when they conjugated payloads to brentuximab using MTG.[82] This conjugate outperformed the FDA-approved Adcetris in rodent lymphoma models. The researchers created an aglycosylated variant of brentuximab with an N297Q mutation, resulting in four potential attachment sites for MTG (glutamine residues at positions 295 and 297 on each heavy chain). They discovered that the two-step chemoenzymatic procedure for conjugating MMAE derivatives produced ADCs with better uniformity (DAR = 4.0) compared to the one-step enzymatic procedure (DAR = 3.7). Analysis of deglycosylated commercially available Adcetris, conjugated through disulphide bridge reduction as described earlier, revealed heterogeneous functionalisation of both the heavy and light chains, with an approximate average DAR of 4, allowing comparison between Adcentris and the new conjugates both *in vitro* and *in vivo*.

In vitro cell toxicity experiments conducted on two CD30⁺ cell lines demonstrated that Adcetris and the MTG conjugates exhibited comparable EC_{50} values. *In vivo* studies on rodents also showed higher tumour uptake, lower non-targeted liver and spleen uptake, and a higher maximum tolerated dose for the MTG-coupled ADC compared to Adcetris. These findings provide further evidence that controlling the DAR of ADCs is

crucial, as increased homogeneity leads to improved pharmacokinetic properties and therapeutic indices.

Strop *et al.* produced a series of ADCs by incorporating MTG recognition tags into antibodies.[83] Whereas other enzymes are often restricted to only recognising terminal sites, MTG can recognise internal positions. This allowed the team to introduce MTG conjugation points wherever they liked on the antibody and investigate the effect the location had. The method gave them precise control over the site of conjugation and DAR.

They further investigated the impact of this site-specific conjugation technology on the pharmacokinetic (PK) properties and therapeutic index (TI) of ADCs with high drug loading. Previous reports have indicated that ADCs with high DAR (> 4) suffer from issues such as compromised PK properties, increased toxicity, and reduced TI. The group discovered that this problem can be partly attributed to the conjugation of multiple hydrophobic payloads in close proximity. However, by employing site-specific MTG conjugation, this challenge can be overcome by identifying conjugation sites that minimise payload density and solvent accessibility. Additionally, these sites should be combined in a manner that avoids excessive clustering of hydrophobic payloads.

To illustrate this, the researchers synthesised ADCs with high drug loading using their MTG site-specific procedure and compared them to conventionally synthesised (cysteine-maleimide) ADCs with similar drug loading. They observed that while both sets of ADCs exhibited similar *in vitro* potency, the site-specific conjugates demonstrated enhanced *in vivo* efficacy, favourable PK properties, and good tolerability, resulting in an improved TI. Moreover, when tested in mouse xenograft models with low expression of the target antigen, the high-loading site-specific ADCs displayed superior efficacy compared to both conventionally synthesised conjugates with similar loading and site-specific conjugates with lower loading. These findings highlight the potential of using the customisable, site-specific conjugation enabled by MTG to target tumours that would otherwise pose challenges for ADC treatment due to factors such as low target expression, slow internalisation, or inefficient intracellular processing, leading to insufficient payload concentration in the target cells.

Rachel and Pelletier also investigated a chemoenzymatic system using MTG and CuAAC, but they developed their conditions to allow the conjugation to be carried out in one pot, without the need for an intermediate purification.[84] MTG had been observed to be inactive in the presence of Cu^{2+}, making it incompatible with the CuAAC conditions.[85] The reason behind this could be chelation of copper to the thiolate ion of catalytically active Cys64, rendering the enzyme unable to form the necessary thioester intermediate. They hypothesised that adding the reduced form of glutathione to the reaction could recover MTG activity in the presence of copper, by keeping Cys64 as the free thiol. This hypothesis was correct and they were able to carry out MTG conjugations in the presence of CuAAC reagents. Additionally they confirmed that the presence of glutathione didn't impact the CuAAC reaction itself. They found that in order for their one-pot methodology to work, the rate of MTG conjugation had to be much faster than the CuAAC rate. This is because the triazole product **22** between the free azide and alkyne was not itself an effective substrate for MTG. Therefore the only productive reaction sequence is conjugation of an amine-alkyne to their model peptide, followed by a CuAAC with the model azide-payload. Under their optimised conditions the rate of MTG reaction was significantly faster than the CuAAC reaction, allowing them to observe conversions of up to 95%. They exemplified this methodology by conjugating the fluorophore Cy5 onto α-lactalbumin.
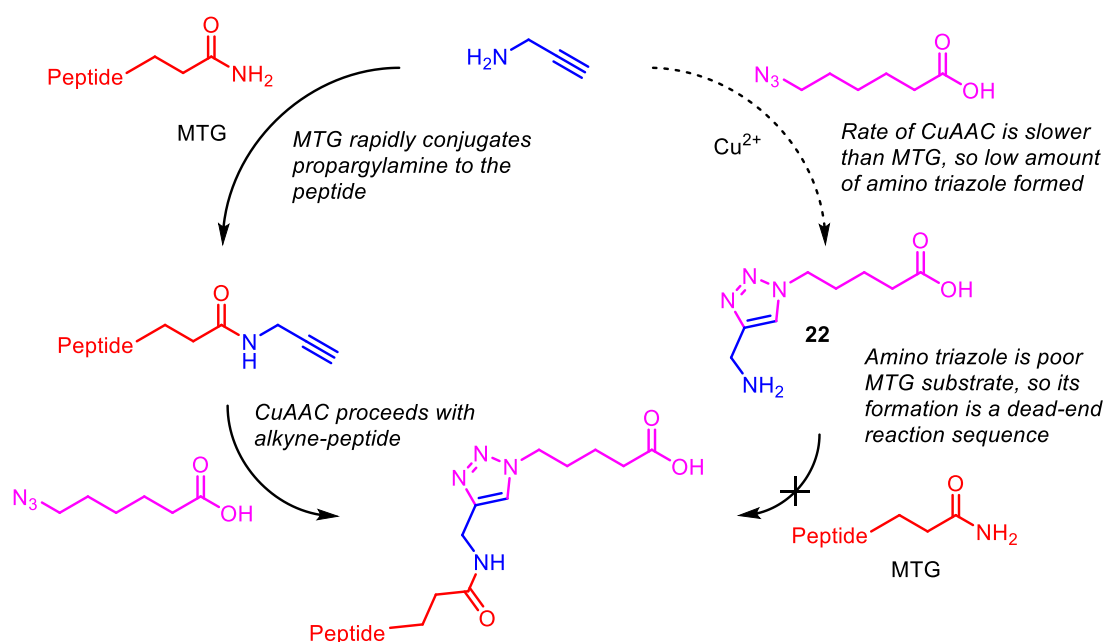
Figure 1.23 Overview of the possible reaction sequences in Rachel and Pelletier's one-pot MTG chemoenzymatic conjugation. Crucially, MTG conjugation occurs more rapidly than the CuAAC. If the CuAAC were to occur faster, the amino triazole product is not an effective MTG substrate and would lead to low levels of product formation.

The group followed this work up with a new methodology, this time incorporating MTG and SPAAC.[74] Copper has a significant cytotoxic effect, so is often avoided in biological contexts. Moreover proteins can be inactivated or precipitated in its presence, highlighting the need for alternative click reactions. In contrast to their earlier work, the metal-free click reactions they investigated proceeded on much faster timescales than the MTG conjugation. The overall yield of the process therefore depends on how good an MTG substrate the click product is. As with their previous work triazoles were relatively ineffective, although they could recover respectable reactivity by including a spacer between the MTG reactive amine and the triazole, allowing all sequences of reactions to be productive.

Of note in both these pieces of work, is that only two equivalents of amine were used with respect to the protein (or model peptide) they were to be attached to. As discussed earlier, this has the potential to allow protein-protein cross-linking. The initial work didn't comment on this, but the metal-free follow-up observed cross-linking of their protein. Although this work has successfully optimised conditions such that MTG chemoenzymatic conjugations can now be performed without intermediate

purification, the fact that cross-linking can occur could be a significant disadvantage to this method, especially for a protein that had surface glutamine/lysine residues that were particularly susceptible to MTG recognition.

Transglutaminases represent a diverse group of enzymes that are abundantly present in various microorganisms. Despite their wide distribution, only a few members of the transglutaminase family, such as MTG derived from *Streptomyces mobaraensis*, have been extensively studied for biotechnological applications. However, exploring other transglutaminases with distinct properties would be highly valuable. One promising example is the recently discovered KalbTG derived from the actinobacterium *Kutzneria albida*. Unlike MTG, KalbTG exhibits no cross-reactivity with known MTG substrates or commonly targeted proteins such as antibodies.[86]

Steffen *et al.* identified KalbTG as having orthogonal reactivity compared to MTG, enabling the dual labelling of a substrate containing recognition sequences for both enzymes.[86] This was achieved by initially treating the substrate with the more specific KalbTG, followed by the less specific MTG. By incorporating the recognition sequence of KalbTG into an antibody, site-specific and precisely controlled labelling became achievable using a lower excess of labelling agent. This is a significant difference to MTG, for which high excesses of amine substrate are required to prevent cross-linking. While the study did not present any ADCs, it showcased the potential of alternative transglutaminases and the ability to perform dual labelling by using orthogonal transglutaminases.

1.5 Payloads

The long process before the cytotoxic payload is released from the ADC means only a small amount of the payload reaches the cell. If each of these steps has a 50% efficiency, only around 1.6% of the administered payload dose will actually reach the intended intracellular target.[87] This shows the importance of using highly potent cytotoxic small molecules as payloads for ADCs. Additionally, the chosen drug must possess prolonged stability in aqueous environments, be structurally compatible with

linker conjugation, minimise immunogenicity, and have minimal impact on the properties of the mAb.

Early ADCs used chemotherapies such as doxorubicin and methotrexate as payloads, due to their well-established toxicity profiles in humans.[88] However, as it became evident that increased potency resulted in more effective ADCs, the range of small-molecule payloads expanded. Some drugs previously considered too cytotoxic for conventional chemotherapy were now included. Typically, the drugs selected for ADCs are 100-1000 times more potent than traditional therapeutics, exhibiting sub-nanomolar potencies.

Three groups of cytotoxins have classically been used in modern ADCs: auristatins, maytansines, and calicheamicins. Auristatins and maytansines function as microtubule inhibitors, targeting rapidly dividing cells and inducing cell cycle arrest.[89] Calicheamicins, along with less common duocarymycins and pyrrolobenzodiazapine (PBD) dimers, induce DNA damage.[90,91] Regardless of the specific group, all of these payloads lead to cancer cell death by triggering apoptosis.[92]

Auristatins, specifically monomethyl auristatin E (MMAE, **23**) and monomethyl auristatin F (MMAF), are derived from natural peptides found in the marine mollusc *Dolabella auricularia*, known as dolastatins. These compounds exhibit a similar mode of action to conventional taxane therapeutics by binding to the β-subunit of cytoplasmic α-β tubulin dimers. This interaction prevents guanosine triphosphate (GTP) hydrolysis on the β-subunit, a biological process critical in regulating cell processes, leading to excessive and uninterrupted microtubule growth, thereby inhibiting the cell from exiting the metaphase stage of mitosis.[93] As MMAE is hydrophobic, it can easily diffuse out of the target cell and enter neighbouring cells, resulting in bystander killing.[94] This property can be advantageous or disadvantageous depending on the specific circumstances. In solid tumours, it may offer benefits, but in the treatment of haematological cancers, it may lead to undesirable off-target toxicity. Besides serving as the cytotoxic payload in Adcetris, MMAE has been extensively studied and employed in various clinical candidates.[34,81,93–97]

Maytansinoids (DMs), which are derivatives of maytansines, exert their effects on microtubule formation in a similar manner to vinca alkaloids. They bind to and block the "plus" end of the growing tubule, hindering the polymerisation of tubulin dimers and thereby preventing the formation of fully developed microtubules. Once the GTP molecule on the β-subunit of the α-β tubulin dimer undergoes hydrolysis, existing microtubules disassemble, effectively arresting the cell in metaphase and inhibiting proliferation.[98] The most commonly utilised maytansinoids are DM1 (**24**) and DM4, with DM1 featuring as the payload in Kadcyla.[99]

Calicheamicins, duocarymycins, and PBD dimers cause DNA damage. When DNA forms a double helix with two anti-parallel strands, it creates a major groove and a narrower minor groove with fewer exposed base pairs. It is within this minor groove that calicheamicins bind, similar to anthracyclines, forming a reactive diradical species that leads to the breaking of DNA strands at multiple sites.[100] Calicheamicin is an exceptionally potent anti-tumour antibiotic and served as the cytotoxic payload in the first approved ADC, Mylotarg.[101] Duocarmycins and PBD dimers also bind to the minor groove, functioning as alkylating and cross-linking agents, respectively.[102,103] As in healthy cells, DNA damage ultimately triggers cell death through apoptosis.
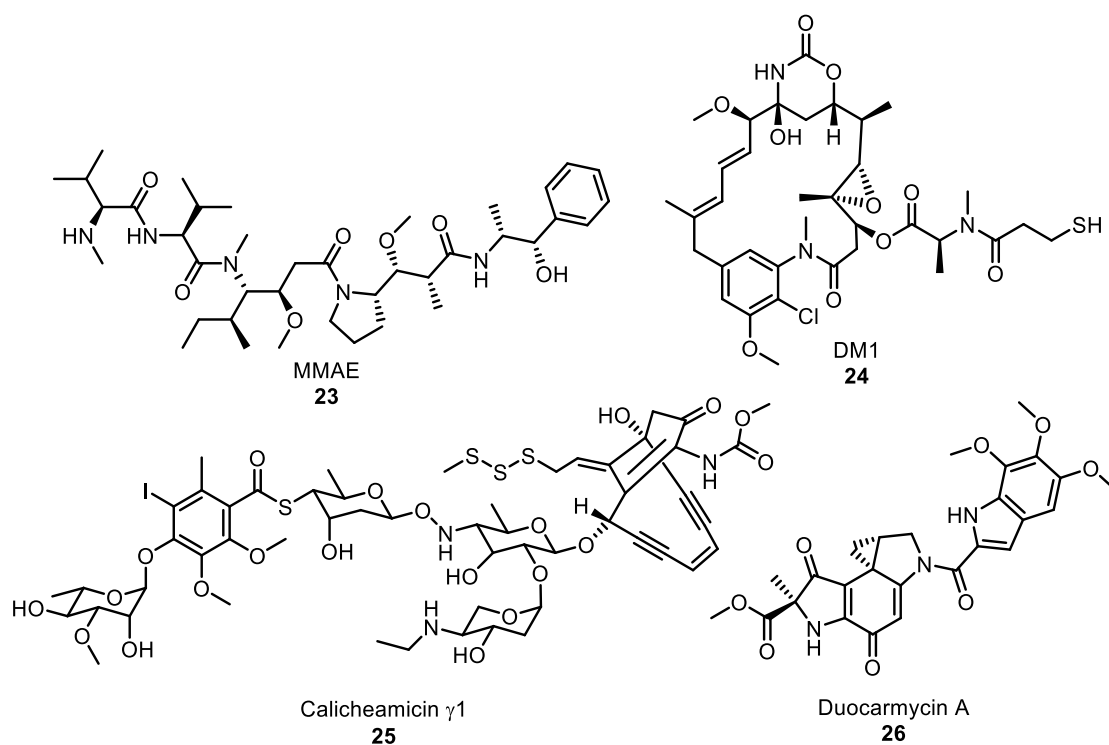
Figure 1.24 Chemical structures of some potent cytotoxic payloads used in ADC synthesis.

1.5.1 Future payload development

Currently approved ADCs have payloads with mechanisms of action similar to those of traditional chemotherapy agents and are, as discussed above, most commonly microtubule disruptors.[104] Cure of an advanced disease is generally achieved by combining therapies with complementary mechanisms of actions and, if possible, non-redundant toxicities. In order to apply this concept to ADC design, future work in the field is beginning to explore alternative payloads that exploit novel mechanisms of action, some of which may have been written off until now due to their excessive toxic effects.[105]

The benefits of payload diversification are exemplified by Enhertu, an ADC approved in the EU in 2021.[106] It can be considered a second generation version of Kadcyla, a previously approved ADC. Both drugs use trastuzamab to target HER2$^+$ cells in order to treat breast cancers (Enhertu is also approved for the treatment of HER2$^+$ gastric or gastroesophageal junction adenocarcinoma). Enhertu is more effective in treating breast cancer and is particularly important in the treatment of Kadcyla-resistant and

HER2-low cancers. In order to develop this improved activity the linker and payload have been changed.

Kadcyla uses DM1 (**24**) as a payload, a microtubule inhibitor. Although effective and in clinical use today, in HER2-low breast cancers Kadcyla can prove ineffective. Enhertu uses a novel topoisomerase I (Top1) inhibitor, deruxtecan (**27**), as its payload. In cells Top1 allows DNA relaxation during replication and transcription. It forms a complex with cleaved DNA and allows the rotation of the cleaved strand allowing subsequent re-ligation, restoring the double strand. Inhibition of Top1 prevents re-ligation, introducing cytotoxic DNA strand breaks.[107]
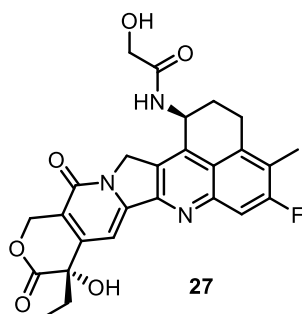
Figure 1.25 Chemical structure of deruxtecan, the payload of Enhertu

The DAR of Enhertu is around twice that of Kadcyla (8 compared to 3-4).[104] This leads to a higher concentration of payload in the target cells, giving the conjugate a higher potency. Although high DAR conjugates can often lead to increased toxicity through premature release of payload in circulation, Enhertu has avoided this pitfall by careful design of their enzymatically cleavable linker that has prevented release until the ADC is internalised.[108]

A key feature of deruxtecan is that it has a higher cell permeability than DM-1. This means that once the 8 payloads per ADC are delivered to the target cells, these toxins can enter other neighbouring cells and extend their cytotoxic effect. This is a crucial way in which Enhertu can address lower antigen-expressing cancers.[109]

Clearly, exploring a diverse range of ADC payloads should be a significant priority for ADC research going forward, potentially resulting in the discovery of improved second generation conjugates such as Enhertu.[105] Not only is it diverse mechanisms of actions

that are of interest, but the development of more potent payloads that have the potential to address low antigen expressing cancers, especially if the payloads can exploit the bystander effect. Although this can be achieved to some extent by simply increasing the DAR of conjugates, there is a limit to this and the possibility of introducing undesirable physical properties to the conjugates such as increased hepatic clearance and aggregation.[110]

1.6   Aims

1.6.1   Investigation of MTG amine donor scope

Investigations into the accepted amine substrate scope of MTG remain fairly limited. Therefore, although it's known that MTG will accept a wide range of amine donors, the structure activity relationships (SAR) of various amine donors is not well understood.

A better knowledge of the tolerated amine substrates for MTG will allow rational design of substrates for specific uses and may allow predictions to be made about the suitability of previously untested amines.

To this end we aim to further explore the amine donors MTG can accept and quantify their reactivity. By comparing reactivity with chemical structure we will develop a structure-activity relationship (SAR) for the amine donors, allowing us to attempt to rationalise and predict reactivity.

1.6.2   Development of an optimised amine donor for payload conjugation

MTG is a widely used and versatile conjugation method to produce ADCs and other functionalised biomolecules. Current one-step conjugation methodologies require a payload excess of 50-80 equivalents to encourage conjugation and prevent protein-protein crosslinking. This is manageable for small scale laboratory reactions, but represents a major cost and materials wastage if production is to be scaled up, as many payloads for ADCs are expensive and labour intensive to produce.

To overcome this issue two-step chemoenzymatic strategies have been developed, that install a click handle on the protein using MTG and attach the payload through a subsequent click reaction. The amine-functionalised click handle still has to be used in high excess to prevent cross-linking during the MTG reaction, but if the unreacted, free amine is removed through purification the payload can be used in only moderate excess.

Although effective, the necessity of an intermediate purification step may lead to reduced yields of conjugate, which may represent a significant cost penalty on scale.

Additionally the inclusion of a second click step means either cytotoxic copper has to be used, or a SPAAC-compatible alkyne incorporated into the system. These alkynes, such as bicyclononyne, are often very lipophilic and can alter the properties of the final conjugate in undesirable ways.

It is therefore desirable to develop a one-step, direct MTG conjugation that doesn't require a large excess of amine-payload. To do this, we hope to find an amine donor motif that is significantly more active than MTG's native amine donor, lysine, such that during a conjugation the optimised amine-payload will react preferentially to surface lysine residues on the protein. This will supress protein-protein crosslinking whilst only requiring the payload to be used in moderate excess, representing a potentially significant saving of cost and material.

1.7 Results and discussion

1.7.1 Establishing methodology

In order to investigate the amine donor substrate tolerance of MTG we first needed to identify a method that allowed us to quantify how well each substrate was accepted and converted by MTG. To do this, we established a set of reaction conditions that were kept constant except for the identity of the amine donor, and measured the conversion of the substrates over a fixed period of time. This allowed us to measure a percentage conversion for each substrate, which could be interpreted as an indication of how well the amine substrate was accepted by MTG. With this number in hand, we could then compare how well different classes of substrates were accepted by MTG, and start to extract a structure-activity relationship (SAR) from the substrates. This quantification of activity also allowed us to compare unnatural substrates to a model of peptidic surface lysine residues, which is the comparison we need to make if we are to address the protein-protein crosslinking issue.
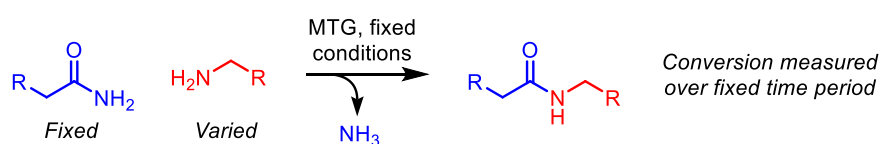
Figure 1.26 Schematic overview of method used to measure substrate conversion.

We decided to use the Cbz-protected dipeptide Z-glutamine glycine (ZGQ, **9**) as our model acyl donor, as it has widely been used in the literature as a model substrate for MTG catalysed reactions, as well as the standard MTG activity assay.[75–77,84] Additionally it contains a chromophore, enabling us to monitor its consumption by LCMS. Using this to measure conversion, rather than quantifying product formation, means that the UV absorbance profile of the varying amine substrates will not affect the measurement.

MTG that is available for biotechnology research applications is pure and highly active, but can represent a significant cost. For example, MTG purchased from Zedira, a company specialising in transglutaminases, can cost around €11 per unit.[111] Alternatively MTG can be expressed and purified in-house, but this requires specialist

equipment and knowledge. MTG intended for food applications can be obtained in large quantities for a comparatively low cost, although it is often mixed with various stabilisers and bulking agents. For example, MTG branded as "Moo Gloo" can be purchased as 50 g or 500 g packages, with an enzyme content of 60-70 units per gram.[112] The 50 g package costs $14.99, making the cost per unit about $0.005. Using this type of MTG (herein referred to as "food grade") would significantly decrease the cost of the project, but would also demonstrate that these cheaper sources of MTG can still be used for research applications.

The temperature chosen for the assay should allow a reasonable MTG activity, but not induce any thermal inactivation of the enzyme. Umezawa *et al.* measured the response of MTG derived from *S. mobaraense* to temperature.[113] They found that the relative activity (determined over the course of a 10 minute reaction) rose steadily from 10 ℃ to ~60 ℃, then rapidly declined. They also investigated the thermal stability of the enzyme by pre-incubating the enzyme at various temperatures for 10 minutes and then measuring the remaining activity. They found that at temperatures above 40 ℃ the remaining activity began to decrease. Taken together these results suggest a temperature just under 40 ℃ will give the maximum activity of enzyme without inducing thermal deactivation. We therefore chose 37 ℃ as the assay temperature, in line with previous literature.[76]

The same team also measured the response of MTG to changes in pH level.[113] They found that MTG had the greatest relative activity at pH 6-7, but was stable up to pH 9 and down to pH 5. This stability window is confirmed in other literature.[114] We chose pH 7.6 for the assay for the following reasons:

- MTG shows good relative activity at this pH (~90%).

- MTG is stable at this pH.

- Although MTG is most active at neutral pH, ZQG is only soluble in water under slightly basic conditions. pH 7.6 proved to be the closest pH to neutral that allowed the complete dissolution of ZQG at the desired concentrations.

- We want to develop a general bioconjugation strategy that is useful in as many situations as possible. Proteins and antibodies are most stable around pH 7, so a versatile bioconjugation method must work well at near-neutral conditions. We therefore want our results to hold true for conditions as close to pH 7 as possible.

When preparing stock solutions of the amine donors to be tested, it was important to measure and adjust the pH to 7.6: many of the amines were reasonably basic, and when dissolved in phosphate-buffered saline (PBS) produced solutions with extremely high pHs.

As discussed in section 1.4.2, when Gundersen *et al.* performed their amine donor screen they did not keep the pH constant, and reactions were carried out at a pH that matched the estimated pK_a of the amine donor being tested. If the pK_a fell outside the range of 6-9, the reaction was performed at the limit of this range closest to the pK_a.[76] They state that this was to aid compound dissolution while maintaining nucleophilicity of the reactive amine (if the pH is adjusted to the pK_a of the amine, then there will be a 1:1 mixture of neutral and protonated amine present). According to Umezawa *et al.*, however, the relative activity of MTG at pH 9 is just under 50%, compared to 100% at pH 6.[113] Clearly this will affect the conversions measured irrespective of the amine donor being investigated. This makes it impossible to draw comparisons between substrates tested at different pHs, and makes it difficult to establish a concrete SAR from their results.

Preliminary experiments with food grade MTG revealed that the formulation of the product posed difficulties with the LCMS analysis of the reactions. We hypothesised that this was likely due to the poor solubility of the undefined excipients included to stabilise the enzyme or improve bulk or flow properties, leading to blockages of the instrument during sample analysis.

It is also desirable to have as few superfluous entities in the reaction mixture as possible, so we began to purify the food grade MTG. This was carried out through dialysis, using a 10 kDa molecular weight cut-off. The purified product was visibly less viscous, and solved the issue with instrument blockages. In order to ensure that results

from batched or classes of enzyme could be compared, the activity of the enzyme was then measured using a standard commercial hydroxylamine-based assay, and the enzyme split into aliquots. The measured activity of the enzyme was surprisingly close to the manufacturer's estimation of activity, despite the fact that this wasn't a product for technical use.

In order to quench the reactions after the predetermined time course we added formic acid and allowed the mixture to stand for 5 minutes. This was informed by the instability of MTG at low pH levels,[113] and is in line with previous work.[76] It is important to consider that although we did not observe any product degradation upon analysis, the reaction mixture should be analysed as soon as possible after quenching to minimise any acid-promoted degradation. An internal standard was also added as soon as the time course was over to correct for any losses that may occur during sample preparation. Again, according to Gundersen *et al.*, we used a 1 mg/mL solution of 4-methoxybenzamide as an internal standard. Its retention time is sufficiently different to ZQG, it has a sharp peak shape at the concentration used, and it ionises well so can be clearly identified in the reaction mixture.

As a model of a peptidic surface lysine residue, we used the doubly protected N_α-Ac-*L*-Lys-OMe (**28**). This would be our benchmark for MTG substrate reactivity. The substitutions on the α-NH$_2$ and the carboxylate mimic those in a peptidic lysine, although the extended bulk of a peptide is absent. In order to compare unnatural substrates that were both more and less active than **28**, its conversion needed to be around 50% over the course of the assay. Preliminary investigations revealed that using 0.56 U of MTG, 2 equivalents of **28** and 1 equivalent of ZQG, and running the reaction for 90 minutes at 37 °C gave a conversion of 48±3.1%.

We also ran a control reaction for each substrate to ensure there was no residual reaction between ZQG and each amine in the absence of MTG. This was true for every substrate tested.

The conversion for each amine substrate could then be calculated from the consumption of ZQG according to the following formula:

$$Conversion = \left(1 - \frac{y}{y_{control}}\right) \times 100$$

Where

$$y = \frac{UV\ peak\ area\ of\ ZQG}{UV\ peak\ area\ of\ internal\ standard}$$

A limitation of this approach is the fact that it's impossible to distinguish between a substrate that reached 100% conversion in 10 minutes or 90 minutes. In this case their activity is outside of the upper bound of the assay, however such compounds can then be investigated under modified assay conditions, for example lower MTG loading and/or shorted incubation times, if required.

Additionally this method of measuring conversion doesn't account for other products forming from ZQG, such as hydrolysis. Hydrolysis has been observed with some less reactive substrates in the literature, although when compared to other transglutaminases MTG has relatively low rates of hydrolysis. The formation of the hydrolysis product was monitored during investigations, but it was never observed – the only product formed (if any) was the expected amide product.
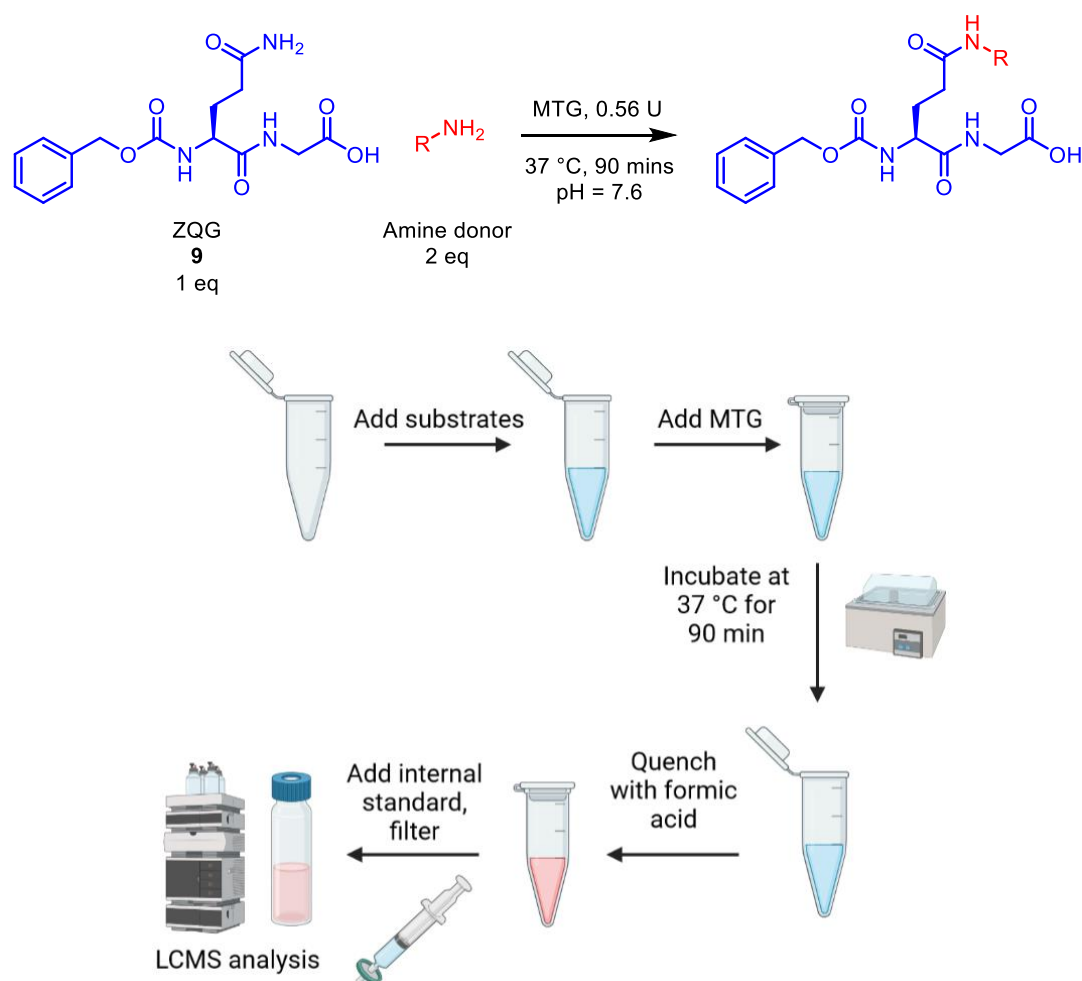
Figure 1.27 Above: chemical reaction occurring during assay. Below: schematic overview of workflow (colour changes are for illustration purposes only).

1.7.2 Straight-chain amino acids, and the various protected forms of lysine

Initially a series of straight-chain amino acids were tested, of the form $NH_2\text{-}(CH_2)_n\text{-}COOH$, where n varied from 1-6. We also tested the methyl esters of these compounds, to investigate the effect of masking the negative charge of the carboxylate. Although these compounds have been tested in prior work, the exact conversion will depend on the specific reaction set-up making it necessary to retest these compounds under our conditions, and verify published data.[75,76]

Compound	Structure	R	Conversion/%	SD
29	H_2N—$\overset{O}{\overset{\|}{C}}$—OR	H	0.0	6.0
30		Me	100	0.0
31	H_2N—$\overset{O}{\overset{\|}{C}}$—OR	H	0.0	1.0
32		Me	72	7.3
33	H_2N—$\overset{O}{\overset{\|}{C}}$—OR	H	0.0	4.1
34		Me	45	1.8
35	H_2N—$\overset{O}{\overset{\|}{C}}$—OR	H	2.0	3.6
36		Me	45	1.8
37	H_2N—$\overset{O}{\overset{\|}{C}}$—OR	H	10	5.0
38		Me	49	2.7
39	H_2N—$\overset{O}{\overset{\|}{C}}$—OR	H	14	3.0
40		Me	23	5.7

Table 1.1 Conversions of straight-chain amino acids and their esters.
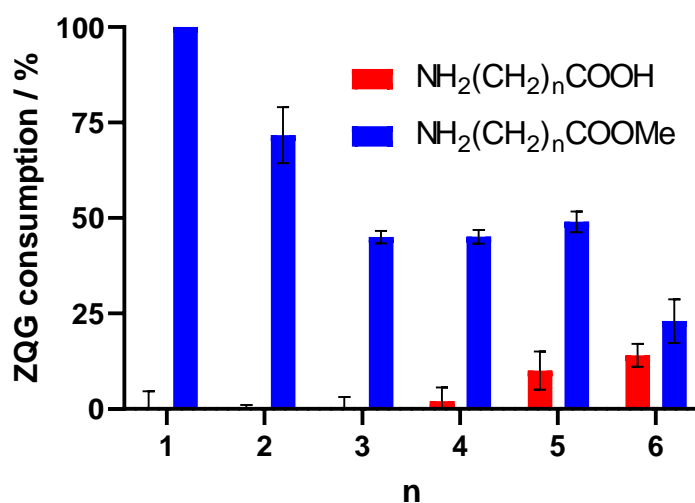
Figure 1.28 Graph of conversions of the straight-chain amino acids and their esters. Acids are shown in red, and esters in blue. Conversions are quoted as the average of three repeats, each repeat using a different batch of purified enzyme. The error bars show the standard deviation of the three repeats.

The most obvious conclusion to draw from these data is that the free carboxylic acids are poor amine donor substrates for MTG. The shortest three compounds show no conversion, and the maximum conversion seen is only 14% for the longest chain

compound, **39**. This can be fairly easily rationalised by considering the active site of MTG. As discussed in section 1.4.2, the net charge around the active site is negative and therefore it follows that amine substrates with areas of negative charge in them, such as carboxylic acids, will experience a significant degree of electrostatic repulsion in the active site. This makes their binding less favourable and leads to lower conversion to product. The reluctance of MTG to accept negatively charged substrates has been noted in the literature before both in the context of amino acids such as these, and other compounds such as phosphonates and sulphonates.[75] The trend in carboxylic acids can also be explained this way: as the intervening chain length increases, the negative carboxyl group can be further away from the active site and has more flexibility to assume a binding mode that minimises negative electrostatic interactions while the amine reacts with the thioester intermediate, leading to less repulsion and better substrate acceptance.

Another obvious observation is that esterification, i.e. masking the negative charge, leads to significant recovery of activity. For example glycine and its methyl ester, **29** and **30**, show a 0% and 100% conversion, respectively. The trend of esters performing better is true for all lengths of chain tested.

Interestingly, as the chain length in the ester series is increased conversion decreases. One possibility is that a favourable interaction is occurring between the ester group and one or more residues in the active site, and as the chain length increases this interaction can occur less, decreasing the conversion. Another possibility is simple sterics – as the chain length increases, there is more steric bulk to accommodate in the active site that may lead to increased steric repulsion and a decrease in conversion. One final factor that could influence this trend is the entropy of binding. Part of the entropy of binding is determined by the extent of conformational freedom lost upon binding. As the chain length increases from **30** to **40**, the molecules have more degrees of rotational freedom, and can adopt more conformations, consequently binding of the longer molecules leads to a higher entropy penalty.

Next the various protected forms of lysine were tested to observe the effects of exposing or masking the α-NH$_2$ and the carboxylate. As observed with the compounds

above, methylation of the lysine carboxylic acid to produce Lys-OMe (**41**) improved conversion by a moderate amount from 60% to 67%. This was also true when considering the N_α-acetyl protected analogues, **42** and **28**. In this case the conversion was improved from 24% to 48% upon esterification.

Something that hasn't been explored in the literature is the effect of the N_α acetylation. It's clear that the acetylation has a detrimental effect on conversion. From lysine (**43**) to N_α-acetyl lysine (**42**) the conversion decreases from 60% to 24%, and in the esters from 67% (**41**) to 48% (**28**). Not only does it seem that acetylation has a detrimental effect, these data suggest that the free α-NH_2 actually has a promoting effect. The addition of an α-NH_2 from 6-aminocaproic acid (**37**) to lysine (**43**) corresponds to an increase in conversion from 10% to 60%, and from the methyl ester of 6-aminocaproic acid (**38**) to Lys-OMe (**41**) an increase from 49% to 67% is seen.
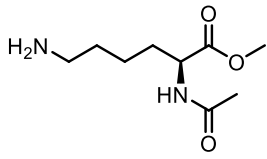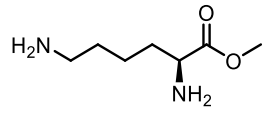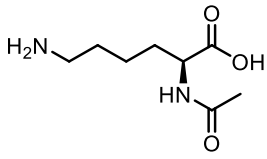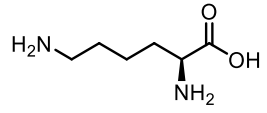
Compound	Structure	Conversion/%	SD
28		48	3.1
41		67	7.2
42		24	3.7
43		60	2.5

Table 1.2 Conversions of the various protected forms of lysine.

78
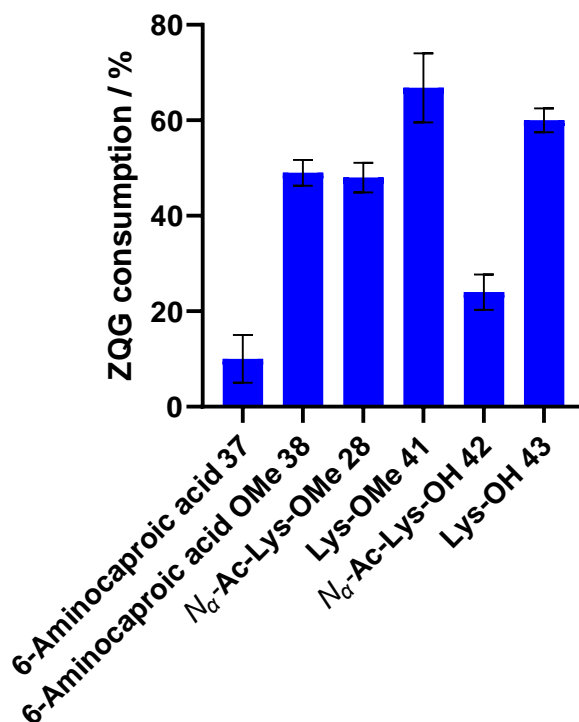
Figure 1.29 Graph of conversions of the various protected forms of lysine.

The data also show that this is not just a steric effect, with the acetyl group producing more steric clash. Comparing the methyl ester of 6-aminocaproic acid (**38**) and the methyl ester of N_α-acetyl lysine (**42**), almost identical conversions are seen (49% and 48%, respectively). This comparison corresponds to adding the whole N_α-Acetyl moiety, suggesting that the associated increase in steric bulk is perfectly tolerated five carbons away from the reactive amine.

A hypothesis to explain this is that an additional free NH_2 gives rise to the possibility of more overall positive charge. For example, 6-aminocaproic acid (**37**) can only carry a maximum possible charge of +1, when both the amine and the acid are protonated. Lysine (**43**), though, can carry a maximum possible charge of +2, when both amines and the acid are protonated. Obviously the various protonation states exist in equilibrium, the balance of which is determined by the pH of the solution; but some proportion of the lysine molecules will occupy the +2 protonation state. These will be strongly attracted to the negative active site, and, once the terminal amine has been neutralised by an active site residue, attack the thioester intermediate to generate

product. Even if the proportion of molecules that exist in the +2 state is low, the strong attraction to the active site could still drive this high reactivity – as the concentration of the +2 protonation state decreases through this reaction the equilibrium will shift to counteract this according to Le Chatelier's principle, generating more +2 molecules.

1.7.3 Glycine upgrade strategy

Glycine methyl ester (**30**) is a highly active substrate, showing full conversion in our assay. If this is a result of favourable interactions in the active site, rather than simply lack of steric bulk, it may represent a way to "upgrade" amine donors by simply coupling them onto glycine to generate a new, more reactive terminal amine (figure 1.30).
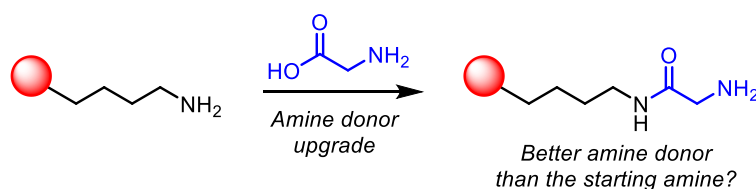
Figure 1.30 Schematic illustrating the concept of using glycine to upgrade an amine donor. A payload is represented as a red circle.

To explore this we tested 2-amino-*N*-methylacetamide (**44**). Upgraded donors containing an ester linkage are unlikely to be hydrolytically stable under biological conditions, but constructing them with amide linkages increases the hydrolytic stability whilst keeping the electronic and structural properties similar.

Unfortunately both **44** and **45**, the one-carbon homologated version, showed only middling to poor conversion (table 1.3). Neither was significantly more reactive than the benchmark compound, **28**, so this strategy was abandoned.

The finding that glycine amide **44** is similarly reactive to the lysine analogues is interesting given the accepted selectivity of MTG for lysine side chains, however. It raises the possibility that *N*-terminal glycine may also be a potential conjugation site for MTG (and perhaps tranglutaminases in general), although we did not investigate this further.
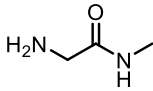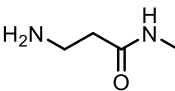
Compound	Structure	Conversion/%	SD
44	H₂N, O, N, H (structure)	52	1.3
45	H₂N, H, N, O (structure)	17	1.0

*Table 1.3 Conversions of amides **44** and **45**.*

1.7.4 Rational design of an alkoxyamino lysine mimic

Nucleophiles with adjacent heteroatoms can show far greater nucleophilicity than would be expected from their basicity. This is known as the α-effect, and representative examples include the hydroperoxide ion (HOO⁻), and hydrazine (N_2H_4). Many hypotheses have been proposed to explain this effect, but the exact origins are still under debate. A 2021 paper by Hansen *et al.* used computational methods to quantum chemically analyse α-effect nucleophiles, and determine the criteria an α-nucleophile needs to fulfil in order to demonstrate the α-effect.[115]

They established that an adjacent heteroatom led to a smaller highest occupied molecular orbital (HOMO), as the electron withdrawing nature of the heteroatom (O, N) pulled electron density away from the nucleophilic atom. When interacting with the electrophile, this smaller $HOMO_{Nu}$ experienced less electrostatic repulsion with the filled molecular orbitals (MOs) of the substrate.
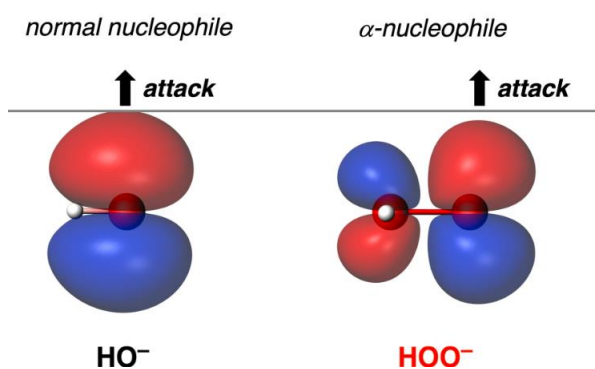
Figure 1.31 Representation of the calculated spatial extent of the HOMOs of both hydroxide (a normal nucleophile, in black) and hydroperoxide (an α-effect nucleophile, in red). The grey line represents the maximum spatial extent of the HOMO, showing the hydroperoxide HOMO extends less far. Figure reproduced unmodified from Hansen et al.[115]

A smaller $HOMO_{Nu}$, however, also leads to poorer spatial MO overlap with the lowest occupied molecular orbital (LUMO) of the electrophile, which should lead to decreased reactivity. The nucleophile therefore has to satisfy a second criterion to experience increased reactivity. The energy of the $HOMO_{Nu}$ is increased through electrostatic repulsion between the filled orbitals of the nucleophilic atom and the α atom. This decreases the $HOMO_{Nu}$-$LUMO_E$ gap, making orbital overlap more energetically favourable.

For α-effect nucleophiles, therefore, the decrease in nucleophile-substrate repulsion, combined with decreased $HOMO_{Nu}$-$LUMO_E$ gap, leads to increased reactivity, but only if the change in HOMO-LUMO gap compensates for the decreased spatial overlap.

Nu:⁻	ε $HOMO_{Nu:-}$ (eV)	⟨$HOMO_{Nu:-}$	$LUMO_{C_2H_5Cl}$⟩
HO⁻	3.0	0.12
HOO⁻	3.5	0.10
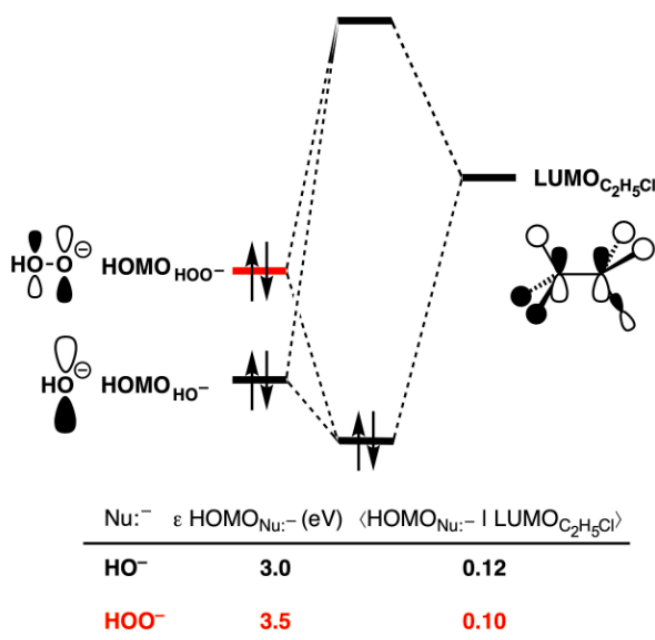
Figure 1.32 Computed molecular orbital diagram of the critical nucleophile-electrophile interaction between the $HOMO_{Nu}$ and $LUMO_E$ for the S_N2 reaction between chloroethane and both hydroperoxide (an α-effect nucleophile, in red) and hydroxide (a normal nucleophile, in black). The HOMO of hydroperoxide is calculated to be closer in energy to the LUMO of chloroethane. Figure reproduced unmodified from Hansen et al.[115]

The deviation from linearity comes from the fact that the basicity of a compound doesn't depend on electrostatic repulsion between the nucleophile and proton, as a proton contains no electrons.

Gundersen *et al.* observed hydroxylamine to be an extremely active MTG substrate, and the α-effect could offer an explanation for this.[76] They attempted to exploit this high reactivity to produce more complex but still highly active amine donor substrates. They reported data on a single example, *O*-benzylhydroxylamine, but it showed only 3% conversion.[76] The authors proposed that this was as a result of increased steric bulk compared to hydroxylamine.

We therefore attempted to exploit the α-effect to produce more active amine donors using a derivative that is structurally closer to the natural substrate, lysine (**43**). We therefore set out to synthesise the alkoxyamine (**46**).
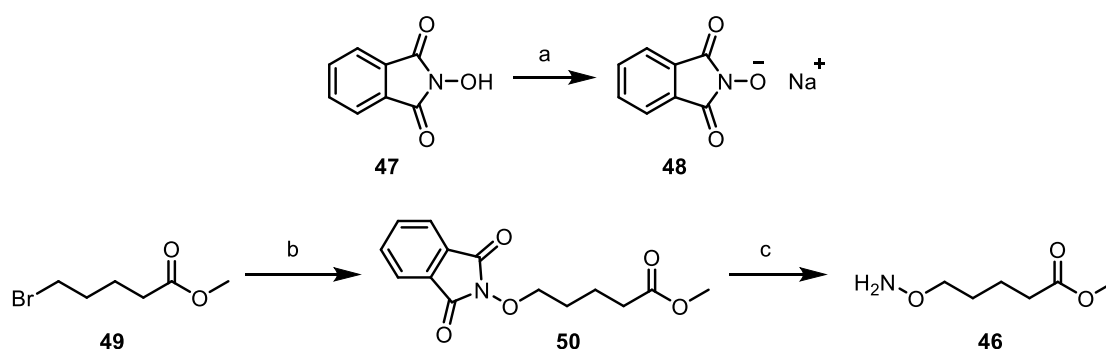
*Figure 1.33 Synthetic route to alkoxyamino **46**. a: Na(s) (1.0 eq), EtOH, 0 ℃ to RT, 82%. b: **48** (1.0 eq), NEt₃ (2.0 eq), MeCN, reflux, 3.0 h, 74%. c: N₂H₄.H₂O (2.0 eq), EtOH, RT, o/n, 26%.*

The sodium salt of *N*-hydroxyphthalimide, **48**, was prepared using sodium metal. **48** Was then used to displace the bromide in 5-bromo-methylvalerate (**49**), generating the phthalimido compound **50**. Standard phthalimide deprotection conditions, hydrazine hydrate in ethanol, were used to remove the phthalimide group and generate alkoxyamino ester **46**, along with the phthalhydrazide by-product (**51**).
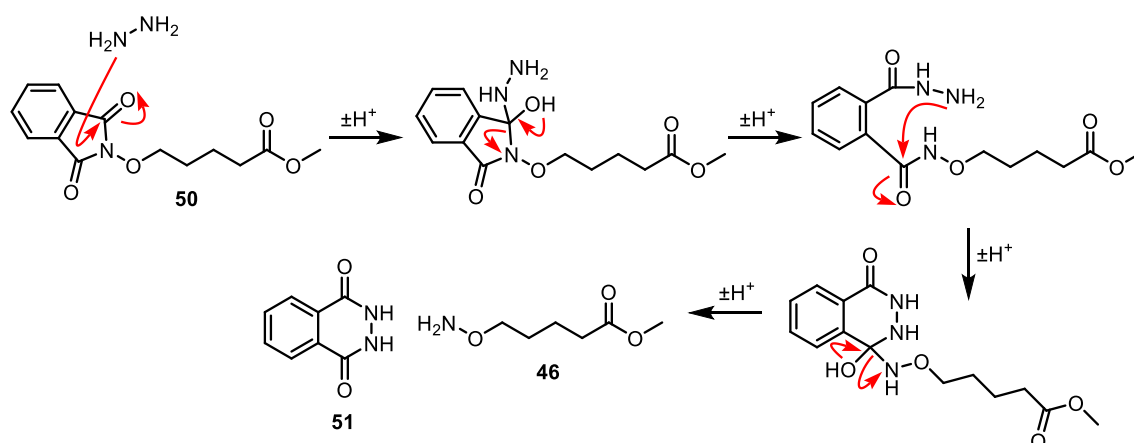
Figure 1.34 Mechanism of phthalimide deprotection with hydrazine.

When subjected to our MTG substrate assay, alkoxyamino ester **46** only showed a 6.7% conversion (table 1.4). Although the terminal NH_2 may be more nucleophilic than the all-carbon analogue, the basicity of **46** will be less because of the electron withdrawing effect of the oxygen. This means the pK_a will be lower, and at a given pH less of **46** will exist in the protonated state.

Given the high reactivity of hydroxylamine reported in the literature, we hypothesise that this loss of activity is not driven by unfavourable interactions between the polar oxygen and the active site. It instead may result from reduced electrostatic attraction to the negative active site, and consequently lower rates of formation of enzyme-amine donor complex, consistent with MTG preferentially binding the ionised amine before accepting a proton to revel the nucleophilic form. Overall therefore, it seems the decrease in pK_a of **46** compared to 6-aminocaproic acid (**37**) significantly outweighs any benefit from increasing the nucleophilicity of the terminal NH_2.
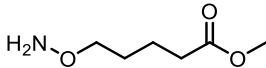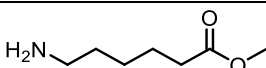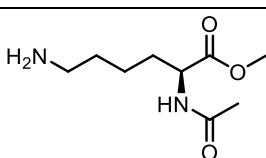
Compound	Structure	Conversion/%	SD
46		6.7	1.5
38		49	2.7
28		48	3.1

*Table 1.4 Conversion of alkoxyamino ester **46** and comparable substrates.*

1.7.5   Aromatic ring-containing amines

Following these results we sought to expand on the limited aromatic substrate scope that exists in the literature. We began by testing benzylamine (**10**) under our conditions, which had a conversion of 63%, moderately more than the benchmark doubly protected lysine (**28**) at 48%. We systematically examined substitution at the 2, 3, and 4 positions of the ring, by testing all the isomers of methoxybenzylamine (**52**, **53**, and **54**). All of the substituted rings showed lower conversions, with the 2 substituted ring giving the lowest conversion of 13%. 3-Picolylamine (**55**) was also tested, to examine whether a heterocycle would behave differently to a carbocycle. Picolylamine had a conversion of 63%, the same as benzylamine, showing that replacement of a carbon with a nitrogen at the 3 position in benzylamine doesn't lead to an overall change in conversion.

Three five-membered aromatic heterocycles were also tested, a class of substrates that has not been examined in the literature. 2-Aminomethyl furan (**56**) showed excellent reactivity, resulting in a conversion of 100% under these conditions. 2-Aminomethyl thiophene (**57**) performed slightly worse, at 72% conversion, and 5-aminomethyl-1,3-oxazole (**58**) showed poor reactivity with a conversion of only 7.5%.

The explanation for the trends observed for these aromatic substrates is not immediately obvious. Hydrogen bond acceptor potential decreases in the order pyridine, oxazole, furan.[116] As this does not match the trend in observed conversions, it seems that hydrogen bond acceptor potential is not the dominant effect behind

these results. Considering the electron density of the rings, both electron poor rings (oxazole **58**) and electron rich rings (all isomers of methoxybenzylamine) show poor conversions. This suggests that electron density in the ring is also not a dominant effect.

The observed conversions could be determined by a combination of factors, including hydrogen bonding potential, electron density, lipophilicity, and sterics. The fact that a significant single point change from benzylamine (**10**) to 3-picolylamine (**55**) has no effect on conversion supports the idea that there are multiple properties determining conversions, some of which may be working against one another.
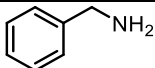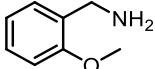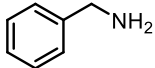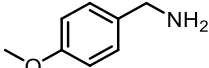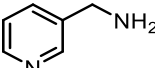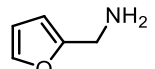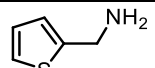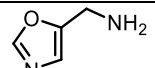
Compound	Structure	Conversion/%	SD
10		63	3.0
52		13	1.4
53		35	1.7
54		30	0.4
55		63	1.7
56		100	0.0
57		72	2.0
58		7.5	0.84

Table 1.5 Conversions of aromatic ring-containing amines.
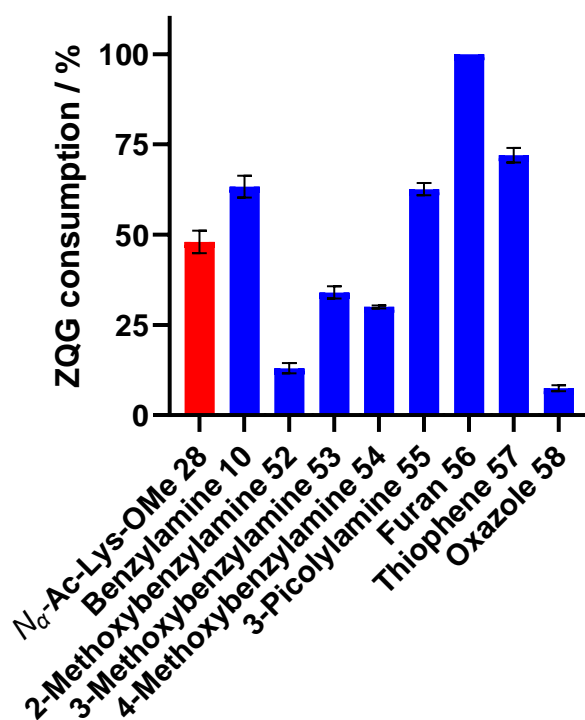
*Figure 1.35 Graph of conversions of aromatic ring-containing amines. The benchmark compound, **28**, is shown in red.*

1.7.6 Furan upgrade strategy

The excellent conversion of 2-aminomethyl furan (**56**) led us to investigate using it as the basis for another upgrade strategy, outlined in figure 1.34. To this end we aimed to synthesis the 2,5-difunctionalised furan **59**, that would allow us to examine whether additional substituents on the furan ring were tolerated.
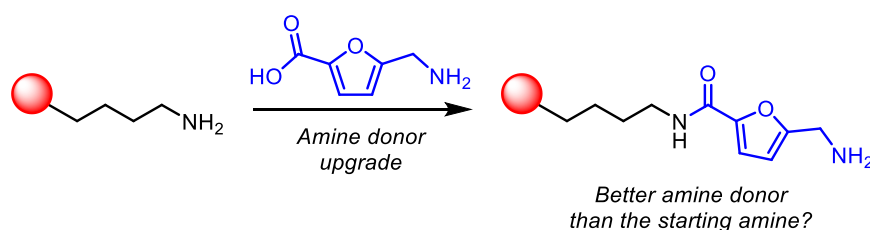
*Figure 1.36 Schematic of the furan upgrade strategy to generate amine donors that exploit the high conversions seen with **56**. Payload represented as red circle.*

In order to prepare this substrate 5-(hydroxymethyl)furan-2-carboxylic acid (**60**) was methylated using methyl iodide and potassium carbonate to form methyl ester **61**. The

alcohol was then converted to the mesylate with mesyl chloride, producing mesylate **62**, which was subsequently displaced with sodium azide to form azide **63**. A Staudinger reduction using triphenylphosphine and water in THF reduced the azide to the amine, affording **59**. The mass of **59** was clearly seen during reaction monitoring by LCMS, but the compound unfortunately appeared to decompose under ambient conditions during purification, preventing full characterisation and testing.
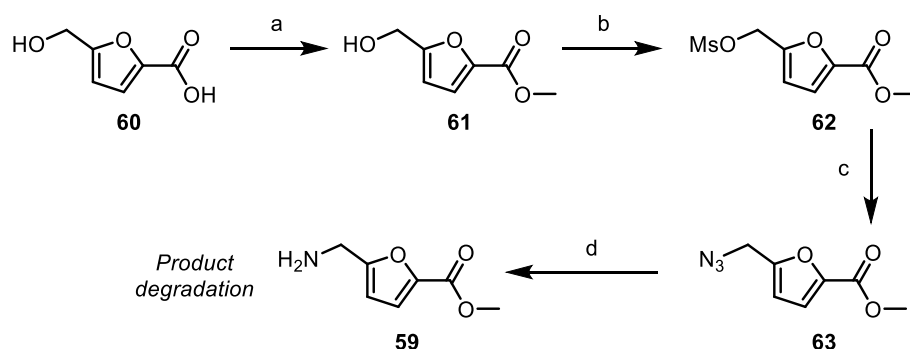
*Figure 1.37 Synthetic route to amino furan **59**. a: K_2CO_3 (5.0 eq), MeI (5.0 eq), DMF, RT, 3.5 h, 72%. b: MsCl (1.5 eq), NEt_3 (3.0 eq), DCM, RT, 2.0 h. c: NaN_3 (3.0 eq), KI (0.25 eq), DMF, 60 °C, o/n, 45% over two steps. d: PPh_3 (6.0 eq), H_2O (6.0 eq), THF, reflux.*
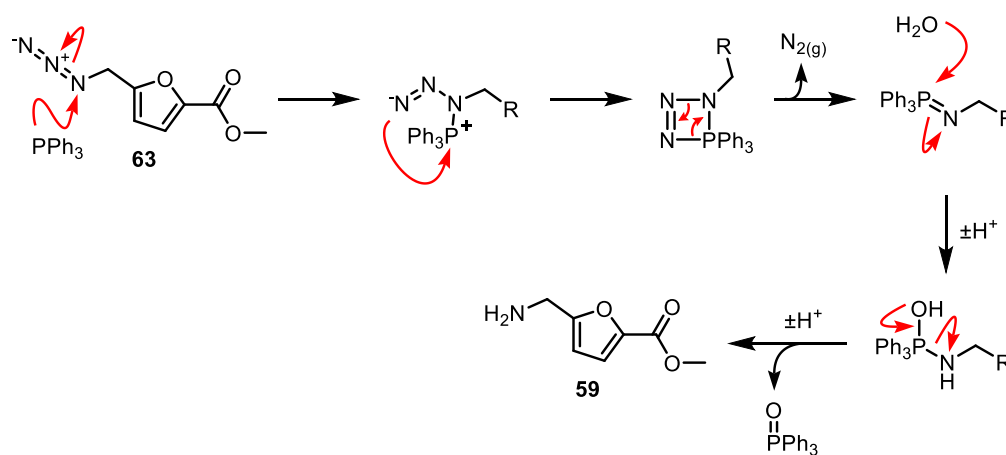
Figure 1.38 Mechanism of the Staudinger reduction.

A possible degradation pathway is a dimerisation or oligomerisation that occurs through attack of the NH_2 in **59** on the methyl ester, forming an amide.

We then aimed to make amide **64** in the hope that the lower electrophilicity of the amide would suppress this mode of degradation and allow compound **64** to be isolated

successfully. 5-(Hydroxymethyl)furan-2-carboxylic acid (**60**) was coupled with *n*-propylamine using HATU to generate **65**. Alcohol **65** was mesylated using standard conditions, but the product **66** quickly decomposed in the reaction mixture.
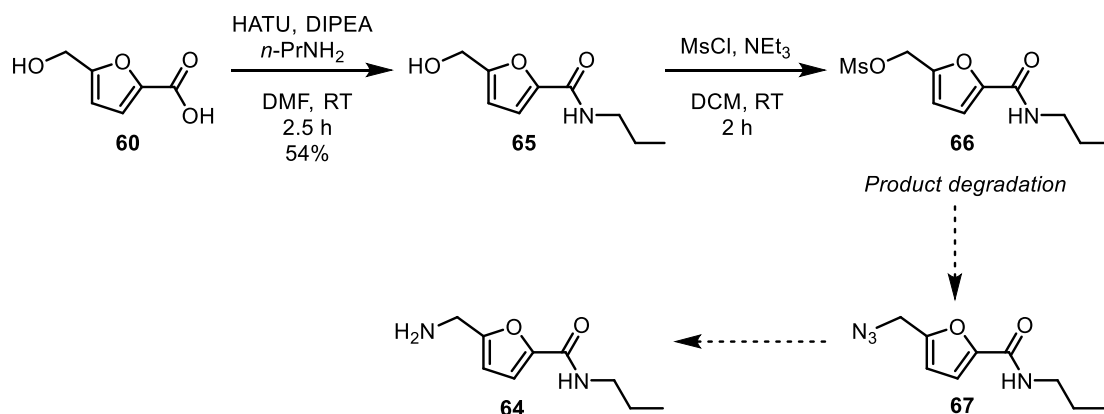
*Figure 1.39 Attempted synthetic route to amino amide **64**.*

Owing to the consistent instability observed with these 2,5-difunctionalised furans this avenue of investigation was ultimately abandoned.

1.7.7 Miscellaneous other substrates

Some miscellaneous amine donors were also tested. The PEG-amine **68** is particularly interesting, as this moiety is commonly used as a conjugation handle during the synthesis of ADCs and other bioconjugates. It shows a conversion of 53%, slightly better than the doubly protected lysine benchmark of 48%. Although this is a reasonable conversion, and will lead to an acceptable extent of conjugation over a reasonable reaction time, it's clear that MTG will show little preference between a surface lysine residue and a PEG-amine functionalised payload.

Cysteamine, **69**, is known to be an extremely active substrate for tissue transglutaminase.[117] With our conditions and MTG, however, no conversion was observed. This highlights the differences between enzymes of the same family and that substrate tolerance doesn't necessarily track across enzymes.

1-Boc-3-aminomethyl azetidine (**70**) was selected as it represents a previously unexplored structural motif, and showed a reasonable conversion of 30%. Finally the methyl ester of alanine (**71**) was tested, to confirm that alpha-branched amines were

ineffective substrates for MTG. Although some reaction was observed the conversion was only 4.7%, confirming previous reports that alpha-branched amines are not well tolerated by MTG.[76]
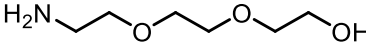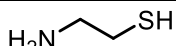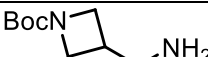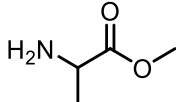
Compound	Structure	Conversion/%	SD
68	H₂N~~O~~O~~OH	53	0.3
69	H₂N~~SH	0.0	17
70	BocN (azetidine) ~NH₂	30	5.5
71	H₂N~~C(=O)O~ (alanine methyl ester)	4.7	3.2

Table 1.6 Conversions of miscellaneous substrates.

1.7.8 Alkyne-containing amine donors

Propargylamine is reported to be an extremely active amine donor substrate for MTG.[76] This could be because it is small, and has little conformational freedom in solution so has a relatively favourable entropy of binding. In addition to this effect there may also be a favourable interaction between the alkyne and residues in the active site that, if a general phenomenon, could enable the synthesis of highly active alkyne-containing amine donors.

We probed the role of the alkyne in propargylamine (**18**) by testing it alongside its partially (allyl amine, **72**) and fully (*n*-propylamine, **73**) reduced analogues. This revealed that propargylamine (**18**) was also an extremely reactive substrate in our hands, showing full conversion. Allyl amine (**72**) had a decreased conversion of 69%, and *n*-propylamine (**73**) even lower at 47%. This shows the high activity of propargylamine is not simply down to its small size, but doesn't clearly delineate the relative impact of entropic or enthalpic changes on the interaction with MTG.

Compound	Structure	Conversion/%	SD
18	H_2N⟶≡	100	0.0
72	H_2N	69	1.1
73	H_2N	47	2.4
74	H_2N	97	4.2
75	H_2N	92	11
76	H_2N	46	0.6
77	H_2N	58	2.4

Table 1.7 Conversions of initial alkyne-containing substrates.
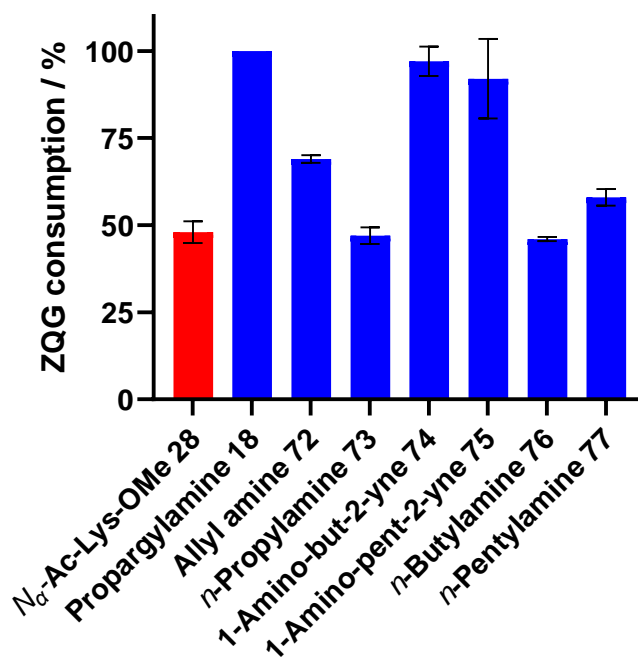
Figure 1.40 Graph of conversions of initial alkyne-containing substrates.

Given the high activity of propargylamine, we investigated the one and two carbon homologated alkynes, **74** and **75** (synthesised according to figure 1.39) to understand whether alkyne substitution could be tolerated by MTG and still give a good conversion. This was indeed the case, with **74** showing a conversion of 97% and **75** a conversion of 92%. Testing commercially available saturated versions of these

compounds, **76** and **77**, confirmed that the C-C triple bonds were responsible for the high activity, as the reduced compounds showed decreased conversions.

78 R = Me
79 R = Et

80 R = Me
81 R = Et

74 R = Me
75 R = Et
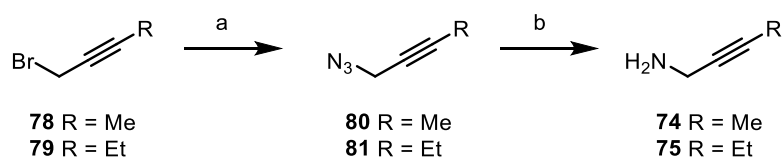
*Figure 1.41 Synthetic route to homologated alkynes **74** and **75**. a: NaN₃ (5.0 eq), DMF, RT, 24 h. b: PPh₃ (2.0 eq), Et₂O, RT, o/n, R = Me (**74**) 37%, R = Et (**75**) 34%.*

Encouraged by the still high conversion of the substituted alkynes **74** and **75**, we began to investigate the possibility of an alkyne upgrade strategy, as outlined in figure 1.40.

Amine donor upgrade

Better amine donor than the starting amine?
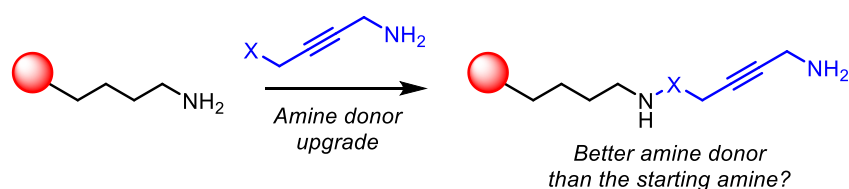
Figure 1.42 Schematic illustrating the concept of using a propargylamine-based molecule to upgrade an amine donor. A payload is represented as a red circle, and an appropriate linking group as X.

We began by synthesising the propargyl alcohol **82**, which would provide a starting point from which we could attempt to incorporate this into payloads in a variety of ways (figure 1.41). The synthetic route involves mono-tosylation of the diol **83** to produce tosylate **84**, and then displacement of the tosyl group with ammonium hydroxide. The amine product was immediately Boc protected, allowing facile purification to produce **82**. With **82** in hand, we could begin to explore ways of reacting it to allow its incorporation into payloads.

83

84

82
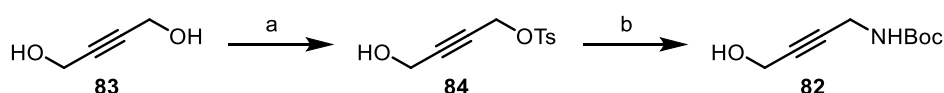
*Figure 1.43 Synthetic route to alcohol **82**. a: TsCl (1.0 eq), Ag₂O (1.5 eq), KI (0.10 eq), DCM, RT, o/n, 44%. b: (i) NH₄OH (as solvent), RT, 1 h (ii) Boc₂O (1.2 eq), NEt₃ (1.2 eq), THF, 0 ℃ to RT, o/n, 57% over two steps.*

We first attempted to oxidise **82** to the acid **83**, which would allow a simple amide coupling to attach the alkyne unit to an amine-functionalised payload (figure 1.42). Literature precedent exists for the direct conversion of primary alcohols to carboxylic acids using sodium chlorite ($NaClO_2$), catalysed by (2,2,6,6-tetramethylpiperidin-1-yl)oxidanyl (TEMPO) and bleach (NaOCl).[118] The scope of this method also included 3-phenylpropargyl alcohol, which is structurally similar to our substrate. However, although a trace of the product mass could be observed by LCMS under these conditions, the starting alcohol **82** remained largely unchanged. NaOCl is known to oxidise double bonds and electron rich aromatic rings, so it's possible that the triple bond in **82** also underwent oxidation. This could potentially quench the small amount of NaOCl that is continuously regenerated throughout the reaction (figure 1.42), thereby breaking the catalytic cycle without causing significant degradation.
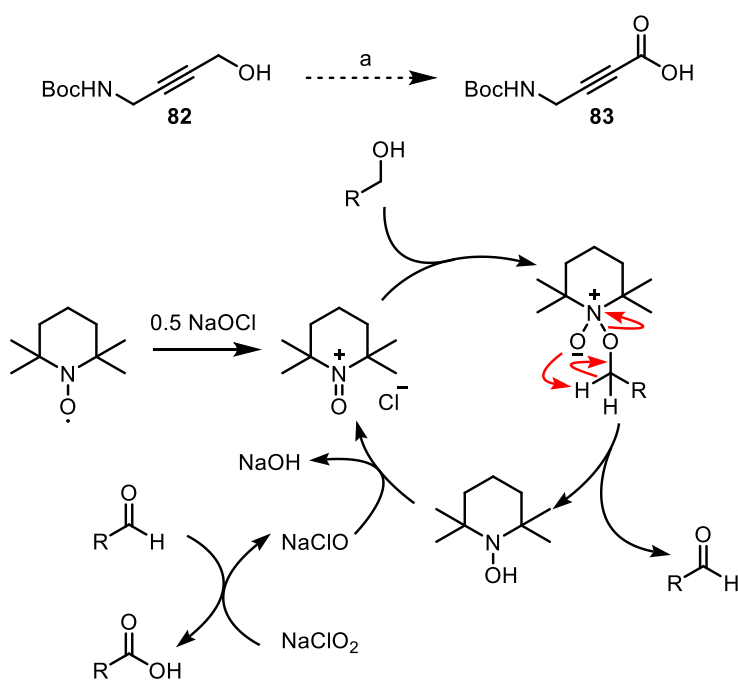
*Figure 1.44 Above: Attempted synthetic route to acid **83**. a: NaOCl₂ (2.0 eq), NaClO (~0.02 eq), TEMPO (0.07 eq), sodium phosphate buffer, MeCN, RT to 35 ℃, o/n. Below: Mechanism of TEMPO and bleach catalysed oxidation of primary alcohols to acids.*

A literature search yielded a method to produce 4-aminotetrolic acid, **84**, by treating imine **85** with ethyl Grignard followed by carbon dioxide, then working the reaction up under acidic conditions to hydrolyse the imine and reveal the desired product (figure

1.43). This method could conceivably be modified to add the deprotonated imine-protected alkyne to a number of electrophiles, allowing access to a range of propargylamine derivatives. Unfortunately in our hands the formation of imine **85** was not observed, despite trying multiple imine formation conditions.[119,120] It's possible that the reactions could not be made sufficiently anhydrous without a Schlenk line.
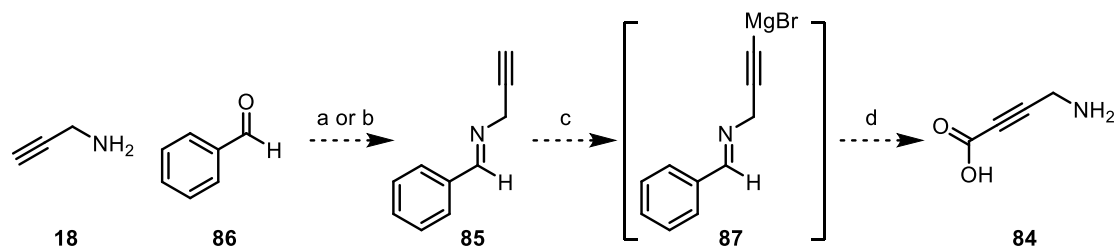
*Figure 1.45 Attempted synthetic route to 4-aminotetrolic acid **84**. a: 4 Å molecular sieves, DCM, RT, 24 h. b: AcOH (0.10 eq), MeOH, RT, 24 h. c: EtMgBr. d: CO_2, acidic workup.*

Returning to propargyl alcohol **82**, we prepared the mesylate **88** and tried to access derivatised compounds by nucleophilic displacement. Initially mesylate **88** was subjected to NH_4OH, under the same conditions used in the synthesis of **82** itself (figure 1.41). This produced a complex mixture of reaction products in which the mass of protected diamine **89** was observable but appeared to be a minor component by LCMS mass trace.

Displacement of mesylate **88** was also attempted with two oxygen-based nucleophiles, benzyl alcohol and methyl-3-hydroxypropanoate (figure 1.44). With benzyl alcohol the mesylate was consumed, but many products were formed, including material that stuck to the baseline of a TLC plate. This is perhaps due to decomposition of the alkyne when subjected to the basic conditions necessary to generate an alkoxide. Reaction with methyl-3-hydroxypropanoate also led to failure, with the whole reaction mixture sticking to TLC baseline. Presumably this is a combination of alkyne decomposition, and methyl-3-hydroxypropanoate oligomerising with itself once deprotonated.
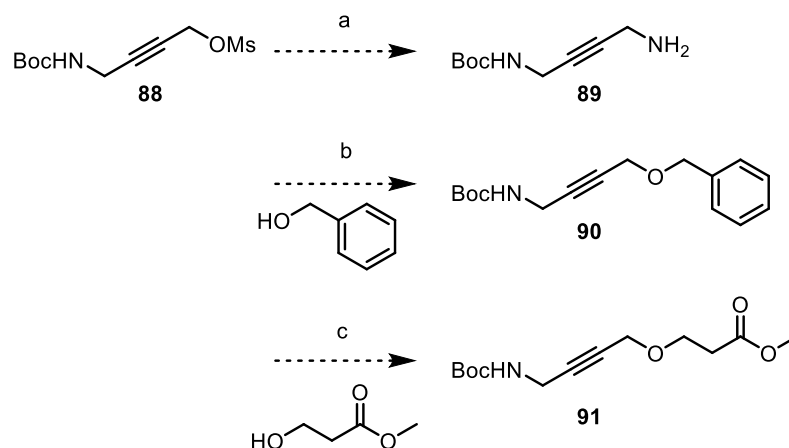
*Figure 1.46 Attempts to displace mesylate **88** to produce extended alkyne products. a: NH₄OH, RT, 2 h. b: benzyl alcohol (2.0 eq), tBuOK (1 M in THF, 2.0 eq), THF, 0 ℃ to RT, 2 h. c: methyl-3-hydroxypropanoate (2.0 eq), tBuOK (1 M in THF, 2.0 eq), THF, 0 ℃ to RT, 1 h.*

Commonly terminal alkynes are deprotonated and used to attack electrophiles, owing to their reasonably low pK_a values (ethyne has a pK_a of 25). In order to investigate this method to synthesise functionalised propargylamines, it was first necessary to protect the amine as it would also react with any electrophile added. The choice of protecting group must also be able to survive the strong basic conditions needed to deprotonate the terminal alkyne, which is typically achieved using *n*-BuLi, and not contain any acidic protons (for example, carbamate protons).

To this end three protected propargylamines were selected for synthesis: phthalimide **92**, di-Boc protected **93**, and di-TMS protected **94** (figure 1.45). **92** was synthesised by refluxing propargylamine (**18**) with phthalic anhydride in acetic acid, and **93** was synthesised by reacting propargylamine (**18**) with an excess of Boc₂O, in the presence of DMAP. An attempt to synthesise **94** was made using TMSCl and NEt₃, but this led to an extremely complicated reaction mixture including lots of baseline material. This may have been due to the reaction being insufficiently anhydrous, and the moisture sensitivity of silylamines.[121]

Attempts to deprotonate phthalimide **92** using NaH led to significant amounts of the hydrolysis product **95** being produced, presumably on account of NaOH in the NaH or water in the reaction. To rule out the possibility of NaOH from the NaH, *n*-BuLi and LiHMDS were also tested as they are likely to be dryer. Use of these bases led to

complicated reaction mixtures though, possibly because of phthalimide instability in strongly basic conditions. Additionally, phthalimides are unstable towards strongly nucleophilic entities such as organometallic reagents, so decomposition may have also occurred through reaction between the metallo-alkyne formed and the phthalimide group.[122]

Di-boc protected **93** was subjected to LDA and then benzyl bromide in an attempt to test the synthetic route with an electrophile containing a chromophore, making the reaction analysis easier. The product mass was not detected by LCMS, although a new UV peak was formed. Attempts to isolate and characterise this compound, however, were unsuccessful. This could be because the UV peak corresponded to something that had a very high UV absorbance but was produced in only trace amounts.
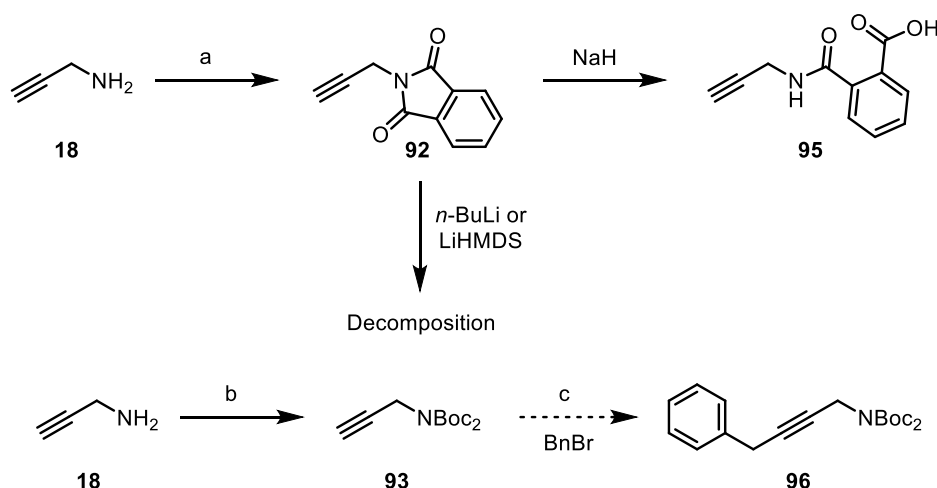
Figure 1.47 Attempts to protect propargylamine and functionalise through deprotonation of the terminal alkyne. a: phthalic anhydride (1.0 eq), AcOH (as solvent), reflux, 5.0 h, 29%. b: Boc$_2$O (2.5 eq), DMAP (1.0 eq), MeCN, RT, o/n, 72%. c: (i) LDA (made in situ, 1.5 eq), THF, -78 ℃ to RT, 1.0 h (ii) BnBr (1.5 eq), NaI (0.5 eq), THF, -78 ℃ to RT, o/n.

Ultimately rearranging the reaction sequence to avoid the requirement for double amine protection reliably allowed us to synthesise functionalised propargylamines (figure 1.46). This relies on having the functionalised side of the alkyne already installed, and then substituting the alkyne to install the CH$_2$NH$_2$ group.

Initially 4-phenyl-1-butyne (**97**) was treated with *n*-BuLi, then formaldehyde was added, both at -78 ℃. Slowly warming to room temperature produced propargyl

alcohol **98**. Standard mesylation conditions afforded mesylate **99**, which was then treated with NH_4OH to give propargylamine **100**. In order to produce a matched alkyl pair, **100** was hydrogenated to produce 5-phenylpentan-1-amine (**101**).

Gratifyingly, propargylamine **100** showed full conversion in the MTG substrate assay, compared to its reduced analogue **101** which showed only 33% conversion. This clearly shows such alkyne-containing amine substrates possess increased reactivity, even when substituted with more complex groups than methyl and ethyl.
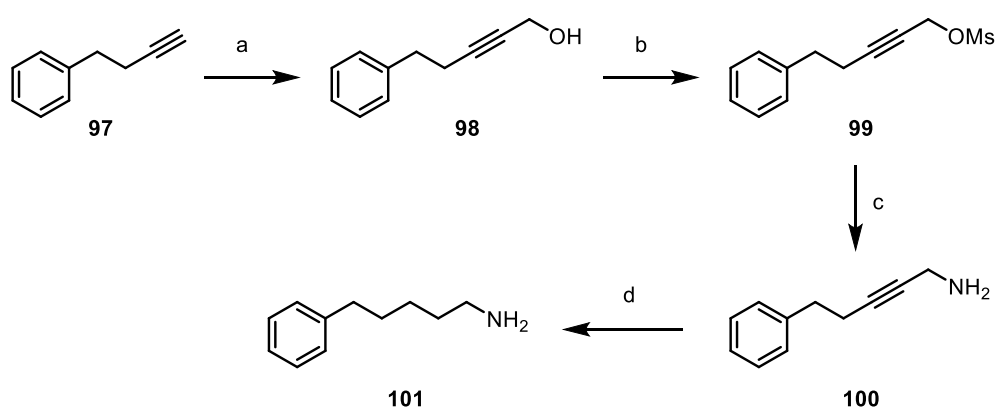
*Figure 1.48 Successful synthetic route to produce **100**, a functionalised propargylamine. a: (i) n-BuLi (1.5 eq), THF, -78 ℃, 2.0 h (ii) (CH₂O)ₙ (1.2 eq), THF, -78 ℃ to RT, o/n, 46%. b: MsCl (3.0 eq), DMAP (0.25 eq), NEt₃ (4.0 eq), DCM, 0 ℃ to RT, o/n. c: NH₄OH, MeOH, RT, 3.0 h, 19% over two steps. d: H₂₍g₎, Pd/C, MeOH, RT, o/n, 51%.*

Compound	Structure	Conversion/%	SD
100		100	0.0
101		33	2.7

*Table 1.8 Conversions of unnatural alkyne-containing amine substrate **100**, and its reduced analogue **101**.*

We then set out to use this route to create compounds with a reactive handle to allow attachment to a payload. Starting with pent-4-yne-1-ol (**102**), the alcohol was protected with a TBDPS group to produce terminal alkyne **103**. **103** was then treated with *n*-BuLi, followed by paraformaldehyde to generate propargyl alcohol **104**. Mesylation gave **105**, followed by displacement with ammonia gave **106**. To release

the alcohol for functionalisation, **106** was deprotected with TBAF. An unforeseen difficulty was that the tetrabutylammonium hydroxide by-product was challenging to separate from the desired amino alcohol **107**. To overcome this, **107** was Boc protected to allow for easy purification through flash column chromatography, affording Boc-protected **108** that was also later used to produce an alkyne-containing substrate with a model payload.

We also wanted to test the parent compound, free amino alcohol **107** (figure 1.47). To this end **108** was treated with TFA in DCM to remove the Boc group. The product was then purified by strong cation exchange (SCX) column to freebase the compound. Puzzlingly this resulted in a mixture of desired product **107**, and amide **109**. This conclusion is based on the following experimental evidence:

- The mass of amide **109** was observed in the LCMS analysis of the reaction mixture.
- ^{1}H NMR analysis showed a proton signal at 4.02 ppm, plausibly corresponding to the α-protons of the amide (compared to a chemical shift of 3.35 ppm for the protons α to the amine in **107**).
- ^{13}C NMR analysis revealed a peak at 157 ppm, plausibly corresponding to the amide carbonyl carbon. Additionally this carbon signal coupled to the assumed α-protons by HMBC.
- A second SCX purification afforded amino alcohol **107** as a pure sample, demonstrating that the by-product didn't contain a free amine, confirming it was the amide rather than the corresponding ester formed on the alcohol.
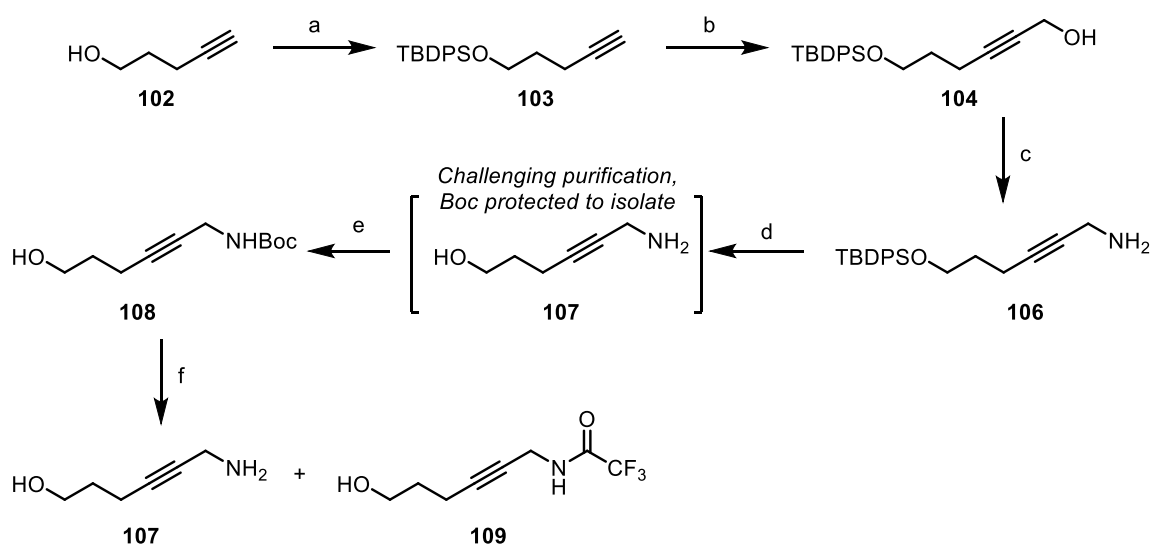
*Figure 1.49 Synthetic route to amino alcohol **107**. An unexpected by-product from the Boc deprotection was observed. a: TBDPSCl (1.1 eq), imidazole (1.3 eq), DCM, 0 ℃ to RT, 2.5 h, 99%. b: (i) n-BuLi (1.1 eq), THF, -78 ℃, 2.0 h (ii) (CH$_2$O)$_n$ (1.2 eq), THF, -78 ℃ to RT, o/n, 46%. c: (i) MsCl (3.0 eq), DMAP (0.25 eq), NEt$_3$ (4.0 eq), DCM, 0 ℃ to RT, 30 min (ii) NH$_4$OH, MeOH:THF 1:1, RT, o/n, 32% over two steps. d: TBAF (2.0 eq), THF, RT, o/n. e: Boc$_2$O (2.0 eq), DCM, RT, 3.5 h, 31% over two steps. f: 10% TFA in DCM, RT, 1.0 h.*

We hypothesise that this occurred as follows: during the TFA deprotection of **108** the desired product was formed, with the amine in a protonated state. Under these acidic conditions some of the alcohol reacted with TFA to form the TFA ester **110** (classical acid catalysed ester formation from an alcohol and carboxylic acid). The reaction mixture was then purified through an SCX column, which removed species that didn't contain a free amine. The left a mixture of desired product **107** and TFA ester **110**. Crucially the SCX column had now desalted the mixture and the amines had been deprotonated, revealing their nucleophilic nature. An acyl transfer reaction then occurred, forming the more stable TFA amide **109**. This acyl transfer could either happen intermolecularly or intramolecularly, as nine membered transition state should be large enough to accommodate the alkyne. This proposed sequence of reactions is outlined in figure 1.48.
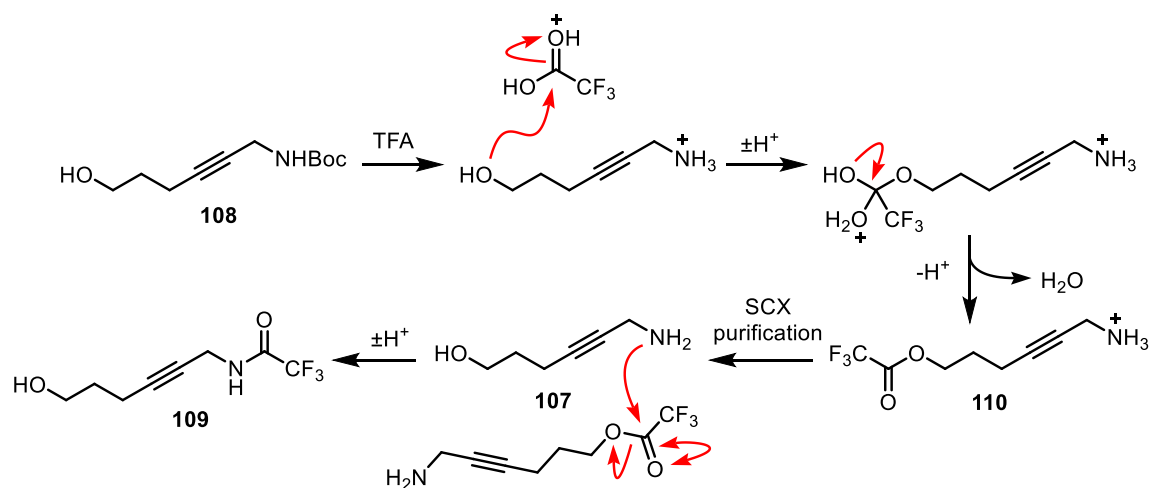
*Figure 1.50 Proposed mechanism of formation for amide by-product **109**. The attack of the amine on the ester could happen either intramolecularly or intermolecularly. Only the intermolecular mode is shown for clarity.*

Deprotection of a Boc group in the presence of an alcohol does not usually result in the formation of amides like these. This specific substrate must be predisposed to this reactivity pathway. Nonetheless, a second SCX purification removed the amide **109** and afforded the desired amino alcohol **107**.

When subjected to our MTG substrate activity assay, **107** only showed a conversion of 72% (table 1.9). We then synthesised compound **111**, which consists of the parent compound **107** attached to a model payload.

108 was mesylated to give **112**, and then displaced with 2-(2-(2-(2-azidoethoxy)ethoxy)ethoxy)ethan-1-amine. To aid purification, the reaction mixture was then subject to Boc protection conditions to afford a mixture of **113** and Boc-protected 2-(2-(2-(2-azidoethoxy)ethoxy)ethoxy)ethan-1-amine. Column chromatography allowed easy isolation of double-Boc protected **113**, which was deprotected without incident to afford **111**.

When subjected to our MTG substrate activity assay, **111** showed an even lower conversion of 42% (table 1.9).

Compound	Structure	Conversion/%	SD
107	HO⟍⟍⟍≡⟍NH$_2$	72	3.0
111	N$_3$⟍⟍O(⟍⟍O)$_2$⟍N(H)⟍⟍⟍≡⟍NH$_2$	42	1.8

*Table 1.9 Conversions of propargylamines **107** and **111**.*
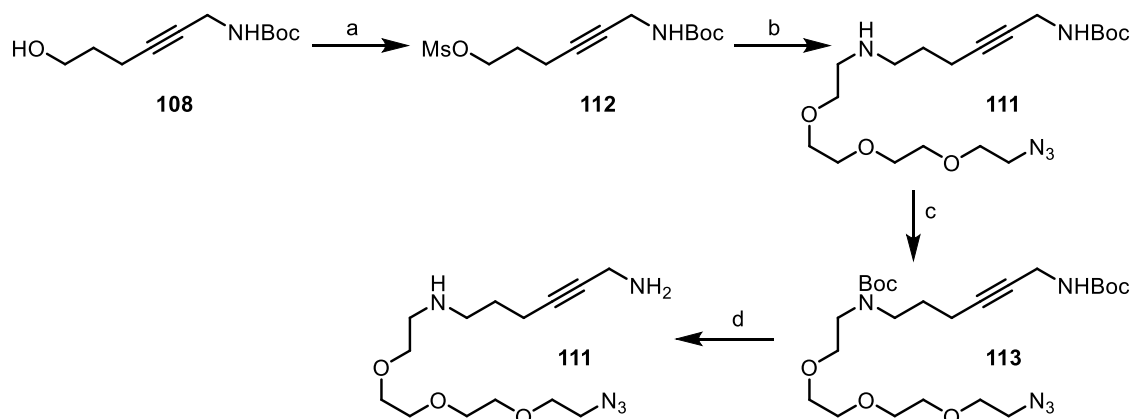
*Figure 1.51 Synthetic route to model payload-containing propargylamine **111**. a: MsCl (2.0 eq), NEt$_3$ (3.0 eq), DCM, 0 °C to RT, 30 min. b: 2-(2-(2-(2-azidoethoxy)ethoxy)ethoxy)ethan-1-amine (5.0 eq), KI (0.25 eq), THF, 80 °C, o/n. c: Boc$_2$O (6.0 eq), THF, RT, 19% over two steps. d: 10% TFA in DCM, RT, 2.0 h, 94%.*

These middling conversions are clearly significantly worse than the phenyl-containing test compound **100**. There are a number of factors that could contribute to this drop-off:

- A hydrogen bond donor at that position on the left-hand side of the alkyne may lead to unfavourable interactions in the MTG active site.

- The increase in polarity caused by either the free alcohol in **107** or the secondary amine and PEG chain in **111** could be interacting unfavourably with the large number of aromatic and lipophilic residues around the MTG active site.

- Sterics are unlikely to contribute to this decrease in activity; the PEG chain in **111** is flexible, and therefore able to adopt a number of conformations, allowing it to avoid the worst of any steric repulsion. Also, when compared to

101

the phenyl group in **100**, this PEG chain likely represents a decrease in steric bulk.

- Adding a long, flexible chain to the substrate may have increased the conformational freedom to such an extent that the entropy of binding as become a significant factor in how well this substrate binds to the MTG active site, although this does not appear to negatively impact the reactivity of PEG-amine **68**.

In terms of number of atoms, the secondary amine in **111** is approximately the same distance from the reactive NH_2 as the α-NH_2 in lysine is from the reactive NH_2 in lysine (6 and 5 atoms, respectively), yet the α-NH_2 in lysine appears to promote reactivity (section 1.7.2), an effect we hypothesise is because the substrate can exist in a more positively charged state, leading to increase attraction for the negative MTG active site. A caveat here is that even though the distances are similar in terms of number of atoms, the triple bond in **111** will change the geometry of the molecule and alter where in space the internal amine can sit.

This may lead one to conclude that it is therefore the PEG chain in **111** that is contributing to its poor reactivity, possibly because of poor interactions with the lipophilic MTG active site. But substrate **68**, a PEG chain with a terminal amine, has a conversion of 53%, showing that a more polar PEG-based substrate (it lacks the lipophilic alkyne-alkyl portion) still shows a higher conversion.

Perhaps it's not that substrates **107** and **111** are bad; after all **107** has a higher conversion than the doubly protected lysine benchmark (48%), and **111** only has a 6% worse conversion than this. Perhaps **100** is just *particularly* active, possibly because its phenyl ring is correctly placed to engage in effective π interactions with aromatic active site residues. Even if this holds true, **111** seems to be underperforming. It contains a propargylamine, and an amine 6 carbons away from the reactive NH_2. Both of these structural features have led to high conversions in other substrates.

Compound	Structure	Conversion/%	SD
107	HO—alkyne—NH$_2$	72	3.0
11	N$_3$—O(—O)$_2$—N(H)—alkyne—NH$_2$	42	1.8
43	HO(O=)C—CH(NH$_2$)—NH$_2$	60	2.5
68	HO—O—O—NH$_2$	53	0.3
100	Ph—alkyne—NH$_2$	100	0.0

*Table 1.10 Conversions of substrates compared to amino alcohol **107** and PEG-containing **111**.*
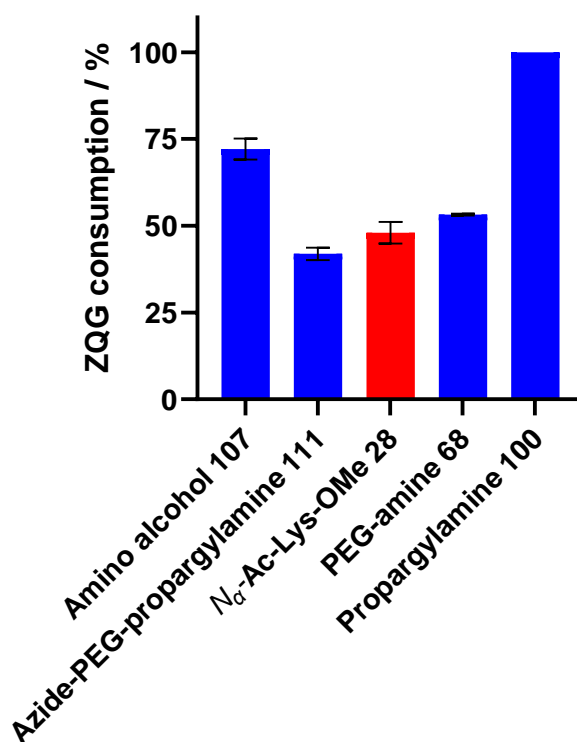
Figure 1.52 Graph comparing conversions of extended alkyne substrates and related compounds.

1.7.9 Reversibility of the system

If we engineer an MTG amine substrate to be more active than the natural substrate, it may follow that the amide product of the MTG-catalysed reaction is also better accepted by MTG, and may consequently experience higher rates of hydrolysis or even amine exchange. This can be thought of in terms of substrate-enzyme interactions: if we install groups on the amine substrate that have favourable interactions with the active site, MTG more readily accepts this substrate. These promoting groups will also exist in the amide product, though, and may also promote the MTG-mediated reverse reaction by making the product a better MTG substrate.

This reasoning can also be illustrated on a reaction energy profile, as shown below (figure 1.51). Consider the left-hand side of the figure, which represents the reaction for a normal, moderately active amine substrate such as doubly protected lysine **28**. An initial energy barrier is overcome to arrive at intermediate 1 (**Int1**) which is the thioester intermediate formed by attack of MTG Cys64 on the glutamine residue in the acyl donor substrate. A second energy barrier must then be overcome (ΔE_1) which corresponds to the amine donor attacking **Int1**, which results in the product forming (**Prod1**). If the reaction then proceeds in reverse, Cys64 of MTG must attack **Prod1** to regenerate **Int1**. This is associated with an energy barrier, ΔE_2. **Int1** can then either undergo hydrolysis, or reform **Prod1** through attack of another amine molecule.
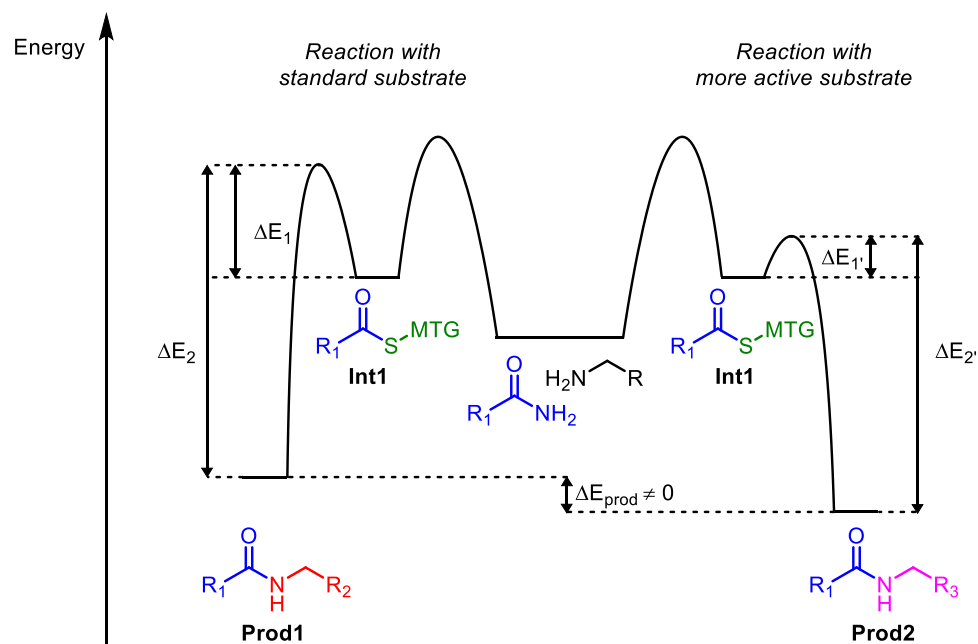
Figure 1.53 Reaction profile of a model MTG reaction with a standard substrate (left), and a highly active substrate (right). The magnitudes of energies shown are arbitrary, and for illustrative purposes only.

The reaction profile on the right-hand side represents the reaction with an optimised, highly active amine substrate. The overall shape of the profile is the same, as the substrates undergo the same reaction, but the energies are altered: the energy barrier of amine attack ($\Delta E_{1'}$) is lower, as the amine substrate interacts more favourably with the MTG active site. A consequence of this lowered activation energy is that the initial energy barrier for the reverse reaction, $\Delta E_{2'}$, is also lowered. This means the re-formation of **Int1** from **Prod2** is more facile, and that the overall reverse reaction (hydrolysis, or interception of the thioester by another nucleophile) would be expected to occur more rapidly.

There are two other factors to consider: the ground state energies of **Prod1** and **Prod2** are different, as they are different molecules formed from different amine donors. The exact ground state energies will affect ΔE_2 and $\Delta E_{2'}$, as can be seen in figure 1.51. This will therefore affect the relative reversibility. For example, the difference between the energies of **Prod1** and **Prod2** (ΔE_{prod}) may be equal to the difference in activation energies, $\Delta E_1 - \Delta E_{1'}$. In this specific scenario we would therefore not expect any

difference in the rates of backwards reaction between the standard substrate and an engineered, active one.

Additionally the relative sizes of the activation energies must be considered. ΔE_1 and $\Delta E_{1'}$ are small enough to be overcome at reaction temperature – this is clear, as the forward reaction occurs. The sizes of ΔE_2 and $\Delta E_{2'}$ are larger – the formation of an amide from a thioester is thermodynamically favourable. The difference in these energies, $\Delta E_2 - \Delta E_{2'}$, may be proportionally very small, meaning it won't affect the rate of backwards reaction significantly.

Generally this equilibrium is driven to the desired product by using a large excess of amine donor, and by the fact that the initially formed volatile ammonia by-product is likely lost from the system. In early control reactions where we investigated using lower concentrations of amine donor, however, we observed hydrolysis product by LCMS in some cases, at the expense of product formation. We were therefore concerned that in the regime of low amine equivalents, and when using more reactive and therefore potentially more reversible amines, this unwanted side-reactivity might also be accelerated.

In order to assess the contribution of reversibility to the product distribution obtained, we synthesised on preparative scale amides **114** and **115**, using MTG as a catalyst. Doing this also allowed us to fully characterise these MTG products, confirming the reactivity is as expected. The amines we chose to form these products were **28**, which represents a moderately active donor (48% conversion in our assay), and **56**, which represents a highly active amine donor (100% conversion in our assay).
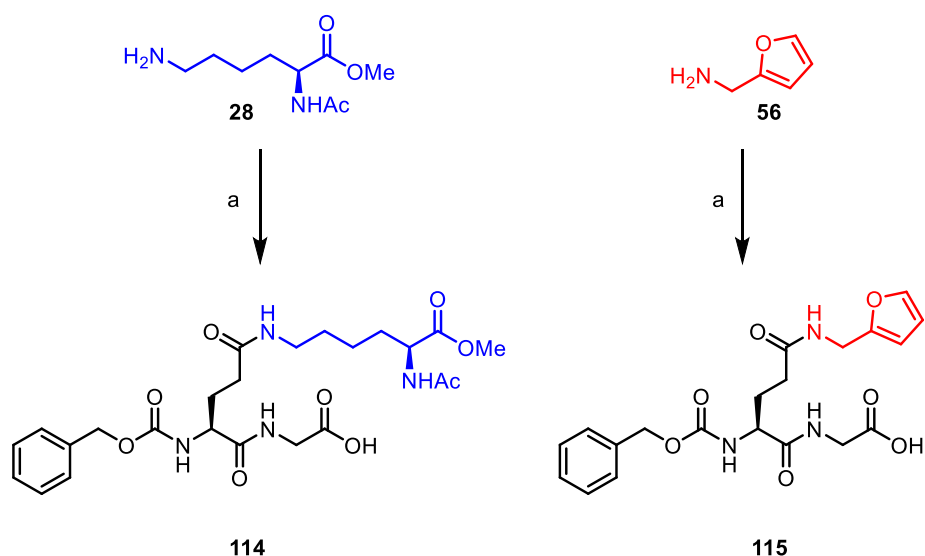
*Figure 1.54 Preparative scale synthesis of MTG products **114** and **115**. a: amine (2.0 eq), ZQG (1.0 eq), MTG (50 U), PBS (pH = 7.6), 37 ℃, o/n, **114** = 28%, **115** = 50%.*

First, to measure hydrolytic stability, **114** and **115** were incubated in PBS at 37 ℃ with MTG for 6 h and 24 h. The amount of hydrolysis product formed (Z-Glu-Gly, **116**), if any, is an indication of the hydrolytic stability. No production of the hydrolysis product was observed for either amide over the course of both 6 h and 24 h. This indicates not only the amide produced from the standard amine substrate is hydrolytically stable under these conditions, but the amide produced from the more reactive amine is too.
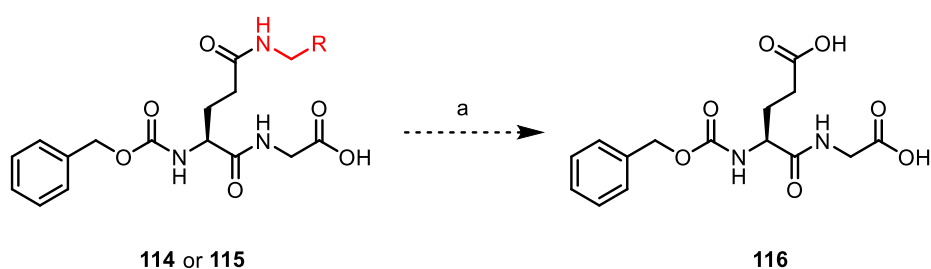
*Figure 1.55 Schematic of reaction to measure hydrolytic stability of MTG-produced amides **114** and **115**. Presence of hydrolysis product Z-Glu-Gly, **116**, was measured. a: MTG (1.0 U), PBS (pH = 7.6), 37 ℃, 6.0 h and 24 h.*

Next, to probe whether amine-exchange reactions might occur, we repeated the experiment but with the inclusion of the alternate amine. So **115** was incubated with N_α-Ac-Lys-OMe (**28**), and **114** was incubated with 2-aminomethyl furan (**56**). These experiments were performed for 2 h and 17 h. These experimental conditions mimic

the presence of peptidic surface lysine residues during a conjugation, which could result in amine-exchange reactions leading to protein-protein crosslinking.
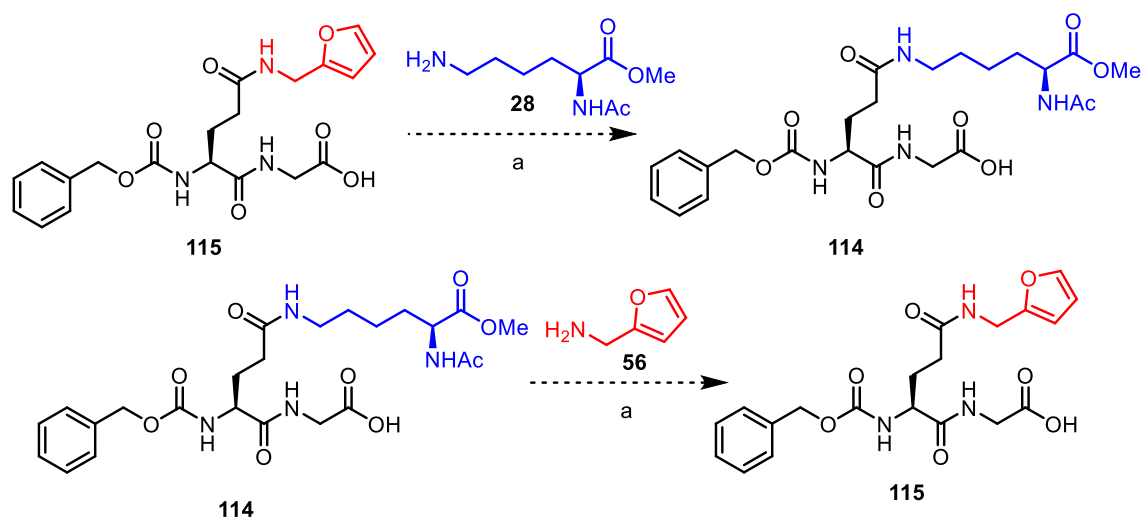
*Figure 1.56 Schematic of reaction to investigate amine-exchange reactions of MTG-produced amides **114** and **115**. a: amine (2.0 eq), MTG (0.56 U), 37 ℃, 2.0 h and 17 h.*

The results of these experiments are summarised in table 1.11. Broadly, both amides are stable under all conditions tested (<10% consumption of starting amide). The furan amide **115**, formed from the more active amine substrate, may be expected to suffer more cross-reactivity if more active substrates do indeed lead to products that are more susceptible to the reverse reaction. Over 2 hours 7.6% of the amide is consumed and 17 hours 0.70%. Traces of the "opposite" amide **114** mass were seen, but no significant UV peak. These results were obtained from two separate reactions, rather than aliquots from the same reaction, so the apparent decrease in conversion as the reaction time is increased may be down to natural variation of the system.

114 also appears stable at all lengths of experiment, even in the presence of reactive amine **56**.
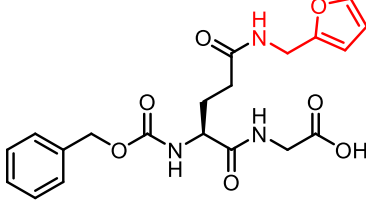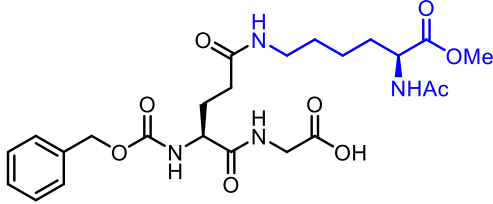
Compound	Structure	Time /h	Conversion /%	SD
115		2.0	7.6	1.3
		17	0.70	0.50
114		2.0	1.0	0.10
		17	2.7	3.3

*Table 1.11 Results of amine-exchange investigation with amides **114** and **115**.*

Another observation is that none of the hydrolysis product **116** was observed at any point during these experiments, confirming again that these amides are stable in aqueous solutions in the presence of MTG.

From these data we can conclude the following:

- The amides produced in MTG-catalysed reactions are essentially stable under all conditions tested, and there is no clear evidence that any reverse reactivity is occurring under these conditions.
- No hydrolysis was observed, even after 24 h.

1.7.10 Conclusions and future work

This work examined how MTG accepted a range of unnatural amine donors, selected through an approach of iterative optimisation with the aim of understanding the SAR for amine donors in MTG-mediated conjugations. We have confirmed the findings reported in the few pieces of literature that exist on this subject, and we have tested many compounds for the first time. Gaps in the existing substrate scope have been filled, and we have attempted to rationally design amine donors that are more active than peptidic surface lysine residues to overcome the challenge of protein-protein crosslinking during MTG-mediated bioconjugations.

Glycine was examined as a potential way to upgrade amine donors, but this approach failed when amides of glycine showed poor conversions. 2,5-Disubstituted furans were then explored, but this class of substrates had a propensity to decompose, precluding the successful synthesis of a test compound. Finally alkyne-containing amines were investigated, as a number of test compounds had shown particularly good conversions.

After a number of unsuccessful synthetic attempts, alkynes with reactive handles were made and used to generate an alkyne substrate with a model payload attached. Unfortunately this compound performed poorly in the MTG assay, even though comparisons with other substrates suggest it should react well. The exact reason this final compound performed so poorly is unknown, and time constraints meant further analogues could not be synthesised.

Judging by the excellent conversion of 5-phenylpent-2-yn-1-amine, **100**, future work should include synthesising analogues of this compound with reactive handles to attach model payloads to. It seems that a phenyl ring at this position leads to effective binding and excellent conversion, but it remains to be seen whether substitution on the ring will be tolerated. Our proposed synthesis is outlined in figure 1.55.
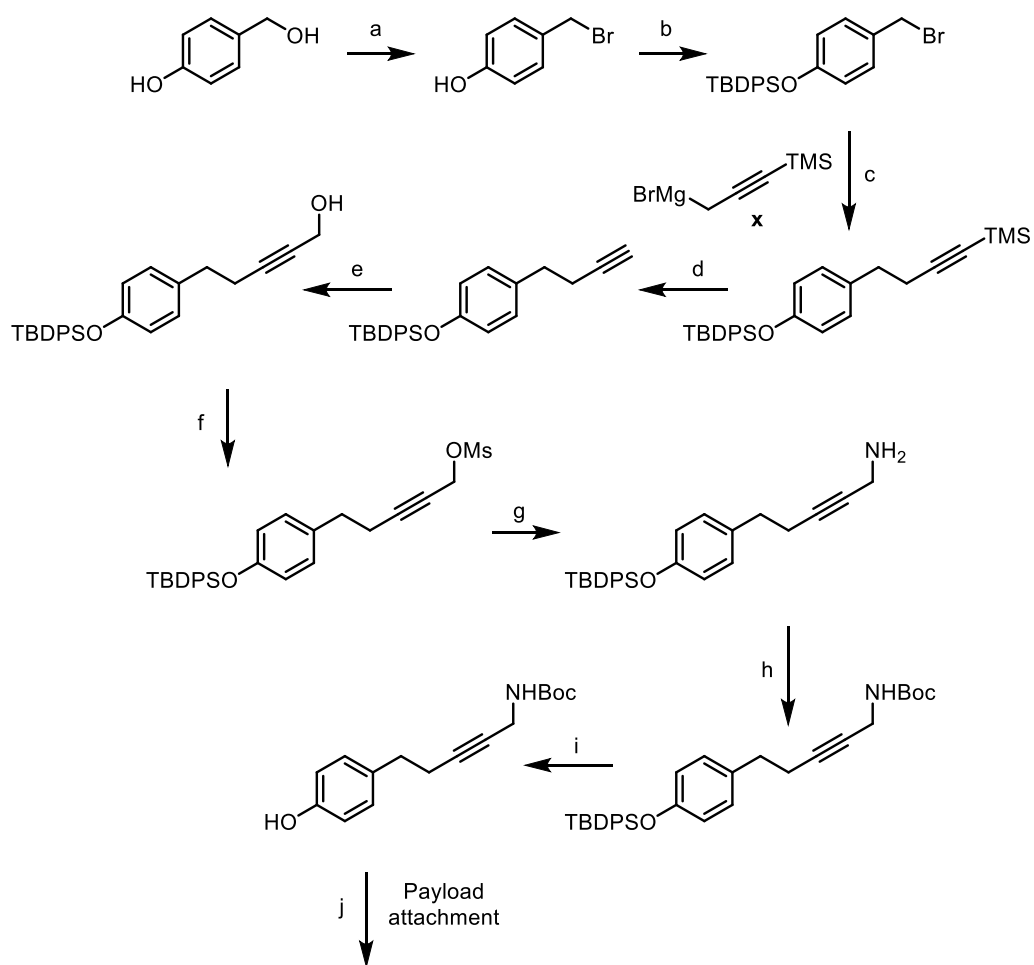
Figure 1.57 a: Appel reaction. b: TBDPS protection. c: Displacement of bromide by Grignard. d: TMS selective silyl deprotection. e: BuLi/formaldehyde homologation. f: Mesylation. g: Displacement of mesylate with ammonia. h: Amine protection. i: Silyl deprotection. j: Phenol alkylation to attach payload.

Although our attempts to synthesise a highly reactive amine donor with a model payload attached fell short, we have shown that there is chemical space in the MTG amine scope in which highly active substrates can be found. It is just a matter of further exploration and optimisation before a system can be developed that allows the upgrade of a normal amine-functionalised payload to a highly active one. This would allow payloads to be conjugated to proteins in a one-step MTG-catalysed step, without the need for large excesses of payload. The potential cost and material savings that this process represent mean it will remain an attractive target.

Specific results we obtained also suggest areas that may warrant additional research. In addition to the phenyl-alkyne described above, aromatic rings may still have

potential to generate a suitable upgrade strategy. Although we explored all points of substitution on benzylamine, we only did this with a methoxy group. Substituting benzylamine with an electron withdrawing group may give different properties. In addition, the excellent conversion seen with 2-aminomethyl furan (**56**) suggests that there may be other five-membered rings that can act as efficient substrates. Ideally they would also avoid the stability issues we encountered with furan derivatives. Finally, varying the distance between the reactive amine and the aromatic ring may yield some SAR.

Our hypothesis that the extra amine in lysine (**43**) compared to 6-aminocaproic acid (**37**) allowing a greater positive charge, and therefore more attraction to the MTG active site, could be tested. For example, a substrate with a permanent positive charge could be synthesised, such as an *N*-substituted pyridine, or a quaternised amine.

2 Design and synthesis of NAMPT PROTACs

2.1 Natural function of NAMPT

Nicotinamide phosphoribosyltransferase (NAMPT) is a critical enzyme in mammalian cells. It's expressed in all mammalian tissues and primarily located in the nucleus and cytosol. NAMPT is the rate limiting enzyme in the pathway salvaging nicotinamide adenine dinucleotide (NAD, **117**) from nicotinamide (NAM, **118**).[123] In addition to this pathway, NAD can be synthesised *de novo* from the catabolism of tryptophan, or salvaged from the other two forms of vitamin B3: nicotinic acid (NA) and nicotinamide riboside (NR).[124]

Nicotinamide
117

NAD
118
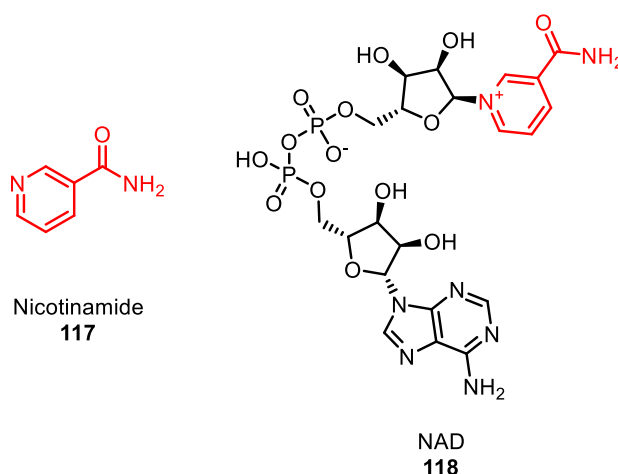
*Figure 2.1 Chemical structures of nicotinamide (**117**) and NAD (**118**).*

NAD is a key cofactor in many redox reactions that generate adenosine triphosphate (ATP), the cellular source of energy. NAD is also the substrate for a number of NAD-consuming enzymes, such as poly-ADP-ribose polymerases (PARPs), CD38, and sirtuins.[125] Through its role as substrate for so many enzymes, NAD levels impact energy metabolism, DNA repair, epigenetic modification, inflammation, circadian rhythm, and stress resistance. Additionally NAD deficiency can contribute to a range of diseases such as cancer, metabolic diseases, and neurodegenerative disorders.[126]

NAMPT catalyses the transformation of nicotinamide and 5-phosphoribosyl-1-pyrophosphate (PRPP, **119**) into nicotinamide mononucleotide (NMN, **120**), which is then combined with adenosine by the enzyme NMN adenylyltransferase (NMNAT), of

which there are three isoforms in different locations within the cell. This pathway represents the primary source of NAD in mammals, with NAMPT function in particular being essential for the maintenance of the NAD pool in many cell types.[127,128]
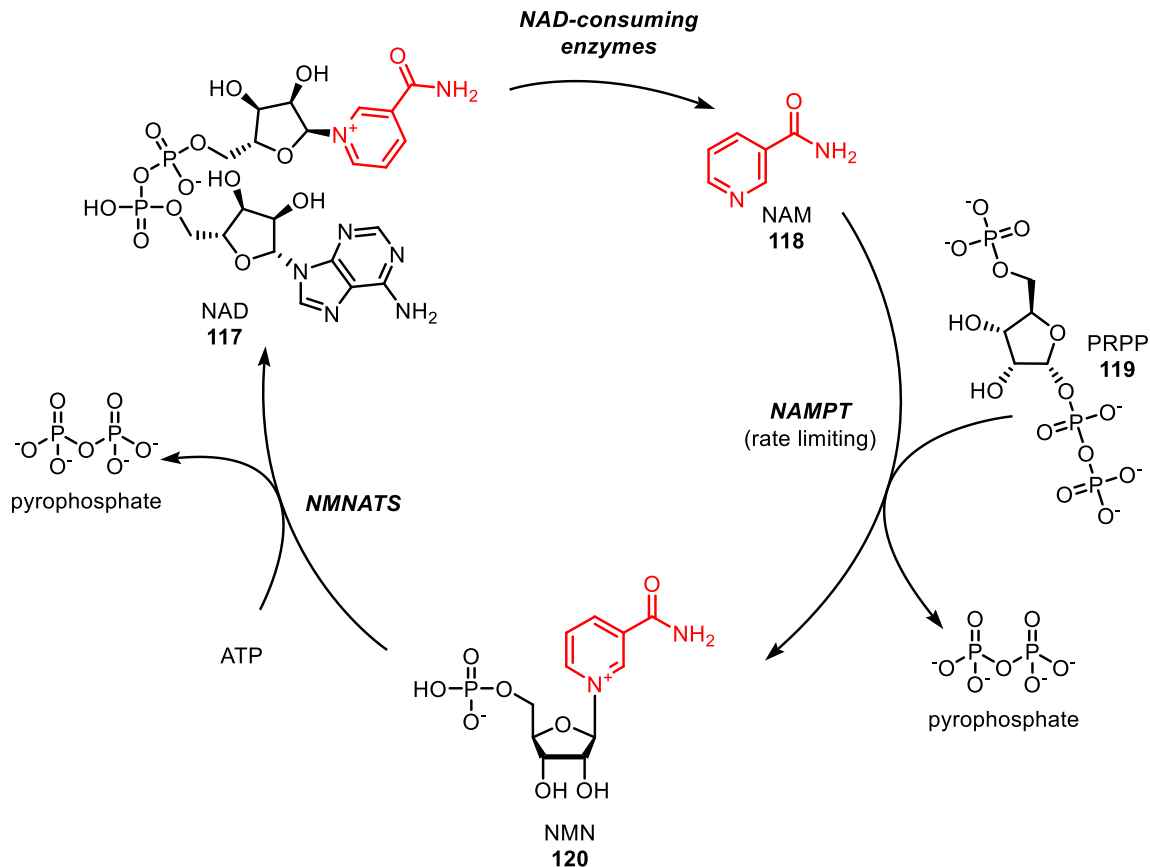
Figure 2.2 NAD salvage pathway from NAM. NAMPT is the rate-limiting enzyme of the cycle.

2.1.1 Extracellular NAMPT

NAMPT can also secreted from cells, leading to an extracellular build-up of enzyme known as eNAMPT. This has been observed in a range of cell types including cancer cells, immune cells, hepatocytes, and adipocytes, in response to stresses including oxidative stress and inflammatory signalling.[127] Compared to intracellular NAMPT, much less is known about the functions of eNAMPT.

It has been shown that eNAMPT exists as a dimer, meaning it can be enzymatically active.[129] Reports have demonstrated that eNAMPT can contribute to intracellular NAD synthesis in mouse tissues,[130,131] with additional research suggesting that the

actual eNAMPT-catalysed reaction doesn't happen in the blood plasma, based on the almost complete lack of PRPP and ATP measured.[132] But conversely, Zamporlini *et al.* demonstrated that enzymatic activity of eNAMPT can be detected in human blood plasma.[133]

Independently of this, eNAMPT also has another set of roles as a cytokine-like protein. As well as modulating immune responses, eNAMPT can trigger intracellular signalling that leads to effects such as promoting differentiation of myeloid cells, activation of the inflammasome, and secretion of further pro/anti-inflammatory cytokines.[128,134]

2.2 NAMPT and cancer

Intracellular NAMPT overexpression has extensively been reported in various cancerous cells, including colorectal, breast, gastric, pancreatic, ovarian, prostate, well-differentiated thyroid and endometrial cancer, brain tumours, melanoma, sarcoma, and haematological malignancies.[135] Additionally higher NAMPT expression has been correlated with poorer prognoses, more aggressive tumours, metastasis, and treatment resistance.[136]

2.2.1 Cancer metabolism and NAMPT

One of the key ways in which improperly regulated NAMPT levels contribute to cancer is by supporting the altered metabolic state that cancer cells exist in. The rapid proliferation of tumours requires an increased and constant supply of energy. To meet this need cancer cells rely on aerobic glycolysis. Glycolysis is a less efficient source of ATP than aerobic respiration, but can provide energy faster.[137] This gives cancerous cells a survival advantage as they are in constant competition with nearby healthy cells for their nutrient supply, a phenomenon known as the Warburg Effect.[138]

In healthy, normoxic cells glycolysis produces pyruvate and 2 ATP molecules from glucose in the cytoplasm, which is then shuttled to mitochondria to be fed into the citric acid cycle and oxidative phosphorylation, producing around 30 further molecules of ATP per glucose molecule. This is the basis for aerobic respiration. In anaerobic conditions the pyruvate instead remains in the cytoplasm and undergoes fermentation. This process oxidises NADH to NAD, which is required for further

glycolysis. In skeletal muscle cells the waste process is lactic acid and this is the process that occurs when insufficient oxygen is present for aerobic respiration (figure 2.3). The only ATP molecules produced are the 2 from glycolysis, although they are produced much more rapidly.[137] Cancer cells reprogram their metabolism to follow this anaerobic pathway even in the presence of oxygen and sufficient nutrients, a process termed aerobic glycolysis.[138]

It has been proposed that the switch to aerobic glycolysis is an adaptation to the hypoxic environment that develops as cancer cells grow further away from their blood supply.[139] Increased rates of glycolysis also modulate the cancer microenvironment, as a result of the lactic acid produced. The pH of the microenvironment is decreased,[140] which the cancer cells can adapt to. This gives them a survival advantage over nearby healthy cells which suffer the toxic effects of the acidic environment. Additionally angiogenesis is promoted and pro-tumour immune cells are generated.[141]
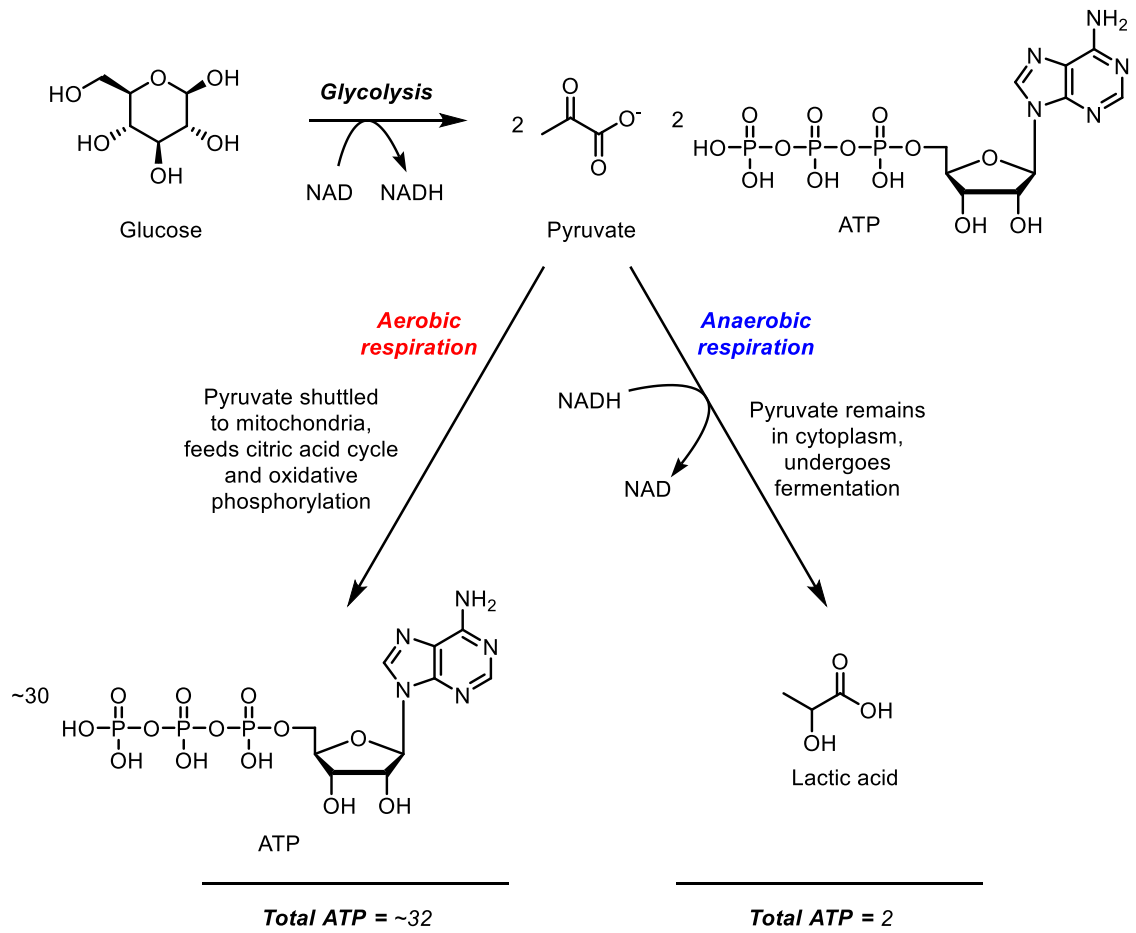
Figure 2.3 Schematic summary of aerobic and anaerobic respiration in cells. Cancer cells reprogram their metabolism to follow the anaerobic pathway even with sufficient oxygen, which is known as aerobic glycolysis.

As glycolysis is not terribly efficient, the large energy output required means cancer cells consume a vastly increased amount of glucose. This forms the basis for fluoro-deoxy glucose positron emission tomography (FDG-PET) imaging of tumours, where a radioactive form of glucose is administered and the increased uptake in tumours compared to healthy tissues reveals cancerous sites.[142]

Additionally there are multiple intermediates of glycolysis that are involved in other pathways highly activated in cancers, such as the pentose phosphate pathway and the serine synthesis pathway. Clearly the Warburg Effect is a crucial part of cancer metabolism, supporting both the energy requirements of invasion and other biosynthetic pathways.[136]

To sustain glycolysis cancer cells need two things, glucose and NAD. Glucose is the fuel and NAD is required as a co-factor. A higher ratio of NAD to its reduced form, NADH, is observed in cancer cells than in healthy cells, suggesting that NAD is crucial to support the altered metabolism of cancer cells.[143]

Mechanisms such as the phosphatidylinositol 3-kinase (PI3K/Akt/mTOR) pathway and transcription factors such as hypoxia-inducible factor 1 (HIF-1) and c-Myc upregulate genes that code for glucose transporters, allowing cancer cells to take in significantly increased amounts of glucose.[144]

To satisfy their NAD requirements cancer cells upregulate its biosynthesis. Most NAD comes from salvage pathways, of which NAMPT is the rate-limiting enzyme. Expressing more NAMPT therefore allows cancer cells to increase their NAD pool and sustain their high rate of glycolysis, leading to NAMPT being described as a "potent oncogene".[136,145] Its increased expression leads to tumour progression and development and many studies have correlated NAMPT levels with an overall poorer prognosis.[146,147]

In addition to its function keeping NAD supplies plentiful, increased levels of NAMPT have been shown to activate the pluripotency transcription factors SOX2, OCT4, KLF4, and Nanog. Activation of these transcription factors gives cancer cells stem cell-like properties, allowing increased levels of self-renewal.[136]

2.2.2   NAMPT inhibition in cancer therapy

Research has shown NAMPT inhibition to be a promising strategy in cancer therapy. Inhibition reduces levels of NAD in the cells, which in turn supresses the production of ATP, restricting the growth of cancer cells.[145,148–150] As inhibition of NAMPT does not affect the mitochondrial concentration of NAD, healthy cells are typically less sensitive to NAMPT inhibition than cancerous cells.[151] Despite this, a key challenge in developing a safe and effective therapy based on NAMPT inhibition is that healthy cells also fundamentally rely on NAMPT for their normal function. Dose-limiting toxicity is a recurring theme in the development of inhibitors and has led to combination therapies

being investigated with the hope they will allow a lower concentration of NAMPT inhibitor to be administered, potentially reducing the severity of side effects.[152]

Despite the challenges associated with inhibiting NAMPT, a number of clinical trials of NAMPT inhibitors to treat various cancers have been carried out, and a number are still ongoing.[153]

2003 saw the discovery of FK866 (**121**), a NAMPT inhibitor that induced delayed cell death by apoptosis in HepG2 human liver carcinoma cells with an EC_{50} of approximately 1 nM.[154] This inhibitor has been widely studied and now represents the benchmark for NAMPT inhibitors. Shortly after this the previously published cytotoxic agent GMX1778 (**122**) was also determined to target NAMPT. Comparisons between the two structures were drawn (figure 2.4) and a common binding pharmacophore was identified, namely a pyridine (or pyridine-like ring) as a capping group (shown in red), that can mimic the binding of the natural substrate nicotinamide. Both structures then feature a hydrogen bond-acceptor section (shown in blue), such as an amide, a hydrophobic linker (shown in purple), and finally a tail group (shown in black) that is exposed to solvent.
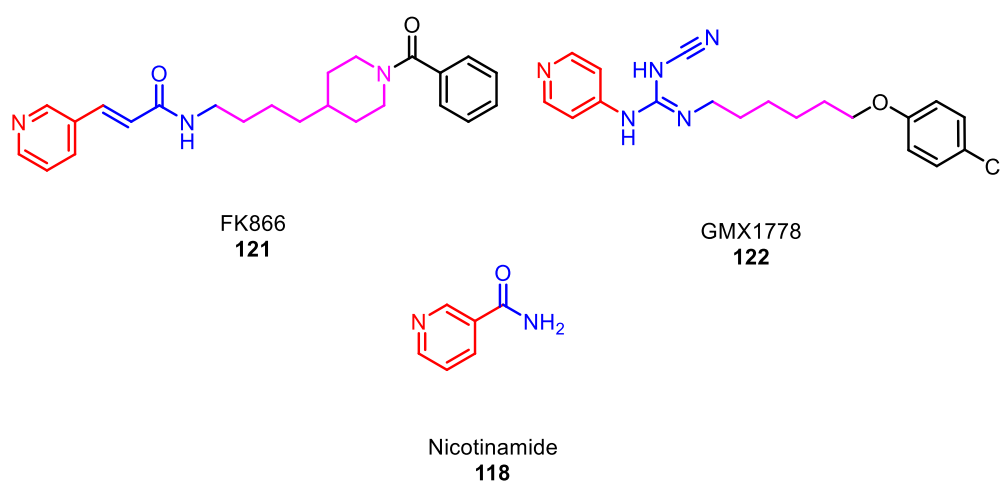
*Figure 2.4 Chemical structures of the synthetic inhibitors FK866 **121** and GMX1778 **122** and the natural substrate of NAMPT, nicotinamide **118**. Corresponding chemical groups are shown in the same colours.*

Crystal structures of NAMPT show it exists as a head-to-tail homodimer, forming two active sites along the interface between the two monomers. The active sites are only

accessible through a narrow hydrophobic tunnel, rationalising the need for a hydrophobic linker in the middle of these inhibitors. Crystal structures of NAMPT in complex with FK866 show the pyridyl moiety positioned between residues Phe193 and Tyr18, forming π-π interactions that mimic the binding of the natural substrate, nicotinamide. The amide bond is seen to form two hydrogen bonds. One to the OH sidechain of Ser275 and one to a water of crystallisation. The water molecule acts as a hydrogen bond bridge, forming further interactions with Asp219, Ser241, and Val242.[155] The lipophilic tail group of the molecules occupies a shallow hydrophobic cleft on the surface of the protein. Although the binding mode of the pyridyl end of the molecules remains consistent, two conformations of the lipophilic phenyl ends of the molecules have been observed with the inhibitor GMX1778 in complex with NAMPT.[156] This suggests that the hydrophobic surface cleft has a reasonable amount of space and may be able to tolerate a range of inhibitor structures.
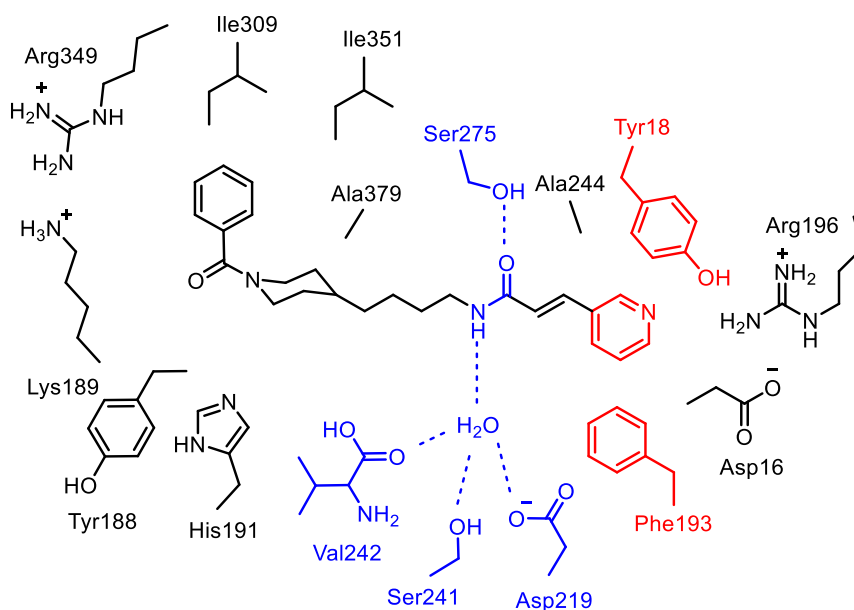
Figure 2.5 2D representation of FK866 in the binding site of NAMPT.[155] Components involved in π-π interactions are shown in red and components involved in hydrogen bonding are shown in blue.

The discovery of this general molecular structure leading to effective NAMPT binding was then widely explored, leading to a plethora of NAMPT inhibitors that broadly shared the same structure. Changes in the exact nature of the building blocks whilst

staying true to the overall model have allowed the absorption, distribution, metabolism, and excretion (ADME) properties of the drugs to be modified.

Bai *et al.* discovered compound **123** in 2016.[157] The pyridinyl acrylamide end of the molecule mimics FK866 and allows the favourable π-π and hydrogen bonding interactions to be maintained. They modified the hydrophobic end of the molecule, introducing an indole-based capping group to replace the phenyl ring of FK866. They hypothesised that the indole group would be able to occupy the two possible positions for the hydrophobic tail, or at least form π-π interactions with Tyr188, which should increase the binding affinity compared to FK866. Docking studies confirmed that either of these two hypotheses could explain the effective binding of **123**, which has an IC_{50} of 25.3 nM, compared to their measured value of IC_{50} = 32.0 nM for FK866. Compound **123** also showed promising anti-proliferative properties in a number of cell lines (HeLa, MCF7, HI975, U937, MDA-MB-231) and exhibited anti-tumour activity in an MDA-MB-231 xenograft tumour model of triple-negative breast cancer. The same group also discovered compound **124**, demonstrating that biarylsulphanilamides could serve as effective tail groups.[158] Again their design principle was based around creating molecules that can occupy more of the large lipophilic cleft that the tail portion of the molecule occupies, which should generate more favourable binding interactions.

123
IC_{50} = 25.3 nM

124
IC_{50} = 5.08 nM
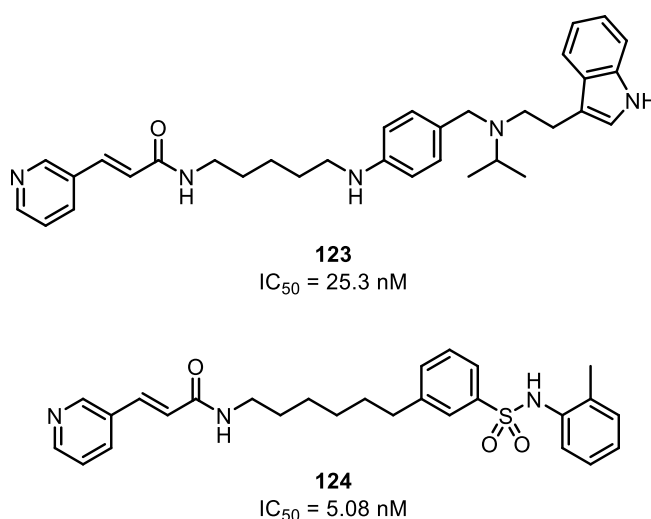
Figure 2.6 Structures of pyridinyl acrylamide-based NAMPT inhibitors developed in the Jiang Group. They illustrate that by generating FK866-like molecules effective NAMPT inhibitors can be discovered.

Compounds that don't rely on the pyridinyl acrylamide moiety have also been developed. Colombano *et al.* discovered the novel NAMPT inhibitor **125** in 2010, using a triazole formed in a click reaction to replace the amide as the hydrogen-bond acceptor.[159] **125** had an IC_{50} of 10.2 nM and an EC_{50} = 3.8 nM for cytotoxicity in human neuroblastoma SH-SY5Y cells.[160] Further work within the group to increase the metabolic stability of their compounds led to compounds **126** and **127**, through introducing more hydrolytically stable groups into the solvent-exposed tail end of the molecule. Both compounds possessed improved stability and had IC_{50} values lower than the original inhibitor **125** of 3.1 nM and 3.8 nM, respectively. They also retained sub-10 nM potency with respect to SH-SY5Y cell viability, albeit lower potency than **125**, with EC_{50} values of 5.8 nM and 5.2 nM, respectively.[160] The authors note that **126** lacked retinal and cardiac toxicity, which they hypothesise is due to the increased polarity compared to **125**. Replacing the amide group of **125** and **126** with a novel 2-biphenyl-1,2,3-triazole was also tolerated leading to compound **128**, but showed comparatively modest properties of an IC_{50} = 114 nM and EC_{50} for SH-SY5Y viability of 20 nM.[161]

125
IC_{50} = 10.2 nM
EC_{50} = 3.8 nM

126
IC_{50} = 3.1 nM
EC_{50} = 5.8 nM

127
IC_{50} = 3.8 nM
EC_{50} = 5.2 nM

128
IC_{50} = 114 nM
EC_{50} = 20 nM
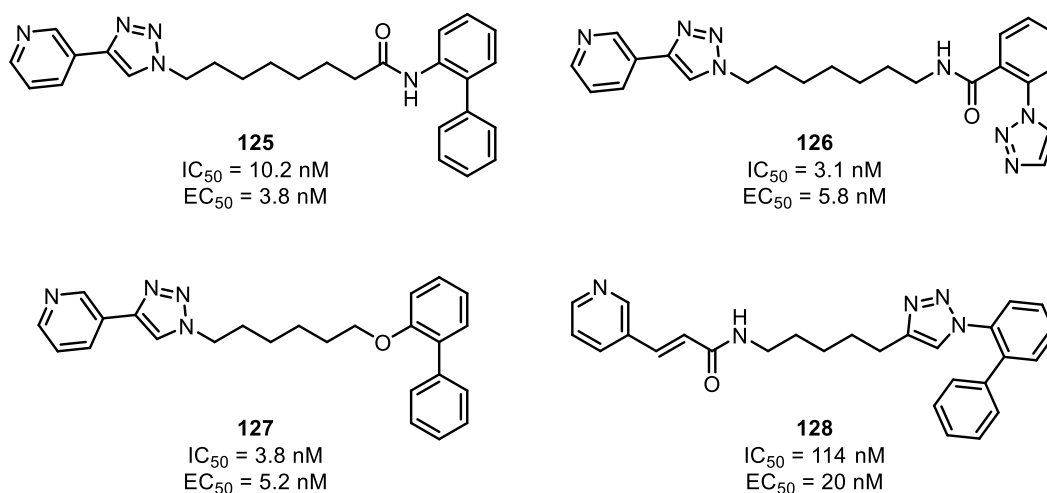
Figure 2.7 Chemical structures of some triazole containing NAMPT inhibitors developed by the Genazzani Group. EC50 refers to the effect on cell viability in SH-SY5Y cells.

Pyridine-like heteroaromatic rings such as isoindolines can also evoke nicotinamide-like binding in inhibitors, such as in compound **129** developed by Genentech, a potent NAMPT inhibitor with an IC_{50} of 14 nM.[162] This compound exemplifies an undesirable

property of many pyridine (or pyridine-like ring) containing NAMPT inhibitors: they can inhibit CYP2C9, an enzyme that makes up a considerable percentage of the human liver microsomal P450 content. CYP2C9 plays an important role in metabolism and is implicated in the phase 1 metabolism in a large proportion of drugs.[162] Consequently co-administration of a drug metabolised by CYP2C9 and a CYP2C9-binding NAMPT inhibitor could lead to unintended drug-drug interactions. The Genentech team therefore worked to retain the on-target NAMPT binding, whilst eliminating the undesirable CYP2C9 inhibition. As the same motif contributes to both NAMPT and CYP2C9 binding, it was challenging to separate the two and increase NAMPT binding whilst reducing that to CYP2C9. Attempts to shut down CYP2C9 binding by introducing more steric bulk around the pyridine usually resulted in lower NAMPT inhibition also. One exception was introducing a 2-NH_2 group to the pyridine ring. In some compounds they tested this maintained NAMPT binding and greatly reduced CYP2C9 binding, although the increased electron density of the molecules led to time-dependent inhibition of another CYP enzyme, CYP3A4. Finally, by increasing the saturation and structural rigidity of the inhibitor to supress the CYP-binding ability of the isoindoline, they arrived at compound **130**, possessing a NAMPT IC_{50} = 5.5 nM, with a CYP2C9 IC_{50} >10 µM.

Optimisation
to suppress
CYP2C9
inhibition

129
NAMPT IC_{50} = 14 nM
CYP2C9 IC_{50} = 5 nM

130
NAMPT IC_{50} = 5.5 nM
CYP2C9 IC_{50} = >10 µM
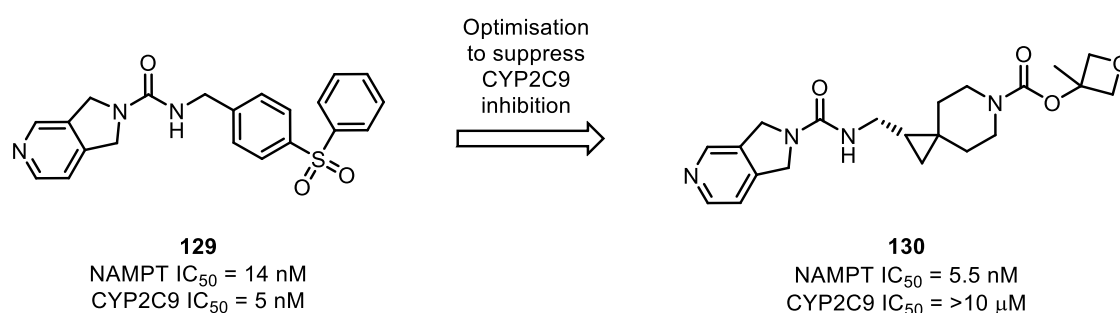
*Figure 2.8 Optimisation of **129** allowed improvement of NAMPT binding, while supressing the CYP2C9 inhibition observed with many pyridine-containing NAMPT inhibitors.*

NAMPT inhibitors often also have poor aqueous solubility, for example GNE-617 (**131**), which has a solubility <2 µM and also happens to inhibit CYP3A4 in a time-dependent way. Genentech once again underwent an optimisation campaign with the hope of addressing these issues.[163] Through *in vitro* metabolism studies using human

hepatocytes, they identified epoxide **132** as a short lived, potentially highly reactive metabolite. They hypothesised that this was the source of CYP3A4 inhibition and sought to move to an all-carbon bridgehead replacement. The azabenzofuran, azaindole, and azabenzothiophene analogues all exhibited no signs of time-dependent CYP3A4 inhibition, and the focus of their work shifted to improving the aqueous solubility of these compounds. Their general strategy was to reduce the number of aromatic rings present and/or the cLogD$_{7.4}$. Through this they arrived at compound **133**, with aqueous solubility of 265 μM and no evidence of CYP3A4 inhibition.
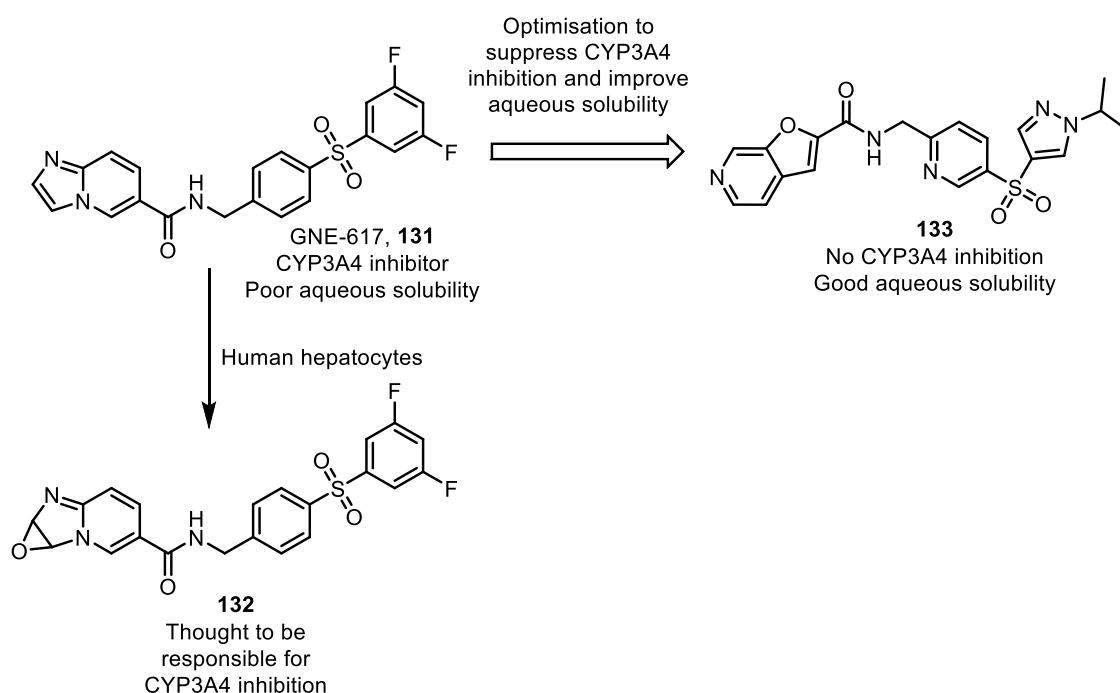
*Figure 2.9 Optimisation of GNE-617 (**131**) improved aqueous solubility and suppressed the inhibition of CYP3A4 whilst maintaining anti-tumour activity. Epoxide **132** was identified in an* in vitro *metabolism study and was thought to be the compound responsible for time-dependent inhibition of CYP3A4.*

It has long been considered that the pyridine, or pyridine-like ring in NAMPT inhibitors is crucial for their function. These rings not only form a favourable π-π stack with Phe193 and Tyr18, but they mimic nicotinamide enough to be phosphoribosylated by NAMPT in the presence of 5-phosphoribosyl-1-pyrophosphate. Research has demonstrated that for many examples, the presence of an N-containing aromatic ring is necessary to achieve good potency, as the phosphoribosylated inhibitor has increased affinity for NAMPT. In some cases this prevents the inhibitor adduct from

124

leaving the active site, essentially producing an irreversible inhibitor.[156] Crystal structures of these adducts bound to NAMPT have been obtained,[150] including for GNE-617 (figure 2.10).[156]
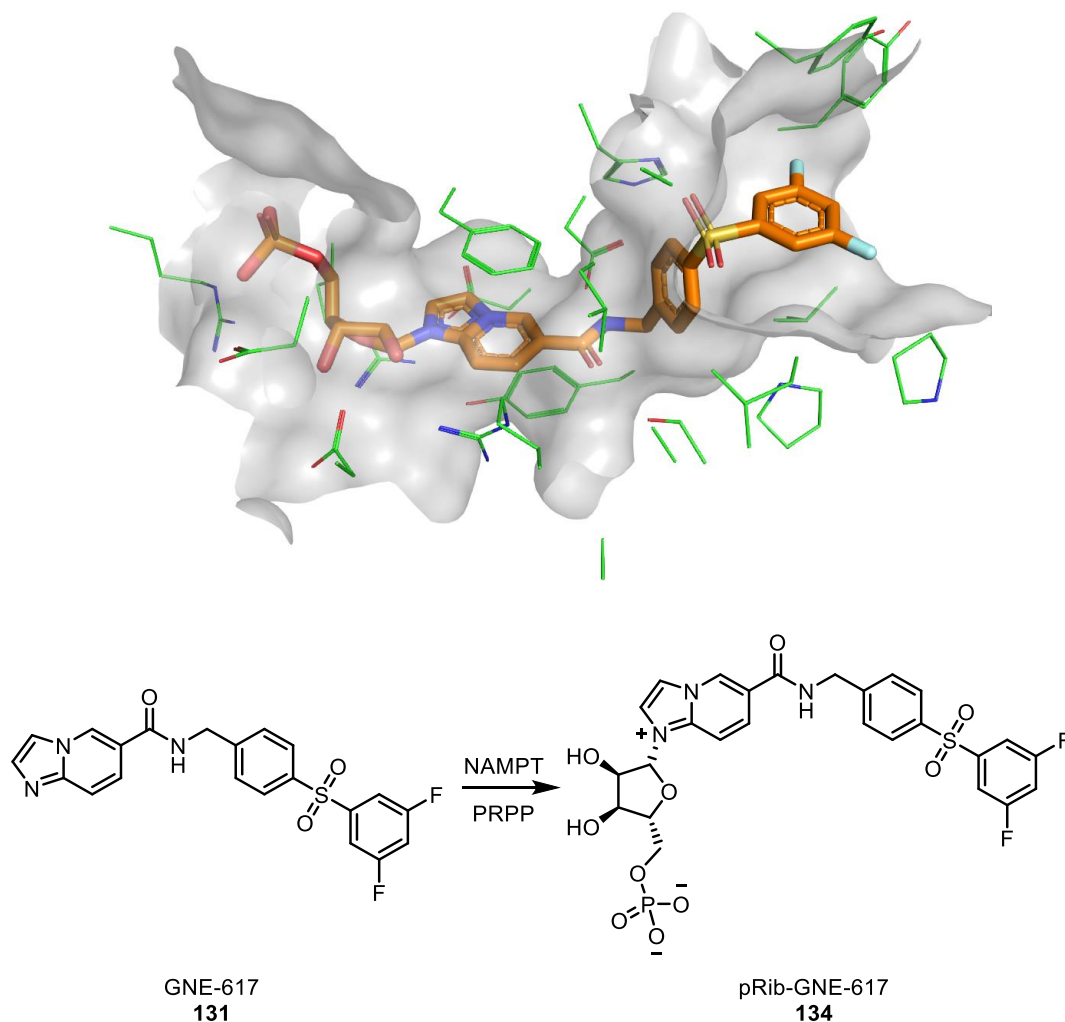
Figure 2.10 Above: Crystal structure of pRib-GNE-617 in complex with NAMPT (PDB: 4L4L). Below: Chemical structures of GNE-617 and the product of phosphoribosylation, pRib-GNE-617.

Although in most cases replacing the pyridine-like ring with the corresponding carbocycle suppresses inhibition, it's now known that NAMPT inhibitors can be generated without this motif. In 2016 AbbVie discovered A-1293201 (**135**).[164] This compound inhibits NAMPT effectively, with an IC_{50} of 83 nM and anti-proliferative action against human colorectal carcinoma HCT116 cells (EC_{50} = 19 nM), but lacks a pyridine-like nitrogen to be phosphoribosylated within the NAMPT active site. A crystal structure of A-1293201 was obtained in complex with NAMPT and revealed that the

compound binds in a similar way to FK866: π-π interactions are observed between the isoindoline cap group and Phe193/Tyr18, but are weaker than in the binding of FK866. The hydrogen bonds formed to Ser275 and a water of crystallisation are still present for the neighbouring amide and additional hydrogen bonds to the distal amide are observed to waters of crystallisation. It's likely that these additional amide bonds compensate for the weaker π bonding the molecule engages in. The team synthesised a series of matched-pair compounds, with each pair containing a carbocyclic capping group and the corresponding nitrogen-containing analogue. Generally the isoindoline versions had lower IC_{50} values, but the azaisoindoline versions had much lower EC_{50}s for the cell viability overall in PC3 cells (bone metastasis of prostate adenocarcinoma cells). A notable exception is that although aza-A-1293201 (**140**) showed higher potency in PC3 cells, it was less potent than A-1293201 in HCT116 cells. The matched pairs are summarised in table 2.1. Overall this work shows conclusively that a nitrogen-containing ring is not strictly necessary to generate a NAMPT inhibitor, contrary to the general consensus in the community.
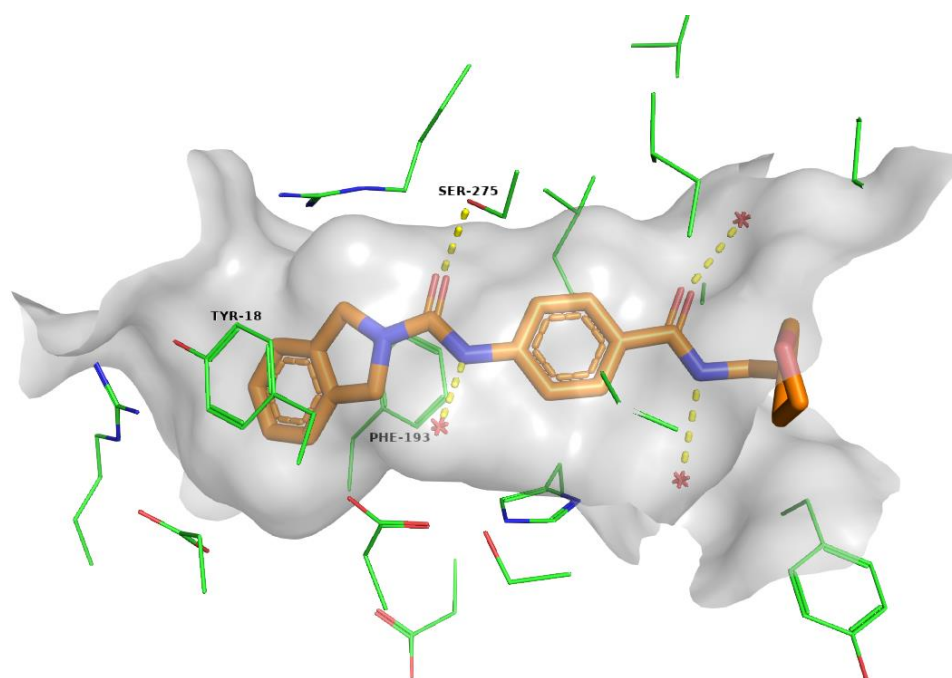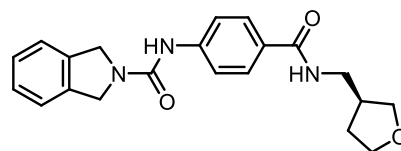
A-1293201
135

Figure 2.11 Above: Crystal structure of A-1293201 in complex with NAMPT (PDB: 5U2M). Hydrogen bonds are shown as yellow dashed lines. The hydrogen bonds on the right hand side of the molecule are not seen in FK866-like binding and likely compensate for the comparatively weaker π-π interactions. Below: Chemical structure of A-1293201, the first NAMPT inhibitor without a pyridine-like ring.

Compound	X	Structure	Inhibitory activity IC_{50} /nM	PC3 cell viability EC_{50} /nM	HCT116 cell viability EC_{50} /nM
136	N		62	5.7	1.0
137	CH		ND	>10,000	ND
138	N		91	8.4	6.1
139	CH		55	38	ND
140	N		107	41.8	32.4
135 (A-1293201)	CH		83	56	19
141	N		112	1.9	0.6
142	CH		98	18	7.7

Table 2.1 Matched pairs of isoindoline and azaisoindoline-based NAMPT inhibitors synthesised by AbbVie.

2.2.3   NAMPT inhibitor-related toxicity

Toxicity associated with NAMPT inhibition is a common feature in the literature, as healthy cells also rely on its function to sustain their normal state. Thrombocytopenia, a low platelet count, has extensively been described as a dose-limiting toxicity. Other

haematological toxicities such as anaemia and neutropenia have also been observed.[152]

A phase I clinical trial of FK866 by Holen *et al.* saw patients with various solid tumours that were not responding to other conventional therapies given FK866 in an escalating dose regime.[165] The treatment didn't appear to have a profound anti-tumour effect in any of the patients, although a handful of patients showed stable disease profiles and one experienced some clinical benefit through a decrease in pain. Thrombocytopenia was reported as a dose-limiting toxicity following occurrence in two of the patients that were given the maximum dose, and one that received the lower phase II-recommended dose. Thrombocytopenia is an abnormally low platelet count in the blood, stemming from the fact bone marrow isn't producing enough platelets. Low platelet levels can prevent blood clotting and cause uncontrollable bleeding. This can be life-threatening if the bleeding is in the brain. Although the degree of thrombocytopenia seen was severe, it didn't lead to any clinically relevant bleeding complications and the patients recovered rapidly once dosing had ceased.

Although mild, cases of lymphopenia (decrease in lymphocyte count) and neutropenia (decrease in neutrophil count) were also observed. Both conditions cause a decrease in types of white blood cell, which in general can leave the patient susceptible to infection. No infections were observed in this trial, however.

Taking the limited efficacy and toxicity together, the authors suggest that FK866 should only be pursued as a potential therapeutic in combination with other drugs that mitigate its toxic effects.

These conclusions were supported by a phase II trial by Goldinger *et al.*[166] Patients with cutaneous T-cell lymphoma (CTCL) were given FK866, again after conventional therapies had failed to address the disease. In this study FK866 led to severe thrombocytopenia and lymphocytopenia. Combined with the minimal effect on the course of the disease, the study was prematurely halted on the grounds of patient wellbeing. The authors don't recommend that FK866 is pursued as a potential treatment for CTCL, but note that other conditions may be more suited to its use.

Olesen *et al.* investigated whether the severe toxicities of FK866 could be mitigated by co-administration with nicotinic acid (vitamin B3).[167] This was a preclinical study, using a murine model. This study was inspired by the co-administration of folinic acid with methotrexante, an early chemotherapy agent developed in the mid-twentieth century. This drug regime decreases the toxic side effects of methotrexate without diminishing the anti-cancer properties of the regime. Methotrexate is an inhibitor of dihydrofolate reductase, a crucial enzyme in the synthesis of tetrahydrofolate from folic acid. This blocks DNA synthesis, halting the rapid division of cells and curtailing with growth of cancers. It also, however, leads to toxic effects in healthy cells as there is no specificity. Folinic acid is readily converted to tetrahydrofolate in a dihydrofolate reductase-independent manor, mitigating the inhibiting effects of methotrexate. When the dose is controlled appropriately, this co-administration can have a protective effect in rapidly dividing healthy cells, whilst retaining a toxic effect in cancerous cells.

The idea was that nicotinic acid would have a similar effect, as it can be converted to NAD independently of NAMPT activity. This effect was seen in healthy mice, with nicotinic acid dosing maintain the platelet count of the mice at a level comparable with the control animals. Lymphocyte levels were similarly protected by nicotinic acid and no change in neutrophil count was observed in any of the treated animals, regardless of the regime.

When this effect was investigated in cancer cell lines, the results varied depending on the cell line. A2780 (ovarian cancer), GLC-2 (small cell lung cancer), and PC-3 (prostate cancer) cell lines were not protected from cell death by nicotinic acid co-administration, whereas ML-2 (myeloid leukaemia), HCT-116 (colon cancer), and A431 (epithelial carcinoma) cells were.

So whilst this research has again demonstrated the toxic effects of NAMPT inhibition, there are strategies that can be used to mitigate it.

2.2.4 NAMPT inhibitor antibody-drug conjugates

In recent years there has been a moderate amount of progress in developing NAMPT inhibitor-antibody conjugates. One of the key and recurring issues with inhibition of NAMPT as a therapeutic strategy is that it's fundamentally toxic to healthy cells, as they also rely on NAMPT for biosynthesis of NAD.[168] The targeted delivery of a NAMPT inhibitor, by conjugation to an antibody, has the potential to alleviate these toxic side-effects by minimising the amount of inhibitor entering healthy cells. The hope is that targeted delivery of a NAMPT inhibitor will give a similar anti-cancer effect as observed with the inhibitors alone, but with a greatly increased therapeutic window. In addition most of the current ADC payloads give rise to their cytotoxic effects by interfering with the cell cycle. This had a much diminished effect if the target cells aren't rapidly dividing, reducing the generality of this approach. Conversely the cytotoxicity derived from NAMPT inhibition is cell cycle-independent, meaning cells that are resting or proliferating slowly can still be targeted.

Karpov *et al.* at Novartis designed and synthesised a series of NAMPT inhibitor ADCs (NAMPTi-ADCs) in 2018.[169] They identified cell lines that were both sensitive to NAMPT inhibition and expressed their target antigens of choice, tyrosine receptor kinases c-Kit and HER2. These cells included the GIST-T1 (gastrointestinal stromal tumour), NCI-H526 (lung carcinoma), and NCI-N87 (gastric carcinoma) lines. They began with inhibitor **143**, produced from internal screening efforts, that demonstrated potent cytotoxicity in a range of cancer cell lines. To introduce a vector for antibody conjugation they arrived at compound **144**, which retained the cytotoxicity of the parent compound (EC$_{50}$ = 5 nM for cell viability in A2780 ovarian cancer cells) but included a suitable chemical handle for linker attachment. Molecular docking studies confirmed that this new vector pointed into solvent when the molecule was bound to NAMPT, allowing attachment of a linker without compromising NAMPT binding.

When optimising the linker, their first choice was the cleavable Val-Cit-PAB linker, as this would release the unmodified drug upon internalisation. Although the resulting conjugate showed good *in vitro* properties, it had a poor aggregation rate of 29% leading to its abandonment. When a series of non-cleavable linkers were investigated

similarly promising *in vitro* properties were observed, but with a greatly reduced rate of aggregation. Their best-in-class ADC, based on an anti-c-Kit antibody, showed an aggregation rate of 6% and an EC_{50} for cell viability of 3 pM and 9 pM in the c-Kit$^+$ cell lines GIST-T1 and NCI-H526, respectively. This inhibitor-linker combination **145** was then attached to an anti-HER2 antibody generating a conjugate that also had an aggregation rate of 6% and an EC_{50} of 17 pM for the cell viability of HER2$^+$ NCI-N87 cells.

Although the conjugates had high potencies in their target cells, the selectivity was only moderate. For example their best-in-class c-Kit-targeting ADC had an EC_{50} of 2.1 nM in HER2$^+$/c-Kit$^-$ cells, still representing a significant effect. Similarly their HER2-targeting ADC had an EC_{50} of 19 nM in c-Kit$^+$/HER2$^-$ cells and the non-binding isotype analogue still had an EC_{50} of 1.4 nM in HER2$^+$ cells, clearly indicating considerable non-specific effects. They then demonstrated that their conjugates provoked concentration-dependent depletion of NAD levels in GIST-T1 cells, supporting the idea that the cytotoxicity of these conjugates arises from NAMPT inhibition. Finally they tested their conjugates *in vivo* and demonstrated that their best-in-class ADCs lead to tumour stasis in a xenograft model, and that the inactive ADC control had a comparable effect to vehicle. The conjugates were "well tolerated", demonstrating that NAMPT-targeting ADCs may represent a valuable line of enquiry.
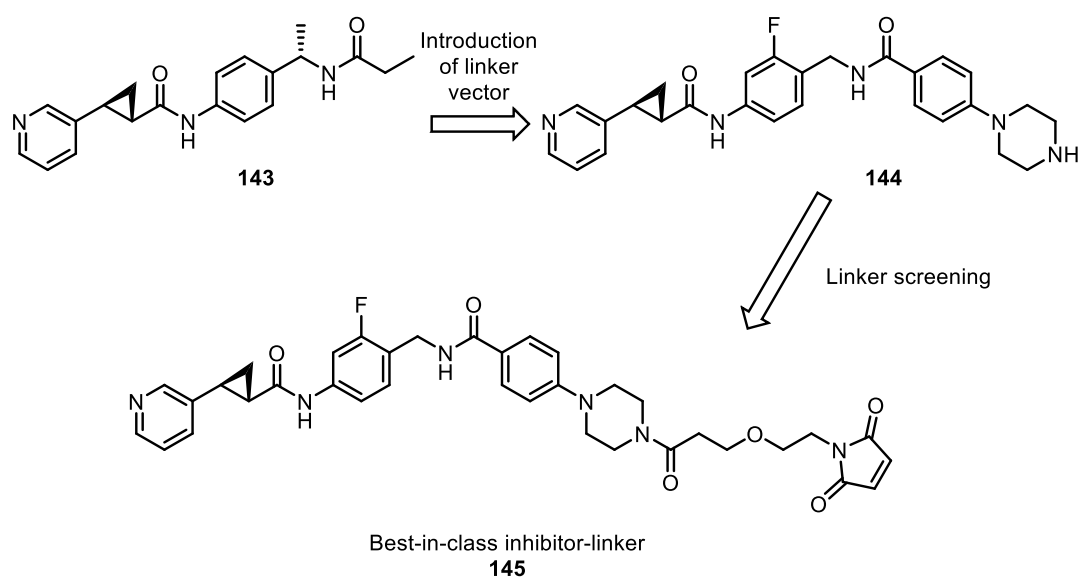
Figure 2.12 Overview of the NAMPTi-ADC development by Novartis, leading to their best-in-class inhibitor-linker 145.

Also in 2018 Seattle Genetics published a series of NAMPTi-ADCs using payloads **146**, **147**, and **148**, the former two based on FK866.[170] The ADCs contained a glucuronide trigger that increased water solubility of the conjugates, but is cleaved off by β-glucuronidase in endosomes and lysosomes. The inhibitors were all joined to the linker by a carbamate, a group that is stable in plasma but cleaves when the glucuronide is triggered after internalisation, releasing the free drug. The inhibitor-linkers were then conjugated by the thiol-maleimide strategy to an anti-CD30 antibody, targeting the tumour necrosis factor receptor CD30.

The ADCs were then tested for NAD depletion in the CD30$^+$ cell line L540cy (Hodgkin's lymphoma) and the CD30$^-$ cell line HepG2 (hepatocellular carcinoma), both of which are sensitive to NAMPT inhibition. The most potent ADC has EC$_{50}$ of 9 ng/mL (~60 pM) for NAD depletion in L540cy and the EC$_{50}$ for all ADCs tested in HepG2 cells was >2,000 ng/mL, representing a considerable increase in selectivity compared to the work of Karpov *et al.*[169]

In vivo studies demonstrated that the conjugates possessed anti-tumour activity in multiple xenograft models of Hodgkin's lymphoma, non-Hodgkin's lymphoma, and acute myeloid leukaemia. Tumour regression was observed with single doses as little as 3 mg/kg in the L540cy xenograft model, whilst a weekly dosage regime could

increase the durability of the regression. Their study found that at lower doses of conjugate an initial decrease in NAD levels was observed, but they subsequently rose again. This suggests sustained inhibition is required for cell death, a phenomenon that has already been observed with free NAMPT inhibitors. Although conjugation to an antibody increases the circulation half-life and may give increased exposure to an inhibitor, the requirement for rapid and significant drug exposure may limit this technology to antigens with high surface expression, or rapid internalisation. Additionally this may require increased dosages, which could decrease the tolerability of the conjugate. Toxicology investigations revealed very few toxic effects compared to the free inhibitors. Notably absent were retinal and cardiac degeneration, effects commonly seen with NAMPT inhibition that are thought to limit their use in humans, and thrombocytopenia, the likely dose-limiting toxicity for untargeted NAMPT inhibitors in humans.[165]
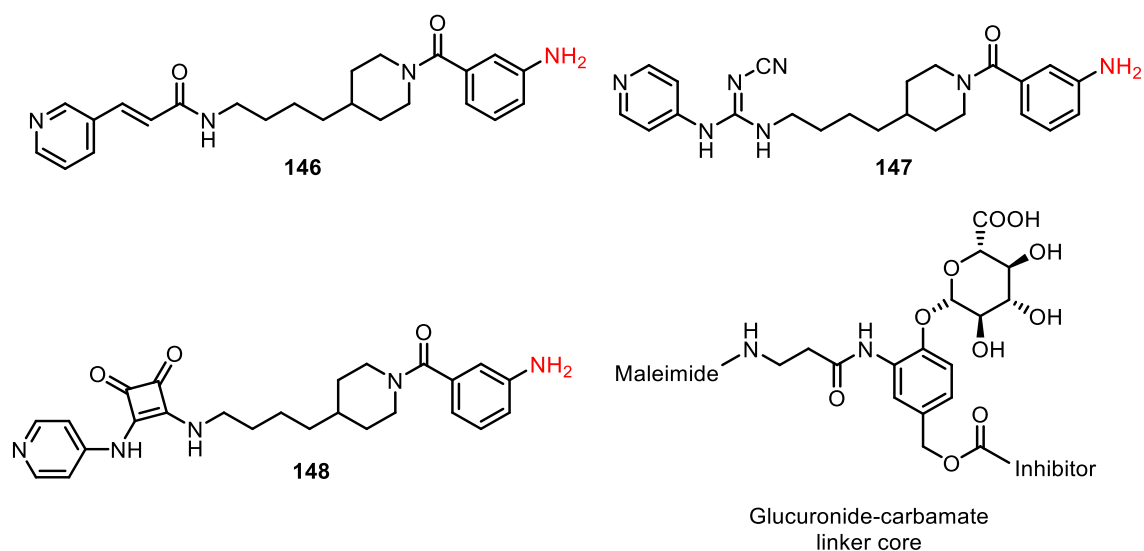
Figure 2.13 Top, and bottom left: Chemical structures of the NAMPTi payloads used by Seattle Genetics to generate their ADCs. Anilines for linker attachment shown in red. Bottom right: Chemical structure of the glucuronide-carbamate linker core, designed to cleave after internalisation.

Finally in 2022 a team from Bayer developed NAMPTi-ADCs based on the payload **149**.[171] For their proof-of-concept studies they conjugated this molecule to antibodies that target C4.4a (a glycolipid-anchored membrane protein), HER2, and B7H3 (the

immune checkpoint protein CD276). As previous studies they also produced a non-targeted control ADC with an isotype control antibody.

A range of linkers were screened, including the cleavable valine-alanine linker and a number of non-cleavable linkers. All ADCs produced showed low levels of aggregation and had DARs ranging from 2.2 to 7.8. Their best performing ADC was with an anti-B7H3 antibody and non-cleavable linker. It had an excellent EC_{50} of 6.9 pM for cell viability in THP-1 cells (a human monocytic leukaemia B7H3$^+$ cell line). As Karpov *et al.* had seen, the Bayer team saw non-specific effects on cell viability. For example the isotype-control ADC had an EC_{50} of 85 pM in THP-1 cells with one of the non-cleavable linkers.

They investigated the *in vitro* metabolism of their conjugates to attempt to understand where the non-specific effects were coming from. They observed the formation of cytotoxic metabolites with intact linkers with both the targeted ADC and isotype control, which led them to conclude payload deconjugation *via* a retro-Michael reaction at the maleimide was contributing significantly to the off-target effects. To remedy this they modified the way in which they conjugated the payload-linker to the antibody. The initial conjugation still proceeded *via* a thio-Michael addition to a maleimide, but once this had occurred they opened the resulting succinimide in basic conditions. This afforded a negatively charged open-chain succinic amide (**150**), which could no longer undergo a retro-Michael to release the cytotoxic payload. Using this new linker design, the targeted ADCs retained their high potency in appropriate cell lines, but the isotype control potency was significantly reduced. For example their new isotype control ADC had an EC_{50} of 30 nM in THP-1 cells, compared to the original 85 pM EC_{50} with the cyclic succinimide linker structure. This work highlights that through careful analysis and optimisation NAMPTi-ADCs can be designed as effective, safe, and selective drug candidates.
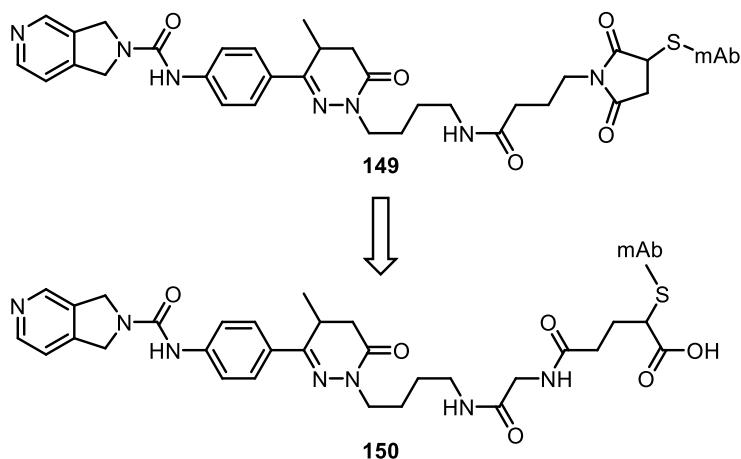
Figure 2.14 Evolution of payload-linker structures developed by Böhnke et al. at Bayer. The move from a cyclic succinimide to an open chain version significantly reduced payload deconjugation and increased the selectivity of the ADCs and correspondingly the therapeutic window.

2.3   PROTACs

Proteolysis-targeting chimeras (PROTACs) are hetero-bifunctional molecules that can induce degradation of a target protein by hijacking the ubiquitin-proteasome system (UPS). The UPS is constantly degrading proteins under normal physiological conditions and is one of the ways cells regulate protein levels. The process proceeds via two steps: first, the protein to be degraded is tagged with ubiquitin, a small (8.6 kDa) protein. The 26S proteasome then recognises the tagged protein and degrades the protein.[172]

In order to tag the substrate protein for degradation, a series of ubiquitin ligases are employed. E1 ligases activate the C-terminal Gly residue of ubiquitin by forming a thioester with a Cys residue on the E1 surface. The ubiquitin then transfers to an E2 ligase, forming another activated thioester intermediate. An E3 ligase then simultaneously binds the E2 and the substrate protein, facilitating the transfer of ubiquitin from the E2 to the substrate. This can either occur directly or via an E3-ubiquitin intermediate. A polyubiquitin chain is then synthesised in successive ligation reactions. In certain contexts E4 ligases have been described, which have roles in elongating the chain.[172,173]
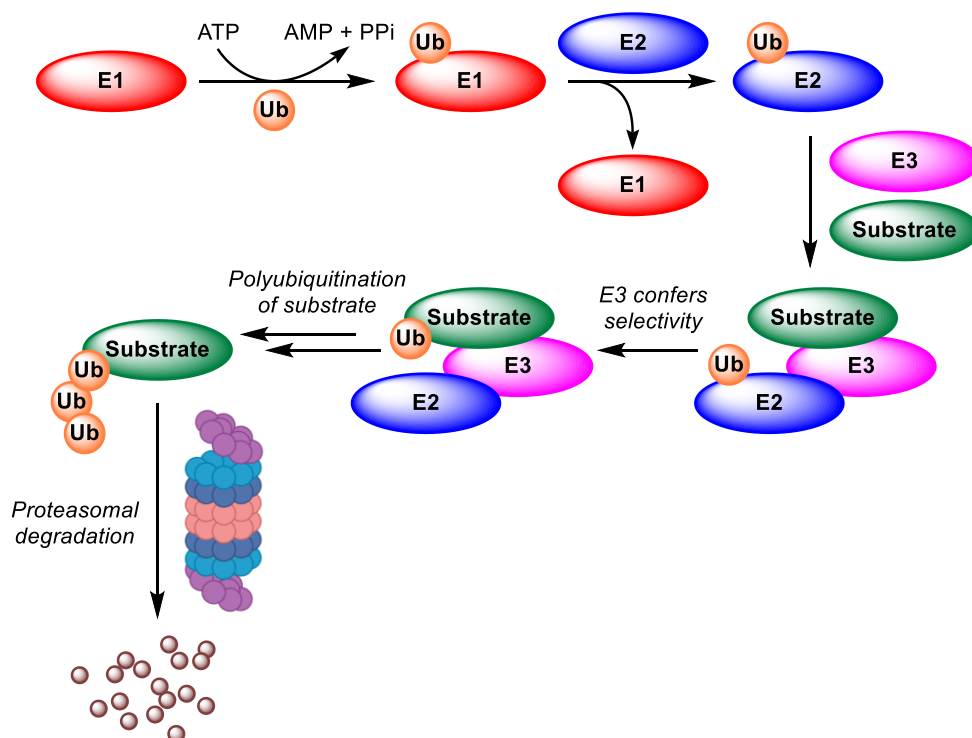
Figure 2.15 Cartoon representation of the ubiquitination process, leading to proteasomal degradation. Ub: ubiquitin, ATP: adenosine triphosphate, AMP: adenosine monophosphate, PPi: pyrophosphate.

The different ligases have differing degrees of substrate selectivity. E1 ligases activate ubiquitin for all modifications and transfer it to an E2. The E3 is the component that confers protein substrate specificity, with specific E3 ligases typically recognising multiple proteins of the same family that share structural similarities. E3 ligases only recognise their substrates if specific criteria are met, for example the substrate has adopted a particular conformation or has been subject to a post-translational modification, such as phosphorylation. This allows the UPS to degrade proteins in response to certain stimuli, transduced through the state of the substrate.[172]

PROTACs are made up of a ligand that binds to the protein of interest (POI), an E3 ligase ligand, and a linker to connect the two ligands.[174] When the PROTAC simultaneously binds both the POI and E3 it forms a ternary complex. This mimics the natural substrate recognition of the E3 and prompts the ubiquitination cascade as described above. The POI is ubiquitinated, then the ternary complex breaks down releasing the tagged POI and the PROTAC. The proteasome then degrades the POI and the PROTAC is free to initiate degradation for another target protein molecule.
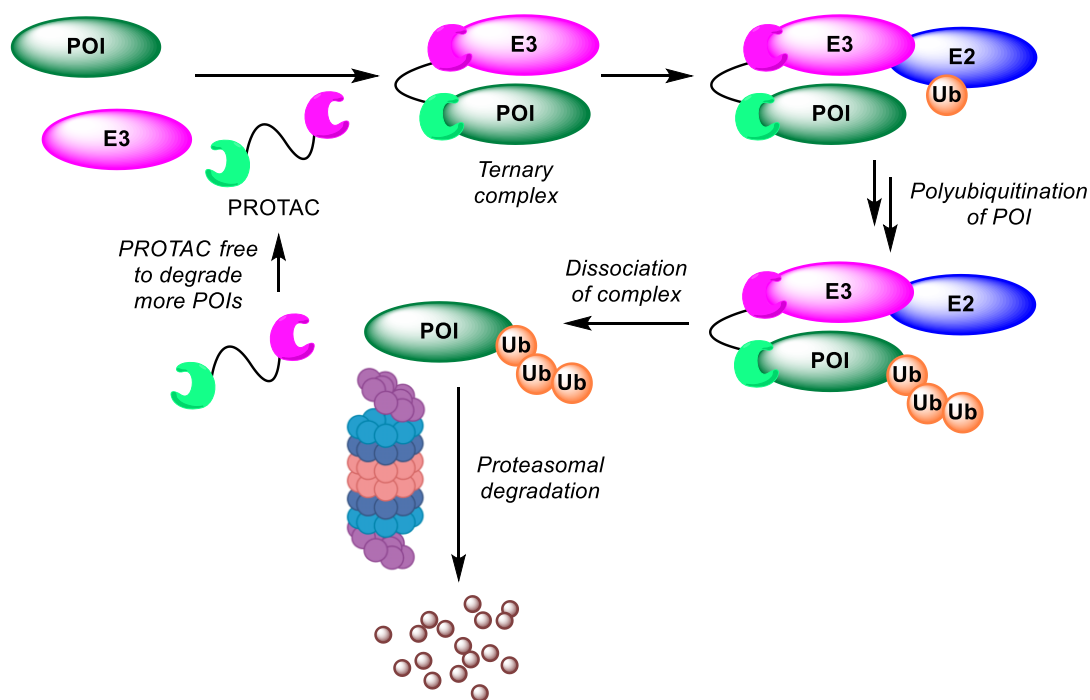
Figure 2.16 Cartoon representation of PROTAC mechanism of action to degrade a protein of interest (POI). Ub: ubiquitin.

The ternary complex formed between the PROTAC, POI, and E3 ligase is of critical importance to the PROTAC's efficacy. If this complex is insufficiently stable the POI will not be ubiquitinated and no degradation will occur. The stability of this complex is not only determined by the binding of the ligand parts of the PROTAC, but of the POI and E3 ligase interactions, mediated by the linker. These interactions are known as protein-protein interactions (PPIs) and are the interactions that should be optimised during PROTAC development.

2.3.1 Event-driven pharmacology

The regime of PROTAC degradation, where one PROTAC molecule can induce the degradation of multiple target protein molecules, is known as "event-driven pharmacology" and means that extremely high degradation potencies can be achieved with PROTACs,[175] even though their cell permeability is often very poor due to their size and high molecular weight. In comparison with the "occupancy-driven pharmacology" of small molecule inhibitors, this in principle allows for PROTACs to target proteins previously considered "undruggable". Proteins with shallow, ill-defined binding pockets prove difficult to develop inhibitors for – the lack of binding

interactions means inhibitors are unlikely to engage the target for the extended periods of time necessary.[176] Conversely as only a transient interaction is required for a PROTAC to induce ubiquitination and subsequent degradation, PROTACs stand a much better chance of producing a therapeutically useful effect.[177]

The extremely high potencies achievable with PROTACs mean it's possible to reduce the systematic drug exposure, which can reduce the risk of off-target adverse effects.[178] The chances of off-target effects are further mitigated by the fact that PROTACs, in certain cases, can show degradation selectivity that exceeds the inhibition selectivity of the parent POI inhibitor.[179,180] Even if the PROTAC engages with structurally similar proteins the ternary complex formed may not be stable enough to result in ubiquitination and degradation. This can be modulated with the choice of linker and/or E3 ligase used, offering a way to further tune the selectivity of the system.

Treatment with small molecule inhibitors can result in feedback loops increasing target expression, leading to an overall loss in activity.[181] If PROTAC therapy is combined with small molecule treatment, a synergistic effect can be obtained: degrading the target protein not only reduces the total number of targets that need to be inhibited, but it can counteract the overexpression of the target that may result from loss of target function.

Mutation-based resistance is another challenge that small molecule inhibitors face. Especially in cancer-associated genes, mutations can occur that lead to changes in the active site of proteins that reduces or destroys the binding capability of the inhibitor.[182–184] The transient nature of PROTAC target engagement means they have the potential to degrade mutated proteins in addition to wild-type. For example, Bruton's tyrosine kinase (BTK) is a target of interest for chronic lympocytic leukaemia. The inhibitor ibrutinib is used to treat the leukaemia, but the C481S mutation that occurs in >80% of patients leads to resistance developing. The BTK-targeting PROTAC MT-802 targets both wild type and mutant BTK for degradation, whilst binding fewer off-target kinases than the parent ligand ibrutinib.[185] Also in 2018 another PROTAC was developed that targeted BTK, which also affected the degradation of both wild

type BTK and the C381S mutant, albeit with a slightly lower DC_{50} for the mutant.[186] Targeted protein degradation clearly has an advantage over inhibition in these situations, especially considering that a potential mutation doesn't even need to be known/characterised for the PROTAC to still target it. Conversely, a whole new campaign to design an inhibitor would have to be undertaken to target the mutant.

Overall the advantages of the PROTAC event-driven regime can result in better performance than the corresponding small molecule inhibitors when inhibiting the proliferation or inducing the apoptosis of cancer cells.[187] For example, the VHL-recruiting c-Met degrader designed by Crews *et al.* inhibited the proliferation of GTL16 cancer cells with an IC_{50} = 66.7 nM, whereas the inactive diastereomeric PROTAC only inhibited proliferation with an IC_{50} = 156 nM.[188] The inactive PROTAC would be expected to act simply as an inhibitor, showing that degradation can be advantageous to inhibition in addressing cancer progression.

2.3.2 Early PROTACs

The first fully synthetic PROTAC, known as Protac-1 (**151**), was published in 2001 by Sakamoto *et al.*[189] and targeted methionine aminopeptidase 2 (METAP2), a metalloenzyme that removes *N*-terminal methionine residues from proteins.[190] Inhibition of METAP2 is known to limit angiogenesis, the creation of new blood vessels, and consequently inhibitors of the enzyme have been explored as anti-cancer agents.[191–193] Protac-1 consisted of the METAP2 ligand ovalicin and 10-amino acid sequence that binds to the E3 ligase β-transducin repeat-containing E3 ubiquitin-protein ligase (β-TRCP) joined by a linker. Simultaneous binding to both METAP2 and β-TRCP resulted in Protac-1-dependent ubiquitination and subsequent degradation of METAP2 in *Xenopus* egg extracts.

R = DRHDSGLDSM
Protac-1, **151**
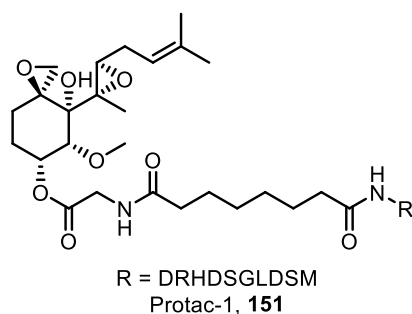
*Figure 2.17 Protac-1 (**151**), the first synthetic PROTAC. It targeted METAP2 for degradation by recruiting the E3 ligase β-TRCP.*

Soon after, a binder for the E3 ligase von Hippel-Lindau tumour suppressor (VHL) was discovered. This binder was an amino-acid sequence derived from the transcription factor hypoxia-inducible factor 1 subunit alpha (HIF-1α). Under normoxic conditions HIF-1α is hydroxylated by prolyl hydroxylases at Pro402 and Pro564. This enables recognition by VHL, leading to polyubiquitination and proteosomal degradation. Under anoxic conditions the hydroxylation ceases and HIF-1α is no longer recognised and degraded. It reaches the nucleus, where it increases the expression of genes involved with a hypoxic response.[194,195] Through point mutations and the testing of truncated sequences, it was found that stereoselective *trans* hydroxylation of the proline residue at position 564 was crucial for successful binding.[196,197]

In 2004 Crews' group then used a peptide derived from the HIF1 sequence (ALAPYIP) to generate PROTACs that recruited the VHL E3 ligase to mediate the ubiquitin-proteasome system (UPS) degradation of target proteins.[198] By linking the VHL-binding peptide to ligands for FKBP12 (a prolyl isomerase) and androgen receptor, they saw degradation of green fluorescent protein-fused versions of the proteins. Finally, a poly-arginine tag was added to the peptide sequence to increase the cell permeability of the compounds. The inclusion of this tag had been shown to increase uptake into cells, by a mechanism mimicking that of HIV trans-activator of transcription (Tat) proteins.[199] This illustrates a challenge that has persisted with PROTAC research: cell permeability. Through their sheer molecular size (>500 as warned against by Lipinski), PROTACs often struggle to permeate into cells.

It should be noted that the peptide sequence used above doesn't contain hydroxyproline. The researchers envisioned that the PROTACs would enter the cell and be recognised and hydroxylated by a prolyl hydroxylase. The resulting peptide sequence including a Hyp residue would then bind to VHL and the UPS degradation would commence. This is in contrast to subsequent VHL binders that already include the hydroxyproline moiety.

2.3.3 Further development of VHL ligands

Although these early approaches were effectively laying the foundation for the field of PROTAC research, the peptide binders used to recruit VHL had very poor physicochemical properties, severely limiting the cell permeability of the final PROTACs. Attention turned to developing a small molecule VHL binder that would ideally have more drug-like properties, allowing the construction of PROTACs with improved physicochemical properties.[200]

Ciulli and Crews began to rationally design small molecules to bind VHL, building around a hydroxyproline core they hypothesised would maintain the key binding interactions that Hyp564 makes in HIF-1α.[201] After synthesising some computationally designed structures they identified **154** as a minimal pharmacophore binding with an IC$_{50}$ >250 μM, while smaller fragments failed to bind measurably. Through exploring the SAR on the right-hand side of the molecule, they arrived at compound **155** which exhibited binding with an IC$_{50}$ = 4.1 μM. The site and mode of binding of **155** was the same as for HIF-1α and VHL as expected, as determined by the co-crystal structure.
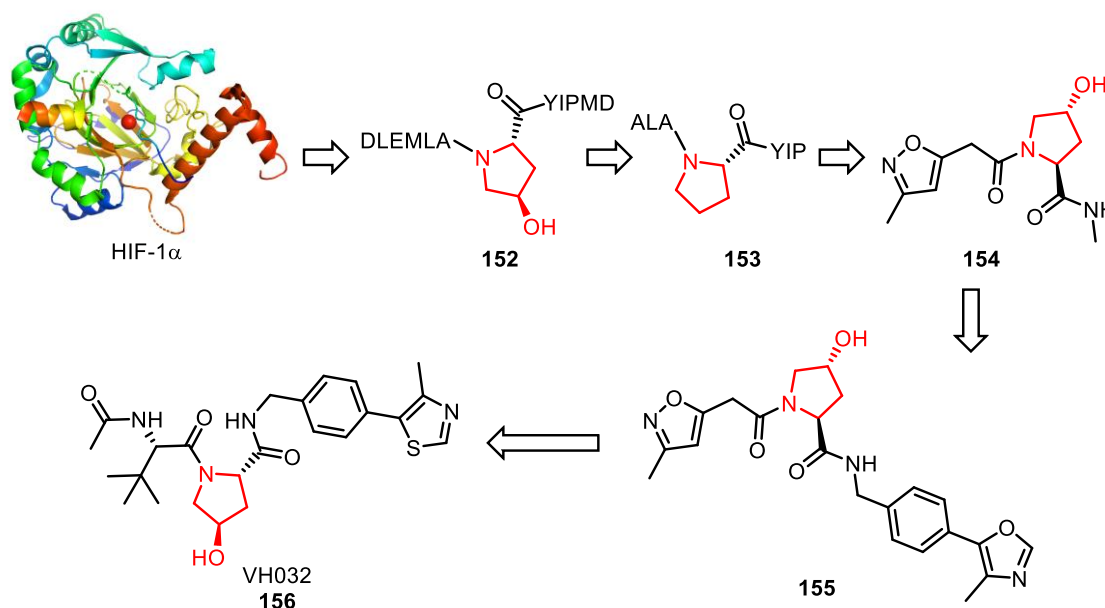
Figure 2.18 Evolution of small molecule VHL binders from HIF-1α, with the key hydroxyproline binding moiety shown in red.

Binding affinity was measured by fluorescence polarisation (FP), a technique that investigates ligand-protein interactions by competing the test ligand against a known ligand. The known ligand is tagged with a fluorescent probe. When the tagged ligand is free in solution, it tumbles rapidly. If the fluorophore is irradiated with plane-polarised light, the rapid tumbling of the fluorophore means it emits light in lots of different polarisation planes, giving overall unpolarised emission. When the fluorophore-ligand is bound to the protein of interest, however, the increase in MW of the complex leads to much slower rotation and tumbling in solution. When the complex is irradiated with plane-polarised light, the fluorophore now emits in mostly the same plane as the radiation source. When the test ligand competes with the known fluorophore-ligand, the extent of binding of the test ligand will correlate with the amount of known fluorophore-ligand free in solution. The extent of polarisation of the emitted light upon irradiation can then be measured and used to deduce the amount of free fluorophore-ligand in solution. This then allows the extent of binding of the test ligand to be calculated and an IC_{50} calculated.

Two years later, in 2014, Ciulli published further optimisation of the hydroxyproline-based small molecule ligands. Addition of a *t*-Bu group gave an increase in binding

affinity due to the exploitation of a new lipophilic binding pocket, and replacing the methylisoxazole with a methylthiazole further boosted binding affinity to arrive at VH032 (**156**), the first VHL ligand more potent than the model peptides based on HIF-1α.[202] VH032 (**156**) now forms the basis for the vast majority of VHL-recruiting PROTACs and variants of it are available commercially.
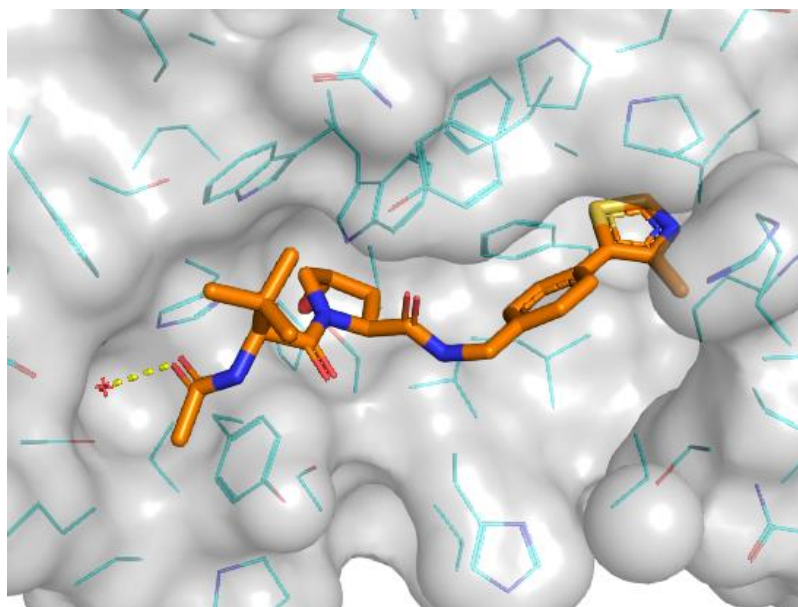
*Figure 2.19 VH032 (**156**) in complex with VHL, showing a key hydrogen bond interaction with water of crystallisation. PDB = 4W9H.*

An example of a VHL-based degrader is MZ1 (**157**), developed by the Ciulli Group.[180] MZ1 targets bromodomain-containing protein 4 (BRD4) and is based on the small molecule inhibitor JQ1 (**158**). BRD4 has been identified as a therapeutic target in acute myeloid leukaemia and ovarian carcinoma, among others, making it an attractive target for protein degradation. As JQ1 is not specific to BRD4 and inhibits its paralogues BRD2 and BRD3, it was surprising when MZ1 exhibited excellent selectivity for degrading BRD4 alone. Moreover, a different pharmacological response was observed when BRD4 was selectively degraded, compared to global inhibition using JQ1. These observations are good examples of how PROTACs can be used to complement existing small-molecule drugs and tune the effects of treatments to exactly what is needed.
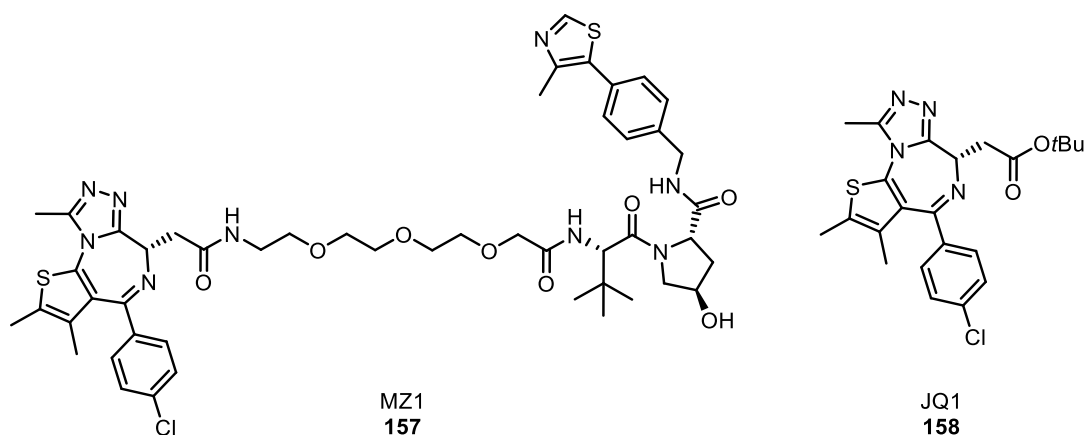
Figure 2.20 The VHL-recruiting PROTAC MZ1 and the BRD4 inhibitor JQ1 on which it's based.

2.3.4 Cereblon ligands

The teratogenic effects of thalidomide (**159**) that arose when it was prescribed to treat morning sickness are well known and often used to illustrate the importance of chirality to chemistry students.[203,204] In 2010, decades after the birth-defect crisis, the protein target of thalidomide was found. It binds to cereblon, a protein that forms an E3 ubiquitin ligase complex together with damaged DNA binding protein 1 (DDB1), Cullin-4A (CUL4A), and regulator of cullins 1 (ROC1).[205]

| Thalidomide | Lenalidomide | Pomalidomide |
| **159** | **160** | **161** |
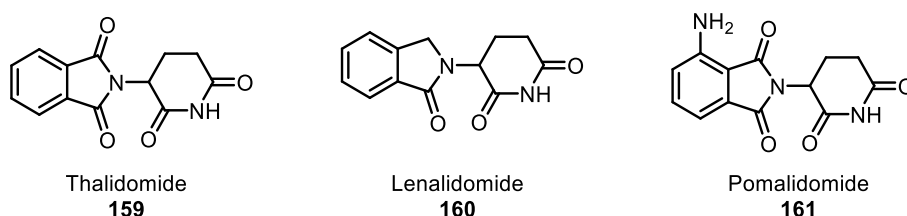
Figure 2.21 Thalidomide and its analogues, known as IMiDs, bind to the E3 ligase cereblon and have been used extensively as the basis for PROTAC development.

Despite the dangers of thalidomide if given to pregnant women, the drug has since been used in attempts to treat a number of different conditions, such as erythema nodosum leprosum (a painful complication of leprosy),[206] Crohn's disease,[207,208] HIV,[209,210] and numerous cancers.[211–217] Once the target of thalidomide and its analogues, known as immunomodulatory imide drugs (IMiDs, figure 2.21) was

144

identified as an E3 ligase, they began to be extensively and successfully used as platforms for PROTAC development.

One such example of a successful CRBN recruiting PROTAC comes from Jin *et al.* in 2020 and degrades epidermal growth factor (EGFR) effectively and selectively.[218] EGFR is a transmembrane protein tyrosine kinase that has a role in regulating cell proliferation, metastasis, apoptosis, and angiogenesis. Many cancers can result from the overexpression, mutation, or amplification of the EGFR gene and as such EGFR has been thoroughly investigated as a therapeutic target. A number of small molecule inhibitors have been developed, but resistance to these can develop as a result of EGFR mutation (specifically T790M). New inhibitors such as afatinib and dacomitinib were developed to target the mutant form, but suffered from extensive side effects owing to their continued activity against wild-type EGFR. Jin *et al.* chose gefitinib as the EGFR ligand on which to base their PROTACs and developed a series of compounds. Their best-in-class CRBN based PROTAC (**162**) possessed a DC_{50} = 11 nM in H3255 cells and DC_{50} = 25 nM in HCC-827 cells (both lung adenocarcinoma). The PROTAC also stopped the proliferation of H3255 and a global proteomic analysis determined that the compound was highly selective for EGFR.

162
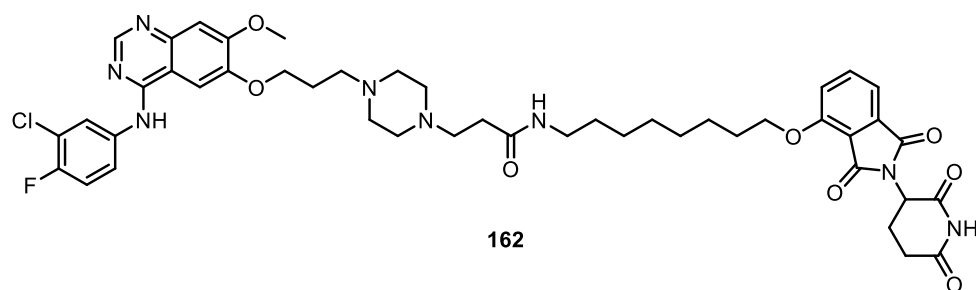
Figure 2.22 Jin et al.'s CRBN based EGFR PROTAC.

2.3.5 PROTACs in the clinic

In 2019, 18 years after the first fully synthetic PROTAC was published, protein degraders entered clinical trials.[219] ARV-110 and ARV-471, both developed by Arvinas, target the androgen receptor (AR) and estrogen receptor (ER), respectively.

The phase 1 testing of ARV-110 was undertaken in patients with metastatic castration resistant prostate cancer (mCRPC), who had already been treated with either

enzalutamide or abiraterone (two existing, approved therapies for mCRPC). This heavily pre-treated subset of patients has limited options of therapies as the usual anti-androgenic therapies often used to treat prostate cancer have little impact on the progression of mCRPC.[220] ARV-110 showed good tolerability and was tested in doses up to 700 mg, with 420 mg being the recommended phase 2 dose.[221] Trial data also showed PROTAC-mediated degradation of the target protein in tumours, and demonstrated the hallmarks of early anti-tumour activity.[220] Clinical activity was greatest in patients with certain AR mutations, possibly indicating a further subpopulation for which ARV-110 could be extremely effective. Trials are ongoing and expected to conclude in late 2023.[222]

ARV-471 was initially tested as a monotherapy in patients with ER$^+$/human epidermal growth factor 2 negative (HER2$^-$) locally advanced or metastatic breast cancer, who had again received extensive pre-treatment including hormonal therapy and chemotherapy.[223] ARV-471 was tolerated acceptably and showed a 42% clinical benefit rate in the heavily pre-treated population.[220] ARV-471 is also now being tested as part of a combination therapy with palbociclib.[223]

Although these trials are still ongoing, the results released are positive. Before this nothing was known about how PROTACs might act in the human body, if they were sufficiently drug-like, or even if they would be safe. ARV-110 and ARV-471 have shown us that PROTAC technology has the potential to generate safe and effective pharmaceuticals and have opened the door to further developments in the field. As such a number of degraders have since entered clinical trials targeting a number of different proteins, mainly concentrated within oncology (see table 2.2).

146

Degrader	Target	Disease area	Company	Trial phase	Trial start
ARV-110[222]	AR	Prostate cancer	Arvinas	1/2	2019
ARV-471[223]	ER	Breast cancer	Arvinas/Pfizer	1/2	2019
AC682[224]	ER	Breast cancer	Accutar Biotech	1	2021
ARV-766[225]	AR	Prostate cancer	Arvinas	1/2	2021
CC-94676[226]	AR	Prostate cancer	Bristol Myers Squibb	1	2020
DT2216[227]	BCL-x$_L$	Liquid/solid tumours	Dialectic Therapeutics	1	2021
FHD-609[228]	BRD9	Synovial sarcoma	Foghorn Therapeutics	1	2021
KT-474[229]	IRAK4	Autoimmune diseases	Kymera/Sanofi	1	2021
KT-413[230]	IRAK4	Diffuse large B cell lymphoma	Kymera	1	2022
KT-333[231]	STAT3	Liquid/solid tumours	Kymera	1	2022
NX-2127[232]	BTK	B cell malignancies	Nurix Therapeutics	1	2021
NX-5948[233]	BTK	B cell malignancies/ autoimmune diseases	Nurix Therapeutics	1	2022
CFT8634[234]	BRD9	Synovial sarcoma	C4 Therapeutics	1/2	2022

Table 2.2 Some heterobifunctional PROTACs in clinical trials as of 2022. AR: Androgen receptor, ER: Estrogen receptor, BCL-x$_L$: B-cell lymphoma-extra large, BRD9: Bromodomain-containing protein 9, IRAK4: Interleukin-1 receptor-associated kinase 4, STAT3: Signal transducer and activator of transcription 3, BTK: Bruton's tyrosine kinase.

2.3.6   Design

2.3.6.1   Ligand selection

The initial step in designing a PROTAC involves selecting ligands that can bind to both the protein of interest (POI) and an E3 ligase. In cases where the POI is a frequently targeted treatment, there are likely to be published and optimised inhibitors that

could be suitable for PROTAC design. However, if such inhibitors are not available, it becomes necessary to develop a small molecule that can bind to the POI. While numerous E3 ubiquitin ligases have been proposed to function in human cells, only a limited number of them have effective ligands documented in the literature. Historically, E3 ligases have been perceived as challenging targets to address, which accounts for the scarcity of available ligands.[235] The most commonly utilised ligases for PROTAC design are the VHL E3 complex and the CRBN E3 complex. It is presently impossible to predict which ligases will or will not yield effective degraders. Furthermore, it remains uncertain whether optimal target-E3 pairs exist at all.[175]

The effectiveness of the ligase being recruited depends heavily on the specific context, making it wise to consider developing parallel series of PROTACs utilising different E3 ligases. For instance, CRBN PROTACs have demonstrated higher activity in certain cases, possibly due to the greater flexibility of the CRBN E3 complex in comparison to the VHL E3 complex which can allow for easier ubiquitination of lysine residues.[177] However, CRBN ligands also have the potential to cause off-target degradation which can lead to undesirable off-target effects.[236] Additionally, predicting protein-protein interactions (PPIs) within the target-E3 complex and determining whether they are beneficial or not is challenging due to their complexity. These PPIs have been identified as vital for the overall stability of the ternary complex, which is crucial for an effective degrader.[237]

Lai *et al.* demonstrated the significant impact of ligase selection on the activity of otherwise identical PROTACs.[179] In their study targeting the oncogenic tyrosine kinase BCR-ABL, they compared two PROTACs: one recruiting VHL and the other recruiting CRBN, both based on the known BCR-ABL ligand bosutinib. Surprisingly, the VHL-based PROTAC showed no degradation of the target, while the CRBN-based compound achieved over 80% BCR-ABL degradation at a concentration of 2.5 µM. This stark difference highlights the crucial role of ligase choice in PROTAC efficacy. The research also explored the influence of the POI ligand by varying it between two other established inhibitors: imatinib and dasatinib. Despite all resulting degraders exhibiting affinity values below 5 nM, only the dasatinib-based PROTAC displayed degradation activity. This comparison was only drawn among the VHL analogues.

These findings emphasise that optimising both the POI ligand and the recruited E3 ligase are equally important. Crucially they also demonstrate that comprehensive investigations can transform an inactive PROTAC into a highly effective compound.

While a strong affinity between the PROTAC and the POI does not always guarantee good activity, it is still important to maintain a high binding affinity for the POI ligand as this is a crucial contributor to the stability of the ternary complex. To achieve this, selecting an attachment point for the linker away from the POI's binding site and exposed to solvent is vital. Crystal structures of the ligand bound to the protein are essential in determining this optimal attachment point. Once an appropriate attachment point has been identified, an easily functionalised group is typically introduced, if not already present, to facilitate chemical conjugation. For example in VH032, a widely used VHL ligand, the acetamide group is often substituted with a free amine group, allowing simple amide bond formation to construct the PROTAC. It is worth noting that there are often multiple suitable attachment points available, providing an additional parameter that can be varied to optimise both degradation activity and selectivity. In VH032, conjugation can also occur through a thioether linkage originating from the *tert*-butyl group or a phenolic linkage, in addition to the terminal amide linkage (figure 2.23).[237,238] These alternative attachment points not only allow for different sites of linker attachment but also represent potential locations for additional derivatisation: this flexibility can be used to conjugate the PROTAC to other biomolecules, such as peptides or antibodies.
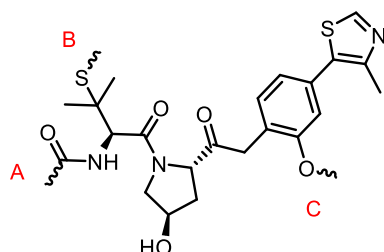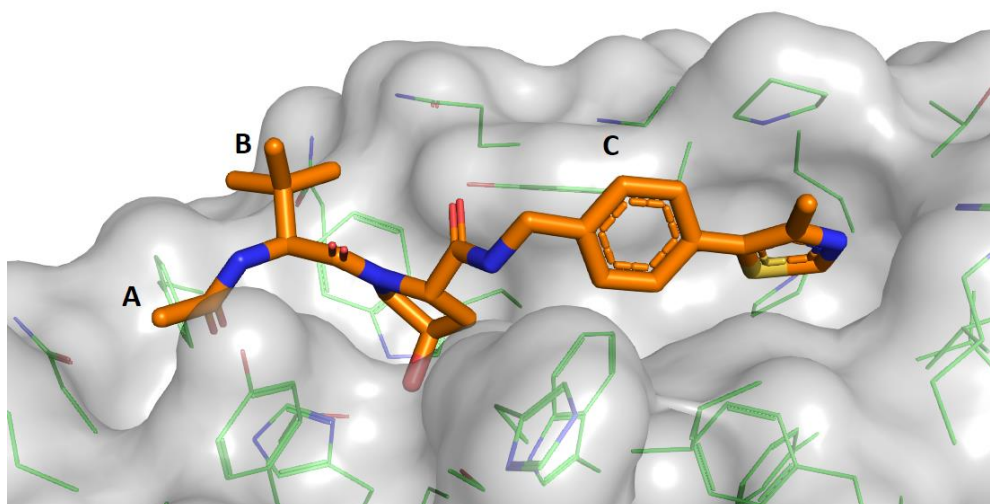
Figure 2.23 Above: Crystal structure of VH032 bound to VHL (PDB: 4W9H). The three potential attachment points can be seen pointing into solvent, labelled A (amide vector), B (tert-butyl vector), and C (phenolic vector). Below: Chemical structures identifying the three potential attachment points on VH032.

2.3.6.2 Linker

The PROTAC linker plays a critical role in the system and significantly impacts the compound's overall degradation capabilities. It directly influences the efficiency of ubiquitination by determining the proximity and relative orientation of the POI and the E3 ligase. Finding the right balance in linker length is crucial: if it is too long, the POI may be out of reach, whereas if it is too short, there may not be enough space for the formation of the ternary complex. The flexibility of the linker is also important in determining the accessible conformations the complex can adopt, as the flexibility determines the availability of lysine residues for ubiquitination. The fundamental substrate specificity of the optimum linker length means linker optimisation is done on a case by case basis.[239] At present, there is no evidence supporting the existence of a general optimum linker length. However, as our understanding of the factors

influencing the stability of the ternary complex expands, it is possible that predicting effective linker lengths and compositions may be possible.

Research by Zoppi *et al.* serves as an excellent illustration of linker optimisation leading to significant improvements in properties.[175] They focused on developing PROTACs targeting BRD9 and recruiting VHL E3, a pair previously considered "non-PROTACable." Through an extensive and iterative design and optimisation process, they established a structure-activity relationship (SAR) that enabled the design and synthesis of a series of degraders exhibiting excellent activity profiles, with the most promising candidate from their efforts demonstrated a DC_{50} value in the single-digit nanomolar range. Their degrader also showed activity against the closely related homologue, BRD7. While this may have potential benefits in an anti-cancer context, it highlights the challenge of achieving perfect selectivity with PROTACs.

Smith *et al.* recently highlighted the crucial role of linker design in achieving target selectivity.[240] Their work demonstrated the ability to selectively target specific isoforms within a protein family by manipulating the linker length and point of attachment on the E3 ligand, which directly influences the orientation of the E3 ligase in the ternary complex. To accomplish this, they utilised the kinase inhibitor foretinib, known for its pan-selectivity for the p38 MAPK family. By incorporating a VHL ligand, they successfully generated PROTACs capable of dual degradation activity against p38α and p38δ. Through single-atom modifications, they further identified degraders with enhanced selectivity for either the α or β isoform (figure 2.24). These findings underscore the significance of linker length and E3 ligase orientation in determining the selectivity of PROTACs, even when targeting structurally similar proteins within the same family.
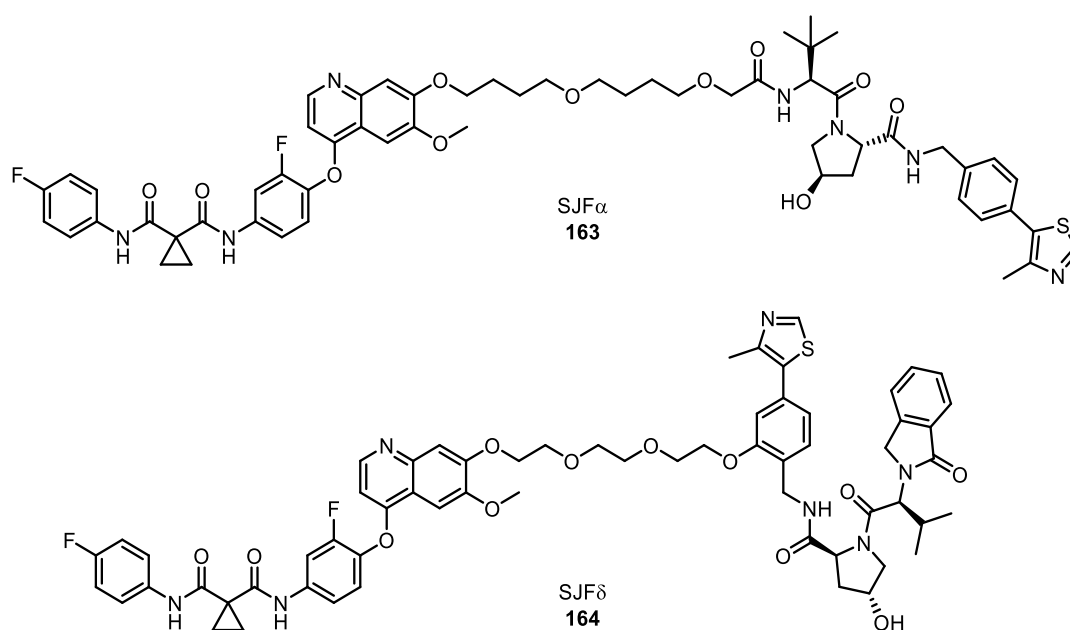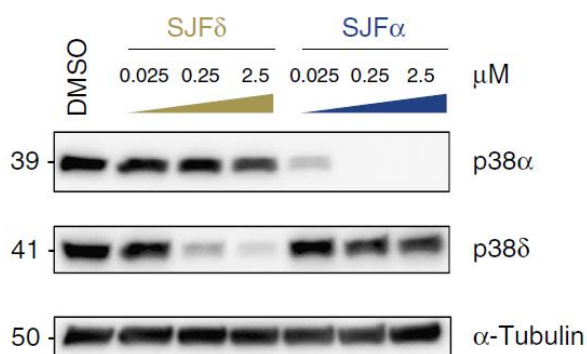
Figure 2.24 Above: Western blot showing the selective degradation of p38α and p38δ by the two degraders. Below: the two PROTACs designed by Smith et al. that share the same two ligands but differ in their p38 selectivity solely because of linker length, composition, and point of attachment on the VHL ligand. Figure reproduced unmodified from Smith et al. (2019).[240]

The composition of the linker in a PROTAC also contributes to the overall efficacy of degradation. Linkers are commonly constructed using polyethylene glycol (PEG) units, alkyl chains, or a combination of both. While alkyl chains can be sufficient for short linker lengths, as the length increases they tend to aggregate in aqueous solutions, resulting in a significant reduction in the distance between the POI and the E3 ligase. PEG linkers are more likely to adopt an extended conformation due to the presence of hydrophilic oxygen atoms that allow favourable interactions with the solvent when the chain is extended. Linker composition, as well as length, should therefore be considered during the design process.[239] Moreover, PROTAC linkers can also be utilised

to modulate the overall pharmacokinetic (PK) properties of the therapeutic. It's crucial to balance PK properties with the activity profile of the compound, however, to avoid developing a drug with excellent PK properties but no therapeutic activity.

In 2017 Gadd *et al.* solved the first crystal structure of a ternary complex between the POI, PROTAC, and E3 ligase.[237] The system they were investigating was their degrader MZ1, which targets BRD4 and recruits VHL. In the crystal structure they observed the PROTAC folding on itself, allowing the ternary structure to adopt a stable conformation. This folding allows burial of extensive surface area and formation of new PPIs that contribute to the stability of the complex. This work marks an important development in our understanding of the factors that confer a PROTAC with its efficacy, or lack thereof: previous strategies largely revolve around a "plug and play" approach, where a panel of linkers is screened and the optimum one is determined empirically. Although this has led to the synthesis of many effective degraders, rationally designing them based on ternary complex crystal structures is a more efficient approach. This has the obvious caveat, though, that obtaining crystal structures isn't always easy, and empirically selecting a linker may actually be quicker and cheaper in many instances. Although obtaining crystal structures may not always be easy or possible, the seminal crystal structure obtained here clearly shows the linker must be considered as more than just a piece of string of varying length holding the PROTAC together; it has a much more significant role in forming and allowing PPIs that contribute significantly to the stability of the ternary complex, and hence the degradation potential of the PROTAC.
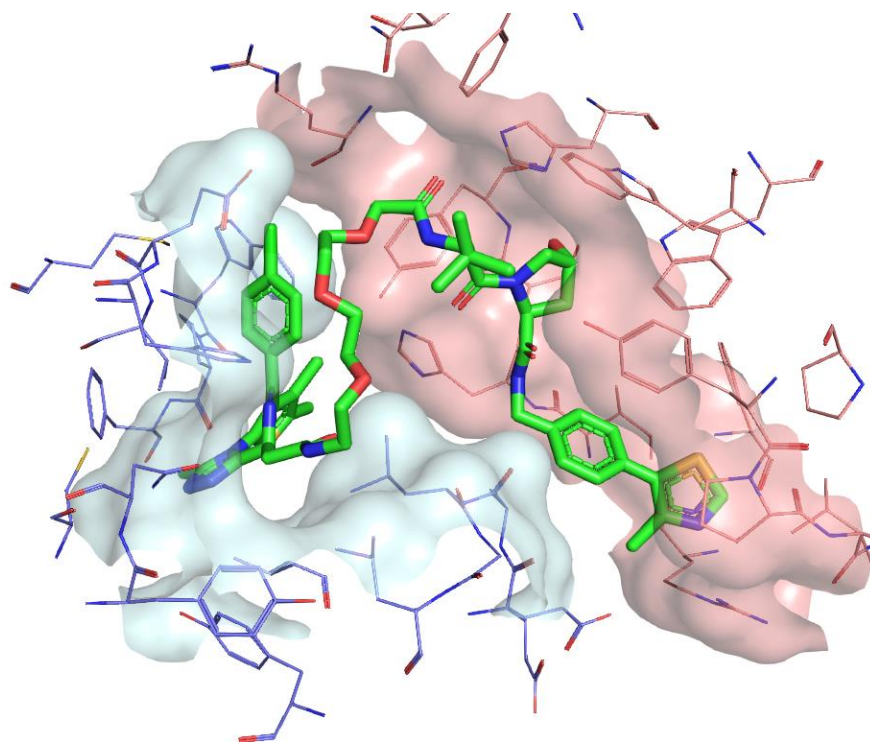
Figure 2.25 Crystal structure of MZ1 (green) in complex with BRD4 (blue) and VHL (peach). The PROTAC can be seen occupying a folded state, maximising PPI and protein-ligand interactions. PDB = 5T35.

2.3.7 PROTAC-antibody conjugates

While conventional small molecule cytotoxins remain the predominant payloads used in modern ADCs, there has been a recent interest in incorporating PROTACs as alternative payloads. PROTACs possess efficient degradation properties but lack tissue selectivity since the E3 ligases they recruit are widely expressed across tissues.[241] Targeting tissue-specific E3 ligases presents a significant challenge, although research into this questions is ongoing and some examples of tissue-specific E3 ligases are beginning to emerge.[220] The current lack of tissue-specific E3 ligases can, however, be overcome by instead achieving tissue selectivity through conjugation to an antibody.

Conjugating PROTACs to antibodies represents a good match for these technologies. PROTACs can achieve spectacularly high potencies, making them well-suited ADC payloads. And the excellent targeting possible with ADCs compensates for the lack of specificity achievable with current PROTAC technology, in addition to providing a way to overcome the often middling cell permeability of large MW PROTACs.

Additionally, as discussed in the context of Enhertu in section 1.5.1, PROTACs represent a class of ADC payload with a completely distinct mechanism of action.[105] The superb potencies they can achieve also make them a promising class of payload to develop treatments for cancers with low antigen expression, as a meaningful therapeutic effect could be achieved as a result of fewer conjugates entering cells.

Maneiro *et al.* used trastuzumab, a HER2-targeting antibody that has demonstrated success in the treatment of breast cancer with Kadcyla, to investigate the potential of mAb-PROTAC conjugates.[241] They opted for a BRD4 degrader as the payload, due to its well established role in inflammation and cancer. The structure of their degrader was based on the published MZ1 PROTAC that targets BRD4 and recruits the VHL E3 complex.

An azido PEG unit was attached to the PROTAC through an ester linkage off the OH group in the central hydroxyproline moiety. This strategy means the PROTAC is rendered inactive, as the hydroxyproline is critical for VHL binding, until the ester linkage is hydrolysed during lysosomal degradation of the conjugate. On the antibody side cysteine rebridging was employed to introduce a novel dibromomaleimide strained alkyne linker, installing precisely four conjugation handles per antibody. The linker-payload was then connected to the antibody using a strain-promoted alkyne-azide cycloaddition (SPAAC), successfully producing the mAb-PROTAC conjugate without the risk of copper contamination.

In vitro experiments demonstrated the degradation of BRD4 in HER2$^+$ cell lines when treated with the mAb-PROTAC conjugate at a concentration of 100 nM, resulting in nearly complete degradation after four hours of incubation. Conversely, no degradation of BRD4 was observed in HER2$^-$ cell lines confirming the selective delivery of the PROTAC to the intended targets.
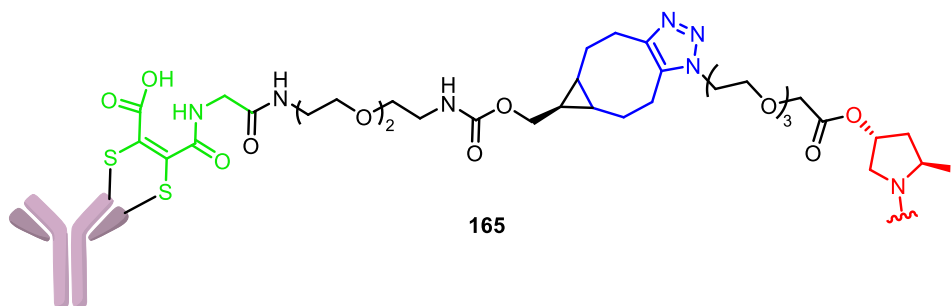
Figure 2.26 Structure of Maneiro et al.*'s mAb-PROTAC conjugate. Green: cysteine rebridging mAb conjugation site. Black: linker. Blue: SPAAC triazole product. Red: hydroxyproline of VHL binding part of the PROTAC payload.*

Pillow *et al.* took a similar approach to address the limitations in the physico-chemical and pharmacokinetic properties of a BRD4 PROTAC they had developed.[242] Their degrader, which was also based on JQ1 and recruited VHL, exhibited enhanced degradation compared to MZ1. To achieve this they functionalised the degrader at the same free hydroxyl position, but instead of an azide they attached a methanethiosulphonyl (MTS) disulphide. These MTS disulphide groups effectively reacted with cysteine residues on the surface of engineered antibodies, forming disulphide bonds to connect the linker-payload to the mAb. Remarkably, despite the high lipophilicity of the linker-drug component, mAb-PROTAC conjugates with a loading of six were successfully prepared without significant aggregation issues. This higher DAR has the potential to increase the concentration of active PROTACs within cells, surpassing similar conjugates with lower DARs. The research team extensively tested the conjugate in rodent xenograft models and observed that a single intravenous dose provided sustained exposure, leading to antigen-specific tumour regressions.

Dragovich *et al.* built upon the previous design discussed above, focusing on degrading oestrogen receptor alpha (ERα).[243] They explored two different degraders and three distinct ADC linker approaches. The PROTACs recruiting the XIAP E3 ligase were connected to the Val-Cit linker using either a carbamate on the XIAP ligand or a phenolic ether on the ERα ligand. For the VHL recruiting degraders they once again used the hydroxyproline OH as a conjugation vector, attaching them through either a disulphide-containing carbonate or a maleimide-containing phosphate linker. Similar

to the study conducted by Pillow *et al.* the anti-HER2 antibody was engineered to incorporate free cysteines. These cysteines formed disulphide links to the degrader, as in the previous study, or reacted with the linker maleimide through a conjugate addition. The researchers observed the delivery of PROTACs to be dependent on the presence of the target antigen, and collected data supporting their hypothesis that conjugation to antibodies can enhance the properties of PROTACs.

166
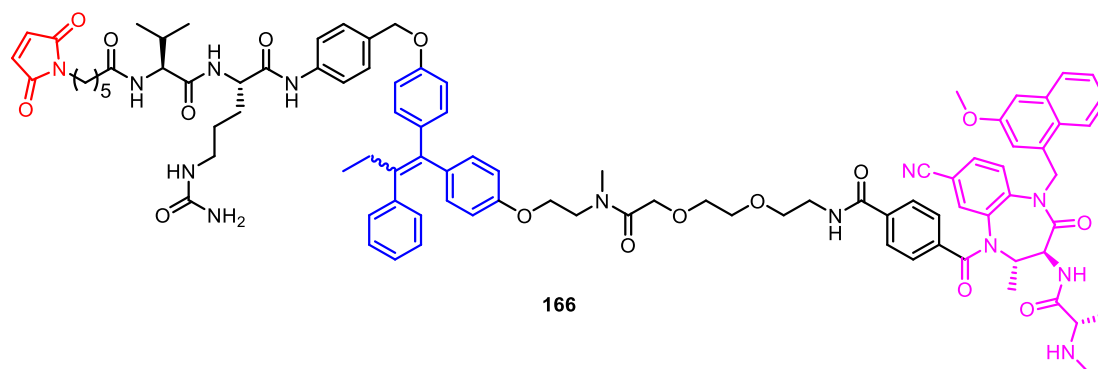
Figure 2.27 An example of a linker-payload compound designed by Dragovich et al. Red: maleimide for mAb conjugation. Black: linker. Blue: ERα ligand. Purple: XIAP ligand.

2.4 Aims

NAMPT is a promising target for cancer therapy, and NAMPT inhibitors have demonstrated significant anti-cancer properties. They have also been associated with a number of on- and off-target toxic side effects, significantly limiting their application. NAMPT inhibitor ADCs have alleviated some of these toxicity issues by allowing the targeted delivery of these inhibitors to cancer cells, with promising results.

The development of NAMPT PROTACs would represent a novel approach to targeting NAMPT for cancer therapy. As NAMPT PROTACs would be expected to suffer from the same toxicity issues as NAMPT inhibitors, and as current PROTAC technology doesn't offer a way to confer cell selectivity, producing NAMPT PROTAC-ADCs would offer a way of selectively delivering the PROTAC payload.

Although NAMPT inhibitor-ADCs have been shown to possess incredibly high potencies *in vitro* and promising anti-tumour properties *in vivo* it has been observed that rapid and sustained high exposure of NAMPT inhibitor-ADCs is necessary to achieve long-term depletion of NAD and effective killing of cancer cells.

Using PROTACs as an alternative ADC payload may offer a way to achieve this target, due to the incredibly high potencies possible as a result of the event-driven pharmacology observed with PROTACs. This could allow a lower dose of ADC that still effectively depleted NAD in the long-term and may also allow the targeting of lower antigen-expressing cells, allowing the treatment of previously elusive disease types, as in the case of Enhertu.

Investigations into novel drug classes for use as ADC payloads also holds general significance, as discussed in section 1.5.1. PROTACs have a distinct mechanism of action from other payload types and developing them as payloads represents a useful diversification of the tools available to treat cancers and other diseases.

We therefore aim to design, synthesise, and test a series of NAMPT PROTACs, with a view to use these as a novel class of potent ADC payloads.

2.5 Results and discussion

2.5.1 PROTAC design and vector selection

The first step in PROTAC design is selecting a POI ligand and identifying a vector from which the ligand can be extended, allowing attachment to the linker and ultimately the E3 ligase ligand. We choose FK866 (**121**) as our NAMPT ligand, as it's highly potent (EC$_{50}$ < 1 nM in THP-1 cells), and crystal structures of it in complex with NAMPT have been published, which should enable PROTAC design.[155,244]

Examining the crystal structure reveals that the 2 position on the phenyl ring is exposed to solvent (black star, figure 2.28), and thus should offer a tolerated position for derivatisation. We therefore embarked upon the synthesis of **167**, a derivatised FK866 analogue that would allow chemical attachment to the PROTAC linker without impacting the binding to NAMPT.

As this pocket is somewhat recessed, we selected a linker with a slightly extended chain to the amine from which the remainder of the linker would be extended. Whilst this limits our ability to prepare PROTACs with <6 atom linkers, it also brings the derivatisation point into a similar region of the protein as seen with other PROTAC projects conducted in our group, potentially enabling the sharing of linker-ligase intermediates.
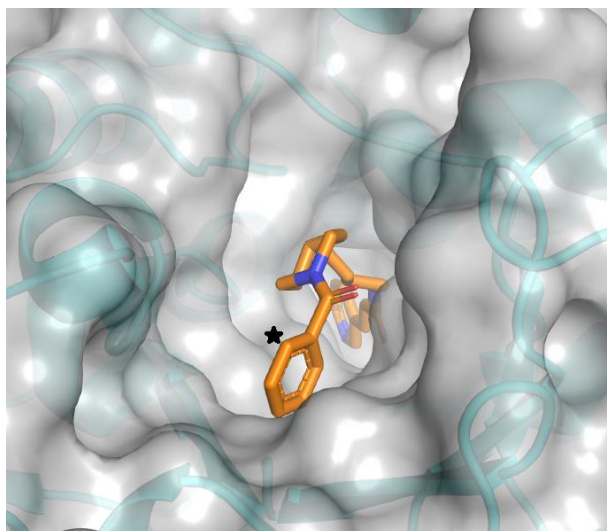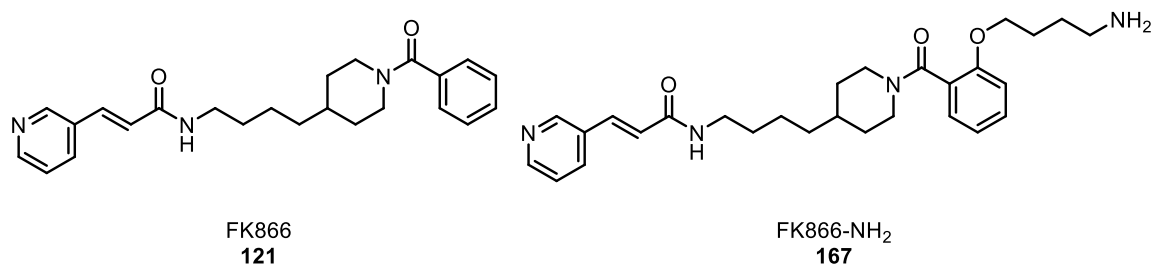
*Figure 2.28 Above: Structures of FK866, the parent ligand, and FK866-NH₂ (**167**), our proposed ligand from which to build a NAMPT PROTAC. Below: Crystal structure of FK866 in complex with NAMPT, showing position 2 of the aryl ring exposed to solvent (indicated with black star).*

2.5.2   Retrosynthetic analysis and forward synthesis of FK866-NH₂ (**167**)

FK866-NH₂ can be split into three main building blocks. The two amides can be made under amide coupling conditions, and the phenol substitution can be affected with simple alkylation chemistry. This retrosynthetic analysis produces the building blocks 3-(3-pyridyl)acrylic acid (**168**), diamine (**169**), and methyl salicylate (**170**). Only the diamine **169** is not commercially available, and therefore needed to be synthesised. Additionally an appropriately building block to install the amine tail was required.
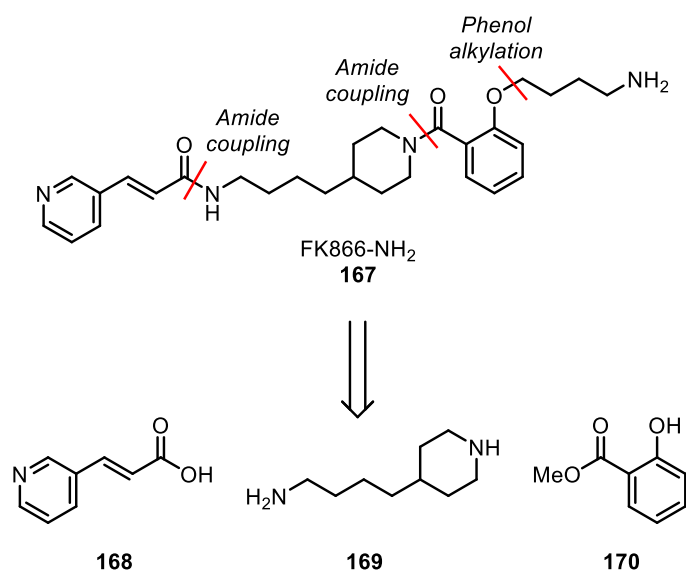
*Figure 2.29 Retrosynthetic analysis of FK866-NH$_2$ (**167**).*

Initially 4-amino-1-butanol (**171**) was Boc protected to afford **172**. An Appel reaction furnished the bromide on **173** that would act as a leaving group during the alkylation of the phenol in methyl salicylate.

The cheapest commercially available material closely related to **169** was 4-piperidine butyric acid hydrochloride (**174**), which we reduced with borane to the corresponding alcohol **175**. With compounds **173** and **175** in hand, we could then start decorating the methyl salicylate core. Methyl salicylate **170** was alkylated with **173** using potassium carbonate to deprotonate the phenol, and sodium iodide as a source of iodide to act as a nucleophilic catalyst by generating trace amounts of the alkyl iodide from the alkyl bromide **173**. Methyl ester **176** was then hydrolysed with sodium hydroxide, to afford acid **177** that was coupled to **175** using HATU to generate alcohol **178**.
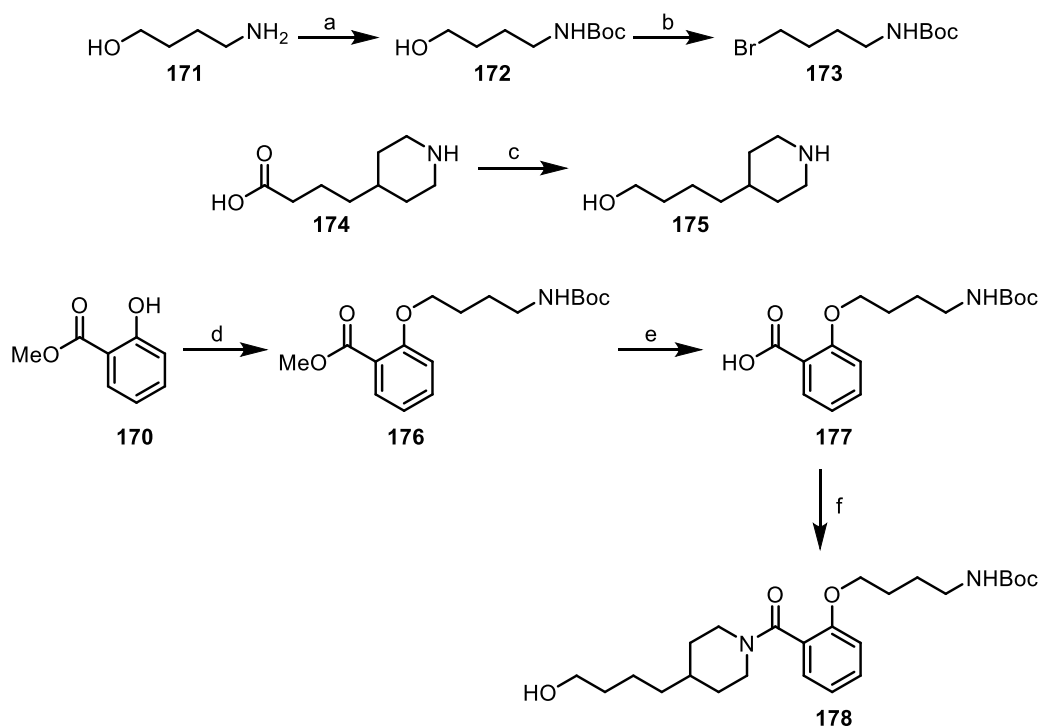
*Figure 2.30 Synthetic route to intermediate **178**. a: Boc₂O (1.0 eq), DCM, 0 ℃ to RT, o/n, 68%. b: PPh₃ (1.5 eq), CBr₄ (1.6 eq), THF, 0 ℃ to RT, 100%. c: BH₃.SMe₂ (1.0 eq), THF, 0 ℃ to reflux, o/n. d: **173** (1.5 eq), K₂CO₃ (3.0 eq), NaI (0.50 eq), DMF, 60 ℃, 24 h, 52%. e: NaOH (2.5 eq), EtOH, 60 ℃, o/n, 68%. f: HATU (1.5 eq), **175** (2.0 eq), DIPEA (4.0 eq), DMF, RT, o/n, 57%.*
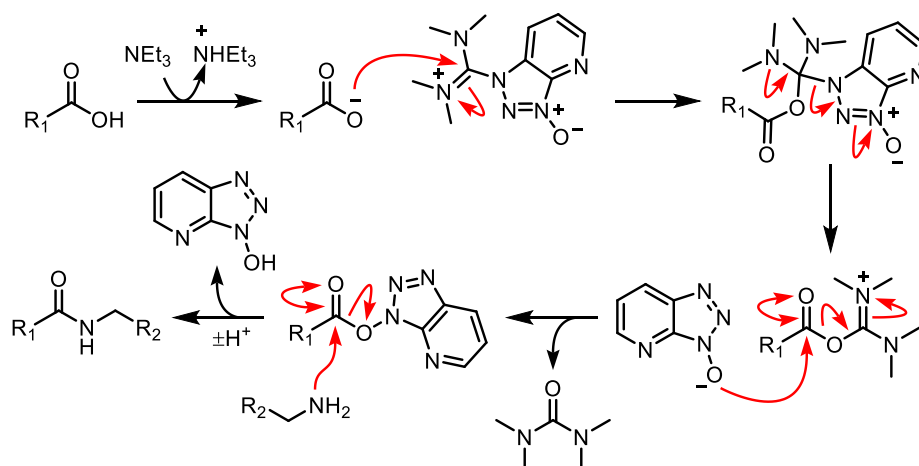
Figure 2.31 Mechanism of HATU coupling. Although the O-linked uronium salt isomer of HATU is more reactive, X-ray crystallography, and both solution and solid state NMR analysis has determined that the true structure in both crystalline and solution state is the N-linked guanidinium salt, as shown here.[245]

A series of functional group interconversions followed. **178** was treated with tosyl chloride to generate tosylate **179**, which was displaced with sodium azide to form

azide **180**. This was reduced using PPh₃ under Staudinger conditions to form amine **181**, which was coupled to 3-(3-pyridyl)acrylic acid (**168**). The product, **182**, was then deprotected using TFA, affording FK866-NH₂ (**167**) as the TFA salt.
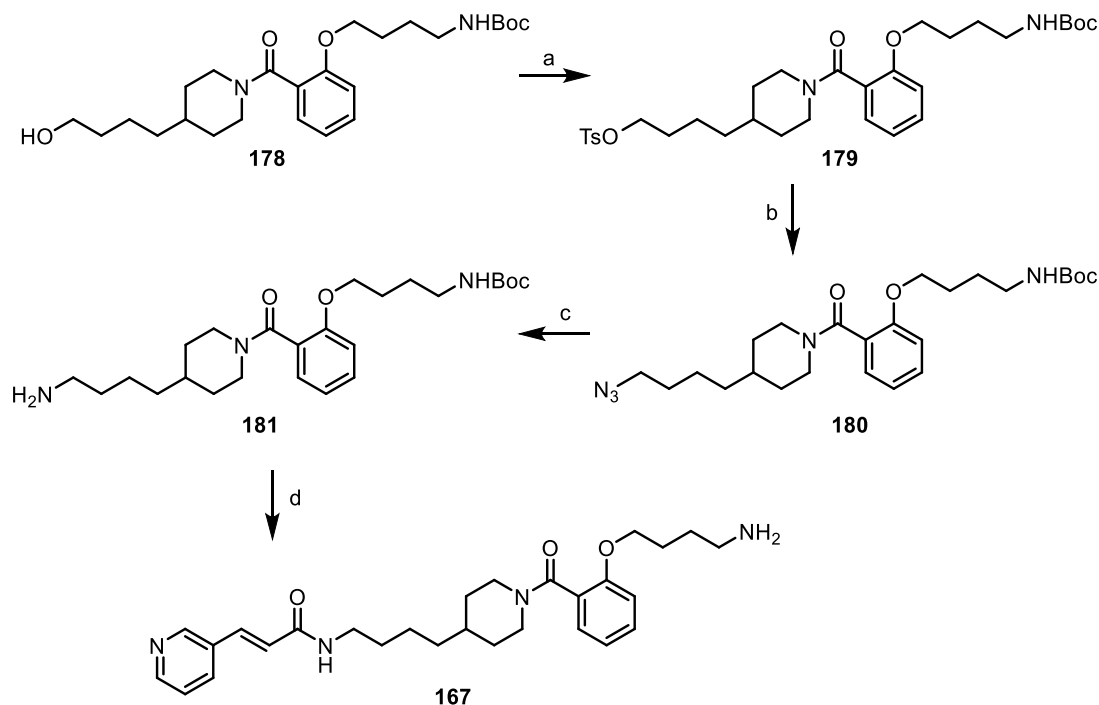
*Figure 2.32 Synthetic route to FK866-NH₂ (**167**). a: TsCl (1.5 eq), NEt₃ (2.0 eq), DCM, RT, o/n. b: NaN₃ (3.0 eq), DMF, 60 ℃, o/n, 51% over two steps. c: PPh₃ (1.5 eq), H₂O (6.0 eq), THF, reflux, 3.0 h, 100%. d: (i) **168** (2.0 eq), HATU (1.5 eq), DIPEA (4.0 eq), DMF, RT, o/n, 42% (ii) 10% TFA in DCM, RT, 2.0 h.*

2.5.3   Testing and validation of FK866-NH₂ (**167**)

Before continuing with the design and synthesis, we tested FK866-NH₂ to ensure the added amine tail hadn't altered its ability to bind NAMPT. **167** was tested in a fluorescence polarisation (FP) assay (experiments performed by Minghao Gao) to examine its binding to NAMPT (assay principle described in section 2.3.3). The results of the assay (figure 2.33) are similar for FK866 and FK866-NH₂, suggesting the binding of the ligand has not been significantly impacted by the attachment of the amine tail.
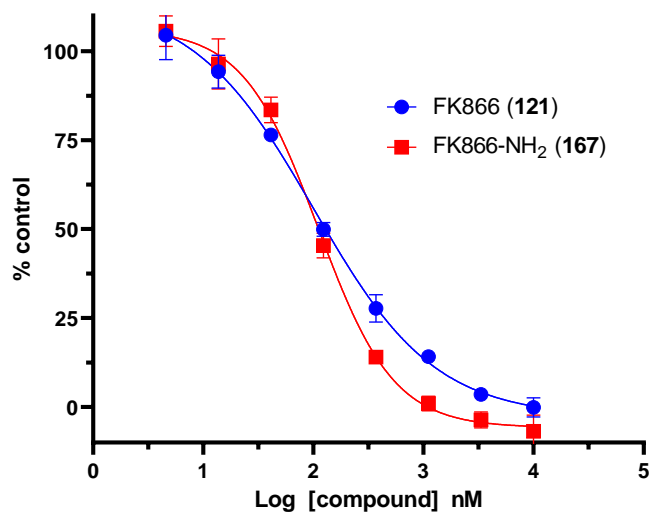
Figure 2.33 FP assay comparing binding of FK866 and FK866-NH$_2$ to NAMPT.

2.5.4 Linkers and E3 ligands

In order to provide the best chance of successfully identifying a NAMPT PROTAC, ligands were chosen that recruit both CRBN and VHL E3 ligases. Within the CRBN ligands both lenalidomide and thalidomide were investigated, while two VH032-based ligands were chosen to recruit VHL: the original amine-linked compound **183**, and the fluorocyclopropyl-capped phenolic analogue **184**.
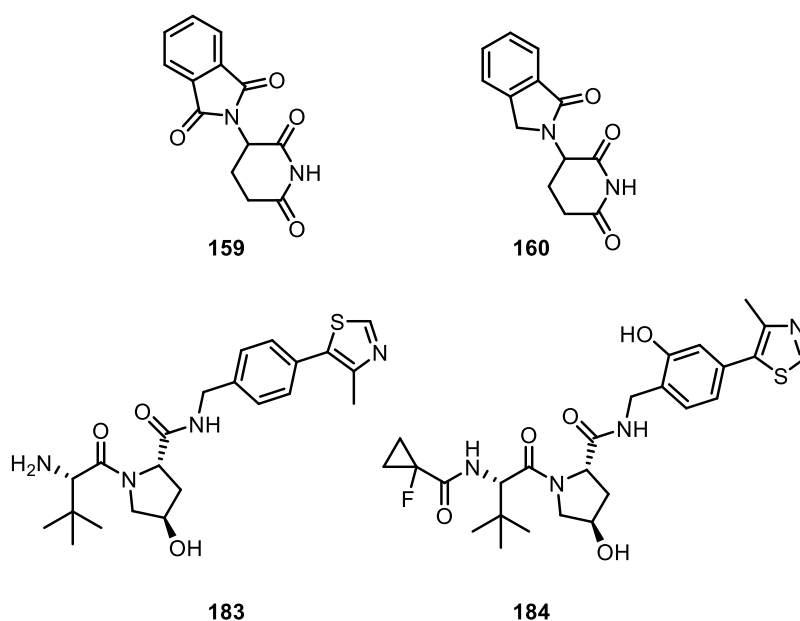
Figure 2.34 Structures of the E3 ligase ligands used in this work.

As described in section 2.3.6.1, choice of E3 ligase can have a great effect on PROTAC action. Activity can be recovered from essentially nothing to a respectable level by changing the E3 ligase recruited.[246] The CRBN E3 complex has been hypothesised to be more flexible than the corresponding VHL complex, which may explain the more active profile of CRBN-based PROTACs in some cases.[175] Given this relatively narrow window for success in VHL-based compounds, we decided to synthesise PROTACs that built from the VHL ligand using different exit vectors: the amide linkage from the *tert*-leucine amine, and the phenolic linkage in a fluorocyclopropyl-capped analogue (**184**). This is another way of exploring different ternary structures – building of the VHL ligand in different places will orient the ligand in different ways relative to the POI, which gives access to slightly different sets of protein-protein interactions, some of which may result in a productive complex.

Three types of linker were investigated. A 13 atom alkyl chain containing an amide, a 12 atom alkyl chain containing an amide, a 12 atom chain containing an amide and an alkyne, and a 20 atom partially PEGylated chain containing an amide (figure 2.35). This doesn't represent a comprehensive survey of linker chemical space, but allows us to potentially generate initial hits that can then be optimised to increase degradation capability.
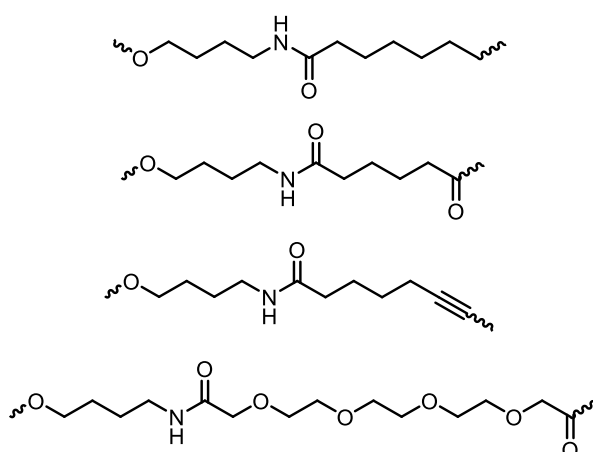
Figure 2.35 Structures of linkers used.

2.5.5 Synthesis of CRBN E3 ligase ligands

To produce a lenalidomide derivative with a reactive handle, bromo-lenalidomide (**185**) was synthesised as follows. A radical bromination of 3-bromo-2-methylbenzoate (**186**) afforded dibromo compound **187**, which was reacted with 3-aminopiperidine-2,6-dione HCl to give the cyclised product bromo-lenalidomide **185**. A Sonogashira coupling was then used to install ester-alkyne **190** on the ring, followed by a TFA deprotection to give alkyne-lenalidomide **188**. Interestingly, no significant reaction was observed with the methyl ester of **189**, however the *t*-butyl ester **190** reacts well under the same conditions. The reason for this is unknown; the esters were both completely soluble in the reaction solvent, and the ester appears to be far enough away from the reactive terminal alkyne that it shouldn't interfere with the reactivity.
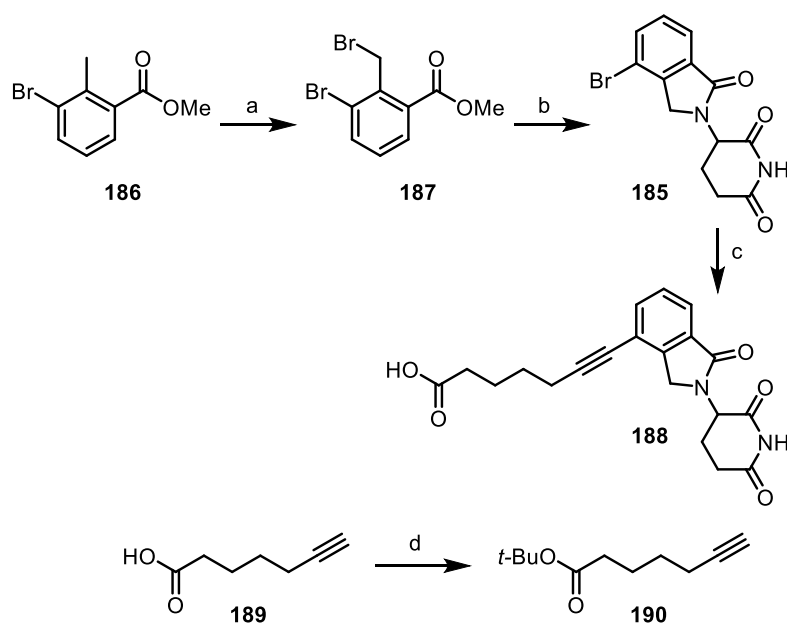
*Figure 2.36 Synthetic route to alkyne-lenalidomide **188**. a: N-bromosuccimide (1.2 eq), benzoyl peroxide (0.10 eq), CCl$_4$, reflux, o/n, 95%. b: 3-aminopiperidine-2,6-dione HCl (1.5 eq), NEt$_3$ (1.7 eq), MeCN, 80 ℃, o/n, 72%. c: (i) **190** (2.0 eq), CuI (0.20 eq), NEt$_3$ (53 eq), Pd(PPh$_3$)$_2$Cl$_2$ (0.10 eq), DMF, 70 ℃, o/n, 55%. (ii) 10% TFA in DCM, RT, 2.0 h. d: Boc$_2$O (2.0 eq), DMAP (0.30 eq), tBuOH, RT, o/n, 79%.*

Bromo-thalidomide **191** was also coupled with alkyne **190** under Sonogashira conditions, giving alkyne-thalidomide **192**. Alkyne-thalidomides are known to be relatively unstable, so we hydrogenated the alkyne to produce the more stable alkyl-thalidomide **193**. A TFA deprotection of the *t*-butyl ester gave alkyl-thalidomide **194**.
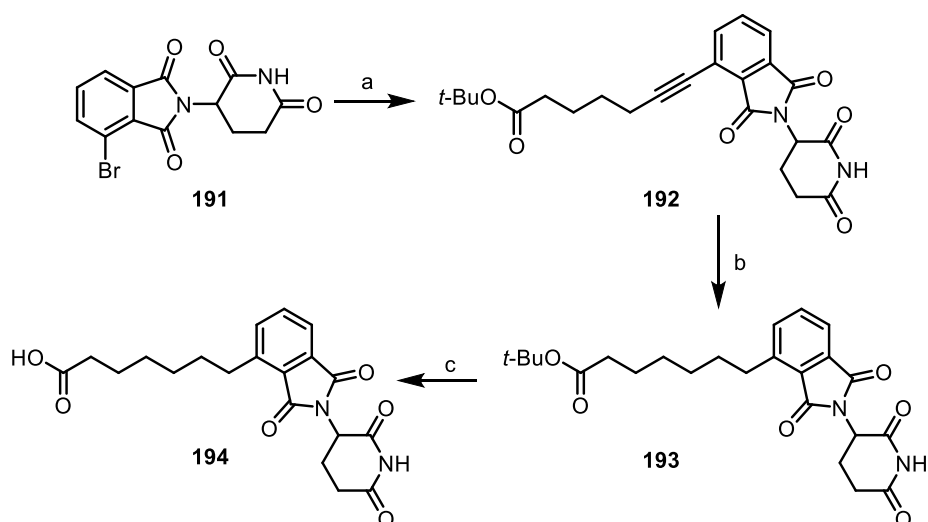
*Figure 2.37 Synthetic route to alkyl-thalidomide **194**. a: **190** (2.0 eq), CuI (0.20 eq), NEt₃ (15 eq), Pd(PPh₃)₂Cl₂, DMF, 80 ℃, 60%. b: Pd/C, H₂(g), EtOAc, RT, o/n, 99%. c: 10% TFA in DCM, RT, 2.0 h.*

The generally accepted mechanism of the copper-cocatalysed Sonogashira coupling is shown in figure 2.38. Despite this reaction's widespread use in forming sp^2-sp carbon-carbon bonds in synthetic chemistry, the mechanism has yet to be fully and definitively characterised.[247] It is thought to proceed through two independent catalytic cycles, one in palladium and one in copper. The copper cycle is relatively poorly understood, although the "textbook" version of events involves copper forming a π-alkyne-Cu complex that increases the acidity of the terminal alkyne proton, allowing deprotonation by the base, usually an amine such as NEt₃.

Recent computational work has also suggested that the copper acetylide that is proposed to form is likely to be anionic, rather than neutral, with the copper coordinated to an anion such as I⁻.[248] This modified version of the mechanism can account for the fact that the rate of reaction is observed to depend on the halide of the Cu(I) salt, as well as the substituent and halide of the aryl halide.

Despite remaining uncertainty of some of the specifics of the mechanism, the mechanism presented in figure 2.38 is generally accepted in the literature.[249]
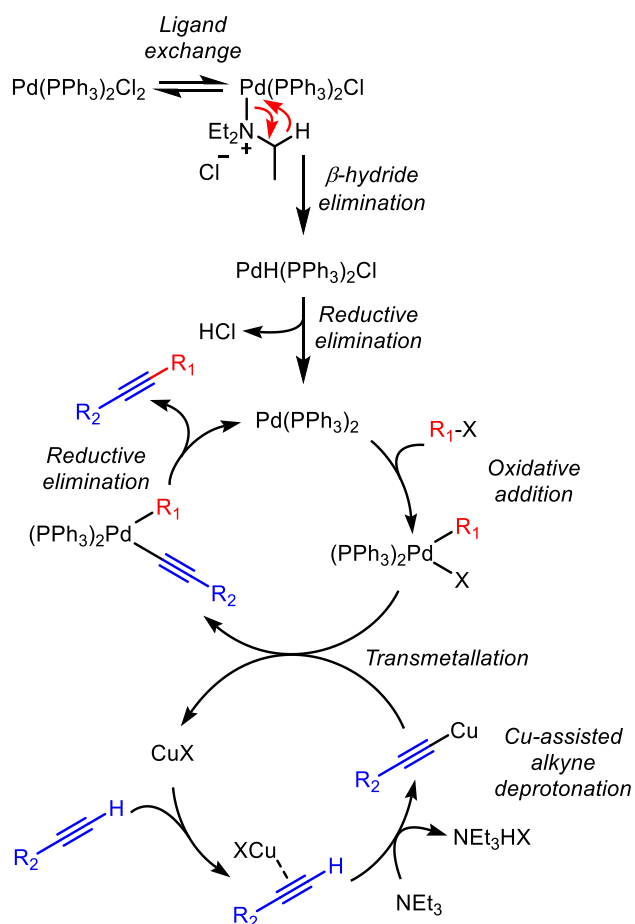
Figure 2.38 Generally accepted catalytic cycle of a Sonogashira coupling.

2.5.6   Synthesis of VHL ligands

The free amine-containing VHL ligand **183** is commercially available. Phenolic version **184** was synthesised in line with the methods published by Crews and Ciulli.[250,251]
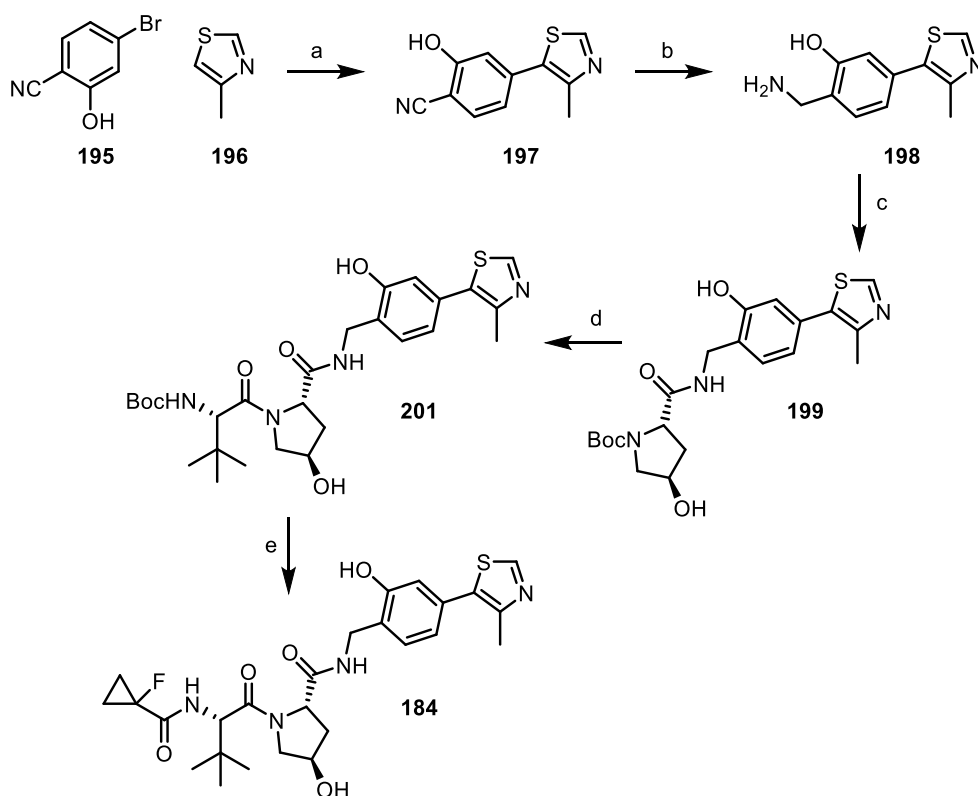
*Figure 2.39 Synthetic route to phenolic VHL ligand **184**. a: **195** (1.0 eq), **196** (1.9 eq), Pd(OAc)$_2$ (0.01 eq), KOAc (2.2 eq), DMA, 150 °C, 3.5 h, 69%. b: BH$_3$.SMe$_2$ (5.0 eq), DIBAL (5.0 eq), RT, o/n, 29%. c: N-Boc hydroxyproline (1.1 eq), HATU (1.25 eq), HOBt.H$_2$O (1.3 eq), DIPEA (2.6 eq), DMF, RT, o/n, 66%. d: (i) 10% TFA in DCM, RT, 2.0 h (ii) N-Boc tert leucine (1.5 eq), HATU (1.9 eq), HOBt.H$_2$O (1.7 eq), DIPEA (5.0 eq), DMF, RT, o/n, 47% over two steps. e: (i) 10% TFA in DCM, RT, 2.0 h (ii) 1-Flurocyclopropyl carboxylic acid (1.8 eq), HATU (2.0 eq), HOBt.H$_2$O (0.99 eq), DIPEA (6.0 eq), DMF, RT, o/n, 34% over two steps.*

First, 4-bromo-2-hydroxybenzonitrile (**195**) was reacted with 4-methylthiazole (**196**) through a palladium-catalysed direct arylation to afford biaryl **197**, the specifics of which are worth mentioning. At high temperatures Pd(OAc)$_2$ can form soluble Pd^0 nanoparticles, which can enter one of two competing pathways. They can aggregate with other nanoparticles eventually forming larger clusters. This process is self-catalysed,[252] and eventually leads to the production of insoluble "palladium black", which effectively removes all active palladium from the reaction, breaking the catalytic cycle. Alternatively, if the concentration of palladium is sufficiently low, the oxidative addition of an aryl halide can compete with the formation of these clusters, adding to palladium atoms at the edges of the nanoparticles.[253] Hence the reaction conditions used to couple **195** and **196** can generate catalytically-active Pd^0, even in the absence

of phosphine ligands or amines, etc. Once the active Pd^0 species has formed, the direct arylation likely proceeds according to a mechanism proposed by Miura, as shown in figure 2.40.[254]
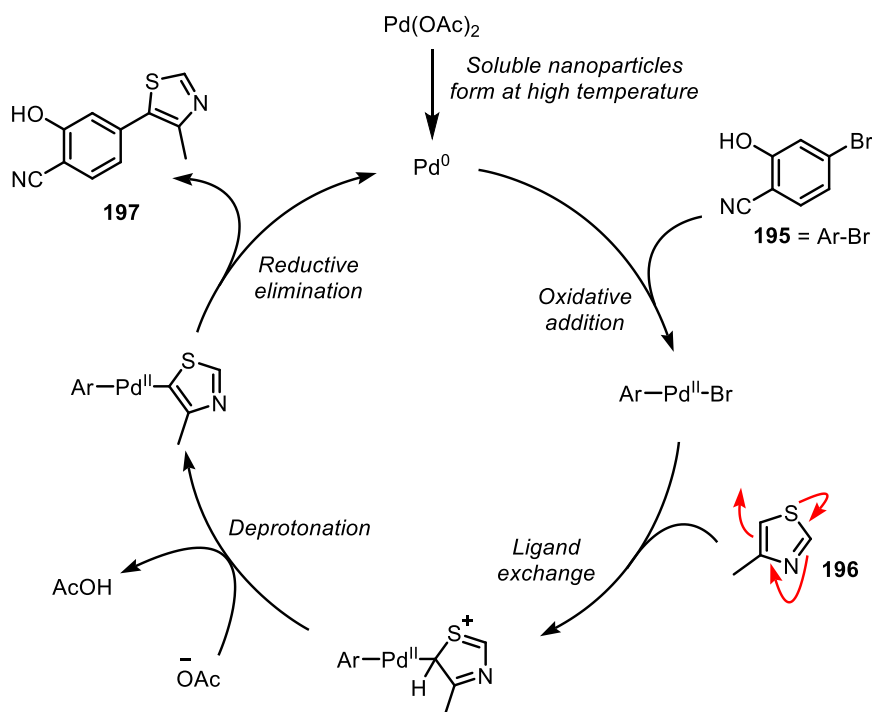
Figure 2.40 Proposed catalytic cycle for Pd-mediated direct arylation.

The reduction of the nitrile in **197** is accomplished with $LiAlH_4$ in the literature. This is a fairly low-yielding reaction, giving the product in about 30% yield. In an attempt to improve on this low yield early in the synthetic route, we investigated the use of diisobutylaluminium borohydride, made by mixing borane and DIBAL. According to first report of this reducing agent, it is able to reduce the structurally similar non-phenol version of **197** (**203**, shown in figure 2.41) in high yield and under mild conditions,[255] a transformation which usually requires more forcing conditions and only gives moderate yields. An additional advantage to this method is that the authors assert that the reactions do not require purification by column chromatography, and that a simple acid base workup will afford the reduced amine in sufficient purity. The presence of an acidic phenol in **197** precluded this method of purification, though, requiring column chromatography to purify the reaction mixture. The isolated yield of **198** was 29%, the same as was obtained using $LiAlH_4$ in the literature. As full conversion of the nitrile to the amine was observed by LCMS during the course of the reaction,

we hypothesise that this greatly diminished yield is due to the purification, rather than insufficient reduction.
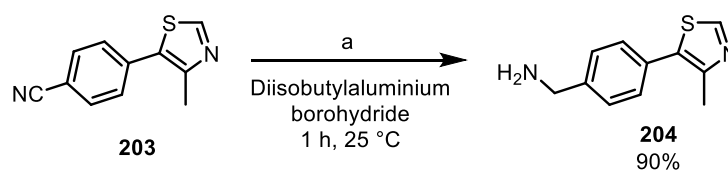
*Figure 2.41 Diisobutylaluminium borohydride can reduce the structurally similar nitrile **203** under mild conditions with high yield. a: (iBu)$_2$AlBH$_4$ (1.0 eq), THF, 25 ℃, 1.0 h, 90%.*

198 Was then coupled to *N*-Boc hydroxyproline with HATU to afford **199**. A TFA deprotection of the Boc group followed by another HATU coupling with *N*-Boc-*tert*-leucine gave **201**. A second TFA deprotection to give free amine **202** and another HATU coupling with 1-fluorocyclopropyl carboxylic acid (**205**) provided the final compound **184**, ready for further derivatisation with the linker and POI ligand.

2.5.7 Unexpected reactivity

During the HATU coupling of **202** with 1-fluorocyclopropyl carboxylic acid some unusual reactivity was observed. Often, the precise order of addition of reagents in a HATU coupling is not important. A typical procedure used in our group pre-forms the activated ester by mixing the carboxylic acid, base (usually DIPEA or NEt$_3$), and HATU, then stirring for around 1 hour, followed by the addition of the amine coupling partner.

When we attempted to synthesis **184** using this procedure, however, we didn't observe any product formation by LCMS analysis. Upon subsequent LCMS analysis of the pre-activation step, we observed the formation of a UV-active species whose mass did not correspond to any of the usual species present in a HATU coupling (including the activated ester, etc.).

Under the assumption that this might be a by-product formed from HATU conditions specifically, we began to investigate other amide coupling conditions. When we attempted to make the acyl fluoride of **205** using BTFFH (fluoro-dipyrrolidinocarbenium hexafluorophosphate) and DIPEA, we again observed the unknown compound forming. We therefore concluded that the compound was

forming from the activated acid of **205**, rather than from the peptide coupling reagents themselves. Repeating the HATU reaction with NEt$_3$, instead of DIPEA, led to the formation of a product with a mass 28 amu lower, suggesting that the unknown product also contained the amine base.

We then scaled up the HATU reaction to isolate and characterise the unknown compound. After NMR analysis, and with a number of possible molecular formulae from high resolution mass spectrometry, we concluded that the unknown compound was **206** – an enaminone (figure 2.42), initially isolated in 13% yield.
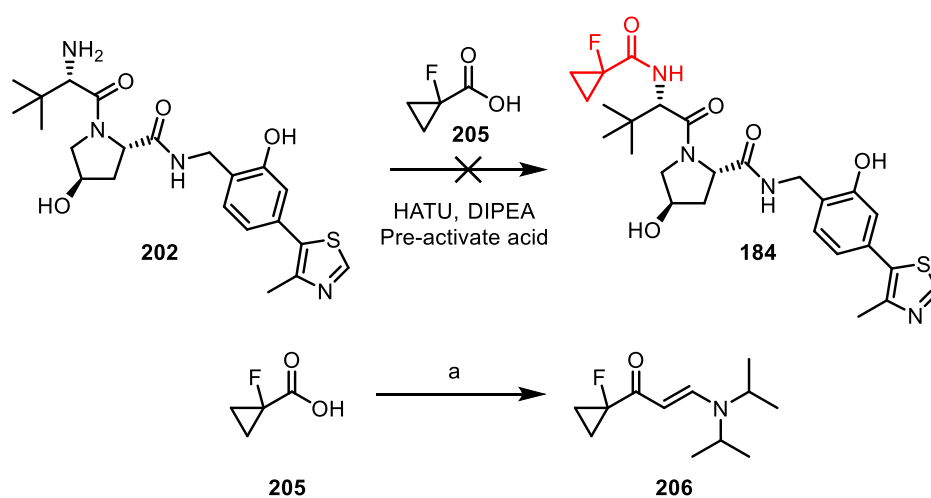
*Figure 2.42 Overview of unexpected reactivity during attempted HATU coupling to make **184**. a: HATU (2.0 eq), DIPEA (3.0 eq), DMF, RT, 1.0 h, 13%.*

There are several key features in the ^{1}H NMR spectrum of **206**. The protons H$_a$ and H$_b$ (figure 2.43) have very high chemical shifts, of 5.81 ppm and 7.87 ppm respectively. These shifts are similar to the alkene protons in an enone. As the nitrogen lone pair is in conjugation with the double bond and carbonyl, the amine cannot freely rotate. This locks it in conformation, making the isopropyl groups magnetically inequivalent. Therefore there are separate signals seen for H$_e$ and H$_f$, and for H$_c$ and H$_d$. The following signals in the ^{13}C spectrum were also split by coupling to the fluorine atom: the cyclopropyl carbons, the carbon geminal to the fluorine, the carbonyl carbon, and the β-enaminone carbon. We would also expect to see the α-enaminone carbon split by the fluorine, but this wasn't observed.
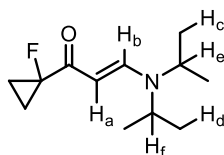
206

*Figure 2.43 Chemical structure of enaminone **206**, with annotations for NMR analysis.*

A literature search revealed that similar products have been formed through the reaction of TFA anhydride (**207**) and NEt₃.[256] The reaction sequence is outlined in figure 2.44. According to the mechanism Schreiber proposes, NEt₃ acts as a hydride donor to TFA anhydride, generating iminium **208**, TFA, and TFA aldehyde (**209**). Imine tautomerisation then gives the imine of NEt₃, **210**, which can attack a further molecule of TFA anhydride to form enaminone **211**. As this product can also act as a nucleophile, the author also observed the formation of the product **212**, produced through an additional attack on TFA anhydride. As well as isolating the enaminone **211**, Schreiber isolated and characterised the trifluoroacyloxy acetal of TFA aldehyde (**213**), supporting the hypothesis that aldehyde **209** is formed, and thus supporting the hydride transfer mechanism.
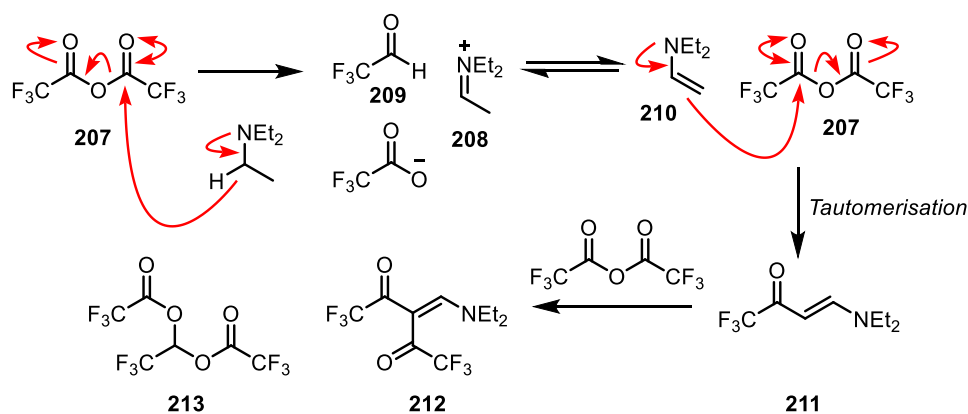
Figure 2.44 Proposed mechanism for the reaction between NEt₃ and TFA anhydride observed by Schreiber.[256]

Schreiber also observed this reactivity with DIPEA, and that the amine exclusively reacted through the ethyl chain, leaving the isopropyl groups intact in the product. This led us to hypothesise that a similar mechanism might be occurring in our system, shown in figure 2.45.

173
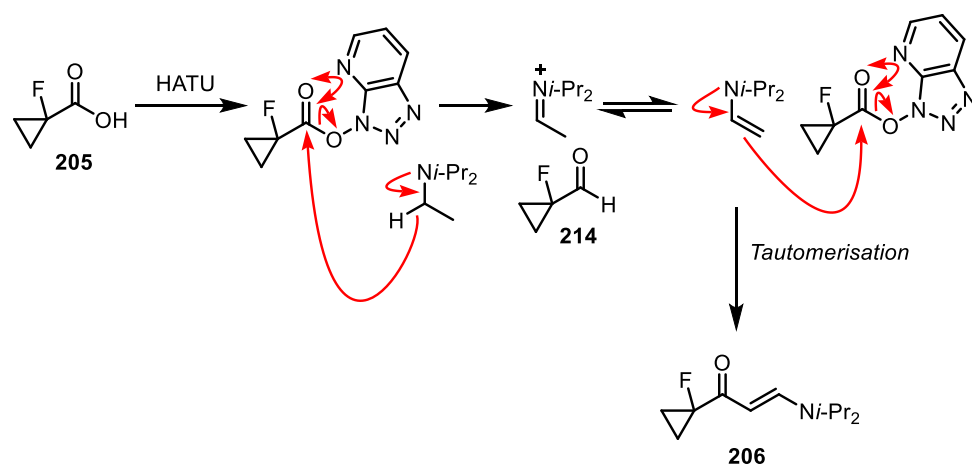
*Figure 2.45 Proposed mechanism for the formation of the enaminone **206**.*

A problem with this hypothesised mechanism is that it should also lead to the production of aldehyde **214**, or derivative thereof. During our investigations we searched for evidence of this aldehyde or related species, but could not find any evidence for these. We didn't observe a peak in the ^{1}H NMR spectrum of crude reaction mixtures that was high enough to be an aldehyde proton, or a signal that could be a hydrate or acetal of the aldehyde (we would expect a peak split by the adjacent fluorine into a doublet, that was at a reasonably high shift). We also didn't observe the mass of either the aldehyde or its derivatives (hydrate, acetal, etc.) in LCMS analyses of the reactions, although this could be because the species don't ionise well, which is plausible. The similarity of our system with the Schreiber system does suggest the two reactions proceed via the same or similar mechanisms, but the fact we haven't been able to observe the aldehyde does call into question whether this reaction could be proceeding via a different mechanism.

As this is an interesting transformation, we put some effort into exploring its scope and limitations. Although not exhaustive, these experiments produced preliminary results that gave us some insight into the reaction and may offer a starting point for future studies.

We briefly investigated some similar carboxylic acids, to attempt to establish the structural features in **205** that promote this reaction pathway. From this point onwards we arbitrarily switched to using NEt$_3$ over DIPEA, as their reactivity was

essentially equivalent. Our initial hypothesis was that the α-fluorine withdraws enough electron density from the carbonyl to make the activated acid reactive enough to act as a hydride acceptor from the amine base – one would not expect a "normal", unactivated acid to behave like this. One might also propose that the α-cyclopropyl ring may have some influence on the reactivity, due to its ring strain and non-standard orbital hybridisation.[257] As controls, we investigated the reactivity of cyclopropyl carboxylic acid **215**, 2-fluoro-2-methylpropanoic acid **216**, and 2,2-difluoro-2-phenylacetic acid **217**. The latter two acids led to product formation determined by LCMS, whereas cyclopropyl carboxylic acid **215** only produces the expected HATU adduct **218**. This suggests it is the α-fluorine(s) that are driving this reactivity, and that the cyclopropyl ring is not necessary.
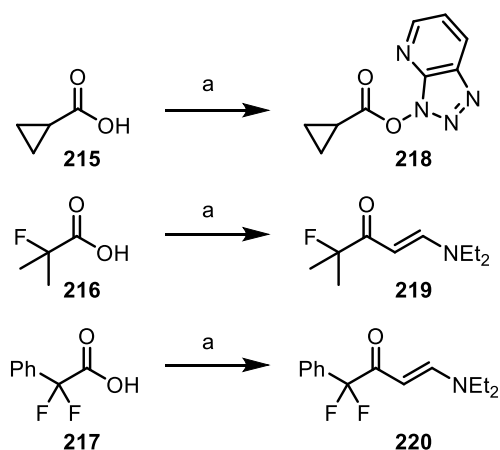
Figure 2.46 Control reactions to investigate what allows carboxylic acids to form enaminones. a: Acid (1.0 eq), HATU (2.0 eq), NEt$_3$ (3.0 eq), DMF, RT, o/n.

Following this finding we also investigated a series of related electron deficient carboxylic acids to determine whether other similarly electron-poor carbonyls could engage in this type of reactivity with NEt$_3$. These experiments are summarised in table 2.3.
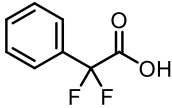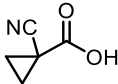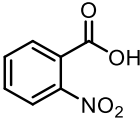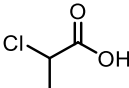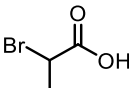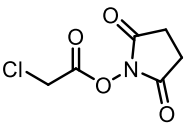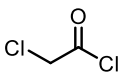
Compound	Structure	Observations based on LCMS analysis of reaction mixture
217		Clean reaction, product isolated in 41% yield.
221		Trace of product mass seen, however reaction profile contains lots of by-products.
222		Trace of product mass seen, major product is HATU adduct.
223		Appreciable formation of product, and some by-product formation.
224		Trace of product mass seen, but limited reactivity.
225		Trace of product mass seen but limited reactivity.
226		Trace of product mass seen, but extensive formation of very polar by-products. Likely decomposition.

Table 2.3 Results of experiments investigated whether various activated acids could engage in hydride acceptor reactivity. Conditions: Acid, NHS ester, or acyl chloride (1.0 eq), HATU (for the acids, 2.0 eq), NEt$_3$ (3.0 eq), DMF, RT, monitored regularly then left o/n.

These results suggests the presence of an α-fluorine puts such a carboxylic acid in a privileged window of reactivity; only traces of product were observed for other electron-poor acids after overnight reactions (except **223** which showed a fair amount of product formation), whereas 1-fluorocyclopropyl carboxylic acid (**205**) and 2,2-difluoro-2-phenylacetic acid (**217**) lead to product formation within hours.

If this reaction could be carried out with the amine as the limiting reagent, the process may have some synthetic utility as a way of functionalising otherwise generally unreactive N-CHX-CHX systems. An excess of amine compared to the acid is currently required, as deprotonation of the acid occurs before the HATU adduct can form. Schreiber describes using NaH as an additional base to overcome this limitation,

preventing the protonation and corresponding deactivation of the amine. Using NaH, and an excess of TFAA compared to NEt$_3$, he observed a yield of 91% for enaminone **212**.

Up to this point the stoichiometry we had been using was acid (1.0 eq), HATU (2.0 eq), NEt$_3$ (3.0 eq). We therefore investigated the effect of varying the number of equivalents of NEt$_3$, to see whether we could reduce the number of equivalents required. We also investigated the effect of including an external base. For these experiments we used the following stoichiometry: acid (2.0 eq), HATU (2.0 eq), NEt$_3$ (1.0 eq), external base (2.0 or 3.0 eq). The results of these experiments are summarised in table 2.4, all of which were performed with 2,2-difluoro-2-phenylacetic acid (**217**).

Acid 217 equivalents	HATU equivalents	NEt$_3$ equivalents	External base	Observation
1	2	3	-	41% isolated yield, almost complete LCMS conversion
1	2	2	-	Moderate conversion, lower product:SM ratio than with 3 eq of base
1	2	1	-	Only a trace of product mass seen by LCMS
2	2	1	DBU 2 eq	No product formation by LCMS
2	2	1	K$_2$CO$_3$ 2 eq	No product formation by LCMS
2	2	1	NaH 3 eq	Full LCMS conversion but <5% isolated yield

Table 2.4 Results from investigating different stoichiometries in the hydride transfer reaction.

In conclusion we were able to isolate enaminone **220** in a maximum of 41% yield, with a significant drop-off in yield seen with reduced amine equivalents. While the use of HATU broadens the scope of this chemistry relative to other related studies,[258] and disclosure of this reactivity may be helpful in optimisation of HATU amide couplings, as a result of the relatively poor conversion see with most substrates alongside the time demands of other projects these investigations were halted.

2.5.8   Construction of PROTACs

With our POI ligand and E3 ligase ligands in hand, we began the final stages of construction of our NAMPT PROTACs. To allow a final amide coupling with FK866-NH$_2$ (**167**), the VHL ligands were decorated with acid-functionalised linkers as shown in figure 2.47. Methyl ester **227** was synthesised through a HATU coupling of VH032-derived **183** with methyl adipate, followed by a basic ester hydrolysis to give **228**. Similarly **183** was reacted with 3,6,9,12-tetraoxatetradecanedioic acid in an amide coupling to afford **229**. Acid **230** was synthesised by alkylating the phenol of **184** with methyl 6-bromohexanoate.
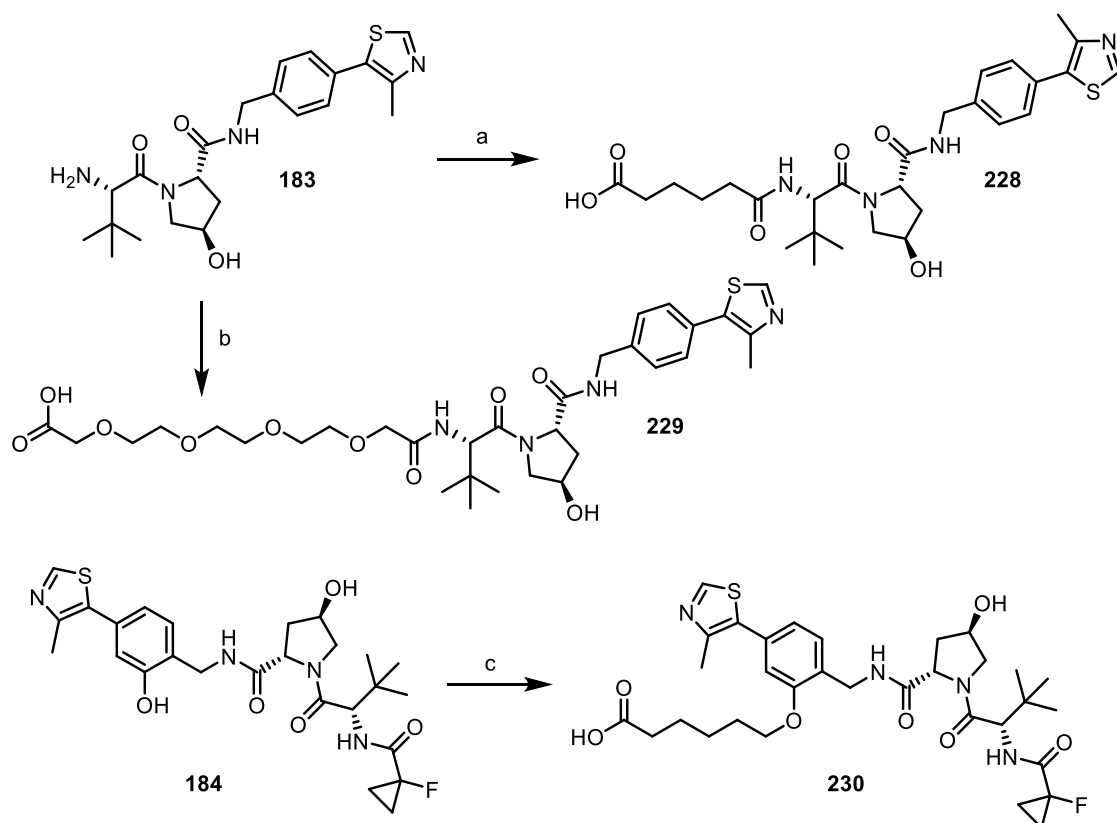
Figure 2.47 Synthetic routes to acid-functionalised VHL ligands. a: (i) Methyl adipate (2.0 eq), HATU (3.0 eq), DIPEA (4.0 eq), DMF, RT, o/n (ii) LiOH.H₂O (20 eq), THF/MeOH/H₂O, RT, 0.5 h, 41% over two steps. b: 3,6,9,12-Tetraoxatetradecanedioic acid (1.5 eq), HATU (2.0 eq), NEt₃ (3.0 eq), DCM, RT, o/n, 52%. c: (i) Methyl 6-bromohexanoate (2.0 eq), K₂CO₃ (3.0 eq), KI (0.25 eq), DMF, 75 °C, o/n (ii) LiOH.H₂O (18 eq), THF/MeOH/H₂O, RT, 1.5 h, 45% over two steps.

A series of amide couplings between FK866-NH$_2$ (**167**) and the acid-functionalised E3 ligands allowed us to synthesise the 5 PROTACs shown in figure 2.48.

Characterisation of PROTACs poses some challenges compared to smaller molecules. As only very small amounts of compound (typically <1 mg) are needed for cell testing, there is usually no need to optimise reaction conditions to maximise yields. Consequently yields are often only moderate, meaning that at the end of a synthetic sequence only small amounts (often <10 mg) of PROTAC are produced. Although more than sufficient for cell testing, this often makes obtaining ^{13}C NMR spectra challenging, due to the inherent insensitivity of carbon NMR, arising because of the low (~1%) abundance of ^{13}C. Even when experiments are run with a high number of scans, it has

been common in our group to not obtain usable carbon spectra, as is the case here too.

Additionally it can be challenging to identify specific peaks in the ^{1}H NMR spectra due to increased peak width and spectral overlap between the many distinct signals present. A possible explanation for the increased peak width is a slower rate of molecular tumbling in solution (due to the large molecular weight), which leads to faster transverse relaxation (shorter T_2).[259] As a result of these factors ^{1}H NMR signals can integrate to lower than their expected values, especially in the aliphatic region where there is an especially high density of peaks.

Despite the challenges associated with the NMR spectra of PROTACs, it is still possible to characterise them beyond reasonable doubt.

- Although the integrations of signals in the ^{1}H NMR signals are sometimes less than expected, the overall spectrum matches what would be expected from the PROTAC. Characteristic proton signals from both halves of the molecule (from FK866-NH$_2$ and the E3 ligase) can be seen, matching the signals observed in the spectra of the two intermediates used to synthesise the PROTAC. Furthermore ^{1}H NMR allows confirmation that no signals are present which suggest the presence of any major organic contaminants.

- Mass spectrometry becomes crucial in confirming the identity of these compounds. Both low-resolution and high-resolution data were obtained and used to confirm the expected identity of the PROTACs.

- The amine and acid coupling partners used to synthesise the final PROTACs were fully characterised by the usual analytical methods, including NMR spectra that were fully assigned. During the HATU-mediated amide couplings to produce the final PROTACs, the two partners were observed by LCMS converting to the product in a smooth and predictable way. This, combined with the general reliability of HATU couplings, suggests the expected reaction has occurred as desired.

- The UV trace from LCMS analysis of the final, purified PROTACs (included in the experimental section) shows a single clean peak, demonstrating purity.

We are therefore confident in the identity and purity of the synthesised PROTACs, despite the lack of ^{13}C spectra and challenges with ^{1}H spectra.
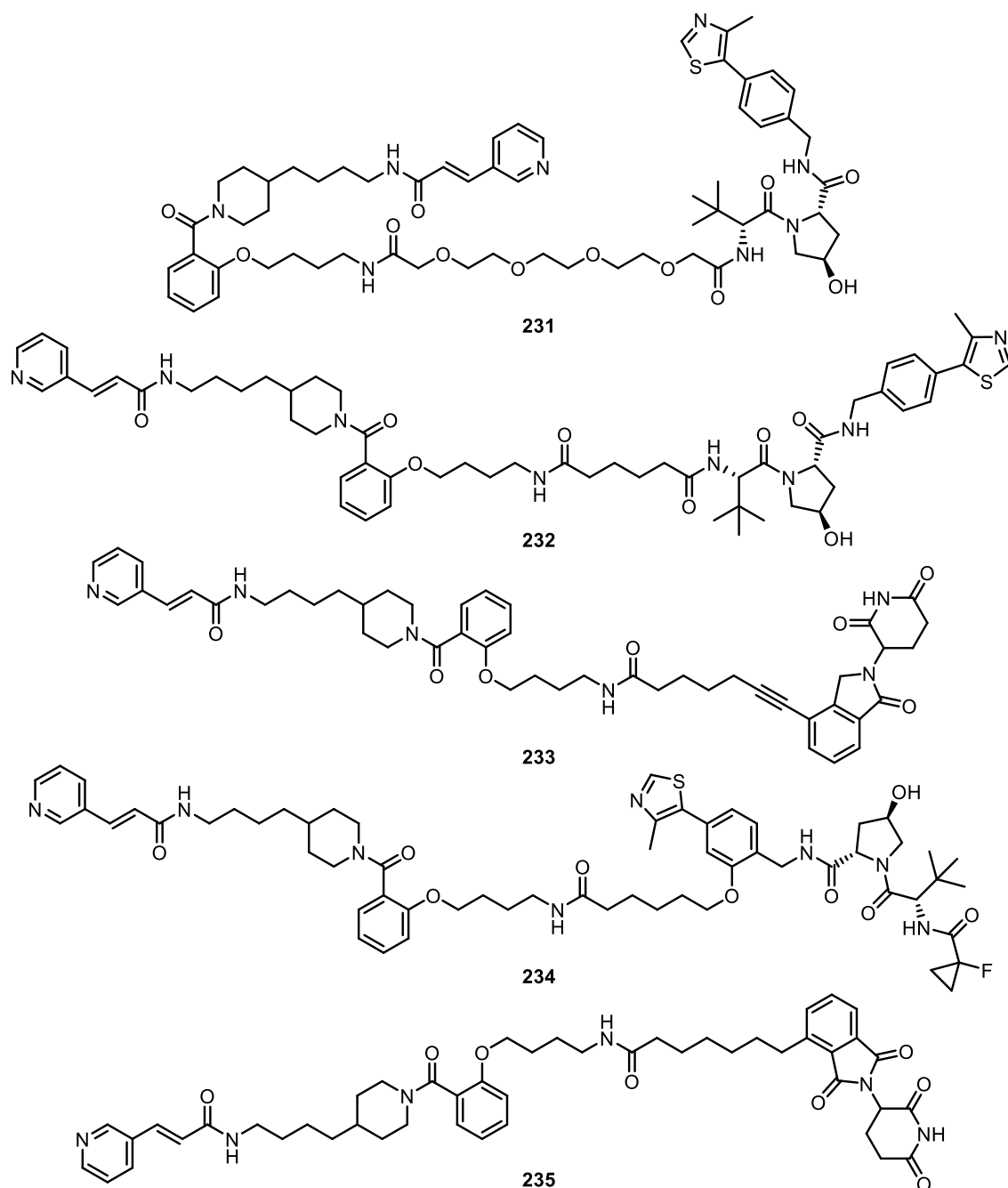
Figure 2.48 Structures of initial PROTACs synthesised.

2.5.9 Cell testing of PROTACs

The PROTACs were first tested in a WST-1 assay. This assay measures cells' ability to cleave the WST-1 dye **236** to a formazan product **237** (figure 2.49), which can be detected colourimetrically. This cleavage is predominantly linked to the activity of

mitochondrial dehydrogenases, and as this is typically linked to the number of metabolically viable cells the WST-1 readout can be used as a surrogate for (metabolically) viable cell number. However as mitochondrial dehydrogenases are NAD-dependent, the whole process is therefore NAD-dependent, and the readout also reflects the NAD levels of the cells. As NAMPT is the rate-limiting enzyme in the NAD salvage pathway, the levels of cellular NAD will decrease if NAMPT enzymatic activity decreases. The WST-1 assay can therefore be used to indirectly measure NAMPT function. There are limitations to this approach, though: the NAD salvage pathway which NAMPT is part of is only one of the ways cells can produce NAD. And likewise, any non-specific antiproliferative off-target effects will be indistinguishable from on-target effects. Consequently the levels of NAD may not directly reflect the levels of NAMPT active in the cells. Additionally, within this assay there is no difference between inhibiting and degrading NAMPT – either action will lead to a loss of NAMPT function, which leads to a decrease in NAD levels. Nonetheless the WST-1 assay is quick, cheap, and simple to run. It is therefore a useful preliminary test, to broadly determine the effect our compounds are having on cells.
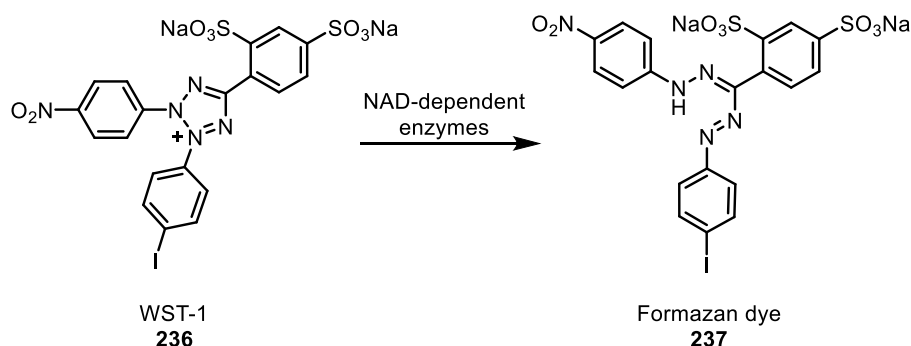
Figure 2.49 Chemical structure of WST-1 and its reduction to a formazan dye.[260]

The WST-1 assay was run by Lucy Li and performed in THP-1 cells, a human leukaemia monocytic cell line commonly used as an *in vitro* model of cancer, with WST-1 added 48 hours following compound administration. In addition to the 5 PROTACs, FK866 (**121**) was also included as a positive comparison. The cells were incubated with the test compound for 48 h with compound concentrations between 0.0170 nM and 1.00 µM (FK866 was tested over the slightly different range of 0.00513 nM to 100 nM). The results are quoted as "percentage of control". The control cells were dosed with

just vehicle (DMSO) and so should retain all of their NAD-dependent enzyme activity. The results are shown in figure 2.50.
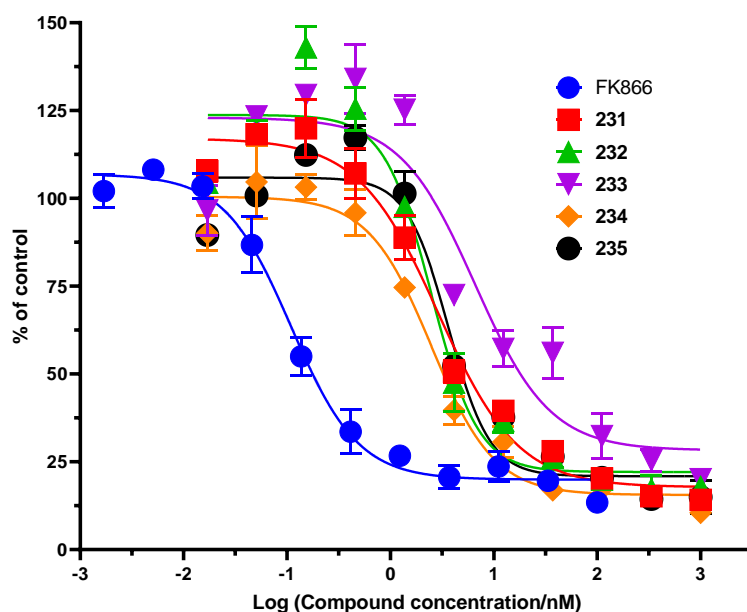
Figure 2.50 Results of WST-1 assay with PROTACs synthesised and FK866.

The results can be summarised as follows: all of the PROTACs tested show a dose-dependent activity in this assay, shown by the sigmoidal dose-response curves. The PROTACs all have EC_{50} values greater than FK866, demonstrating that they are less potent under these conditions. Despite this, they are all still reasonable potent compounds, with EC_{50} values below 10 nM. The EC_{50} values are shown below in table 2.5.

Compound	EC_{50} / nM	95% confidence interval
FK866 (**121**)	0.110	0.0904 to 0.134
231	2.89	2.27 to 3.76
232	2.48	1.88 to 3.34
233	6.57	3.20 to 15.9
234	2.48	1.95 to 3.20
235	3.63	2.81 to 5.19

Table 2.5 Calculated EC_{50} values for PROTACs synthesised and FK866 based on the WST-1 assay. Data reported as average of 3 repeats.

The following conclusions can be drawn from this experiment: the PROTACs appear to be binding to NAMPT in cells and leading to a decrease in its activity, although whether this is through inhibition or degradation cannot be determined from these results.

The compounds are reasonably potent, with all EC_{50} values under 10 nM, but are less active than the parent drug, FK866. These data nonetheless demonstrate that these larger PROTACs are sufficiently cell-permeable to enter the cells, and can bind to and inhibit NAMPT. These compounds don't appear to be significantly more potent than FK866, as indicated by their lesser activity compared to the parent compound. However these data cannot delineate the intrinsic activity of these compounds from the possibly significantly decreased membrane permeability resulting from the compounds' large size and polar surface area – the intracellular concentration of these compounds may simply be very low.

The fact that the PROTACs elicit a response warrants further investigation into whether or not they are degrading NAMPT. Degradation of a protein (and more generally, levels of protein in a sample) can be probed by performing a Western blot. This method allows the semi-quantitative visualisation of specific proteins from biological samples by using antibodies that selectively bind to the target protein, alongside separation of proteins by size to enhance the specificity of the signal.

Western blots can be performed on simple mixtures of proteins, or on cells. If cells are to be used, they are first lysed. This process breaks down the cell membrane, releasing the cellular components (proteins, DNA, RNA, organelles, etc.) into solution, and denatures the proteins. The mixture of interest is then separated by gel electrophoresis; a voltage is applied across a gel, and the proteins migrate towards the positive electrode. Larger proteins will migrate more slowly, moving less distance overall. Once the electrophoresis has occurred, the proteins are transferred to a membrane for visualisation.

A blocking solution is first applied, which binds a protein such as bovine serum albumin (BSA) to the membrane, reducing non-specific antibody binding. The membrane is then incubated with an antibody that binds to the protein of interest. After a suitable

time, any unbound antibody is washed off. The membrane is then incubated with a secondary antibody that binds to the primary antibody. The secondary antibody is also attached to an enzyme, such as horseradish peroxidase (HRP). After a second wash to remove unbound secondary antibody then membrane is ready for visualising. An appropriate substrate for the enzyme is added, one that gives a colourimetric change upon enzyme transformation. The colour can be recorded, and the density of the colour corresponds to the amount of protein of interest in the band. Western blots are considered semi-quantitative – they can give information about relative amounts of protein (darker or lighter bands), but generally cannot give information about the absolute concentrations of protein.

Based on the WST-1 data, THP-1 cells were incubated with our 5 PROTACs at concentrations of 1, 10, and 100 nM with the aim of covering a range of concentrations achieving up to those needed to fully occupy NAMPT. After 24 hour treatment the cells were lysed and a Western blot then taken of the cell lysate to visualise NAMPT. Untreated cells were also included as a control, as were cells treated with vehicle only (1% DMSO). These experiments and Western blots were performed by Lucy Li.
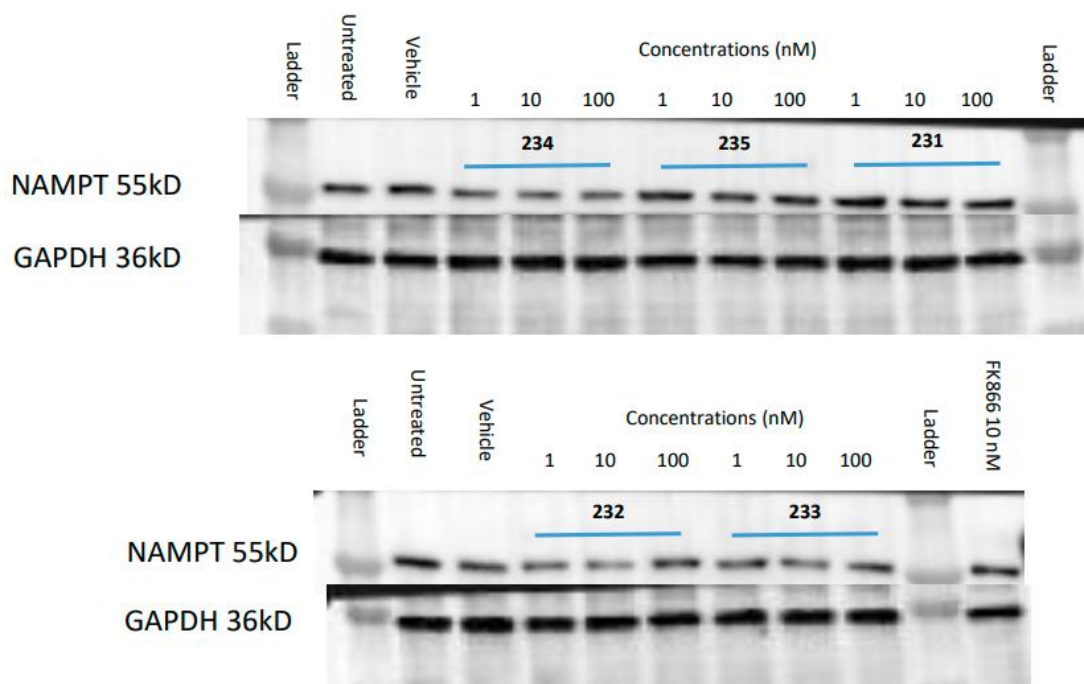
Figure 2.51 Western blots of NAMPT PROTACs. 1×10^6 THP-1 cells/mL were treated with compounds for 24 h at concentrations of 1, 10, and 100 nM. The antibody used was Bethyl A700-058. Data collected by Lucy Li.

The results show that the levels of NAMPT had approximately remained constant in the treated cells compared to the untreated cells, as judged by the intensity of the NAMPT band (figure 2.51). A slight effect can perhaps be seen with compound **232**, with the bands at 1 nM and 10 nM looking slightly fainter than the vehicle band. If this is a real effect, the fact it isn't seen at 100 nM could be explained by the hook effect: when PROTACs are at high concentrations they tend to form binary complexes; some with the POI, and some with the E3 ligase, preventing the formation of ternary complexes that lead to degradation. This means as the concentration of PROTAC is increased, after a point, the degrading effect will decrease.

Alongside the WST-1 data these results show that whilst the compounds are able to enter cells and inhibit NAMPT, concentrations of "PROTACs" that are sufficient to achieve effectively 100% occupancy of NAMPT (based on WST-1 signal compared to FK866) result in little or no degradation of NAMPT. Likewise given the lack of impact of protein levels, there is clearly no evidence of degradation at concentrations that result in lower occupancy (based on WST-1 signal).

As the compounds are entering the cells and engaging NAMPT, the reason for them not inducing degradation of NAMPT could be that they are not forming a stable or productive ternary complex with NAMPT and the E3 ligase, or that the PROTACs aren't engaging the E3 ligase at all. The E3 ligands we have used, and the vectors we have used to functionalise them, have been widely reported in the literature, and used with success in the design of PROTACs towards other targets. This suggests it's the former – the lack of formation of a stable or productive ternary complex – that has led to the lack of degradation activity.

As discussed in the introduction, predicting the protein-protein interactions (PPIs) that govern the stability of the ternary complex is currently essentially impossible. Empirically, though, changing the linker length and composition, and point of attachment on the ligands, is the way to investigate this.

Another possible explanation is the rate of resynthesis of NAMPT in THP-1 cells. If the rate is particularly rapid in THP-1 cells, this could reverse the action of a weakly active PROTAC and lead to Western blots that look as if no protein has been degraded, however there is no information in the literature about NAMPT resynthesis rates in THP-1 cells.

2.5.10 NAMPT PROTACs presented in the literature

During the course of this research, a number of papers have been published on the discoveries of NAMPT PROTACs that are reported to effectively degrade the protein. They are described in brief below.

Wu *et al.* developed the NAMPT PROTAC A7 (**238**) that degraded NAMPT in a dose-dependent way in A2780, HCT-116, and CT26 (murine colorectal carcinoma) cells.[261] Their research found that NAMPT promoted the formation of myeloid-derived suppressor cells (MDSCs) independently of its enzymatic function. MDSCs are a type of immune cell that suppress the immune response, contributing to a pro-tumour environment. They also found that the MDSC promoting effect was not dependent on NAMPT being enzymatically active. The production of MDSCs in decreased in CT26

tumour cells when NAMPT was depleted via short hairpin RNA knockdown, whilst in mice treatment with the NAMPT inhibitor FK866 didn't lead to a decrease in MDSCs.

The team then designed and synthesised a number of NAMPT targeting PROTACs based on their NAMPT inhibitor MS7 (**239**), and an E3 ligase recruiting ligand. They synthesised a number of analogues with varying chain lengths and varying attachment points on the aromatic ring of MS7.

Their best-in-class, A7 (**238**), degraded NAMPT in A2780, HCT-116, and CT26 cells, leading to a decrease in intracellular NAD levels, as well as a decrease in the concentration of extracellular NAMPT in media. They also tested A7 *in vivo*, and showed that NAMPT was successfully depleted in mice. Finally they showed that the anti-tumour effect of A7 was greater in immune-competent mice than in immune-deficient mice, suggesting the depletion of NAMPT by A7 also contributed to anti-tumour immunity.

The same group then published a series of slightly modified degraders, with the best example achieving a DC_{50} of <0.17 nM.[262] Compared to A7 (**238**), B3 (**240**), their best performing PROTAC, contained a urea instead of a thiourea in the NAMPT binding part of the molecule. Additionally the aromatic ring in the linker was removed, and the linker was changed from a PEG chain to an all-alkyl chain. B3 (**240**) had a potent antiproliferative effect against A2780 ovarian cancer cells (EC_{50} = 1.5 nM) and showed promising anti-tumour effects in mouse xenograft models.
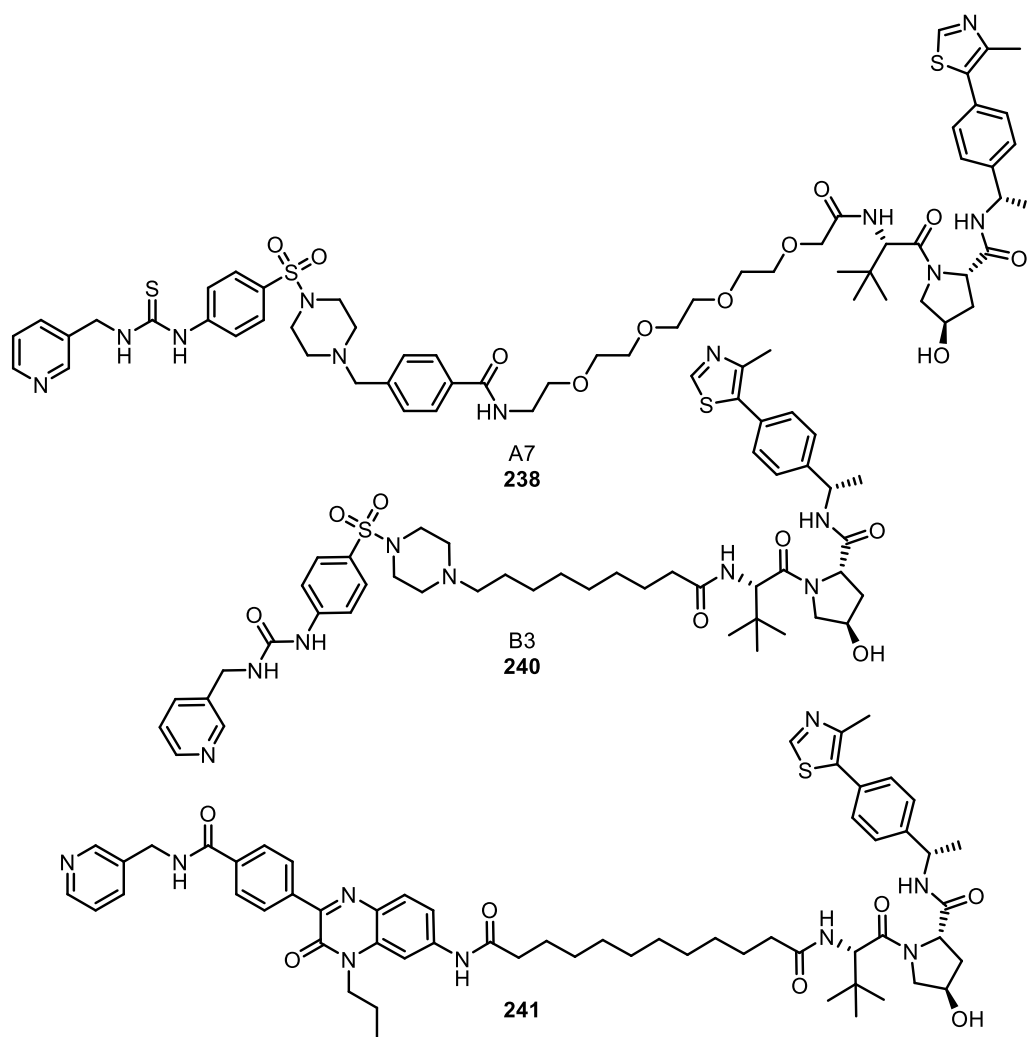
Figure 2.52 Structures of NAMPT PROTACs disclosed by Wu et al., Bi et al., and Zhang et al.

Cheng *et al.*, of the same group as above, published a fluorescent NAMPT PROTAC that degraded NAMPT and allowed the process to be visualised.[263] Their compound, **241**, degraded NAMPT in A2780 cells with a DC_{50} of 8.4 nM. Their compound showed promising anti-tumour effects both *in vitro* and *in vivo*.

Finally Zhang *et al.*, again part of the same group, published a series of NAMPT PROTACs based on FK866.[264] The used the same VHL ligand as in their previous work, and synthesised PROTACs with an alkyl linker of varying length. Their best performing PROTAC **242** had a DC_{50} of 31.7 nM in A2780 cells. Most of their series also showed antiproliferative effects against A2780 cells, with the most potent compound being comparable to FK866 (EC_{50} of 2.4 nM compared to <3.0 nM). Their best degrading

PROTAC **242**, though, was about 10-fold less potent for antiproliferative activity than FK866.

Work in a different group, by Zhu *et al.*, also led to the development of a series of FK866-derived NAMPT PROTACs.[265] Unlike the PROTACs discussed above, they used CRBN recruiting ligands in their design. They designed and synthesised 12 PROTACs, with varying degradation potential.
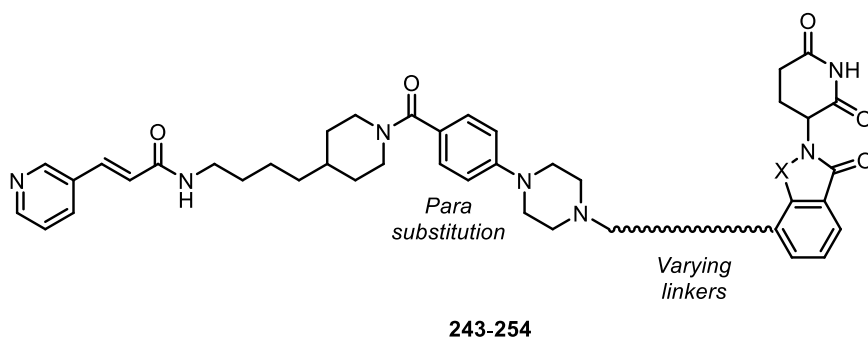
Figure 2.53 General structure of the NAMPT PROTACs designed and synthesised by Zhu et al. Note the para substitution of the aromatic capping group in the FK866-derived part of the structure.

Zhu *et al.* synthesised PROTACs with a variety of linker types, including all-alkyl and PEGylated examples of varying lengths. They also all three of thalidomide-type, lenalidomide-type, and alkyne-lenalidomide-type CRBN ligands. The degrading potential of these different compounds are summarised in table 2.6. Their results seem to show that the overall efficacy of the PROTAC is very sensitive to changes in the linker length and composition.

For example, as seen in table 2.6, increasing the length of alkyl linker **244** by just one carbon to reach **245** transforms the PROTAC from inducing no measurable degradation to effectively degrading NAMPT with a 1.44 nM DC_{50}. Both compounds **245** and **246** are potent degraders, with sub 2 nM DC_{50}s. They have linker lengths of 6 and 8 atoms, respectively. The PEGylated 7-atom linker in **247** however shows no measureable degradation, suggesting oxygen atoms in the linker are poorly tolerated. **248**, one PEG unit longer than **247**, also shows no degradation.

This sensitivity is also seen in the lenalidomide series: Moving from **251**, a 7-atom alkyl linker to **252**, an 8-atom alkyl linker results in a switch from no activity to a 5.58 nM DC$_{50}$. The two alkyne-lenalidomides show almost identical activity, though, despite being one atom different in length.

These results, taken together, suggest that there is an extremely narrow structural window which successful NAMPT PROTACs can occupy, and that it therefore might be quite easy to synthesise a range of NAMPT PROTACs but miss this window and see no activity.

It's possible to draw some very crude comparisons in linker length between these PROTACs from Zhu *et al.* and our PROTACs. The obvious limitations of this are: (1) the linking groups are different – we have used derivatised the aromatic ring with a phenolic ether, whereas Zhu *et al.* have attached a piperazine to the ring. We can crudely approximate the piperazine as 4 atoms long. (2) Both sets of PROTACs derivatise from different positions on the aromatic ring. This changes the effective PROTAC linker length. (3) Our linkers have an amide in the middle, whereas the literature ones don't. As discussed above, this system seems to be incredibly sensitive to linker composition, so this might be a significant factor.

An atom count of our CRBN recruiting PROTACs gives a linker length of 13 atoms. As our PROTACs are *ortho* substituted the effective length is probably slightly less than this. This makes the following compounds vaguely comparable:

- Thalidomide-based **235** (this work) and **246** (Zhu *et al.*)
- Alkyne-lenalidomide **233** (this work), **253**, and **254** (Zhu *et al.*)

In all cases our compounds show no activity whereas the corresponding literature compounds show <10 nM DC$_{50}$s. This difference in activity despite vaguely similar linker lengths could be down to the different linker compositions, or the different attachment point on the aromatic ring.
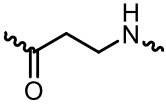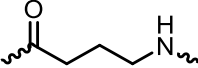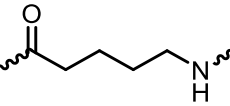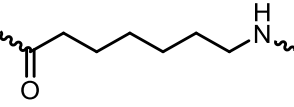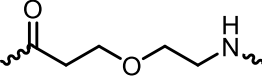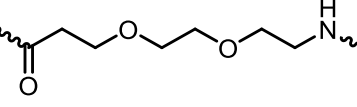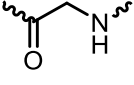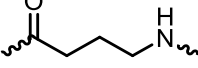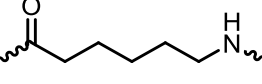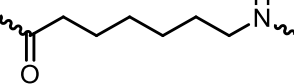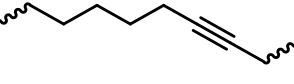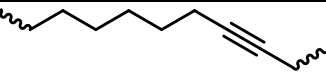
Compound	Linker	Linker length /atoms	X	DC_{50} /nM	D_{max} /%
243	(chemical structure)	4	CO	nd	0
244	(chemical structure)	5	CO	nd	0
245	(chemical structure)	6	CO	1.44	57
246	(chemical structure)	8	CO	<1	75
247	(chemical structure)	7	CO	nd	0
248	(chemical structure)	10	CO	nd	0
249	(chemical structure)	3	CH_2	nd	0
250	(chemical structure)	5	CH_2	nd	38
251	(chemical structure)	7	CH_2	nd	0
252	(chemical structure)	8	CH_2	5.85	73
253	(chemical structure)	8	CH_2	<1	93
254	(chemical structure)	9	CH_2	<1	93

Table 2.6 Summary of the degradation efficacies of the PROTACs made by Zhu et al. DC_{50} values were calculated from Western blot analysis after Jurkat cells were treated with compound for 24 h. nd = not detected.

Whilst we have functionalised the *ortho* position of the aromatic ring, they have functionalised the *para* position (figure 2.53). Inspection of the crystal structure of

FK866 bound to NAMPT (PDB: 2GVJ), the *para* position clearly points towards the surface of the protein, meaning substitution at this position would be expected to disrupt NAMPT binding. The paper mentions no reasoning behind this design choice. The fact that Zhu *et al.*'s PROTACs work, and retain binding affinity for NAMPT, suggests that their PROTACs adopt a different binding pose in the NAMPT active site, and that this altered binding pose may allow the necessary PPIs to form that allow the formation of a stable, productive ternary complex. Some insight into this can be gleaned from considering the crystal structure of NAMPT inhibitor GMX1778 (**122**).
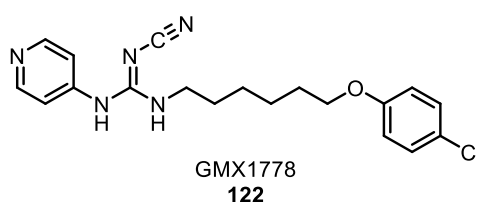
GMX1778
122

*Figure 2.54 Chemical structure of NAMPT inhibitor GMX1778 (**122**). This inhibitor follows the general blueprint for a NAMPT inhibitor, but with the addition of a para substituent on the aromatic capping group.*

GMX1778 (**122**) follows the general NAMPT inhibitor blueprint, of a headgroup, a hydrophobic alkyl linker, and an aromatic capping group. The aromatic capping group is also substituted at the *para* position. The crystal structure obtained of GMX1778 in complex with NAMPT shows the inhibitor adopting two different binding poses.[156] One is essentially the standard binding pose of NAMPT inhibitors, with the *para* position of the ring (and the substituent in this case) pointing into a pocket in the active site. This can be seen by overlaying this with FK866 (figure 2.55). The other binding pose, though, points the *para* position out towards solvent. The rest of the molecule remains in approximately the same position, but the aromatic capping group is just flipped.
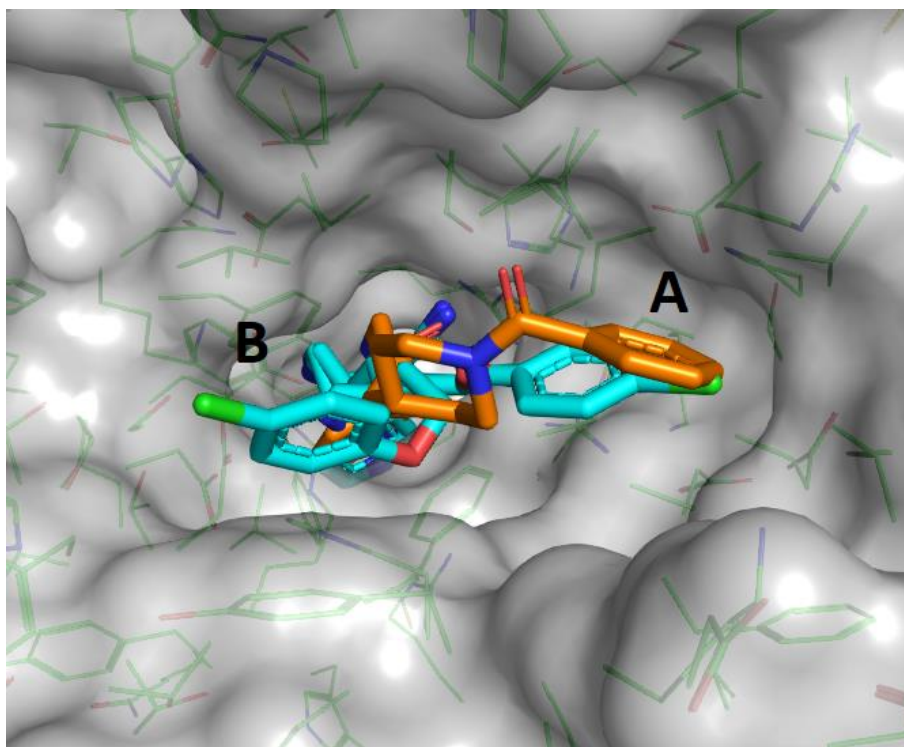
*Figure 2.55 Overlay of the crystal structures of GMX1778 (**122**, light blue) and FK866 (**121**, orange) in complex with NAMPT. The two binding poses of GMX1778 are denoted A and B. Pose A matches the canonical binding of FK866, with the para substituent pointing into a pocket. Pose B points the para substituent out of the pocket, and into solvent. PDB: 2GVJ and 4O12.*

If this tracks over to FK866 derivatives with *para* substituents, it suggests this kind of substitution is tolerated, and leads to a change in binding mode to facilitate the new steric bulk. The binding poses may not track over exactly to FK866-type ligands as the linkage between the aromatic capping group and the alkyl linker is made by a phenolic ether in GMX1778, but a piperidine amide in FK866. The latter is likely to be more rigid, which might mean FK866 is less able to achieve the conformation required to adopt this altered binding pose. As far as we are aware there are no published crystal structures of FK866-based inhibitors with *para* substituents, however the fact that the Zhu PROTACs work means they are binding to NAMPT, whether in the canonical binding pose or otherwise.

2.5.11 Attempting to replicate the findings of Wu *et al.*

Given the success of the first published thiourea based PROTAC A7 (**238**), we decided to make compound **238** and test it to understand its effect relative to our compounds. We followed the synthetic route Wu *et al.* proposed.

4-Nitrobenzenesulphonyl chloride (**255**) was smoothly condensed with *N*-Boc piperazine (**256**) to afford sulphonamide **257**. The nitro group was then reduced under mild conditions with iron filings and aqueous ammonium chloride to give aniline **258**. 1,1'-Thiocarbonyldiimidazole (thio-CDI) was used to generate isothiocyanate **259**, which could be isolated as a bench-stable solid. 3-Aminomethylpyridine was then added into the isothiocyanate, generating thiourea **260**. A Boc deprotection gave **261**, followed by a substitution of methyl 4-(bromomethyl)benzoate to give methyl ester **262**. A basic ester hydrolysis then afforded intermediate **263**, the completed NAMPT-binding part of PROTAC **238**.
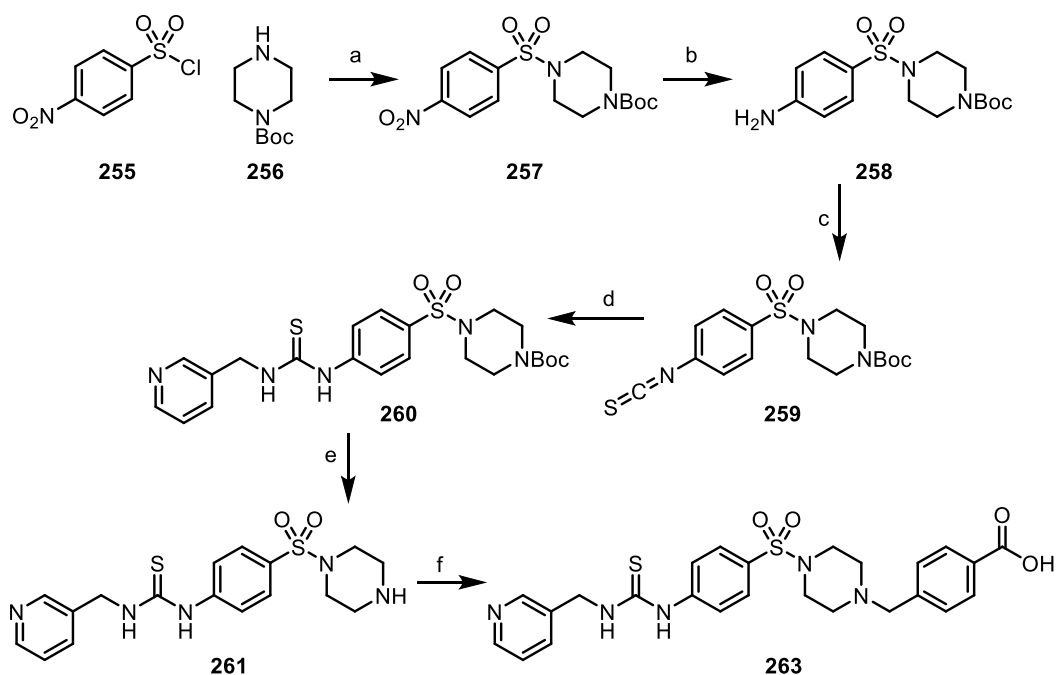
*Figure 2.56 Synthetic route to intermediate **263**. a: **255** (1.0 eq), **256** (2.0 eq), NEt₃ (1.0 eq), DCM, RT, 0.5 h, 96%. b: Fe(s) (2.6 eq), NH₄Cl (aq.), EtOH/H₂O, 75 °C, 1.2 h, 93%. c: TCDI (3.0 eq), NEt₃ (2.0 eq), DCM, 0 °C to RT, o/n, 54%. d: 3-Aminomethylpyridine (1.0 eq), DCM, RT, o/n, 79%. e: 10% TFA in DCM, RT, 2.0 h. f: (i) Methyl 4-(bromomethyl)benzoate (2.5 eq), NEt₃ (6.0 eq), DCM, RT, 2.0 h, 20% over two steps (ii) LiOH.H₂O (6.0 eq), THF/MeOH/H₂O, RT, o/n, 61%.*

To produce the VHL-binding part of PROTAC **238**, commercially available **264** was coupled with 14-azido-3,6,9,12-tetraoxatetradecanoic acid using HATU as an amide coupling reagent. The azide in **265** was then reduced using hydrogen and palladium on carbon, giving amine **266**. This was then coupled to acid **263** again using HATU, to afford PROTAC **238**.
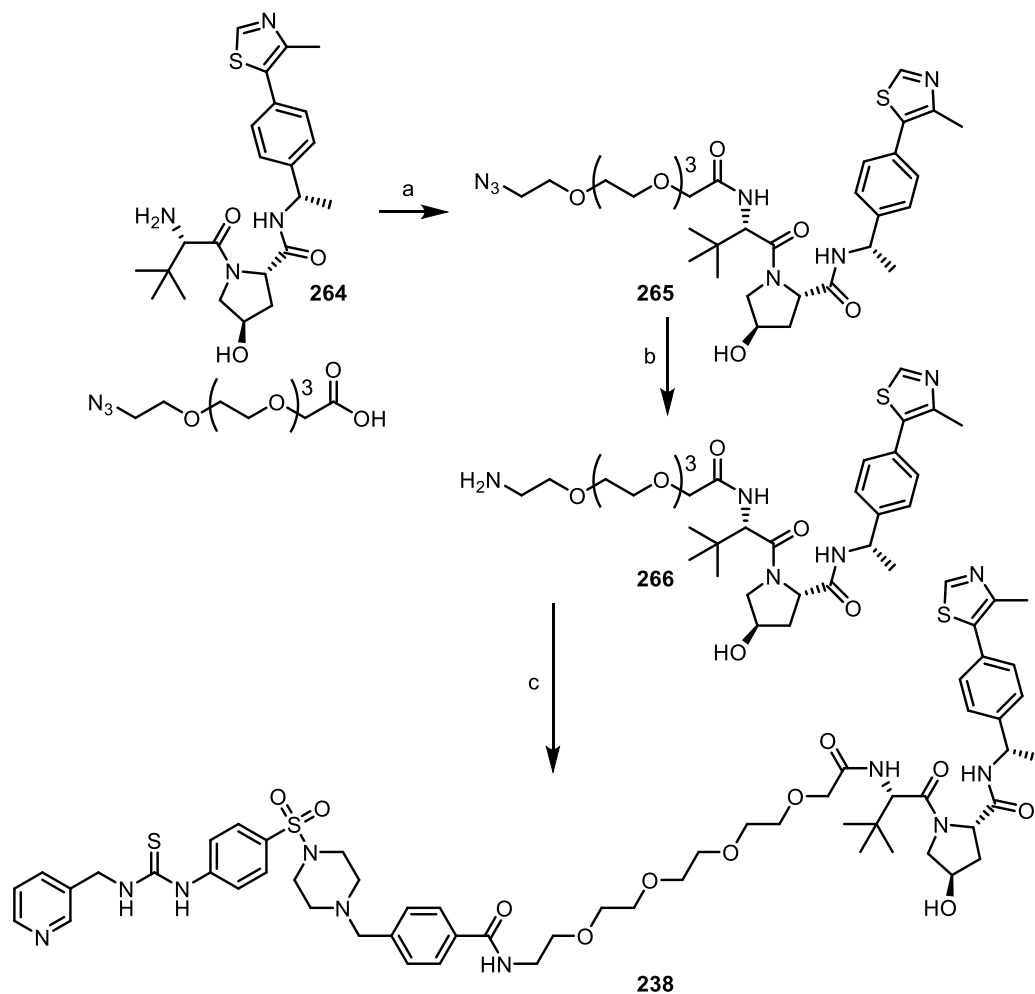
*Figure 2.57 Synthetic route to the E3-binding part of PROTAC **238**, and final coupling to give **238**. a: 14-Azido-3,6,9,12-tetraoxatetradecanoic acid (1.0 eq), HOBt.H$_2$O (2.0 eq), DIPEA (4.0 eq), HATU (2.0 eq), DMF, RT, 2.0 h, 65%. b: H$_{2(g)}$, Pd/C, EtOAc, RT, o/n, 37%. c: **263** (1.5 eq), HOBt.H$_2$O (2.0 eq), DIPEA (6.0 eq), HATU (3.0 eq), DMF, RT, o/n, 19%.*

In order to allow a more direct comparison of our findings with the published results, we decided to first compare the activity of our molecules and the published PROTAC in A2780 ovarian cancer cells. Cells were incubated with our PROTACs (**231**-**235**), and PROTAC **238**. Concentrations of 1, 10, and 100 nM were tested, and the cells incubated

for 24 h. A Western blot was then run to investigate potential depletion of NAMPT. These experiments and Western blots were performed by Lucy Li.

The blots clearly show no degradation of NAMPT for any of the compounds tested at any of the concentrations (figure 2.58). This includes the literature compound **238**, even the highest concentration tested of 0.1 μM, which should be sufficient to cause significant NAMPT degradation based on the published data.
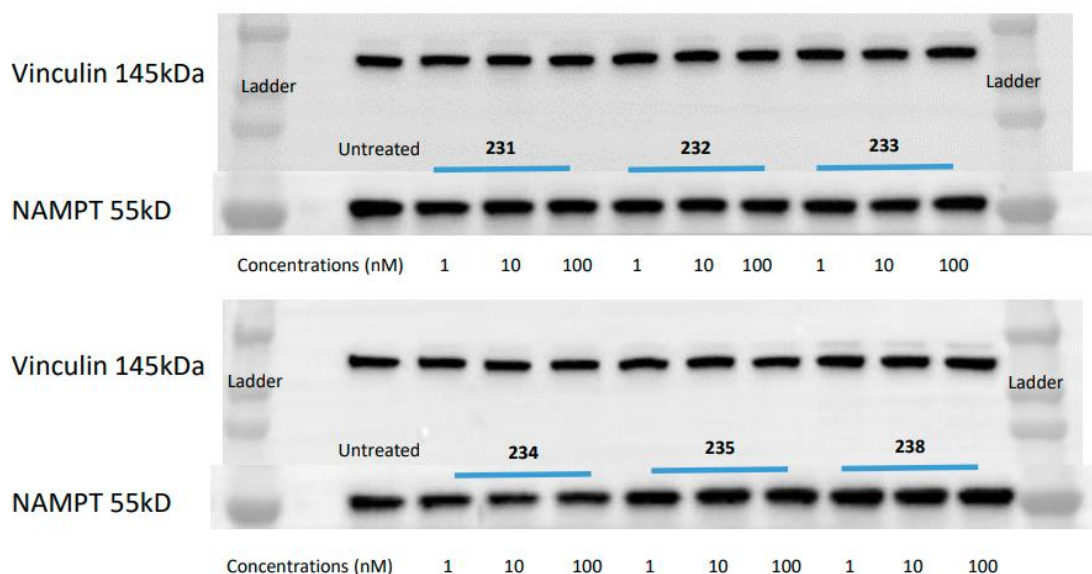
*Figure 2.58 Western blots of compounds **231**-**235** and **238**. 1x10^6 A2780 cells/mL were treated with compounds for 24 h at concentrations of 1, 10, and 100 nM. The antibody used was Bethyl A700-058. Data collected by Lucy Li.*

2.5.12 Conclusions and future work

A series of NAMPT PROTACs were synthesised based on the inhibitor FK866, and recruiting VHL and CRBN E3 ligases. Although these compounds caused a decrease in cell viability in a WST-1 assay, Western blot analysis determined that they weren't inducing the degradation of NAMPT. Crucially though, this evidence suggests that the PROTACs are getting into the cells, and engaging NAMPT. Linker length or composition could be inadequate for formation of effective protein-protein interactions, leading to an unstable ternary complex that doesn't lead to ubiquitination and degradation.

Work in the literature that was published during these studies suggests that the linker length and composition is crucial for a NAMPT PROTAC to degrade effectively, supporting the analysis above.

Future work should involve a more systematic and complete screen of different linker lengths and compositions to determine whether our compound design can generate successful PROTACs.

To investigate the effect of substituting the aromatic capping group in FK866 at different positions, a series of matched pairs could be synthesised, differing only by attachment point on the ring. This will help understand whether *para* substitution on the FK866 core is necessary for an effective PROTAC.

A NAMPT PROTAC disclosed in the literature was also synthesised and tested. Although the compound was made successfully, we did not observe any degradation of NAMPT in our hands at the concentrations we tested. The concentrations covered in the paper disclosing this compound extended to a higher range, so perhaps we were just testing below its effective concentration. This may be the case, but it's reasonable to say that a PROTAC with no observable degradation at 100 nM doesn't warrant further investigation. Ideally the more active PROTACs that have been published since this work was undertaken should also be made for comparison, with a more comprehensive analysis of concentrations required for target engagement and degradation in matched cell lines.

So far the only NAMPT ligands that have been used to make PROTACs are FK866 (**121**) and MS7 (**239**). It may be fruitful to explore alternative ligands from which to build PROTACs, as better performance may be achievable. There are a plethora of NAMPT ligands in the literature, many of which are commercially available.

During the synthetic work to generate the PROTACs, some unusual reactivity that formed enaminones was observed. Brief investigations were carried out, and it was found that the reactivity was only apparent for carboxylic acids bearing an α-fluorine. A hypothesis was put forward for the mechanism by which the reaction proceeds, supported by literature precedent. A crucial piece of evidence, the formation of

aldehyde **214**, was missing though. This raises the possibility that the reactivity we observed proceeds via a different mechanism to the similar literature. Further optimisation and investigation could provide mechanistic insight, and possibly make this reaction a useful synthetic tool.

3   Experimental

3.1   General experimental

Anhydrous solvents were obtained from Acros Organics over 3 Å molecular sieves and were stored under nitrogen. All other reagents and solvents were purchased from Sigma-Aldrich, Fisher Scientific, VWR International and Fluorochem and were used as received. Room temperature (RT) refers to 21– 25 °C. Temperatures of 0 °C were maintained using an ice-water bath and temperatures below 0 °C were maintained using dry ice-acetone baths. The progress of reactions was monitored by thin-layer chromatography (TLC) or if appropriate, liquid chromatography-mass spectrometry (LCMS). TLC was performed on Merck 60 F_{254} silica gel plates which were visualised using short-wave UV light (254 nm) and staining with $KMnO_4$, anisaldehyde, vanillin or ninhydrin. During work-up brine refers to a saturated solution of NaCl in H_2O. Column chromatography was performed using silica gel (Geduran silica gel 60, 40–63 μm). Silica gel was neutralised (where necessary) by the addition of NEt_3 to the solvent system. Hexane refers to *n*-hexane. Unless otherwise stated, all reactions were carried out under an inert atmosphere using oven-dried glassware. SCX chromatography refers to the use of a Teledyne ISCO RediSep R_f SCX (strong cationic exchange) column to retain basic compounds. Compounds requiring purification by reverse-phase chromatography were purified using a Teledyne ISCO automated column system using RediSep R_f C18 Gold 15.5 g or 30 g columns. MeCN was obtained from Fisher Scientific (HPLC grade) and deionised H_2O was modified by the addition of 0.1% v/v formic acid (VWR, 80% aq. solution) or 0.1% v/v NH_3 (Fisher, 28% v/v aq. solution). Columns were maintained at room temperature through acquisition. The UV detector scanned between 200–300 nm and at 254 nm. All components were maintained at room temperature throughout separation. NMR data were recorded on a Bruker AV400 (400 MHz ^{1}H, 101 MHz ^{13}C, T = 293 K) or a Bruker AV500 (500 MHz ^{1}H, 126 MHz ^{13}C, T = 293 K). Spectra were recorded in an appropriate deuterated solvent, and referenced to the residual solvent peak. Data were processed on Mestrenova 11.0. Chemical shifts, δ, are reported in ppm and coupling constants, J, are reported in Hz to the nearest 0.1 Hz. Coupling constants that were non-identical are reported as averages. The following

abbreviations are used to describe the multiplicity of resonances in 1H NMR spectra: s (singlet), d (doublet), t (triplet), q (quartet), p (pentet) m (multiplet), app. (apparent). Proton-decoupled ^{13}C NMR spectra were recorded using the PENDANT pulse sequence and/or the UDEFT pulse sequence. Proton assignments were determined either on the basis of unambiguous chemical shift or coupling pattern, by patterns observed in 2D experiments or by analogy with fully interpreted spectra for related compounds. The numbering of compounds for NMR assignment is consistent with that used in the literature. Where it is not possible to resolve individual resonances due to multiple peaks stacking in 1H NMR, the stack has been labelled as 'residual protons'. Two dimensional ($^1H^1H$, $^1H^{13}C$) NMR data were recorded on a Bruker AV400 or AV500 spectrometer (T = 293 K). LC data was obtained using a Waters ACQUITY UPLC PDA detector scanning between 210-400 nm. Mass spectrometry data was acquired using a Waters ACQUITY QDa detector scanning in the positive (ES+) and negative (ES–) modes between m/z 100-1000. Separation of components was achieved using a Waters ACQUITY UPLC BEH C18 1.7 μm 2.1 × 50 mm column coupled to a Waters ACQUTY UPLC BEH C18 1.7 μm VanGuard pre-column 2.1 × 5 mm. Columns were maintained at 40 °C throughout acquisition. The table below details a schematic for the standard four-minute run on the instrument using a flow rate of 0.60 mL min^{-1}:

Start Time / min	End Time / min	H$_2$O:MeCN (% v/v)
0	0.50	95:5
0.50	2.50	95:5 → 5:95
2.50	3.00	5:95
3.00	3.10	5:95 → 95:5
3.10	4.00	95:5

All solvents obtained were of LC-MS grade (Fisher Optima) and were modified by the addition of 0.1% v/v formic acid (Fisher Optima) referred to as method 1 or NH$_4$OH (Fisher, 28% v/v aq. solution) referred to method 2. Samples were prepared in MeOH (Fisher Optima) and a 2.0 μL aliquot was extracted from each sample for analysis. Samples were maintained at 10 °C prior to acquisition. Solvents were combined using a Waters ACQUITY UPLC H-Class Quaternary Solvent Manager (QSM) with in-built

degasser. Inert gas was provided using a Genius NM32LA nitrogen generator. The switch method consisted of 95:5 H2O:MeCN (with appropriate acidic or basic modifiers) running at 0.60 mL min^{-1} for two minutes immediately prior to acquisition. Data was processed using MassLynx V4.1. Values of purity were obtained through analysis of the peak areas in the LC trace between 0.40 min. and 3.50 min. Infrared spectra were recorded on a Bruker Tensor 27 with ATR attachment between 4000-600 cm^{-1} and are reported in cm^{-1}.

3.2 Development of a microbial transglutaminase bioconjugation method for the production of antibody-drug conjugates

3.2.1 MTG substrates obtained commercially

N_α-Ac-L-lysine (**42**), N_α-Ac-L-lysine methyl ester HCl (**28**), L-lysine HCl (**43**), Glycine methyl ester HCl (**30**), 2-amino-N-methylacetamide (**44**), L-alanine methyl ester HCl (**71**), β alanine (**31**), n-propylamine (**73**), n-butylamine (**76**), n-pentylamine (**77**), allyl amine (**72**), propargylamine (**18**), cysteamine (**69**), 2-(2-(2-aminoethoxy)ethoxy)ethan-1-ol (**68**), glycine (**29**), benzylamine (**10**), 2-methoxybenzylamine (**52**), 3-methoxybenzylamine (**53**), 4-methoxybenzylamine (**54**), 2-(aminomethyl)thiophene (**57**), 2-(aminomethyl)furan (**56**), 3-picolylamine (**55**), (1,3-oxazol-5-yl)methanamine (**58**).

3.2.2 Chemical synthesis

2-Hydroxyisoindoline-1,3-dione sodium salt (48)
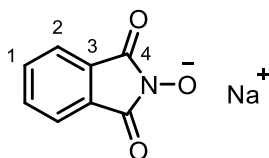
A flame dried flask was charged with N-hydroxyphthalimide (4.08 g, 25.0 mmol, 1.0 eq) and EtOH abs. (25 mL), then the mixture was cooled to 0 °C with an ice bath. Sodium metal (575 mg, 25.0 mmol, 1.0 eq) was added in portions, then the reaction stirred at room temperature for 30 min. The resulting red precipitate was recovered

by vacuum filtration and washed with EtOH (20 mL), then dried at 120 °C overnight to afford the title compound as a brick red solid (3.81 g, 82%)

^{1}H NMR (400 MHz, Deuterium Oxide) δ 7.45 – 7.40 (m, 2H), 7.37 – 7.31 (m, 2H).

^{13}C NMR (101 MHz, Deuterium Oxide) δ 169.4 (C4), 133.4 (C1), 129.4 (C3), 121.6 (C2).

t_R (method 1) = 1.61 min

Analytical data matches that found in the literature.[266]

Methyl 5-((1,3-dioxoisoindolin-2-yl)oxy)pentanoate (50)
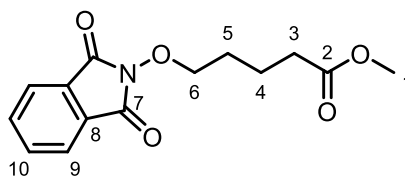
5-bromo-ethylvalerate (717 μL, 5.00 mmol, 1.0 eq), *N*-hydroxyphthalimide sodium salt (**48**) (815 mg, 5.00 mmol, 1.0 eq), and NEt$_3$ (1.39 mL, 10.0 mmol, 2.0 eq) were dissolved in MeCN (10 mL) and stirred at reflux for 3.0 h. The mixture was cooled to 0 °C and filtered. The filtrate was concentrated under reduced pressure and redissolved in EtOAc (10 mL), then washed with H$_2$O (3 x 5.0 mL), then brine (5.0 mL). The organic layer was then dried over MgSO$_4$, filtered, and concentrated under reduced pressure. The residue was purified by recrystallisation from EtOH, to afford the title compound as beige needle crystals (1.02 g, 74%).

^{1}H NMR (400 MHz, CDCl$_3$) δ 7.78 – 7.74 (m, 2H, H9 or H10), 7.70 – 7.67 (m, 2H, H9 or H10), 4.14 (t, *J* = 6.1 Hz, 2H, H6), 3.60 (s, 3H, H1), 2.36 (t, *J* = 7.0 Hz, 2H, H3), 1.86 – 1.68 (m, 4H, H4 and H5).

^{13}C NMR (101 MHz, CDCl$_3$) δ 173.7 (C2), 163.6 (C7), 134.5 (C9 or C10), 128.9 (C8), 123.5 (C9 or C10), 77.9 (C6), 51.6 (C1), 33.4 (C3), 27.5 (C4 or C5), 21.1 (C4 or C5).

MS: *m/z* (ES+) 186.2 (100%, [M+H]$^+$)

v$_{max}$ (thin film, ATR)/cm^{-1}: 3103, 2939, 1789, 1715, 1610, 1584, 1467, 1451, 1440, 1431, 1422, 1402, 1371, 1323, 1294, 1245, 1188, 1165, 1129, 1104, 1097, 1084, 1067, 1054, 1018, 1003, 982, 952, 915, 876, 803, 787, 777, 697, 621, 587, 519

Analytical data matches that found in the literature.[267]

Methyl 5-(aminooxy)pentanoate (46)
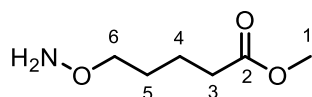
Methyl 5-((1,3-dioxoisoindolin-2-yl)oxy)pentanoate (**50**) (1.02 g, 3.69 mmol, 1.0 eq) was dissolved in EtOH (15 mL). $N_2H_4.H_2O$ (365 µL, 7.38 mmol, 2.0 eq) was added at room temperature, and the reaction stirred overnight. The mixture was concentrated to dryness under reduced pressure. The residue was redissolved in DCM (5.0 mL), and filtered. To afford the product that was used without further purification (142 mg, 26%).

^{1}H NMR (400 MHz, CDCl$_3$) δ 3.57 – 3.55 (m, 5H, stack of H1 and H6), 2.24 (t, *J* = 7.2 Hz, 2H, H3), 1.62 – 1.46 (m, 5H, stack of H4 and H5).

N.B. signal for H4 and H5 overintegrates by 1H

^{13}C NMR (101 MHz, CDCl$_3$) δ 173.9 (C2), 75.3 (C6), 51.4 (C1), 33.7 (C3), 27.7 (C4 or C5), 21.4 (C4 or C5).

MS: *m/z* (ES+) 148.3 (100%, [M+H]$^+$)

HRMS calculated for $C_6H_{14}NO_3$ [M+H]$^+$ 148.0895, found 148.0901

Methyl 5-(hydroxymethyl)furan-2-carboxylate (61)
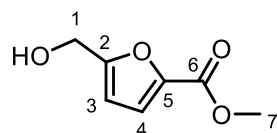
5-(Hydroxymethyl)furan-2-carboxylic acid (500 mg, 3.52 mmol, 1.0 eq), K$_2$CO$_3$ (2.43 g, 17.6 mmol, 5.0 eq), and MeI (1.10 mL, 17.6 mmol, 5.0 eq) were dissolved in DMF

(6.0 mL) at room temperature. The reaction was stirred for 3.5 h then diluted with H_2O (10 mL). The mixture was extracted with EtOAc (5 x 5.0 mL), then the combined organics washed with H_2O (3 x 5.0 mL) then brine (5.0 mL). The organics were then dried over $MgSO_4$, filtered, and concentrated under reduced pressure. The residue was purified by flash column chromatography (1:1 EtOAc:hexane) to afford the title compound as a colourless oil (397 mg, 72%).

^{1}H NMR (500 MHz, CDCl$_3$) δ 7.13 (d, J = 3.4 Hz, 1H, H4), 6.41 (d, J = 3.5 Hz, 1H, H3), 4.67 (s, 2H, H1), 3.89 (s, 3H, H7).

^{13}C NMR (126 MHz, CDCl$_3$) δ 159.2 (C6), 158.3 (C2), 144.1 (C5), 118.9 (C4), 109.5 (C3), 57.6 (C1), 52.0 (C7).

MS: m/z (ES+) 157.0 (100%, [M+H]$^+$)

R$_t$ (method 1) = 1.49 min

R$_f$ (1:1 EtOAc:hexane) = 0.34

Methyl 5-(((methylsulfonyl)oxy)methyl)furan-2-carboxylate (62)
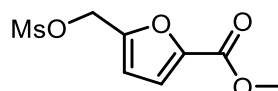
Methyl 5-(hydroxymethyl)furan-2-carboxylate (**61**) (44.0 mg, 0.282 mmol, 1.0 eq), MsCl (32.9 µL, 0.423 mmol, 1.5 eq), and NEt$_3$ (118 µL, 0.846 mmol, 3.0 eq) were dissolved in DCM (2.0 mL) at room temperature and stirred for 2.0 h. The mixture was diluted with H_2O (5.0 mL) and extracted with DCM (3 x 5.0 mL). The combined organics were washed sequentially with H_2O (5.0 mL) and HCl (1 M, aq., 5.0 mL), then dried over $MgSO_4$, filtered, and concentrated under reduced pressure to afford the title compound that was used without further purification.

Methyl 5-(azidomethyl)furan-2-carboxylate (63)
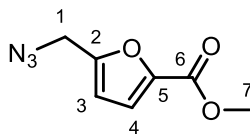
Methyl 5-(((methylsulfonyl)oxy)methyl)furan-2-carboxylate (**62**) (assumed 0.282 mmol), NaN_3 (55.0 mg, 0.846 mmol, 3.0 eq), and KI (11.7 mg, 0.0705 mmol, 0.25 eq) were dissolved in DMF (1.5 mL) at room temperature. The reaction was heated to 60 °C and stirred overnight. The mixture was diluted with water (3.0 mL) and extracted with EtOAc (5 x 5.0 mL). The combined organics were washed with H_2O (3 x 5.0 mL) and brine (5.0 mL), dried over $MgSO_4$, filtered, and concentrated under reduced pressure to afford the title compound that was used without further purification (23.0 mg, 45% over two steps).

^{1}H NMR (500 MHz, $CDCl_3$) δ 7.14 (d, *J* = 3.5 Hz, 1H, H4), 6.47 − 6.45 (m, 1H, H3), 4.37 (s, 2H, H1), 3.89 (s, 3H, H7).

^{13}C NMR (126 MHz, $CDCl_3$) δ 158.8 (C6), 153.2 (C2), 144.9 (C5), 118.7 (C4), 111.0 (C3), 52.1 (C7), 46.9 (C1).

MS: *m/z* (ES+) 154.1 (100%, $[M+H-N_2]^+$)

R_t (method 1) = 2.13 min

Methyl 5-(aminomethyl)furan-2-carboxylate (59)
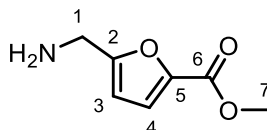
Methyl 5-(azidomethyl)furan-2-carboxylate (**63**) (145 mg, 0.801 mmol, 1.0 eq), PPh_3 (314 mg, 1.20 mmol, 1.5 eq), and H_2O (86.8 μL, 4.81 mmol, 6.0 eq) were dissolved in THF (3.0 mL) at room temperature. The mixture was heated at reflux for 3.0 h, then cooled to room temperature and concentrated to dryness under reduced pressure. The residue was purified by reverse phase flash column chromatography (acid

modifier) to afford the title compound as a yellow oil that degraded under ambient conditions.

5-(Hydroxymethyl)-*N*-propylfuran-2-carboxamide (65)
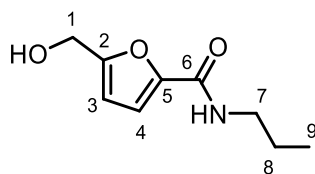
5-(Hydroxymethyl)furan-2-carboxylic acid (169 mg, 1.19 mmol, 1.0 eq), *n*-propylamine (196 μL, 2.38 mmol, 2.0 eq), and DIPEA (848 μL, 4.77 mmol, 4.0 eq) were dissolved in DMF (3.0 mL) at room temperature. HATU (680 mg, 1.79 mmol, 1.5 eq) was added, and the reaction stirred for 45 minutes. The mixture was diluted with H_2O (5.0 mL) and extracted with EtOAc (5 x 5.0 mL). The combined organics were then washed with water (3 x 5.0 mL), and brine (5.0 mL), then dried over $MgSO_4$, filtered, and concentrated under reduced pressure. The residue was purified by flash column chromatography (4:1 EtOAc:hexane) to afford the title compound as a yellow oil (118 mg, 54%).

^{1}H NMR (500 MHz, MeOD) δ 7.05 (d, *J* = 3.5 Hz, 1H, H4), 6.45 (d, *J* = 3.4 Hz, 1H, H3), 4.59 (s, 2H, H1), 3.33 – 3.30 (m, 2H, H7), 1.62 (h, *J* = 7.4 Hz, 2H, H8), 0.96 (t, *J* = 7.5 Hz, 3H, H9).

^{13}C NMR (126 MHz, MeOD) δ 159.5 (C6), 157.2 (C2), 147.0 (C5), 114.4 (C4), 108.9 (C3), 56.1 (C1), 40.6 (C7), 22.4 (C8), 10.3 (C9).

MS: *m/z* (ES+) 184.2 (100%, [M+H]$^+$)

R$_t$ (method 1) = 1.61 min

HRMS calculated for $C_9H_{13}O_3NNa$ [M+Na]$^+$ 206.0788, found 206.0783

(5-(Propylcarbamoyl)furan-2-yl)methyl methanesulfonate (66)
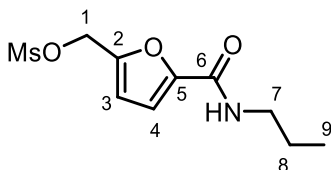
5-(Hydroxymethyl)-*N*-propylfuran-2-carboxamide (**65**) (118 mg, 0.645 mmol, 1.0 eq), MsCl (75.2 µL, 0.968 mmol, 1.5 eq), and NEt$_3$ (270 µL, 0.1.94 mmol, 3.0 eq) were dissolved in DCM (2.0 mL) at room temperature and stirred overnight. This led to complete degradation of product in the reaction mixture.

But-2-yn-1-amine HCl (74)
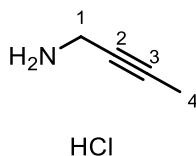
Known compound made by known procedure[268]

1-Bromo-2-butyne (160 µL, 1.83 mmol, 1.0 eq) and NaN$_3$ (595 mg, 9.15 mmol, 5.0 eq) were stirred in DMF (5.0 mL) at room temperature for 24 h. Et$_2$O (10 mL) was added to precipitate excess NaN$_3$, and the mixture filtered through a celite pad and washed with Et$_2$O (8.0 mL). The organics were washed with H$_2$O (6 x 5.0 mL) and brine, then dried over MgSO$_4$ and filtered. The organics were then concentrated under reduced pressure. The residue was re-dissolved in Et$_2$O (10.0 mL), and PPh$_3$ (959 mg, 3.66 mmol, 2.0 eq) was added in four portions over 5 min, and the reaction stirred at room temperature overnight. The reaction mixture was quenched with HCl (5.0 mL, 2.0 M, aq.) and stirred for 30 min. The aqueous layer was washed with EtOAc (3 x 5 mL) and concentrated under reduced pressure to yield the title product as a tan solid (71.8 mg, 37%).

^{1}H NMR (400 MHz, MeOD) δ 3.73 (q, *J* = 2.7 Hz, 2H, H1), 1.86 (t, *J* = 2.5 Hz, 3H, H4).

^{13}C NMR (101 MHz, MeOD) δ 84.8 (C2), 71.5 (C3), 30.4 (C1), 3.2 (C4).

HRMS calculated for C$_4$H$_8$N [M+H]$^+$ 69.0578, found 69.0580

Pent-2-yn-1-amine HCl (75)
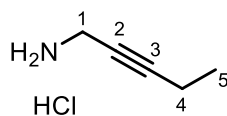
Known compound made by known procedure[269]

1-Bromo-2-pentyne (307 μL, 3.00 mmol, 1.0 eq) and NaN_3 (975 mg, 15.0 mmol, 5.0 eq) were stirred in DMF (3.0 mL) at room temperature for 24 h. Et_2O (10 mL) was added to precipitate excess NaN_3, and the mixture filtered through a celite pad and washed with Et_2O (8.0 mL). The organics were washed with H_2O (6 x 5.0 mL) and brine, then dried over $MgSO_4$ and filtered. The organics were then concentrated under reduced pressure. The residue was re-dissolved in Et_2O (10.0 mL), and PPh_3 (1.57 g, 6.0 mmol, 2.0 eq) was added in four portions over 5 min, and the reaction stirred at room temperature overnight. The reaction mixture was quenched with HCl (5.0 mL, 2.0 M, aq.) and stirred for 30 min. The aqueous layer was washed with EtOAc (3 x 5 mL) and concentrated under reduced pressure to yield the title product as a tan solid (122 mg, 34%).

^{1}H NMR (400 MHz, D_2O) δ 3.75 (t, J = 2.3 Hz, 2H, H1), 2.21 (qt, J = 7.5, 2.3 Hz, 2H, H4), 1.09 (t, J = 7.5 Hz, 3H, H5).

^{13}C NMR (101 MHz, D_2O) δ 90.4 (C3), 70.1 (C2), 29.4 (C1), 12.7 (C5), 11.6 (C4).

HRMS calculated for $C_5H_{10}N$ [M+H]$^+$ 83.0735, found 83.0734

4-Hydroxybut-2-yn-1-yl 4-methylbenzenesulfonate (84)
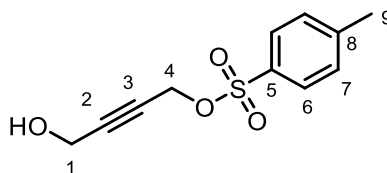
1,4-Butynediol (2.58 g, 30.0 mmol, 1.0 eq), Ag_2O (9.40 g, 40.9 mmol, 1.4 eq), and KI (498 mg, 3.00 mmol, 0.10 eq) were dissolved in DCM (80 mL) at room temperature. TsCl (5.70 g, 30.0 mmol, 1.0 eq) was added at room temperature, and the reaction stirred overnight. The mixture was filtered, concentrated under reduced pressure, and

the residue purified by flash column chromatography (1:2 EtOAc:hexane) to afford the title compound as a colourless oil (3.16 g, 44%).

¹H NMR (400 MHz, CDCl₃) δ 7.81 (d, J = 8.4 Hz, 2H, H6), 7.35 (d, J = 8.1 Hz, 2H, H7), 4.73 (t, J = 1.8 Hz, 2H, H1), 4.16 (t, J = 1.8 Hz, 2H, H4), 2.45 (s, 3H, H9).

¹³C NMR (101 MHz, CDCl₃) δ 145.3 (C5), 133.0 (C8), 129.9 (C7), 128.2 (C6), 87.7 (C3), 77.5 (C2), 57.9 (C1), 50.8 (C4), 21.7 (C9).

R$_f$ (2:3 EtOAc:hexane) = 0.28

MS: m/z (ES+) 241.6 (100%, [M+H]⁺)

***Tert*-butyl (4-hydroxybut-2-yn-1-yl)carbamate (82)**
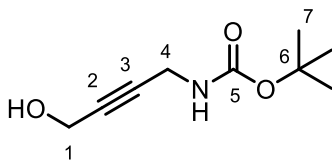
4-Hydroxybut-2-yn-1-yl 4-methylbenzenesulfonate (**84**) (276 mg, 1.15 mmol, 1.0 eq) was dissolved in NH₄OH (35%, aq., 2.3 mL) at room temperature and stirred for 2.0 h. The mixture was then evaporated to dryness, and the residue redissolved in THF (7.5 mL), and NEt₃ (192 μL, 1.38 mmol, 1.2 eq) added. The mixture was cooled to 0 °C, and Boc₂O (301 mg, 1.38 mmol, 1.2 eq) added. The mixture was allowed to warm to room temperature and stirred overnight. The solvent was removed under reduced pressure and the residue redissolved in DCM (5.0 mL), then washed with H₂O (3 x 5.0 mL). The aqueous washings were then extracted with DCM (3 x 5.0 mL). The combined organics were washed with brine (5.0 mL), dried over MgSO₄, filtered, and concentrated under reduced pressure. The residue was purified by flash column chromatography (2:3 EtOAc:hexane) to afford the title compound as a colourless oil (66.0 mg, 31% over two steps).

¹H NMR (500 MHz, CDCl₃) δ 4.19 (t, J = 2.0 Hz, 2H, H1), 3.90 – 3.86 (m, 2H, H4), 1.38 (s, 9H, H7).

13C NMR (126 MHz, CDCl$_3$) δ 155.7 (C5), 81.7 (C3), 81.5 (C2), 80.2 (C6), 50.7 (C1), 30.6 (C4), 28.3 (C7).

R$_f$ (1:1 EtOAc:hexane) = 0.48

HRMS calculated for C$_9$H$_{16}$O$_3$N [M+H]$^+$ 186.1125, found 186.1126

v$_{max}$ (thin film, ATR)/cm^{-1}: 3342, 2978, 2933, 1688, 1512, 1454, 1393, 1366, 1273, 1249, 1157, 1114, 1048, 1018, 931, 917, 859, 779, 763, 546.

2-(Prop-2-yn-1-yl)isoindoline-1,3-dione (92)
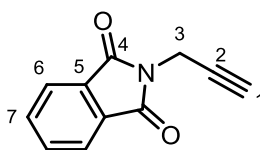
A flask was charged with propargylamine (64.0 μL, 1.00 mmol, 1.0 eq), phthalic anhydride (148 mg, 1.00 mmol, 1.0 eq), and acetic acid (2.0 mL) then the mixture was heated at reflux for 5 h. After cooling to room temperature, the reaction mixture was diluted with water and the precipitate collected and washed with water to yield the title compound as a tan crystalline solid (52.0 mg, 29%).

1H NMR (400 MHz, Chloroform-*d*) δ 7.88 (dd, *J* = 5.5, 3.1 Hz, 2H, H6), 7.74 (dd, *J* = 5.5, 3.1 Hz, 2H, H7), 4.45 (d, *J* = 2.5 Hz, 2H, H3), 2.22 (t, *J* = 2.5 Hz, 1H, H1).

13C NMR (101 MHz, Chloroform-*d*) δ 167.0 (C4), 134.2 (C7), 132.0 (C5), 123.6 (C6), 77.2 (C2), 71.5 (C1), 27.0 (C3).

t$_R$ (method 1) = 2.11 min

MS: *m/z* (ES+) 186.2 (100%, [M+H]$^+$)

Tert-butyl (*tert*-butoxycarbonyl)(prop-2-yn-1-yl)carbamate (93)
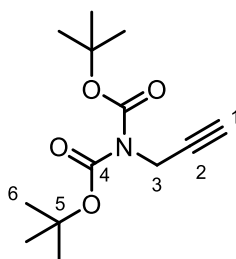
Propargylamine (64.1 µL, 1.00 mmol, 1.0 eq) was dissolved in MeCN (5.0 mL). Di-*tert*-butyl dicarbonate (546 mg, 2.50 mmol, 2.5 eq) and DMAP (122 mg, 1.00 mmol, 1.0 eq) were added at room temperature and the mixture stirred overnight at room temperature. The reaction was then quenched with water and partitioned with Et_2O. The organic phase was then washed sequentially with HCl (1 M, aq.) and water. The organics were dried over $MgSO_4$, filtered, and concentrated under reduced pressure to afford the title compound (183 mg, 72%) that was used without further purification.

^{1}H NMR (400 MHz, Chloroform-*d*) δ 4.27 (d, *J* = 2.5 Hz, 2H, H3), 2.13 (t, *J* = 2.4 Hz, 1H, H1), 1.45 (s, 18H, H6).

^{13}C NMR (101 MHz, Chloroform-*d*) δ 151.5 (C4), 82.9 (C5), 79.6 (C2), 70.5 (C1), 35.7 (C3), 28.0 (C6).

R$_f$ (EtOAc/hexane 1:9) = 0.39

HRMS calculated for $C_{13}H_{21}NO_4Na$ [M+Na]$^+$ 278.1363, found 278.1351.

Analytical data matches that found in the literature.[270]

5-Phenylpent-2-yn-1-ol (98)
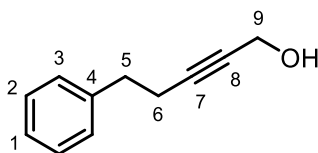
But-3-yn-1-ylbenzene (250 µL, 1.78 mmol, 1.0 eq) was dissolved in THF (10 mL) and cooled to -78 °C *n*-BuLi (1.6 M in hexanes, 1.67 mL, 2.67 mmol, 1.5 eq) was added dropwise and the reaction stirred at -78 °C for 2 h. A suspension of paraformaldehyde

(64.2 mg, 2.14 mmol, 1.2 eq) in THF (5.0 mL) was added dropwise at -78 °C and the mixture allowed to slowly warm to room temperature overnight. The reaction was quenched with NH_4Cl (sat. aq., 5.0 mL), and the THF removed under reduced pressure. The aqueous residue was extracted with EtOAc (3 x 5.0 mL), and the combined organics washed with brine (5.0 mL), dried over $MgSO_4$, filtered, and concentrated under reduced pressure. The residue was purified by flash column chromatography (EtOAc:hexane 1:4) to afford the title compound as a colourless oil (130 mg, 46%).

^{1}H NMR (500 MHz, $CDCl_3$) δ 7.31 (m, 2H, H3), 7.23 (m, 3H, stack of H1 and H2), 4.23 (t, J = 2.2 Hz, 2H, H9), 2.84 (t, J = 7.6 Hz, 2H, H5), 2.52 (tt, J = 7.6, 2.2 Hz, 2H, H6).

^{13}C NMR (126 MHz, $CDCl_3$) δ 140.6 (C4), 128.43 (C2 or C3), 128.42 (C2 or C3), 126.4 (C1), 85.8 (C7), 79.1 (C8), 51.4 (C9), 35.0 (C5), 20.9 (C6).

R_t (method 1) = 2.25 min

R_f (1:4 EtOAc:hexane) = 0.25

HRMS calculated for $C_{11}H_{12}ONa$ $[M+Na]^+$ 183.0780, found 183.0782

v_{max} (thin film, ATR)/cm^{-1}: 3339, 3062, 3027, 2928, 2863, 2224, 1604, 1496, 1453, 1429, 1341, 1224, 1133, 1078, 1010, 747, 698, 578, 506

5-Phenylpent-2-yn-1-yl methanesulfonate (99)
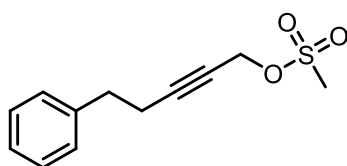
5-Phenylpent-2-yn-1-ol (**98**) (130 mg, 0.813 mmol, 1.0 eq), NEt_3 (452 μL, 3.23 mmol, 4.0 eq), and DMAP (24.8 mg, 0.203 mmol, 0.25 eq) were dissolved in DCM (10 mL) at room temperature. The mixture was cooled to 0 °C and MsCl (190 μL, 2.44 mmol, 3.0 eq) was added dropwise, and the reaction stirred overnight whilst warming to room temperature. The reaction was quenched with H_2O (5.0 mL), and extracted with DCM (3 x 5.0 mL). The combined organics were washed sequentially with H_2O (5.0 mL) and HCl (1.0 M, aq., 5.0 mL), dried over $MgSO_4$, filtered, and concentrated under

reduced pressure to afford the title compound that was used without further purification.

5-Phenylpent-2-yn-1-amine (100)
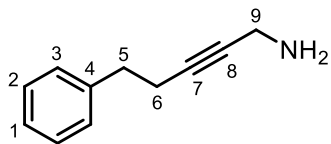

5-Phenylpent-2-yn-1-yl methanesulfonate (**99**) (assumed 0.813 mmol) was dissolved in MeOH (2.0 mL), and NH_3 (~35% aq., 5.0 mL) was added at room temperature. The mixture was stirred for 3.0 h, then concentrated to dryness under reduced pressure. The residue was purified by reverse phase flash column chromatography (acid modifier) to afford the title compound as a colourless oil (24.0 mg, 19% over two steps).

^{1}H NMR (400 MHz, MeOD) δ 7.30 – 7.21 (m, 4H, stack of H2 and H3), 7.21 – 7.16 (m, 1H, H1), 3.73 (t, J = 2.3 Hz, 2H, H9), 2.82 (t, J = 7.4 Hz, 2H, H5), 2.54 (tt, J = 7.5, 2.3 Hz, 2H, H6).

^{13}C NMR (101 MHz, MeOD) δ 140.3 (C4), 128.10 (C2 or C3), 128.08 (C2 or C3), 126.0 (C1), 87.03 (C7), 71.9 (C8), 34.1 (C5), 29.0 (C9), 20.1 (C6).

HRMS calculated for $C_{11}H_{14}N$ [M+H]$^+$ 160.1121, found 160.1122

MS: *m/z* (ES+) 160.2 (100%, [M+H]$^+$)

R$_t$ (method 1) = 1.63 min

5-Phenylpentan-1-amine (101)
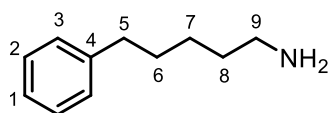
5-Phenylpent-2-yn-1-amine (**100**) (19.0 mg, 0.119 mmol) was dissolved in MeOH (4.0 mL) at room temperature and degassed with Ar for 15 min. Pd/C (10.0 mg) was added, and H_2 bubbled through the mixture for 10 min. The reaction was then stirred

under an atmosphere of H_2 at room temperature for 6.0 h. The mixture was filtered through celite and the pad washed with MeOH (10 mL). The resulting solution was concentrated to dryness under reduced pressure and the residue purified by reverse phase flash column chromatography (acid modifier) to afford the title compound as a yellow oil (10.0 mg, 51%).

¹H NMR (500 MHz, MeOD) δ 7.25 (t, J = 7.6 Hz, 2H, H2), 7.21 – 7.11 (m, 3H, stack of H1 and H3), 2.89 (t, J = 7.6 Hz, 2H, H9), 2.64 (t, J = 7.6 Hz, 2H, H5), 1.68 (app. p, J = 7.7 Hz, 4H, stack of H6 and H8), 1.47 – 1.37 (m, 2H, H7).

¹³C NMR (126 MHz, MeOD) δ 142.0 (C4), 128.0 (C2 or C3), 127.9 (C2 or C3), 125.4 (C1), 39.2 (C9), 35.2 (C5), 30.7 (C6 or C8), 27.1 (C6 or C8), 25.6 (C7).

MS: *m/z* (ES+) 164.2 (100%, [M+H]⁺)

R$_t$ (method 1) = 1.84 min

***Tert*-butyl(pent-4-yn-1-yloxy)diphenylsilane (103)**
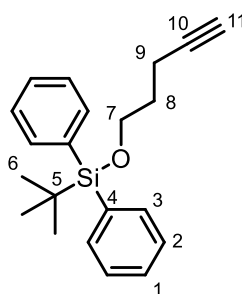
Pent-4-yn-1-ol (1.10 mL, 11.8 mmol, 1.0 eq) and imidazole (1.04 g, 15.3 mmol, 1.3 eq) were dissolved in DCM (30 mL) and cooled to 0 ℃. TBDPSCl (3.38 mL, 13.0 mmol, 1.1 eq) was added dropwise at 0 ℃, and the reaction then allowed to slowly warm to room temperature and stirred for 2.5 h. The reaction was quenched with H_2O (10 mL) and extracted with DCM (3 x 10.0 mL). The combined organics were dried over MgSO$_4$, filtered, and concentrated under reduced pressure. The residue was purified by flash column chromatography (pure hexane) to afford the title compound as a colourless oil (3.78 g, 99%).

¹H NMR (500 MHz, CDCl₃) δ 7.74 – 7.69 (m, 4H, H4), 7.49 – 7.38 (m, 6H, stack of H1 and H2), 3.79 (t, *J* = 6.0 Hz, 2H, H7), 2.39 (td, *J* = 7.2, 2.7 Hz, 2H, H9), 1.94 (t, *J* = 2.7 Hz, 1H, H11), 1.82 (app. ddd, *J* = 13.2, 7.2, 6.0 Hz, 2H, H8), 1.10 (s, 9H, H6).

¹³C NMR (126 MHz, CDCl₃) δ 135.6 (C3), 133.9 (C4), 129.6 (C1), 127.7 (C2), 84.3 (C10), 68.4 (C11), 62.3 (C7), 31.5 (C8), 26.9 (C6), 19.3 (C5), 15.0 (C9).

R$_f$ (1:95 EtOAc:hexane) = 0.56

Analytical data matches that found in the literature.[271]

6-((T*ert*-butyldiphenylsilyl)oxy)hex-2-yn-1-ol (104)
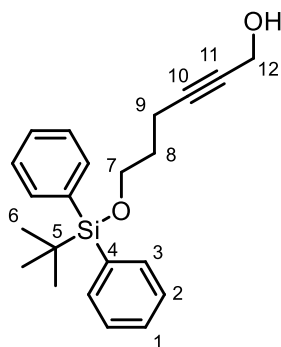
Tert-butyl(pent-4-yn-1-yloxy)diphenylsilane (**103**) (100 mg, 0.310 mmol, 1.0 eq) was dissolved in THF (3.0 mL) and cooled to -78 °C *n*-BuLi (1.6 M in hexanes, 213 µL, 0.341 mmol, 1.1 eq) was added dropwise and the reaction stirred at -78 °C for 2 h. A suspension of paraformaldehyde (11.2 mg, 0.372 mmol, 1.2 eq) in THF (1.5 mL) was added dropwise at -78 °C, and the mixture allowed to slowly warm to room temperature overnight. The reaction was quenched with NH₄Cl (sat. aq., 5.0 mL), and the THF removed under reduced pressure. The aqueous residue was extracted with EtOAc (3 x 5.0 mL), and the combined organics washed with brine (5.0 mL), dried over MgSO₄, filtered, and concentrated under reduced pressure. The residue was purified by flash column chromatography (EtOAc:hexane 1:4) to afford the title compound as a colourless oil (50.0 mg, 46%).

¹H NMR (400 MHz, CDCl₃) δ 7.69 (dt, *J* = 6.4, 1.7 Hz, 4H, H3), 7.48 – 7.35 (m, 6H, stack of H1 and H2), 4.21 (t, *J* = 2.2 Hz, 2H, H12), 3.75 (t, *J* = 6.0 Hz, 2H, H7), 2.38 (tt, *J* = 7.1, 2.2 Hz, 2H, H9), 1.82 – 1.71 (m, 2H, H8), 1.07 (s, 9H, H6).

¹³C NMR (101 MHz, CDCl₃) δ 135.6 (C3), 133.8 (C4), 129.6 (C1), 127.7 (C2), 86.1 (C10), 78.5 (C11), 62.3 (C7), 51.4 (C12), 31.5 (C8), 26.9 (C6), 19.3 (C5), 15.3 (C9).

R_f (1:4 EtOAc:hexane) = 0.36

ν_max (thin film, ATR)/cm⁻¹: 3351, 3071, 2930, 2857, 1589, 1472, 1463, 1427, 1389, 1361, 1326, 1189, 1135, 1105, 1070, 1007, 963, 822, 770, 740, 699, 686, 622, 613, 503

Analytical data matches that found in the literature.[271]

6-((*Tert*-butyldiphenylsilyl)oxy)hex-2-yn-1-yl methanesulfonate (105)
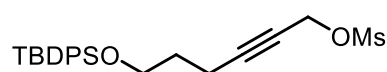
6-((T*ert*-butyldiphenylsilyl)oxy)hex-2-yn-1-ol (**104**) (50.0 mg, 0.142 mmol, 1.0 eq), NEt₃ (79.0 µL, 0.568 mmol, 4.0 eq), and DMAP (4.33 mg, 0.0355 mmol, 0.25 eq) were dissolved in DCM (3.0 mL) and the solution cooled to 0 °C. MsCl (33.1 µL, 0.426 mmol, 3.0 eq) was added dropwise at 0 °C. The solution was allowed to warm to room temperature and stirred for 30 min, the quenched with H₂O (5.0 mL). The mixture was extracted with DCM (3 x 5.0 mL), and the combined organics washed sequentially with H₂O and HCl (1.0 M, aq., 5.0 mL each), dried over MgSO₄, filtered, and concentrated under reduced pressure to afford the title compound that was used without further purification.

6-((*Tert*-butyldiphenylsilyl)oxy)hex-2-yn-1-amine (106)
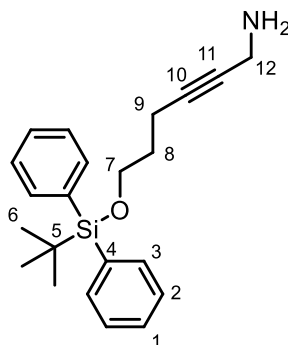
6-((*Tert*-butyldiphenylsilyl)oxy)hex-2-yn-1-yl methanesulfonate (**105**) (assumed 0.142 mmol) was dissolved in MeOH:THF (1:1, 2.5 mL). NH₃ (~35% aq. solution, 3.0 mL) was added at room temperature and the reaction stirred overnight. The mixture was

evaporated to dryness under reduced pressure, and the residue purified by reverse phase flash column chromatography (acid modifier) to afford the title compound as a colourless oil (16.0 mg, 32% over two steps).

^{1}H NMR (500 MHz, MeOD) δ 7.68 – 7.64 (m, 4H, H3), 7.48 – 7.35 (m, 6H, stack of H1 and H2), 3.76 (t, *J* = 6.0 Hz, 2H, H7), 3.57 (s, 2H, H12), 2.37 (t, *J* = 6.9 Hz, 2H, H9), 1.80 – 1.70 (m, 2H, H8), 1.04 (s, 9H, H6).

^{13}C NMR (126 MHz, MeOD) δ 135.3 (C3), 133.4 (C4), 129.5 (C1), 127.4 (C2), 85.4 (C10), 74.0 (C11), 62.1 (C7), 31.2 (C8), 29.4 (C12), 25.9 (C6), 18.6 (C5), 14.4 (C9).

HRMS calculated for $C_{22}H_{30}ONSi$ [M+H]$^+$ 352.2091, found 352.2100

R$_t$ (method 1) = 2.49 min

MS: *m/z* (ES+) 352.2 (100%, [M+H]$^+$)

v$_{max}$ (thin film, ATR)/cm^{-1}: 2930, 2857, 1589, 1472, 1428, 1382, 1361, 1187, 1110, 1043, 998, 962, 823, 773, 740, 701, 688, 614, 555, 506

6-Aminohex-4-yn-1-ol (107)
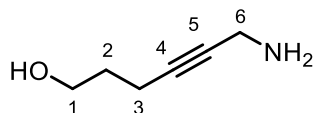
Tert-butyl (6-hydroxyhex-2-yn-1-yl)carbamate (**108**) (9.00 mg, 0.0423 mmol) was dissolved in DCM (0.80 mL). TFA (0.20 mL) was added at room temperature, and the reaction stirred for 3.0 h. The mixture was concentrated to dryness, and purified twice by SCX to afford the title compound (4.6 mg, 96%).

^{1}H NMR (500 MHz, MeOD) δ 3.63 (t, *J* = 6.3 Hz, 2H, H1), 3.34 (t, *J* = 2.3 Hz, 2H, H6), 2.27 (tt, *J* = 7.2, 2.3 Hz, 2H, H3), 1.69 (app. p, *J* = 6.7 Hz, 2H, H2).

^{13}C NMR (126 MHz, MeOD) δ 81.7 (C4), 79.3 (C5), 60.2 (C1), 31.3 (C2), 30.1 (C6), 14.4 (C3).

MS: *m/z* (ES+) 114.1 (100%, [M+H]$^+$)

HRMS calculated for $C_6H_{12}ON$ [M+H]$^+$ 114.0913, found 114.0920

v_{max} (thin film, ATR)/cm^{-1}: 3355, 2928, 1592, 1436, 1381, 1058, 932.

Tert-butyl (6-hydroxyhex-2-yn-1-yl)carbamate (108)
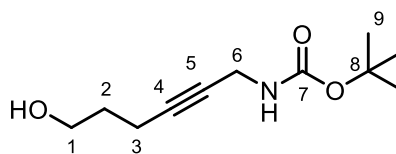
6-((*Tert*-butyldiphenylsilyl)oxy)hex-2-yn-1-amine (**106**) (195 mg, 0.553 mmol, 1.0 eq) was dissolved in THF (2.5 mL). TBAF (1.0 M in THF, 1.11 mL, 1.11 mmol, 2.0 eq) was added at room temperature, and the reaction stirred overnight. The mixture was concentrated to dryness under reduced pressure and redissolved in DCM (4.0 mL). Boc$_2$O (242 mg, 1.11 mmol, 2.0 eq) was added at room temperature and the reaction stirred for 3.5 h. The mixture was diluted with H$_2$O and extracted with DCM (3 x 5.0 mL), and the combined organics washed with HCl (1.0 mL, aq., 5.0 mL). The organics were then dried over MgSO$_4$, filtered, and concentrated under reduced pressure. The residue was purified by flash column chromatography (EtOAc:hexane 2:3) to afford the title compound as a colourless oil (37.0 mg, 31% over two steps.

^{1}H NMR (400 MHz, CDCl$_3$) δ 3.87 (t, *J* = 2.4 Hz, 2H, H6), 3.73 (t, *J* = 6.1 Hz, 2H, H1), 2.29 (tt, *J* = 7.0, 2.3 Hz, 2H, H3), 1.73 (app. p, *J* = 6.6 Hz, 2H, H2), 1.44 (s, 9H, H9).

^{13}C NMR (101 MHz, CDCl$_3$) δ 155.4 (C7), 82.8 (C4), 79.9 (C8), 76.7 (C5), 61.6 (C1), 31.2 (C2 or C6), 30.9 (weak, C2 or C6), 28.4 (C9), 15.2 (C3).

HRMS calculated for $C_{11}H_{19}O_3NNa$ [M+Na]$^+$ 236.1257, found 236.1258

R_f (2:3 EtOAc:hexane) = 0.21

v_{max} (thin film, ATR)/cm^{-1}: 3335, 2932, 1689, 1518, 1454, 1392, 1366, 1329, 1274, 1250, 1166, 1119, 1049, 931, 862, 782, 762, 580

6-((*Tert*-butoxycarbonyl)amino)hex-4-yn-1-yl methanesulfonate (112)
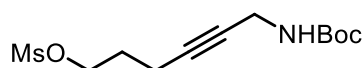
Tert-butyl (6-hydroxyhex-2-yn-1-yl)carbamate (**108**) (9.00 mg, 0.0423 mmol, 1.0 eq) and NEt$_3$ (17.7 µL, 0.127 mmol, 3.0 eq) were dissolved in DCM (1.5 mL) and the solution cooled to 0 °C MsCl (6.57 µL, 0.0846 mmol, 2.0 eq) was added dropwise at 0 °C The solution was allowed to warm to room temperature and stirred for 30 min, the quenched with H$_2$O (5.0 mL). The mixture was extracted with DCM (3 x 5.0 mL), and the combined organics washed sequentially with H$_2$O and HCl (1.0 M, aq., 5.0 mL each), dried over MgSO$_4$, filtered, and concentrated under reduced pressure to afford the title compound that was used without further purification.

Tert-butyl (2-(2-(2-(2-azidoethoxy)ethoxy)ethoxy)ethyl)(6-((*tert*-butoxycarbonyl)amino)hex-4-yn-1-yl)carbamate (113)
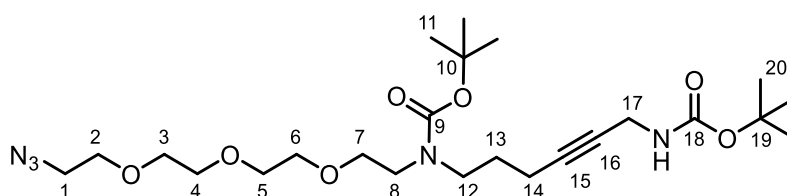
6-((*Tert*-butoxycarbonyl)amino)hex-4-yn-1-yl methanesulfonate (**112**) (assumed 0.0704 mmol, 1.0 eq), KI (2.92 mg, 0.0176 mmol, 0.25 eq), and 2-(2-(2-(2-azidoethoxy)ethoxy)ethoxy)ethan-1-amine (76.7 mg, 0.352 mmol, 5.0 eq) were dissolved in THF (2.5 mL). The mixture was heated to 80 °C and stirred overnight. The mixture was cooled to room temperature, and Boc$_2$O (92.0 mg, 0.422 mmol, 6.0 eq) was added. The mixture was stirred at room temperature for 5.0 h, then concentrated to dryness under reduced pressure. The residue was purified by flash column chromatography (EtOAC:hexane 45:55) to afford the title compound (7.0 mg, 19% over two steps).

^{1}H NMR (500 MHz, CDCl$_3$) δ 3.87 (app. s, 2H, H17), 3.74 – 3.56 (m, 12H, stack of H1 and H3-7), 3.42 – 3.35 (m, 4H, stack of H8 and H2), 3.32 (t, *J* = 7.0 Hz, 2H, H12), 2.16 (tt, *J* = 7.3, 2.4 Hz, 2H, H14), 1.72 (app. p, *J* = 7.1 Hz, 2H, H13), 1.45 (s, 9H, H11 or H20), 1.44 (s, 9H, H11 or H20).

HRMS calculated for C$_{24}$H$_{43}$O$_7$N$_5$Na [M+Na]$^+$ 536.3055, found 536.3063

R$_f$ (1:1 EtOAc:hexane) = 0.37

N^6-(2-(2-(2-(2-azidoethoxy)ethoxy)ethoxy)ethyl)hex-2-yne-1,6-diamine (111)
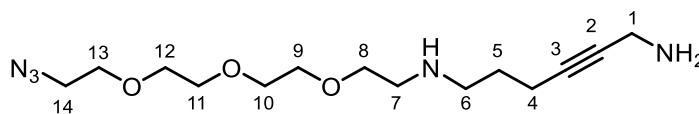
Tert-butyl (2-(2-(2-(2-azidoethoxy)ethoxy)ethoxy)ethyl)(6-((*tert*-butoxycarbonyl)amino)hex-4-yn-1-yl)carbamate (**113**) (7.00 mg, 0.0136 mmol) was dissolved in DCM (0.80 mL). TFA (0.20 mL) was added at room temperature, and the reaction stirred for 2.0 h. The mixture was concentrated to dryness, and purified by SCX to afford the title compound (4.0 mg, 94%).

^{1}H NMR (500 MHz, MeOD) δ 3.70 – 3.60 (m, 12H, stack of H8-12 and H14), 3.42 – 3.36 (m, 4H, stack of H1 and H13), 2.93 (t, *J* = 5.2 Hz, 2H, H7), 2.88 – 2.83 (m, 2H, H6), 2.33 – 2.27 (m, 2H, H4), 1.77 (app. p, *J* = 7.1 Hz, 2H, H5).

^{13}C NMR (126 MHz, MeOD) δ 81.6 (C3), 80.9 (C2), 70.19 (one of C8-13), 70.18 (one of C8-13), 70.1 (one of C8-13), 69.9 (one of C8-13), 69.7 (one of C8-13), 68.0 (one of C8-13), 50.4 (C14), 30.0 (C1), 26.9 (C5), 15.7 (C4).

N.B. ^{13}C signals for C6 and C7 not observed.

MS: *m/z* (ES+) 314.4 (100%, [M+H]$^+$)

HRMS calculated for $C_{14}H_{28}O_3N_5$ [M+H]$^+$ 314.2187, found 314.2187

$ν_{max}$ (thin film, ATR)/cm^{-1}: 3364, 2923, 2870, 2106, 1621, 1590, 1457, 1347, 1286, 1116.

3.2.3 General procedure for synthesis of amino acid methyl esters (GP1)[272]

Amino acid (1.0 eq) was dissolved in anhydrous MeOH and the solution cooled to 0 ℃. Thionyl chloride (1.8 eq) was added dropwise and the reaction allowed to warm to room temperature whilst stirring overnight. The mixture was concentrated to dryness under reduced pressure to afford the title compound without the need for further purification.

Methyl 3-aminopropanoate HCl (32)
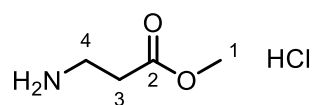
Synthesised according to GP1 using beta-alanine (500 mg, 5.62 mmol) and $SOCl_2$ (717 µL, 9.82 mmol) dissolved in MeOH (20.0 mL). The title compound was obtained as an off-white solid (758 mg, 97%).

^{1}H NMR (400 MHz, D_2O) δ 3.81 (s, 3H, H1), 3.38 (t, J = 6.6 Hz, 2H, H4), 2.92 (t, J = 6.4 Hz, 2H, H3).

^{13}C NMR (101 MHz, D_2O) δ 173.1 (C2), 52.8 (C1), 35.2 (C4), 31.2 (C3).

MS: *m/z* (ES+) 104.1 (100%, [M+H]$^+$)

Analytical data matches that found in the literature.[273]

Methyl 4-aminobutanoate HCl (34)
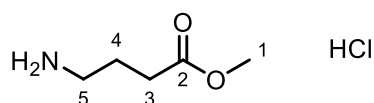
Synthesised according to GP1 using 4-amino butanoic acid (103 mg, 1.00 mmol) and $SOCl_2$ (153 µL, 2.10 mmol) dissolved in MeOH (2.50 mL). The title compound was obtained as an off-white solid (116 mg, 99%).

^{1}H NMR (400 MHz, D_2O) δ 3.70 (s, 3H, H1), 3.04 (t, J = 7.0 Hz, 2H, H5), 2.52 (t, J = 6.6 Hz, 2H, H3), 1.96 (app. t, J = 7.2 Hz, 2H, H4).

^{13}C NMR (101 MHz, D_2O) δ 175.4 (C2), 52.2 (C1), 38.6 (C5), 30.4 (C3), 21.8 (C4).

MS: *m/z* (ES+) 118.1 (100%, [M+H]$^+$)

Analytical data matches that found in the literature.[273]

Methyl 5-aminopentanoate HCl (36)
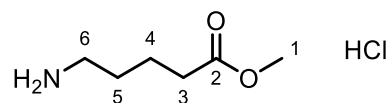
Synthesised according to GP1 using 5-amino pentanoic acid (117 mg, 1.00 mmol) and SOCl$_2$ (153 µL, 2.10 mmol) dissolved in MeOH (2.50 mL). The title compound was obtained as an off-white solid (130 mg, 99%).

^{1}H NMR (400 MHz, D$_2$O) δ 3.70 (s, 3H, H1), 3.01 (app. s, 2H, H6), 2.45 (app. s, 2H, H3), 1.69 (app s, 4H, H4 and H5).

^{13}C NMR (101 MHz, D$_2$O) δ 176.6 (C2), 52.1 (C1), 39.0 (C6), 32.8 (C2), 26.0 (C4 or C5), 21.0 (C4 or C5).

MS: *m/z* (ES+) 132.1 (100%, [M+H]$^+$)

Analytical data matches that found in the literature.[273]

Methyl 6-aminohexanoate HCl (38)
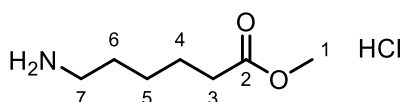
Synthesised according to GP1 using 6-amino hexanoic acid (131 mg, 1.00 mmol) and SOCl$_2$ (153 µL, 2.10 mmol) dissolved in MeOH (2.50 mL). The title compound was obtained as an off-white solid (144 mg, 99%).

^{1}H NMR (400 MHz, D$_2$O) δ 3.68 (s, 3H, H1), 3.00 (t, *J* = 7.2 Hz, 2H, H7), 2.42 (t, *J* = 7.0 Hz, 2H, H3), 1.66 (app. s, 4H, H6 and H4), 1.39 (app. s, 2H, H5).

^{13}C NMR (101 MHz, D$_2$O) δ 177.1 (C2), 52.1 (C1), 39.2 (C7), 33.2 (C3), 26.2 (C4 or C6), 24.9 (C5), 23.6 (C4 or C6).

MS: *m/z* (ES+) 146.2 (100%, [M+H]$^+$)

Analytical data matches that found in the literature.[273]

Methyl 7-aminoheptanoate HCl (40)
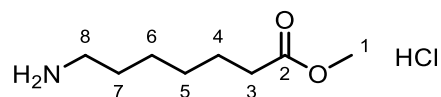
Synthesised according to GP1 using 7-amino heptanoic acid (145 mg, 1.00 mmol, 1.0 eq) and $SOCl_2$ (153 μL, 2.1 mmol, 2.1 eq) dissolved in MeOH (2.5 mL). The title compound was obtained as an off-white solid (143 mg, 90%).

^{1}H NMR (400 MHz, D_2O) δ 3.66 (s, 3H, H1), 2.96 (t, J = 7.3 Hz, 2H, H8), 2.38 (t, J = 7.0 Hz, 2H, H3), 1.69 − 1.53 (m, 4H, stack of H4 and H7), 1.42 − 1.29 (m, 4H, stack of H5 and H6).

^{13}C NMR (101 MHz, D_2O) δ 177.5 (C2), 51.9 (C1), 39.2 (C8), 33.4 (C3), 27.4 (C7), 26.3 (C5), 25.0 (C6), 23.8 (C4).

MS: *m/z* (ES+) 160.5 (100%, [M+H]$^+$)

Analytical data matches that found in the literature.[274]

Methyl *L*-lysinate 2HCl (41)
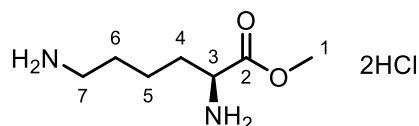
Synthesised according to GP1 using lysine HCl (183 mg, 1.0 mmol, 1 eq) and $SOCl_2$ (153 μL, 2.1 mmol, 2.1 eq) dissolved in MeOH (2.5 mL). The title compound was obtained as a white solid (208 mg, 89%).

^{1}H NMR (500 MHz, DMSO) δ 8.70 (s, 3H, N**H**$_3$), 8.27 − 8.01 (m, 3H, N**H**$_3$), 3.97 (t, J = 6.4 Hz, 1H, H3), 3.75 (s, 3H, H1), 2.74 (t, J = 7.5 Hz, 2H, H7), 1.88 − 1.76 (m, 2H, H4), 1.64 − 1.53 (m, 2H, H6), 1.52 − 1.42 (m, 1H, H5a), 1.42 − 1.31 (m, 1H, H5b).

^{13}C NMR (126 MHz, DMSO) δ 170.3 (C2), 53.2 (C1), 52.0 (C3), 38.6 (C7), 29.7 (C4), 26.6 (C6), 21.6 (C5).

MS: *m/z* (ES+) 161.2 (100%, [M+H]$^+$)

Analytical data matches that found in the literature.[275,276]

3-Amino-*N*-methylpropanamide (45)
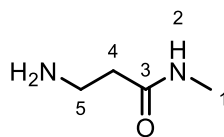
β-alanine methyl ester HCl (300 mg, 2.15 mmol, 1.0 eq) was dissolved in MeNH$_2$ (17.9 mL, 40% wt. solution in H$_2$O) and the mixture stirred at 40 °C for 80 min. The reaction mixture was concentrated under reduced pressure and the residue redissolved in EtOH (10 mL), then cooled to -20 °C. Et$_2$O (10 mL) was added at -20 °C until a white solid precipitated. The white solid was removed by filtration and the remaining solution concentrated under reduced pressure to yield the title compound as a colourless solid (161 mg, 47%) without the need for further purification.

^{1}H NMR (500 MHz, MeOD) δ 3.19 (t, *J* = 6.6 Hz, 2H, H5), 2.74 (s, 3H, H1), 2.62 (t, *J* = 6.6 Hz, 2H, H4).

^{13}C NMR (126 MHz, MeOD) δ 171.3 (C3), 35.9 (C5), 31.5 (C4), 24.9 (C1).

HRMS calculated for C$_4$H$_{11}$ON$_2$ [M+H]$^+$ 103.0866, found 103.0871

MS: *m/z* (ES+) 103.4 (100%, [M+H]$^+$)

3.2.4 Preparative scale MTG reactions

N^5-((*S*)-5-Acetamido-6-methoxy-6-oxohexyl)-N^2-((benzyloxy)carbonyl)-*L*-glutaminylglycine (114)
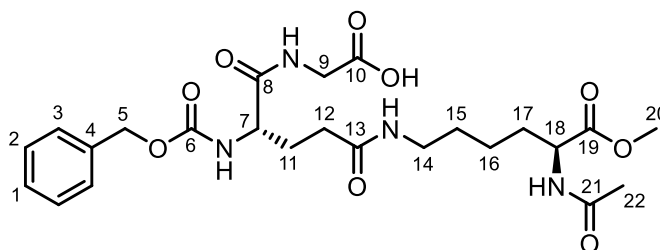
((Benzyloxy)carbonyl)-*L*-glutaminylglycine (ZQG) (36.0 mg, 0.107 mmol, 1.0 eq) and methyl acetyl-*L*-lysinate (51.1 mg, 0.214 mmol, 2.0 eq) were dissolved in PBS (12 mL).

MTG (50 U) in PBS (2.5 mL) was added, and the reaction stirred at 50 rpm at 37 ℃ overnight. A solution of formic acid in MeOH (1% v/v, 5.0 mL) was added, and the mixture cooled to 0 ℃ and left to stand for 5 min. The precipitate was filtered off, and the resulting solution concentrated to dryness under reduced pressure. The residue was purified by reverse phase flash column chromatography to afford the title compound as a white solid (21.0 mg, 38%).

^{1}H NMR (400 MHz, MeOD) δ 7.40 – 7.25 (m, 5H, stack of H1-3), 5.15 – 5.03 (m, 2H, H5), 4.36 (dd, *J* = 8.9, 5.1 Hz, 1H, H18), 4.17 (dd, *J* = 8.6, 5.4 Hz, 1H, H7), 3.95 (d, *J* = 17.7 Hz, 1H, H9a), 3.86 (d, *J* = 17.5 Hz, 1H, H9b), 3.70 (s, 3H, H20), 3.24 – 3.06 (m, 2H, H14), 2.31 (t, *J* = 7.5 Hz, 2H, H12), 2.18 – 2.05 (m, 1H, H11a), 1.97 (s, 3H, H22), 1.94 – 1.88 (m, 1H, H11b), 1.87 – 1.74 (m, 1H, H17a), 1.74 – 1.60 (m, 1H, H17b), 1.56 – 1.44 (m, 2H, H15 or H16), 1.43 – 1.32 (m, 2H, H15 or H16).

^{13}C NMR (101 MHz, MeOD) δ 171.3 (stack of C8, C13, and C19), 155.3 (C6), 135.2 (C4), 126.6 (one of C1-3), 126.1 (one of C1-3), 126.0 (one of C1-3), 64.9 (C5), 53.0 (C7), 50.8 (C18), 49.7 (C20), 39.2 (C9), 37.1 (C14), 30.2 (C12), 29.2 (C17), 26.9 (C15 or C16), 26.5 (C11), 21.2 (C15 or C16), 19.4 (C22).

t$_R$ (method 1) = 1.89 min

MS: *m/z* (ES+) 523.3 (100%, [M+H]$^+$)

HRMS calculated for $C_{24}H_{35}N_4O_9$ [M+H]$^+$ 523.2326, found 523.2324.

N^2-((Benzyloxy)carbonyl)-N^5-(furan-2-ylmethyl)-L-glutaminylglycine (115)
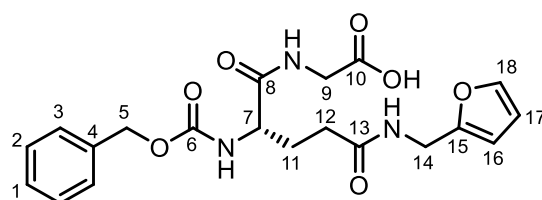
((Benzyloxy)carbonyl)-*L*-glutaminylglycine (ZQG) (50.0 mg, 0.150 mmol, 1.0 eq) and furan-2-ylmethanamine (26.5 μL, 0.300 mmol, 2.0 eq) were dissolved in PBS (10 mL). MTG (50 U) in PBS (2.5 mL) was added, and the reaction stirred at 50 rpm at 37 ℃ overnight. A solution of formic acid in MeOH (1% v/v, 5.0 mL) was added, and the

mixture cooled to 0 ℃ and left to stand for 5 min. The precipitate was filtered off, and the resulting solution concentrated to dryness under reduced pressure. The residue was purified by reverse phase flash column chromatography to afford the title compound as a white solid (32.0 mg, 51%).

^{1}H NMR (500 MHz, MeOD) δ 7.40 (d, *J* = 1.9 Hz, 1H, H18), 7.37 – 7.27 (m, 5H, stack of H1-H3), 6.32 (dd, *J* = 3.2, 1.9 Hz, 1H, H17), 6.23 (d, *J* = 3.2 Hz, 1H, H16), 5.12 – 5.04 (m, 2H, H5), 4.33 (d, *J* = 1.8 Hz, 2H, H14), 4.18 (dd, *J* = 8.5, 5.4 Hz, 1H, H7), 3.96 (d, *J* = 17.8 Hz, 1H, H9a), 3.87 (d, *J* = 17.7 Hz, 1H, H9b), 2.34 (t, *J* = 7.6 Hz, 2H, H12), 2.18 – 2.07 (m, 1H, H11a), 2.00 – 1.91 (m, 1H, H11b).

^{13}C NMR (126 MHz, MeOD) δ 173.4 (C13), 173.3 (C8), 171.4 (C10), 157.0 (C6), 151.6 (C15), 141.9 (C18), 136.7 (C4), 128.1 (one of C1-3), 127.7 (one of C1-3), 127.5 (one of C1-3), 110.0 (C17), 106.7 (C16), 66.4 (C5), 54.5 (C7), 40.4 (C9), 35.8 (C14), 31.5 (C12), 27.9 (C11).

t_R (method 1) = 2.02 min

MS: *m/z* (ES+) 418.3 (100%, [M+H]$^+$)

HRMS calculated for $C_{20}H_{24}N_3O_7$ [M+H]$^+$ 418.1536, found 418.1537.

3.2.5 Purification of MTG

Transglutaminase isolated from *Streptoverticillium mobaraense* (obtained from https://specialingredients.co.uk, approximately 1.00 g) was purified by dialysis using a Slide-A-Lyzer™ MINI Dialysis Device, 10K MWCO, 0.5 mL at room temperature overnight, according to manufacturer's instructions. The sample was recovered, lyophilised, and reconstituted in 1.00 mL of PBS. After measuring the activity, the enzyme was aliquoted into 0.56 U aliquots and stored at -20 ℃. One unit of microbial transglutaminase activity is defined as the amount of enzyme which causes the formation of 1.0 μmol of hydroxamate per minute by catalysing the reaction between Z-Gln-Gly and hydroxylamine at pH 6.0 at 37 °C.[77]

3.2.6 Determination of MTG activity

The activity of MTG was measured using a Zedi*Xclusive* Microbial Transglutaminase Assay Kit purchased from Zedira GmbH and used according to the manufacturer's instructions.

3.2.7 Screening reaction parameters and measurement

MTG substrate conversion was determined through the reaction of amine donors with the amine-acceptor substrate Z-glutamine-glycine (ZQG), extensively used in the literature as a probe for MTG reactivity. ZQG (450 µL of 6.58 mM adjusted to pH = 7.6, 1 eq) and amine (450 µL of 13.2 mM adjusted to pH = 7.6, 2 eq) were combined in a 1.5 mL Eppendorf. MTG was added (100 µL, 0.56 U) and the mixture vortexed before stirring (microwave stir bar, 50 RPM to minimise mechanical degradation of enzyme) at 37 ℃ for 1.5 h.

A 500 µL aliquot of the reaction mixture was added to 250 µL of 95% formic acid, shaken, and allowed to stand for 5 min. 500 µL of methanol and 75 µL of internal standard (4-methoxybenzamide, 1 mg/mL in neat DMSO) were added. The sample was shaken to homogenise then passed through a 0.2 µm syringe filter and submitted for LCMS analysis. Control reactions for each amine substrate were performed as the above, but substituting the MTG for 100 µL of buffer.

Substrate conversion was determined by measuring consumption of ZQG, as this is independent of the UV absorbance profiles of the amine substrates. Consumption of ZQG is calculated as follows:

$$\% \, Consumption = \left(1 - \frac{y}{y_{control}}\right) \times 100$$

Where:

$$y = \frac{LC \, peak \, area \, (ZQG)}{LC \, peak \, area \, (internal \, standard)}$$

For each substrate, the experiment was repeated three times, using different batches of purified enzyme for each repeat. The consumption values are reported as mean ± standard deviation.

The reaction time was chosen as the benchmark compound N_{α}-Ac-L-lysine methyl ester gave a conversion of around 50% after 1.5 h, allowing us to compare both more efficient and less efficient substrates.

3.3 Design and synthesis of NAMPT PROTACs

Tert-butyl (4-hydroxybutyl)carbamate (172)

Known compound made by a known procedure.[277]
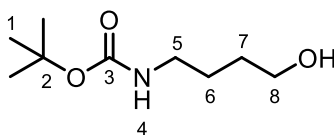
Di-*tert*-butyl dicarbonate (30.6 g, 140 mmol, 1.0 eq) was dissolved in anhydrous DCM (200 mL). The solution was cooled to 0 °C, and 4-amino-1-butanol (12.9 mL, 140 mmol, 1.0 eq) added dropwise over 10 min. The reaction was allowed to warm to room temperature and stirred overnight. The reaction was then cooled to 0 °C and quenched with water (100 mL). The organic layer was washed sequentially with HCl (1 M, aq.) and water, before being dried over MgSO$_4$, filtered, and concentrated under reduced pressure to afford the title compound as a colourless oil (18.0 g, 68%) that was used without further purification.

Tert-butyl (4-bromobutyl)carbamate (173)
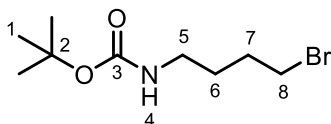
An oven dried flask was charged with *tert*-butyl (4-hydroxybutyl)carbamate (**172**) (189 mg, 1.00 mmol, 1.0 eq), PPh$_3$ (394 mg, 1.50 mmol, 1.5 eq) and anhydrous THF (5.0 mL). The mixture was cooled to 0 °C and a solution of CBr$_4$ (514 mg, 1.55 mmol, 1.6 eq) in anhydrous THF (5.0 mL) was added dropwise. The mixture was stirred and allowed to warm to room temperature overnight. The reaction mixture was then filtered through celite and the residue washed with THF. The combined filtrates were concentrated under reduced pressure and the resulting residue purified with a silica plug eluting with hexane followed by EtOAc/hexane 3:7 to afford the title compound as a light yellow oil (252 mg, quantitative).

¹H NMR (400 MHz, CDCl₃) δ 4.76 (br. s, 1H, H4), 3.36 (t, *J* = 6.7 Hz, 2H, H8), 3.08 (app. q, *J* = 6.6 Hz, 2H, H5), 1.88 – 1.76 (m, 2H, H7), 1.63 – 1.51 (m, 2H, H6), 1.37 (s, 9H, H1).

¹³C NMR (101 MHz, CDCl₃) δ 156.0 (C3), 79.0 (C2), 39.6 (C5), 33.3 (C8), 29.9 (C7), 28.7 (C6), 28.4 (C1).

HRMS calculated for $C_9H_{18}BrNO_2Na$ [M+Na]⁺ 274.0413, found 274.0405

R$_f$ (EtOAc/hexane 1:1) = 0.82

4-(Piperidin-4-yl)butan-1-ol (175)
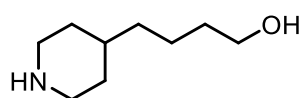
A flame dried flask was charged with 4-(piperidin-4-yl)butanoic acid hydrochloride (**174**) (2.50 g, 12.0 mmol, 1.0 eq) and THF (24 mL) and cooled to 0 °C. BH₃·SMe₂ (2.0 M solution in THF, 24.0 mL, 48.2 mmol, 4.0 eq) was added and the reaction mixture warmed to room temperature before stirring at 65 °C overnight. The reaction was slowly quenched at 0 °C with MeOH (25 mL) and then refluxed for 3 h. The reaction mixture was concentrated under reduced pressure and the product used without further purification (2.97 g).

Methyl 2-(4-((*tert*-butoxycarbonyl)amino)butoxy)benzoate (176)
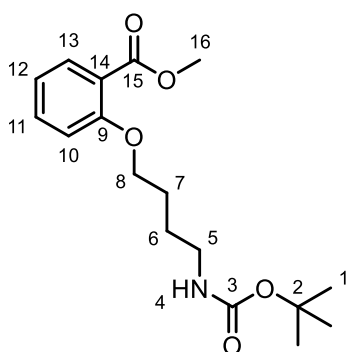
A flask was charged with methyl salicylate (**170**) (696 µL, 5.37 mmol, 1.0 eq), *tert*-butyl (4-bromobutyl)carbamate (2.03 g, 8.06 mmol, 1.5 eq), K₂CO₃ (2.23 g. 16.1 mmol, 3.0 eq), NaI (403 mg, 2.69 mmol, 0.5 eq), and DMF (25 mL). The reaction mixture was heated to 60 ℃ and stirred for 24 h. The reaction was allowed to cool to room

temperature and quenched with water (10 mL), then partitioned with Et$_2$O. The aqueous layer was extracted with Et$_2$O (x5) and the combined organics washed sequentially with water then brine and dried over MgSO$_4$, filtered, and concentrated under reduced pressure. The resulting residue was purified by flash column chromatography using EtOAc/hexane 1:4 to afford the title compound as a pale yellow oil (903 mg, 52%)

^{1}H NMR (400 MHz, CDCl$_3$) δ 7.76 (dd, J = 7.7, 1.8 Hz, 1H, H13), 7.44 – 7.34 (m, 1H, H11), 6.96 – 6.88 (m, 2H, stack of H10 and H12), 4.93 (br. s, 1H, H4), 4.01 (t, J = 6.0 Hz, 2H, H8), 3.85 (s, 3H, H16), 3.17 (t, J = 6.8 Hz, 2H, H5), 1.84 (app. dq, J = 7.8, 6.2 Hz, 2H, H7), 1.73 – 1.64 (m, 2H, H6), 1.39 (s, 9H, H1).

^{13}C NMR (101 MHz, CDCl$_3$) δ 166.7 (C15), 158.5 (C9), 156.1 (C3), 133.5 (C11), 131.7 (C13), 120.1 (stack of C12 and C14), 113.0 (C10), 78.9 (C2), 68.4 (C8), 51.9 (C16), 40.1 (C5), 28.4 (C1), 26.7 (C6), 26.3 (C7).

HRMS calculated for C$_{17}$H$_{26}$NO$_5$ [M+H]$^+$ 324.1733, found 324.1801

R$_f$ (EtOAc/hexane 1:4) = 0.36

t$_R$ (method 1) = 2.71 min

MS: *m/z* (ES+) 224.3 (100%, [M+H]$^+$)

v$_{max}$ (thin film, ATR)/cm^{-1}: 3346, 2978, 2934, 1693, 1601, 1584, 1516, 1492, 1454, 1436, 1390, 1366, 1305, 1246, 1165, 1133, 1109, 1085, 1046, 865, 754, 722, 696, 666, 541

2-(4-((*Tert*-butoxycarbonyl)amino)butoxy)benzoic acid (177)
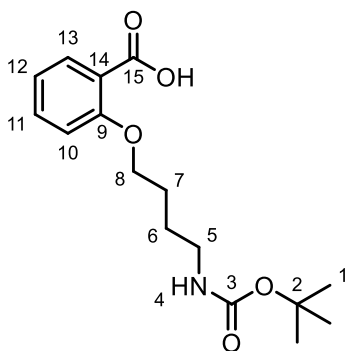
Methyl 2-(4-((*tert*-butoxycarbonyl)amino)butoxy)benzoate (**176**) (903 mg, 2.80 mmol, 1.0 eq) was dissolved in EtOH absolute (5.0 mL), and powdered NaOH added (280 mg, 7.00 mmol, 2.5 eq) at room temperature. The mixture was then stirred at 60 °C for 16 h. Once cooled to room temperature the reaction mixture was evaporated to dryness, before the residue was taken up in Et_2O and partitioned with water. The pH was adjusted to 1 with HCl (37%) and the mixture was extracted with Et_2O (3 x 15 mL). The combined organics were washed with brine, dried over $MgSO_4$, filtered, and concentrated under reduced pressure. The residue was purified by flash column chromatography using MeOH/DCM 0:1 to 1:17 to afford the title compound as a yellow oil (587 mg, 68%).

^{1}H NMR (400 MHz, Chloroform-*d*) δ 8.13 (dd, *J* = 7.8, 1.9 Hz, 1H, H13), 7.52 (ddd, *J* = 8.4, 7.4, 1.9 Hz, 1H, H11), 7.10 (app. td, *J* = 7.6, 1.0 Hz, 1H, H12), 7.02 (d, *J* = 8.4 Hz, 1H, H10), 4.72 (br. s, 1H, H4), 4.25 (t, *J* = 6.5 Hz, 2H, H8), 3.20 (app. q, *J* = 6.7 Hz, 2H, H5), 1.98 – 1.89 (m, 2H, H7), 1.73 – 1.63 (m, 2H, H6), 1.42 (s, 9H, H1).

^{13}C NMR (101 MHz, Chloroform-*d*) δ 165.7 (C15), 157.5 (C9), 156.1 (C3), 135.0 (C11), 133.6 (C13), 122.1 (C12), 117.9 (C14), 112.7 (C10), 79.4 (C2), 69.7 (C8), 39.8 (C5), 28.4 (C1), 26.6 (C6), 26.2 (C7).

HRMS calculated for $C_{16}H_{24}NO_5$ [M+H]$^+$ 310.1649, found 310.1641

t_R (method 1) = 2.41 min

MS: *m/z* (ES-) 308.2 (100%, [M-H]$^-$)

***Tert*-butyl (4-(2-(4-(4-hydroxybutyl)piperidine-1-carbonyl)phenoxy)butyl)carbamate (178)**
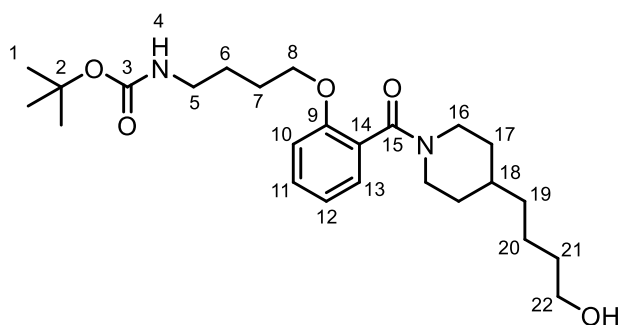
A flame dried flask was charged with HATU (1.04 g, 2.74 mmol, 1.5 eq), a solution of 2-(4-((*tert*-butoxycarbonyl)amino)butoxy)benzoic acid (**177**) (566 mg, 1.83 mmol, 1.0 eq) in anhydrous DMF (10 mL), and DIPEA (1.30 mL, 7.32 mmol, 4.0 eq), and was stirred for 15 min. Crude 4-(piperidin-4-yl)butan-1-ol (902 mg, assumed 3.66 mmol, 2.0 eq) in anhydrous DMF (10 mL) was added and the mixture stirred overnight at room temperature. The reaction was quenched with water (10 mL), extracted with EtOAc (5 x 20 mL), washed with water then brine, and then dried over $MgSO_4$. The mixture was filtered, concentrated under reduced pressure, and the residue purified by flash column chromatography using MeOH/DCM 1:40 to 1:10 to afford the title compound as a viscous yellow oil (469 mg, 57%).

^{1}H NMR (500 MHz, Acetone-d_6) δ 7.36 − 7.30 (m, 1H, H11), 7.19 (dd, J = 7.4, 1.8 Hz, 0.5H, H13), 7.10 (dd, J = 7.4, 1.8 Hz, 0.5H, H13), 7.03 (app. t, J = 7.8 Hz, 1H, H10), 6.96 (app. td, J = 7.3, 5.1 Hz, 1H, H12), 6.05 (m, 1H, H4), 4.71 − 4.62 (m, 1H, H16a), 4.15 − 3.97 (m, 2H, H8), 3.57 − 3.49 (m, 2H, H22), 3.49 − 3.38 (m, 1H, H16'a), 3.18 − 3.09 (m, 2H, H5), 3.08 − 3.01 (m, 0.5H, 16'b), 2.94 − 2.88 (m, 0.5H, 16'b), 2.75 − 2.64 (m, 1H, H16b), 1.86 − 1.73 (m, 3H, stack of H7 and H17a), 1.70 − 1.56 (m, 3H, stack of H6 and H17'a), 1.55 − 1.46 (m, 3H, stack of H18 and H21), 1.40 (s, 10H, stack of H1 and H20), 1.35 − 0.90 (m, 5H, stack of H17b, H17'b, H19, and H20).

^{13}C NMR (126 MHz, Acetone-d_6) δ 166.6 (C15), 166.5 (C15, minor), 155.9 (C3, minor), 155.8 (C3), 154.9 (C9, minor), 154.7 (C9), 129.6 (C11), 127.7 (C13, major), 127.6 (C14, minor), 127.4 (C13, minor), 127.3 (C14, major), 120.54 (C12), 120.52 (C12, minor), 112.2 (C10, minor), 112.0 (C10), 77.5 (C2), 67.9 (C8), 67.7 (C8, minor), 61.5 (C22), 47.0 (C16', minor), 46.7 (C16'), 41.3 (C16), 41.2 (C16, minor), 39.8 (C5), 36.3 (C19), 36.1 (C18), 33.0 (C21), 32.7 (C17'), 32.0 (C17), 27.8 (C1), 26.6 (C6), 26.5 (C7), 22.8 (C20).

N.B. 16 and 16', 17 and 17' refer to the ring-flipped conformations, and rotamers observed.

HRMS calculated for $C_{25}H_{41}N_2O_5$ [M+H]$^+$ 449.3010, found 449.3016

R_f (EtOAc/hexane 1:4) = 0.19

t_R (method 1) = 2.48 min

MS: *m/z* (ES+) 449.5 (100%, [M+H]$^+$)

v$_{max}$ (thin film, ATR)/cm^{-1}: 3358, 2930, 2863, 1709, 1615, 1495, 1453, 1365, 1247, 1172, 1101, 1033, 755, 638

4-(1-(2-(4-((*Tert*-butoxycarbonyl)amino)butoxy)benzoyl)piperidin-4-yl)butyl 4-methylbenzenesulfonate (179)
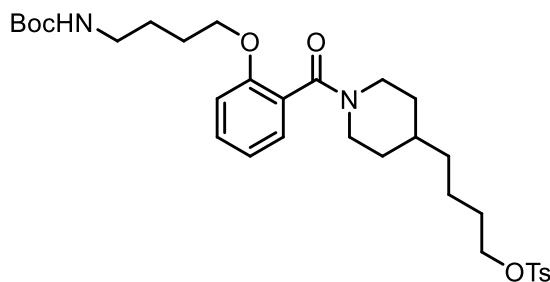
A flame dried flask was charged with *tert*-butyl (4-(2-(4-(4-hydroxybutyl)piperidine-1-carbonyl)phenoxy)butyl)carbamate (**178**) in DCM (15 mL), TsCl (299 mg, 1.57 mmol, 1.5 eq), and anhydrous NEt$_3$ (0.290 mL, 2.09 mmol, 2.0 eq) and the reaction stirred at room temperature overnight. The mixture was diluted with EtOAC, washed sequentially with water, HCl (1 M, aq.), NaHCO$_3$ (sat. aq.), and brine, then dried over MgSO$_4$, filtered, and concentrated under reduced pressure. The crude product (695 mg) was used without further purification.

Tert-butyl (4-(2-(4-(4-azidobutyl)piperidine-1-carbonyl)phenoxy)butyl)carbamate (180)
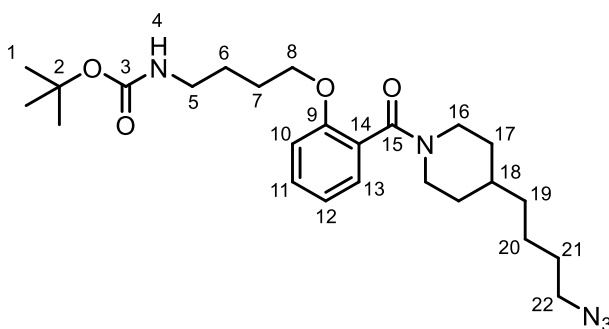
A flame dried flask was charged with 4-(1-(2-(4-((*tert*-butoxycarbonyl)amino)butoxy)benzoyl)piperidin-4-yl)butyl 4-methylbenzenesulfonate (**179**) (695 mg, assumed 1.05 mmol, 1.0 eq) in DMF (12 mL).

NaN$_3$ (205 mg, 3.15 mmol, 3.0 eq) was added, and the mixture stirred at 60 °C overnight. The reaction was diluted with water, and extracted with EtOAc (5 x 30 mL). The combined organics were washed with brine, dried over MgSO$_4$, filtered, and concentrated under reduced pressure. The residue was purified by reverse phase flash column chromatography (acid modifier) to yield the title compound as a yellow oil (245 mg, 51% over two steps).

^{1}H NMR (500 MHz, Acetone-d_6) δ 7.36 – 7.29 (m, 1H, H11), 7.20 (dd, J = 7.5, 1.7 Hz, 0.5H, H13), 7.11 (dd, J = 7.5, 1.7 Hz, 0.5H, H13), 7.01 (app. t, J = 7.8 Hz, 1H, H10), 6.96 (app. q, J = 6.9 Hz, 1H, H12), 6.10 – 6.05 (m, 1H, H4), 4.71 – 4.65 (m, 1H, H16a), 4.13 – 3.94 (m, 2H, H8), 3.44 – 3.39 (m, 1H, H16'a), 3.33 (app. q, J = 7.2 Hz, 2H, H22), 3.16 – 3.07 (m, 2H, H5), 3.06 – 2.86 (m, 1H, H16'b), 2.76 – 2.64 (m, 1H, H16b), 1.84 – 1.71 (m, 3H, stack of H7 and H17a), 1.68 – 1.49 (m, 6H, stack of H6, H17'a, H18, and H21), 1.41 (s, 10H, stack of H1 and H20), 1.36 – 0.88 (m, 5H, stack of H19, H20, H17b, and H17'b).

^{13}C NMR (126 MHz, Acetone-d_6) δ 166.7 (C15), 166.5 (C15, minor), 155.9 (C3), 154.9 (C9, minor), 154.7 (C9), 129.9 (C11), 129.7 (C11, minor), 127.8 (C13), 127.5 (C13, minor), 127.4 (C14, minor), 127.2 (C14), 120.6 (C12), 112.2 (C10, minor), 112.0 (C10), 77.5 (C2), 67.9 (C8), 67.8 (C8, minor), 51.11 (C22, minor), 51.10 (C22), 47.0 (C16', minor), 46.7 (C16'), 41.4 (C16, minor), 41.3 (C16), 39.9 (C5), 35.92 (C18), 35.87 (C19), 32.7 (C17'), 32.0 (C17), 28.9 (C21), 27.9 (C1), 26.6 (C6), 26.5 (C7, minor), 26.4 (C7), 23.7 (C20, minor), 23.6 (C20).

N.B. rotamers observed.

t$_R$ (method 1) = 2.86 min

MS: *m/z* (ES+) 474.4 (100%, [M+H]$^+$)

R$_f$ (EtOAc/hexane 1:1) = 0.25

HRMS calculated for C$_{25}$H$_{40}$N$_5$O$_4$ [M+H]$^+$ 474.3075, found 474.3065

v$_{max}$ (thin film, ATR)/cm^{-1}: 3317, 2928, 2858, 2137, 1705, 1617, 1600, 1495, 1453, 1365, 1274, 1247, 1171, 1101, 1044, 756, 638

Tert-butyl (4-(2-(4-(4-aminobutyl)piperidine-1-carbonyl)phenoxy)butyl)carbamate (181)
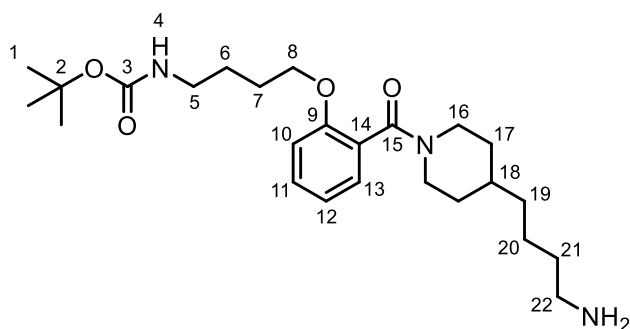
A flask was charged with *tert*-butyl (4-(2-(4-(4-azidobutyl)piperidine-1-carbonyl)phenoxy)butyl)carbamate (**180**) (245 mg, 0.517 mmol, 1.0 eq) and THF (6.0 mL). PPh$_3$ (204 mg, 0.776 mmol, 1.5 eq) and H$_2$O (55.8 μL, 3.10 mmol, 6.0 eq) were added and the reaction heated at reflux for 3 h. Upon completion the reaction mixture was cooled, and concentrated to dryness under reduced pressure. The residue was purified by reverse phase flash column chromatography (acid modifier) to yield the title compound as a yellow oil (232 mg, quantitative yield).

^{1}H NMR (500 MHz, Acetone-d_6) δ 7.33 (app. q, *J* = 7.2 Hz, 1H, H11), 7.21 (d, *J* = 7.4 Hz, 0.5H, H13), 7.12 (d, *J* = 7.4 Hz, 0.5H, H13), 7.03 (dd, *J* = 8.4, 5.7 Hz, 1H, H10), 6.97 (app. q, *J* = 6.9 Hz, 1H, H12), 4.64 (d, *J* = 12.7 Hz, 1H, H16a), 4.13 – 3.95 (m, 2H, H8), 3.39 (d, *J* = 13.2 Hz, 1H, H16'a), 3.14 – 2.86 (m, 5H, stack of H22, H5, and H16'b), 2.71 (app. q, *J* = 12.9, 12.4 Hz, 1H, H16b), 1.83 – 1.47 (m, 9H, stack of H6, H7, H17a, H17'a, H18, and H21), 1.39 (s, 10H, stack of H1 and H20), 1.32 – 0.82 (m, 5H, stack of H17b, H17'b, H19, and H20).

^{13}C NMR (126 MHz, Acetone-d_6) δ 167.0 (C15), 166.9 (C15, minor), 156.1 (C3, minor), 156.0 (C3), 154.8 (C9, minor), 154.7 (C9), 130.2 (C11), 129.9 (C11, minor), 127.7 (C13), 127.4 (C13, minor), 127.1 (C14, minor), 126.9 (C14), 120.7 (C12), 120.6 (C12, minor), 112.3 (C10, minor), 112.1 (C10), 77.6 (C2), 67.9 (C8), 67.8 (C8, minor), 47.0 (C16', minor), 46.8 (C16'), 41.5 (C16, minor), 41.4 (C16), 40.6 (C22), 39.7 (C5), 35.81 (C19), 35.76 (C18), 35.71 (C18, minor), 32.6 (C17'), 31.9 (C17), 29.5 (C21), 28.0 (C1), 26.6 (C6), 26.5 (C7), 23.6 (C20).

N.B. rotamers observed.

t$_R$ (method 1) = 2.07 min

MS: *m/z* (ES+) 448.5 (100%, [M+H]$^+$)

HRMS calculated for C$_{25}$H$_{41}$N$_3$O$_4$Na [M+Na]$^+$ 470.2989, found 470.2984

Tert-butyl (*E*)-(4-(2-(4-(4-(3-(pyridin-3-yl)acrylamido)butyl)piperidine-1-carbonyl)phenoxy)butyl)carbamate (182)
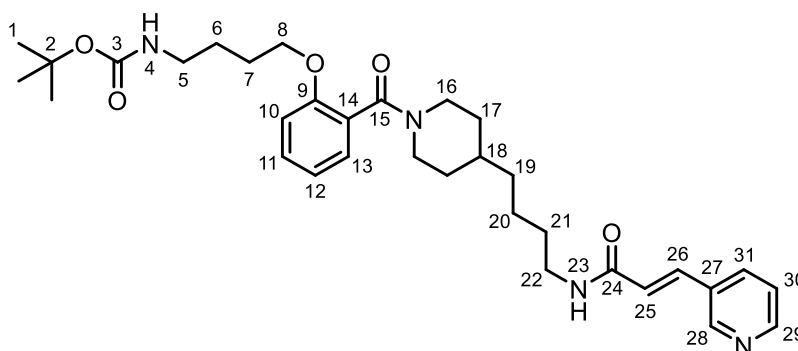
An oven dried flask was charged with HATU (148 mg, 0.389 mmol, 1.5 eq), a solution of (*E*)-3-(pyridin-3-yl)acrylic acid (**168**) (77.4 mg, 0.519 mmol, 2.0 eq) in DMF (1.5 mL), and DIPEA (180 µL, 1.04 mmol, 4.0 eq) then stirred for 40 min at room temperature. *Tert*-butyl (4-(2-(4-(4-aminobutyl)piperidine-1-carbonyl)phenoxy)butyl)carbamate (**181**) (116 mg, 0.259 mmol, 1.0 eq) in DMF (1.5 mL) was added and the reaction stirred overnight at room temperature. The reaction was quenched with H$_2$O (10 mL), extracted with EtOAc (5 x 10 mL), and the organics washed sequentially with water (10 mL) and brine (10 mL) before being dried over MgSO$_4$, filtered, and concentrated under reduced pressure. The resulting residue was combined with the crude product of a second identical reaction and purified by reverse phase flash column chromatography (acid modifier) to afford the title compound as a yellow oil (combined yield of 129 mg, 42%).

^{1}H NMR (400 MHz, Acetone) δ 8.74 (d, *J* = 2.3 Hz, 1H, H28), 8.53 (dd, *J* = 4.8, 1.6 Hz, 1H, H29), 7.91 (d, *J* = 8.0 Hz, 1H, H31), 7.65 – 7.58 (m, 1H, H23), 7.54 (dd, *J* = 15.8, 2.4 Hz, 1H, H26), 7.37 (dd, *J* = 8.0, 4.9 Hz, 1H, H30), 7.34 – 7.29 (m, 1H, C11), 7.21 (dd, *J* = 7.4, 1.8 Hz, 0.5H, H13), 7.11 (dd, *J* = 7.4, 1.8 Hz, 0.5H, H13), 7.02 (dd, *J* = 8.4, 2.8 Hz,

1H, H10), 6.96 (app. td, *J* = 7.4, 4.5 Hz, 1H, H12), 6.79 (dd, *J* = 15.8, 1.6 Hz, 1H, H25), 6.14 – 6.12 (m, 1H, H4), 4.70 – 4.63 (m, 1H, H16a), 4.14 – 3.93 (m, 2H, H8), 3.45 – 3.37 (m, 1H, H16'a), 3.36 – 3.25 (m, 2H, H22), 3.17 – 3.08 (m, 2H, H5), 3.04 (t, *J* = 12.9 Hz, 0.5H, H16'b), 2.96 – 2.86 (m, 0.5H, H16'b), 2.75 – 2.64 (m, 1H, H16b), 1.84 – 1.71 (m, 3H, stack of H7 and H17a), 1.70 – 1.61 (m, 2H, H6), 1.61 – 1.47 (m, 4H, stack of H18, H17'a, H21), 1.39 (s, 11H, stack of H1, H20), 1.34 – 0.88 (m, 4H, stack of H17b, H17'b, H19).

^{13}C NMR (101 MHz, Acetone) δ 166.8 (C15), 166.5 (C15, minor), 164.6 (C24, minor), 164.5 (C24), 155.9 (C3, minor), 155.8 (C3), 154.9 (C9, minor), 154.7 (C9), 150.1 (C29), 149.2 (C28), 135.6 (C26), 133.8 (C31), 131.1 (C27), 130.0 (C11), 129.7 (C11, minor), 127.7 (C13), 127.44 (C14, minor), 127.35 (C13, minor), 127.2 (C14), 124.3 (C25), 123.7 (C30), 120.6 (C12), 112.2 (C10, minor), 112.1 (C10), 77.5 (C2), 67.9 (C8), 67.8 (C8, minor), 47.0 (C16', minor), 46.7 (C16'), 41.4 (C16), 41.3 (C16, minor), 39.9 (C5), 39.1 (C22), 39.0 (C22, minor), 36.1 (C19), 36.0 (C18), 32.7 (C17'), 32.0 (C17), 29.7 (C21), 27.9 (C1), 26.6 (C6), 26.5 (C7), 26.4 (C6, minor), 23.84 (C20), 28.78 (C20, minor).

N.B. rotamers observed, VT NMR of compound **182** in section 3.3.1.

t$_R$ (method 1) = 2.30 min

MS: *m/z* (ES+) 579.4 (100%, [M+H]$^+$)

HRMS calculated for C$_{33}$H$_{46}$N$_4$O$_5$Na [M+Na]$^+$ 601.3360, found 601.3350

v$_{max}$ (thin film, ATR)/cm^{-1}: 3290, 2929, 1704, 1666, 1615, 1538, 1453, 1365, 1245, 1170, 1101, 979, 734, 637

(*E*)-*N*-(4-(1-(2-(4-Aminobutoxy)benzoyl)piperidin-4-yl)butyl)-3-(pyridin-3-yl)acrylamide TFA salt (167)
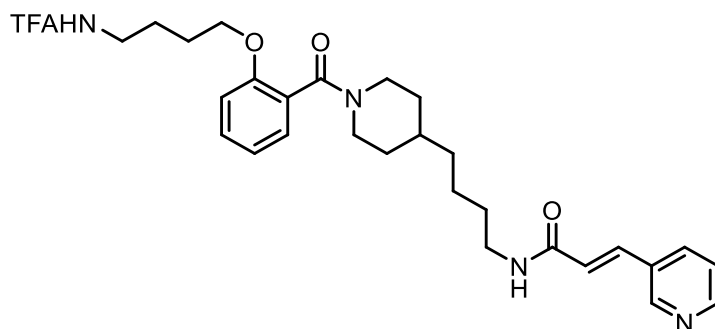
A flask was charged with a solution of *tert*-butyl (*E*)-(4-(2-(4-(4-(3-(pyridin-3-yl)acrylamido)butyl)piperidine-1-carbonyl)phenoxy)butyl)carbamate (**182**) (48.0 mg, 0.0810 mmol) in dry DCM (5.0 mL). TFA (0.5 mL) was added, and the reaction mixture stirred for 1.5 h at room temperature. Upon completion the reaction was concentrated to dryness under reduced pressure to afford the crude title compound as a yellow oil (89.0 mg), which was used without further purification.

Methyl 3-bromo-2-(bromomethyl)benzoate (187)
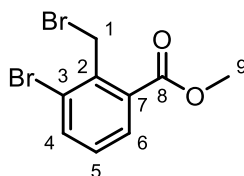
N-Bromosuccinimide (468 mg, 2.63 mmol, 1.2 eq) and benzoyl peroxide (53.0 mg, 0.219 mmol, 0.10 eq, recrystallised from acetone/MeOH) were added to a solution of methyl 3-bromo-2-methylbenzoate (**186**) (500 mg, 2.19 mmol, 1.0 eq) in CCl_4 (4.5 mL) at room temperature. The reaction was heated at reflux overnight. The mixture was concentrated to dryness under reduced pressure, and the residue purified by flash column chromatography (EtOAc:hexane 1:19) to afford the title compound as a white solid (639 mg, 95%).

¹H NMR (500 MHz, $CDCl_3$) δ 7.88 (dd, *J* = 7.8, 1.3 Hz, 1H, H6), 7.75 (dd, *J* = 8.0, 1.3 Hz, 1H, H4), 7.22 (app. t, *J* = 7.9 Hz, 1H, H5), 5.12 (s, 2H, H1), 3.95 (s, 3H, H9).

13C NMR (126 MHz, CDCl$_3$) δ 166.5 (C8), 137.9 (C2), 137.1 (C4), 131.7 (C7), 130.4 (C6), 129.5 (C5), 127.1 (C3), 52.7 (C9), 30.1 (C1).

MS: *m/z* (ES-) 305.7 (100%, [M-H]$^-$)

R$_t$ (method 1) = 2.66 min

3-(4-Bromo-1-oxoisoindolin-2-yl)piperidine-2,6-dione (185)
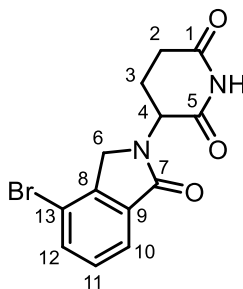
3-Aminopiperidine-2,6-dione hydrochloride (513 mg, 3.11 mmol, 1.5 eq) and NEt$_3$ (490 µL, 3.52 mmol, 1.7 eq) were added to a stirred solution of methyl 3-bromo-2-(bromomethyl)benzoate (**187**) (639 mg, 2.07 mmol, 1.0 eq) in MeCN (12 mL) at room temperature, and the reaction stirred at 80 °C overnight. The mixture was cooled to room temperature and filtered. The solids were washed sequentially with MeCN, MeCN:Et$_2$O 2:3, Et$_2$O, H$_2$O, MeCN, each 10 mL. This afforded the title compound as a purple solid (482 mg, 72%) that was used without further purification.

1H NMR (400 MHz, DMSO) δ 7.87 (dd, *J* = 7.9, 0.9 Hz, 1H, H12), 7.77 (dd, *J* = 7.6, 0.9 Hz, 1H, H10), 7.51 (t, *J* = 7.7 Hz, 1H, H11), 5.15 (dd, *J* = 13.3, 5.1 Hz, 1H, H4), 4.42 (d, *J* = 17.6 Hz, 1H, H6a), 4.26 (d, *J* = 17.6 Hz, 1H, H6b), 2.92 (ddd, *J* = 17.3, 13.6, 5.4 Hz, 1H, H2a), 2.60 (ddd, *J* = 17.6, 4.9, 2.2 Hz, 1H, H2b), 2.44 (dd, *J* = 13.4, 4.4 Hz, 1H, H3a), 2.07 – 1.96 (m, 1H, H3b).

13C NMR (101 MHz, DMSO) δ 173.3 (C1), 171.3 (C5), 167.7 (C7), 142.6 (C8), 135.1 (C9), 134.4 (C12), 131.0 (C11), 123.0 (C10), 117.8 (C13), 52.2 (C4), 48.4 (C6), 31.7 (C2), 22.7 (C3).

MS: *m/z* (ES+) 323.0 (100%, [M+H]$^+$)

R$_t$ (method 1) = 1.97 min

HRMS calculated for $C_{13}H_{12}O_3N_2Br$ [M+H]$^+$ 323.0026, found 323.0028

Tert-butyl hept-6-ynoate (190)
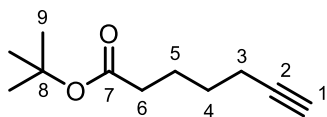
Hept-6-ynoic acid (**189**) (387 μL, 3.00 mmol, 1.0 eq), Boc$_2$O (1.31 g, 6.00 mmol, 2.0 eq), and DMAP (110 mg, 0.900 mmol, 0.30 eq) were dissolved in *t*BuOH (4.0 mL) at room temperature. The mixture was stirred overnight, then evaporated to dryness under reduced pressure. The residue was redissolved in EtOAc (10 mL) and partitioned with H$_2$O (10 mL). The aqueous layer was extracted with EtOAc (5.0 mL x 3), then the organics washed with brine (5.0 mL), dried over MgSO$_4$, filtered, and concentrated under reduced pressure to afford the title compound (429 mg, 79%) that was used without further purification.

^{1}H NMR (400 MHz, CDCl$_3$) δ 2.20 – 2.10 (m, 4H, stack of H3 and H6), 1.88 (t, *J* = 2.6 Hz, 1H, H1), 1.71 – 1.58 (m, 2H, H5), 1.53 – 1.43 (m, 2H, H4), 1.38 (s, 9H, H9).

^{13}C NMR (101 MHz, CDCl$_3$) δ 172.8 (C7), 84.1 (C2), 80.1 (C8), 68.5 (C1), 35.0 (C6), 28.1 (C9), 27.8 (C4), 24.2 (C5), 18.2 (C3).

R$_f$ (1:4 EtOAc:hexane) = 0.83

Analytical data matches that found in the literature.[278]

Tert-butyl 8-(2-(2,6-dioxopiperidin-3-yl)-1-oxoisoindolin-4-yl)oct-7-ynoate (267)
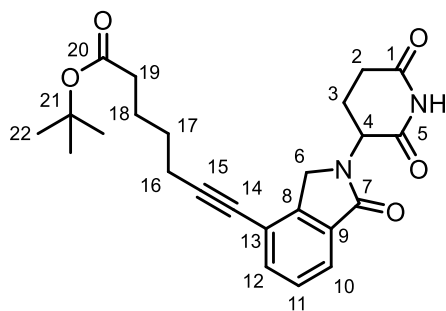
3-(4-Bromo-1-oxoisoindolin-2-yl)piperidine-2,6-dione (**185**) (22.4 mg, 0.0605 mmol, 1.0 eq), CuI (2.3 mg, 0.0121 mmol, 0.20 eq), NEt$_3$ (450 μL, 3.23 mmol,

53 eq), and *tert*-butyl hept-6-ynoate (22.0 mg, 0.121 mmol, 2.0 eq) were dissolved in DMF (1.5 mL) in an oven-dried vessel and degassed with argon for 15 min. Pd(PPh$_3$)$_3$Cl (4.25 mg, 0.00605 mmol, 0.10 eq) was added and the reaction stirred at 70 °C overnight. The mixture was cooled to room temperature, filtered, and the solids washed with EtOAc. The resulting solution was washed with H$_2$O (3 x 10 mL) then brine (10 mL), and the organic layer concentrated to dryness under reduced pressure. The resulting residue was purified by flash column chromatography (EtOAc:hexane 65:35) to afford the title compound as a yellow oil (14.0 mg, 55%).

^{1}H NMR (400 MHz, CDCl$_3$) δ 7.80 (dd, *J* = 7.6, 1.1 Hz, 1H, H10 or H12), 7.56 (dd, *J* = 7.7, 1.1 Hz, 1H, H10 or H12), 7.43 (t, *J* = 7.6 Hz, 1H, H11), 5.25 (dd, *J* = 13.4, 5.0 Hz, 1H, H4), 4.50 (d, *J* = 16.8 Hz, 1H, H6a), 4.39 (d, *J* = 16.8 Hz, 1H, H6b), 3.00 − 2.78 (m, 2H, H2), 2.53 − 2.42 (m, 3H, stack of H16 and H3a), 2.29 − 2.16 (m, 3H, stack of H19 and H3b), 1.83 − 1.71 (m, 2H, H18), 1.69 − 1.57 (m, 2H, H17), 1.43 (s, 9H, H22).

^{13}C NMR (101 MHz, CDCl$_3$) δ 172.9 (C20), 171.1 (C1), 169.4 (C7 or C5), 169.1 (C7 or C5), 143.7 (C8), 134.6 (C10 or C12), 131.5 (C9), 128.4 (C11), 123.3 (C10 or C12), 119.5 (C13), 95.5 (C15), 80.2 (C21), 51.8 (C4), 47.0 (C6), 35.0 (C19), 31.6 (C2), 28.1 (C22), 27.9 (C17), 24.3 (C18), 23.3 (C3), 19.3 (C16).

N.B.: carbon peak for C14 overlaps with solvent peak

MS: *m/z* (ES+) 369.2 (100%, [M+H-*t*Bu]$^+$)

R$_t$ (method 1) = 2.57 min

HRMS calculated for C$_{24}$H$_{28}$O$_5$N$_2$Na [M+Na]$^+$ 447.1890, found 447.1896

v$_{max}$ (thin film, ATR)/cm^{-1}: 2855, 2926, 1709, 1454, 1368, 1233, 1145, 753

7-(2-(2,6-Dioxopiperidin-3-yl)-1-oxoisoindolin-4-yl)hept-6-ynoic acid (188)
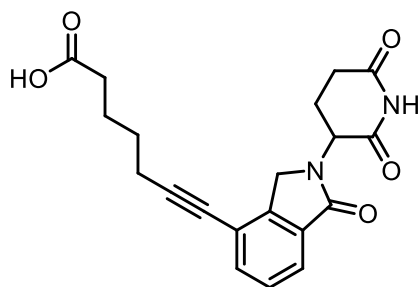
Tert-butyl 8-(2-(2,6-dioxopiperidin-3-yl)-1-oxoisoindolin-4-yl)oct-7-ynoate (**267**) (46.0 mg, 0.108 mmol) was dissolved in DCM (2.0 mL). TFA (0.50 mL) was added at room temperature, and the reaction stirred for 3 h. The mixture was concentrated to dryness under reduced pressure to afford the title compound as a beige gum that was used without further purification.

Tert-butyl 7-(2-(2,6-dioxopiperidin-3-yl)-1,3-dioxoisoindolin-4-yl)hept-6-ynoate (192)
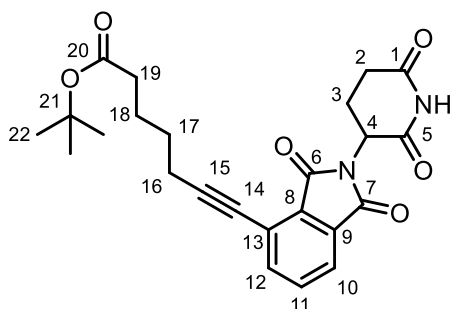
4-Bromo-2-(2,6-dioxopiperidin-3-yl)isoindoline-1,3-dione (**191**) (50.0 mg, 0.148 mmol, 1.0 eq), CuI (5.62 mg, 0.0296 mmol, 0.20 eq), NEt₃ (300 µL, 2.16 mmol, 15 eq), and *tert*-butyl hept-6-ynoate (53.9 mg, 0.296 mmol, 2.0 eq) were dissolved in DMF (1.0 mL) in an oven-dried vessel and degassed with argon for 15 min. Pd(PPh₃)₃Cl (10.4 mg, 0.0148 mmol, 0.10 eq) was added and the reaction stirred at 80 ℃ overnight. The mixture was cooled to room temperature, filtered, and the solids washed with EtOAc. The resulting solution was washed with H₂O (3 x 10 mL) then brine (10 mL), and the organic layer concentrated to dryness under reduced pressure. The resulting residue was purified by flash column chromatography (EtOAc:hexane 45:55) to afford the title compound as a yellow oil (39.0 mg, 60%).

¹H NMR (400 MHz, CDCl₃) δ 7.76 (dd, *J* = 7.2, 1.3 Hz, 1H, H10), 7.71 − 7.61 (m, 2H, stack of H11 and H12), 4.97 (dd, *J* = 12.1, 5.4 Hz, 1H, H4), 2.93 − 2.70 (m, 3H, stack of H2 and 1 of H3), 2.53 (t, *J* = 6.9 Hz, 2H, H16), 2.28 (t, *J* = 7.3 Hz, 2H, H19), 2.15 − 2.09 (m, 1H, 1 of H3), 1.83 − 1.75 (m, 2H, H18), 1.74 − 1.64 (m, 2H, H17), 1.43 (s, 9H, H22).

¹³C NMR (101 MHz, CDCl₃) δ 172.8 (C20), 170.9 (C1), 167.9 (C5), 166.5 (C7), 166.0 (C6), 138.5 (C12), 133.8 (C11), 132.2 (C9), 130.6 (C8), 122.5 (C10), 121.7 (C13), 99.1 (C15), 80.2 (C21), 76.2 (C14), 49.3 (C4), 35.0 (C19), 31.4 (C2), 28.1 (C22), 27.7 (C17), 24.3 (C18), 22.6 (C3), 19.6 (C16).

R$_f$ (45:55 EtOAc:hexane) = 0.24

MS: *m/z* (ES-) 437.2 (100%, [M-H]⁻)

R$_t$ (method 2) = 2.66 min

***Tert*-butyl 7-(2-(2,6-dioxopiperidin-3-yl)-1,3-dioxoisoindolin-4-yl)heptanoate (193)**
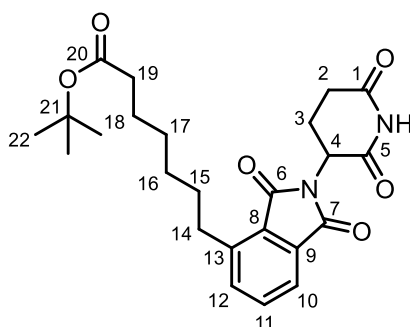
Tert-butyl 7-(2-(2,6-dioxopiperidin-3-yl)-1,3-dioxoisoindolin-4-yl)hept-6-ynoate (**192**) (84.0 mg, 0.192 mmol) was dissolved in EtOAc (6.0 mL) at room temperature and degassed with argon for 15 min. Pd/C (25.0 mg) was added, and H₂ bubbled through the mixture for 10 min. The reaction was then stirred under an atmosphere of H₂ at room temperature overnight. The mixture was filtered through celite and the pad washed with EtOAc (10 mL). The resulting solution was concentrated to dryness under reduced pressure to afford the title compound as a pale yellow oil (84.3 mg, 99%).

¹H NMR (500 MHz, CDCl₃) δ 7.68 (dd, *J* = 7.3, 1.0 Hz, 1H, H10), 7.59 (app. t, *J* = 7.6 Hz, 1H, H11), 7.48 (dd, *J* = 7.8, 1.0 Hz, 1H, H12), 4.97 (dd, *J* = 12.1, 5.3 Hz, 1H, C4), 3.06 − 3.00 (m, 2H, H14), 2.89 − 2.67 (m, 3H, stack of H2 and 1 of H3), 2.17 (t, *J* = 7.5 Hz, 2H,

H19), 2.15 – 2.08 (m, 1H, 1 of H3), 1.66 – 1.59 (m, 2H, H15), 1.58 – 1.51 (m, 2H, H18), 1.40 (s, 9H, H22), 1.39 – 1.29 (m, 4H, stack of H16 and H17).

^{13}C NMR (126 MHz, CDCl$_3$) δ 172.3 (C20), 170.5 (C1), 167.5 (C5), 166.8 (C6), 166.3 (C7), 142.6 (C13), 134.9 (C12), 133.0 (C11), 131.2 (C9), 127.0 (C8), 120.5 (C10), 79.0 (C21), 48.1 (C4), 34.5 (C19), 30.3 (C2), 30.2 (C14), 29.6 (C15), 28.1 (C16 or 17), 27.8 (C16 or 17), 27.1 (C22), 23.9 (C18), 21.6 (C3).

HRMS calculated for C$_{24}$H$_{30}$N$_2$O$_6$Na [M+Na]$^+$ 465.1996, found 465.1988

MS: *m/z* (ES-) 441.3 (100%, [M-H]$^-$)

R$_t$ (method 1) = 2.77 min

7-(2-(2,6-Dioxopiperidin-3-yl)-1,3-dioxoisoindolin-4-yl)heptanoic acid (194)
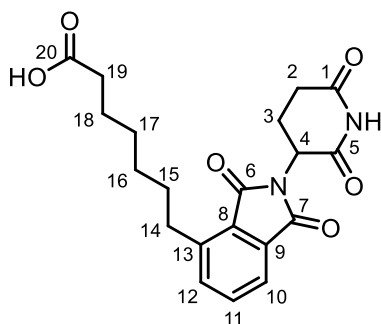
Tert-butyl 7-(2-(2,6-dioxopiperidin-3-yl)-1,3-dioxoisoindolin-4-yl)heptanoate (**193**) (98.4 mg, 0.222 mmol) was dissolved in DCM (2.0 mL). TFA (0.20 mL) was added at room temperature, and the reaction stirred at room temperature for 3 h. The mixture was concentrated to dryness under reduced pressure to afford the title compound as a beige gum that was used without further purification.

2-Hydroxy-4-(4-methylthiazol-5-yl)benzonitrile (197)
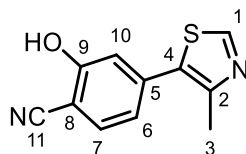
4-Bromo-2-hydroxy-benzonitrile (**195**) (4.85 g, 24.5 mmol, 1.0 eq), 4-methylthiazole (**196**) (4.22 mL, 46.3 mmol, 1.89 eq), Pd(OAc)$_2$ (54.6 mg, 0.245 mmol, 0.01 eq), and

KOAc (5.35 g, 54.4 mmol, 2.22 eq) were dissolved in an. DMA (50 mL). The reaction was heated to 150 °C and stirred for 3.5 h. The reaction mixture was allowed to cool to room temperature and diluted with water (100 mL), then extracted with EtOAc (5 x 50 mL). The combined organics were then washed with brine (3 x 25 mL), dried over MgSO$_4$, filtered, and concentrated under reduced pressure. The resulting residue was purified by flash column chromatography using EtOAc/hexanes (6:1) to afford the title compound as a yellow solid (3.64 g, 69%).

^{1}H NMR (500 MHz, DMSO) δ 11.35 (s, 1H, OH), 9.07 (s, 1H, H1), 7.69 (d, *J* = 8.1 Hz, 1H, H7), 7.13 (d, *J* = 1.7 Hz, 1H, H10), 7.06 (d, *J* = 8.1 Hz, 1H, H6), 2.49 (s, 3H, H3).

^{13}C NMR (126 MHz, DMSO) δ 160.7 (C9), 153.4 (C1), 149.8 (C2), 138.1 (C5), 134.3 (C7), 130.3 (C4), 120.4 (C6), 117.2 (C11), 116.3 (C10), 98.6 (C8), 16.8 (C3).

MS: *m/z* (ES+) 217.11 (100%, [M+H]$^+$)

R$_t$ (acid method) = 2.06 min

HRMS calculated for C$_{11}$H$_7$ON$_2$S [M-H]$^-$ 215.0285, found 215.0279

ν$_{max}$ (thin film, ATR)/cm^{-1}: 3083, 2224, 1607, 1577, 1423, 1302, 1274, 1240, 1187, 1119, 1033, 950, 868, 817, 742, 666, 632, 510

2-(Aminomethyl)-5-(4-methylthiazol-5-yl)phenol (198)
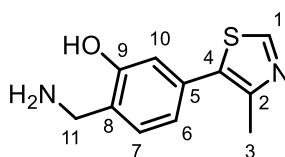
BH$_3$.SMe$_2$ (2.0 M solution in THF, 21.0 mL, 41.0 mmol, 5.0 eq) was added dropwise to DIBAL (1.0 M solution in hexanes, 41.0 mL, 41.0 mmol, 5.0 eq) and the mixture stirred at room temperature for 1.0 h. A solution of 2-hydroxy-4-(4-methylthiazol-5-yl)benzonitrile (**197**) (1.77 g, 8.20 mmol, 1.0 eq) in an. THF (20 mL) was added dropwise at room temperature, and reaction stirred overnight. The reaction was cooled to 0 °C and quenched with MeOH (20 mL) followed by water (20 mL). The resulting gel was filtered, and the solids washed with THF and MeOH. The filtrate was

acidified to pH = 2.0 with HCl (conc.) and heated at reflux for 1 h. The mixture was allowed to cool to room temperature, neutralised with K_2CO_3, and concentrated under reduced pressure. The residue was purified by flash column chromatography using 0.7 M NH_3 in MeOH/DCM (1:4) to give the title compound as a yellow solid (520 mg, 29%).

^{1}H NMR (400 MHz, MeOD) δ 8.82 (s, 1H, H1), 7.19 (d, J = 7.7 Hz, 1H, H7), 6.87 (s, 1H, H10), 6.81 (d, J = 7.6 Hz, 1H, H6), 3.92 (s, 2H, H11), 2.47 (s, 3H, H3).

^{13}C NMR (101 MHz, MeOD) δ 158.2 (C9), 151.2 (C1), 147.3 (C2), 132.4 (C4), 131.7 (C5), 129.1 (C7), 126.0 (C8), 118.9 (C6), 116.3 (C10), 41.6 (C11), 14.6 (C3).

MS: m/z (ES+) 221.2 (100%, [M+H]$^+$)

R_t (method 1) = 1.49 min

HRMS calculated for $C_{11}H_{13}ON_2S$ [M+H]$^+$ 221.0743, found 221.0741

v$_{max}$ (thin film, ATR)/cm^{-1}: 3467, 3372, 2978, 2925, 1683, 1634, 1595, 1504, 1456, 1422, 1367, 1344, 1321, 1282, 1265, 1249, 1220, 1157, 1128, 1088, 1055, 996, 929, 832, 733, 714, 665, 591, 551

Tert-butyl (2_S_,4_R_)-4-hydroxy-2-((2-hydroxy-4-(4-methylthiazol-5-yl)benzyl)carbamoyl)pyrrolidine-1-carboxylate (199)
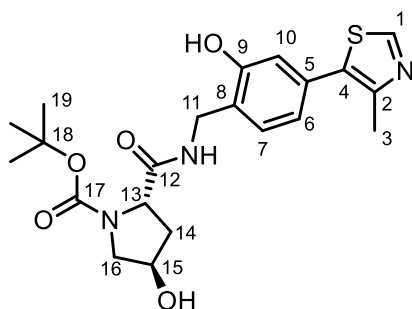
HATU (1.95 g, 5.13 mmol, 1.25 eq), HOBt.H$_2$O (815 mg, 5.33 mmol, 1.30 eq), DIPEA (1.86 mL, 10.7 mmol, 2.60 eq), and Boc-Hyp-OH (996 mg, 4.31 mmol, 1.05 eq) were dissolved in DMF (5.0 mL) and stirred at room temperature for 1 h 45 min. 2-(Aminomethyl)-5-(4-methylthiazol-5-yl)phenol (**198**) (900 mg, 4.10 mmol, 1.00 eq) was added and the reaction stirred at room temperature overnight. HATU (779 mg,

2.05 mmol, 0.500 eq), DIPEA (713 µL, 4.10 mmol, 1.00 eq), and Boc-Hyp-OH (474 mg, 2.05 mmol, 0.500 eq) were stirred in DMF (2.0 mL) for 45 min, and then added to the reaction mixture at room temperature. The reaction mixture was stirred for 3.5 h then diluted with water and extracted with EtOAc (10 mL x 5). The combined organic layers were washed with brine, dried over $MgSO_4$, filtered, and concentrated under reduced pressure. The resulting residue was purified by flash column chromatography (MeOH: DCM 1:9) to afford the title compound as a beige solid (1.18 g, 66%).

^{1}H NMR (400 MHz, DMSO) δ 9.93 (s, 0.7H, OH), 9.82 (s, 0.3H, OH), 8.95 (s, 1H, H1), 8.49 (t, J = 5.9 Hz, 0.7H, NH), 8.34 (t, J = 6.0 Hz, 0.3H, NH), 7.25 (d, J = 7.8 Hz, 0.3H, H7), 7.20 (d, J = 7.8 Hz, 0.7H, H7), 6.92 (d, J = 1.8 Hz, 1H, H10), 6.87 (dd, J = 7.7, 1.8 Hz, 0.7H, H6), 6.84 (dd, J = 7.8, 1.8 Hz, 0.3H, H6), 5.01 (s, 1H, OH), 4.33 − 4.12 (m, 4H, stack of H11, H13, and H15), 3.50 − 3.23 (m, 2H, H16), 2.44 (s, 3H, H3), 2.15 − 2.00 (m, 1H, H14 or H14′), 1.93 − 1.82 (m, 1H, H14 or H14′), 1.24 (s, 9H, H19).

^{13}C NMR (101 MHz, DMSO) δ 173.8 (C12), 173.0 (C12, minor), 155.6 (C17), 155.3 (C17, minor), 154.5 (C9, minor), 154.0 (C9), 151.7 (C9, minor), 151.8 (C1), 148.04 (C2), 147.96 (C2, minor), 131.7 (C5), 129.9 (C7), 125.7 (C8), 119.9 (C6), 119.8 (C6, minor), 116.1 (C10), 115.5 (C10, minor), 79.2 (C18, minor), 79.0 (C18), 69.0 (C15, minor), 68.3 (C15), 59.3 (C13), 55.5 (C16, minor), 55.3 (C16), 40.1 (C14), 37.9 (C11), 37.5 (C11, minor), 28.6 (C19, minor), 28.3 (C19), 16.53 (C3 minor), 16.46 (C3).

N.B. Signal for C4 not observed, rotamers observed.

MS: *m/z* (ES+) 434.3 (100%, [M+H]$^+$)

R$_t$ (method 1) = 2.01 min

HRMS calculated for $C_{21}H_{27}N_3O_5SNa$ [M+Na]$^+$ 433.1671, found 433.1678

v$_{max}$ (thin film, ATR)/cm^{-1}: 3303, 2978, 1668, 1543, 1477, 1408, 1367, 1285, 1250, 1158, 1128, 1085, 982, 943, 882, 854, 773, 734, 702, 624, 550, 463.

(2S,4R)-4-Hydroxy-N-(2-hydroxy-4-(4-methylthiazol-5-yl)benzyl)pyrrolidine-2-carboxamide TFA salt (200)
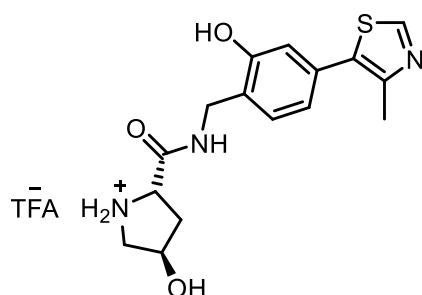
Tert-butyl (2S,4R)-4-hydroxy-2-((2-hydroxy-4-(4-methylthiazol-5-yl)benzyl)carbamoyl)pyrrolidine-1-carboxylate (**199**) (1.18 g, 2.73 mmol) was dissolved in DCM (3.0 mL). TFA (1.0 mL) was added and the reaction stirred at room temperature for 1 h. DCM (1.0 mL) and TFA (1.0 mL) were added and the reaction stirred at room temperature for 16 h. The mixture was concentrated to dryness under reduced pressure to afford the title compound which was used without further purification.

Tert-butyl ((S)-1-((2S,4R)-4-hydroxy-2-((2-hydroxy-4-(4-methylthiazol-5-yl)benzyl)carbamoyl)pyrrolidin-1-yl)-3,3-dimethyl-1-oxobutan-2-yl)carbamate (201)
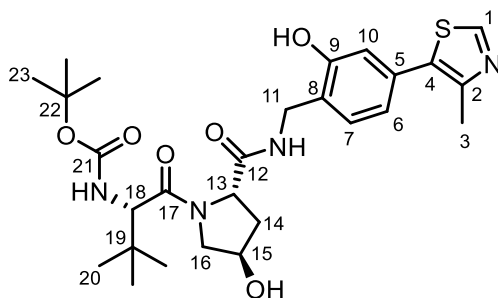
HATU (1.97 g, 5.19 mmol, 1.9 eq), HOBt.H$_2$O (710 mg, 4.64 mmol, 1.7 eq), DIPEA (2.43 mL, 13.7 mmol, 5.0 eq), and Boc-Tle-OH (947 mg, 4.10 mmol, 1.5 eq) were dissolved in DMF (3.0 mL) and stirred at room temperature for 1.25 h. (2S,4R)-4-Hydroxy-N-(2-hydroxy-4-(4-methylthiazol-5-yl)benzyl)pyrrolidine-2-carboxamide TFA salt (**200**) (assumed 2.73 mmol) in DMF (3.5 mL) was added and the reaction stirred for 16 h. HATU (657 mg, 1.37 mmol, 0.5 eq), HOBt.H$_2$O (237 mg, 1.37 mmol, 0.5 eq), DIPEA (1.46 mL, 8.20 mmol, 3.0 eq), and Boc-Tle-OH (316 mg, 1.37 mmol, 0.5 eq) were stirred in DMF (2.0 mL) for 1 h and added to the reaction mixture, which was then

stirred at room temperature for a further 3 h. DIPEA (1.0 mL, 5.62 mmol, 2.05 eq) was added at room temperature and the reaction heated to 40 °C, and the mixture stirred for 48 h. The reaction mixture was allowed to cool to room temperature, then diluted with water and extracted with EtOAc (x5). The combined organic layers were washed with brine, dried over MgSO₄, filtered, and concentrated under reduced pressure. The resulting residue was purified by reverse phase flash column chromatography to afford the title compound as a beige oil (702 mg, 47% over two steps).

¹H NMR (500 MHz, MeOD) δ 8.84 (s, 1H, H1), 7.36 (d, J = 7.7 Hz, 1H, H7), 6.90 – 6.86 (m, 2H, stack of H6 and H10), 4.61 (app. t, J = 8.2 Hz, 1H, H13), 4.52 – 4.48 (m, 1H, H15), 4.42 (d, J = 15.5 Hz, 1H, H11a), 4.36 (d, J = 15.4 Hz, 1H, H11b), 4.29 (s, 1H, H18), 3.87 (d, J = 11.1 Hz, 1H, H16a), 3.78 (dd, J = 11.0, 4.0 Hz, 1H, H11b), 2.47 (s, 3H, H3), 2.23 – 2.17 (m, 1H, H14a), 2.11 (ddd, J = 13.2, 8.8, 4.6 Hz, 1H, H14b), 1.44 (s, 9H, H23), 1.00 (s, 9H, H20).

¹³C NMR (126 MHz, MeOD) δ 173.2 (C12), 171.5 (C17), 156.4 (C21), 155.3 (C9), 151.3 (C1), 147.4 (C2), 132.2 (C4), 131.4 (C5), 129.2 (C7), 124.8 (C8), 120.0 (C6 or C10), 115.4 (C6 or C10), 79.1 (C22), 69.7 (C15), 59.3 (C13), 58.9 (C18), 56.6 (C16), 38.1 (C11), 37.3 (C14), 35.4 (C19), 27.3 (C23), 25.7 (C20), 14.6 (C3).

MS: *m/z* (ES+) 547.2 (100%, [M+H]⁺)

Rₜ (method 1) = 2.29 min

ν_max (thin film, ATR)/cm⁻¹: 3290, 1739, 1641, 1537, 1417, 1203, 1055, 742, 695, 599

(2*S*,4*R*)-1-((*S*)-2-Amino-3,3-dimethylbutanoyl)-4-hydroxy-*N*-(2-hydroxy-4-(4-methylthiazol-5-yl)benzyl)pyrrolidine-2-carboxamide TFA salt (202)
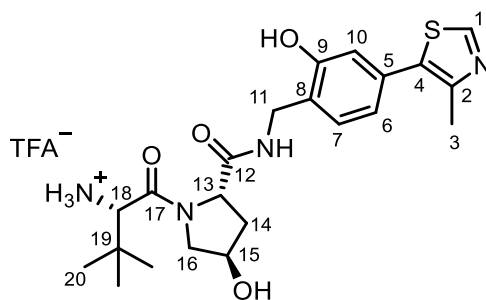
Tert-butyl ((*S*)-1-((2*S*,4*R*)-4-hydroxy-2-((2-hydroxy-4-(4-methylthiazol-5-yl)benzyl)carbamoyl)pyrrolidin-1-yl)-3,3-dimethyl-1-oxobutan-2-yl)carbamate (**201**) (128 mg, 0.234 mmol) was dissolved in DCM (2.7 mL) and TFA (0.3 mL) added at room temperature. The mixture was stirred at room temperature for 3.5 h, then concentrated to dryness under reduced pressure to afford the title compound that was used without further purification.

(2*S*,4*R*)-1-((*S*)-2-(1-Fluorocyclopropane-1-carboxamido)-3,3-dimethylbutanoyl)-4-hydroxy-*N*-(2-hydroxy-4-(4-methylthiazol-5-yl)benzyl)pyrrolidine-2-carboxamide (184)
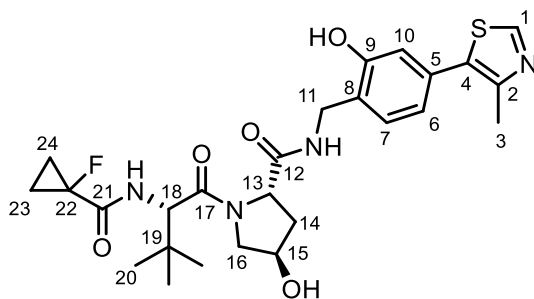
(2*S*,4*R*)-1-((*S*)-2-Amino-3,3-dimethylbutanoyl)-4-hydroxy-*N*-(2-hydroxy-4-(4-methylthiazol-5-yl)benzyl)pyrrolidine-2-carboxamide TFA salt (**202**) (assumed 0.234 mmol), 1-fluorocyclopropanecarboxylic acid (43.8 mg, 0.422 mmol, 1.8 eq), DIPEA (166 µL, 1.40 mmol, 6.0 eq), and HOBt.H_2O (35.5 mg, 0.232 mmol, 0.99f eq) were dissolved in DMF (2.5 mL) at room temperature. HATU (178 mg, 0.468 mmol, 2.0 eq) was added at room temperature and the mixture stirred for 16 h. The reaction mixture was diluted with water (7.0 mL) and extracted with EtOAc (5 x 7.0 mL). The combined organic layers were washed with brine (10 mL), dried over $MgSO_4$, filtered, and concentrated under reduced pressure. The resulting residue was purified by reverse phase flash column chromatography (acid modifier) to afford the title compound (45.6 mg, 34% over 2 steps).

¹H NMR (500 MHz, CDCl₃) δ 9.33 (s, 1H, OH), 8.70 (s, 1H, H1), 8.11 (app. t, *J* = 6.4 Hz, 1H, (O)CN**H**-CH₂), 7.09 (d, *J* = 7.8 Hz, 1H, H7), 7.00 (dd, *J* = 8.8, 3.6 Hz, 1H, (O)CN**H**-CH), 6.92 (d, *J* = 1.8 Hz, 1H, H10), 6.81 (dd, *J* = 7.8, 1.8 Hz, 1H, H6), 4.67 (app. t, *J* = 7.9 Hz, 1H, H13), 4.52 – 4.46 (m, 2H, stack of H15 and H18), 4.39 (dd, *J* = 14.6, 7.2 Hz, 1H, H11),

4.16 (dd, J = 14.6, 5.5 Hz, 1H, H11'), 3.93 – 3.86 (m, 1H, H16), 3.61 (dd, J = 11.1, 3.8 Hz, 1H, H16'), 2.47 (s, 3H, H3), 2.34 (ddd, J = 12.9, 8.0, 4.7 Hz, 1H, H14), 2.09 – 2.00 (m, 1H, H14'), 1.38 – 1.15 (m, 4H, stack of H23 and H24), 0.89 (s, 9H, H20).

^{13}C NMR (126 MHz, CDCl$_3$) δ 172.9 (C12), 171.0 (C17, minor), 170.9 (C17), 170.1 (d, J_{C-F} = 20.2 Hz, C21), 155.8 (C9), 150.6 (C1), 133.0 (C5), 131.8 (C5), 131.1 (C7), 124.1 (C8), 120.6 (C6), 118.0 (C10), 78.14 (d, J_{C-F} = 232.1 Hz, C22, minor), 78.07 (d, J = 232.6 Hz, C22), 70.0 (C15), 58.4 (C13), 57.6 (C18), 56.7 (C16), 39.8 (C11), 36.1 (C14), 35.6 (C19), 26.5 (C20), 26.2 (C20, minor), 16.0 (C3), 13.6 (d, J_{C-F} = 4.3 Hz, C23 or C24), 13.5 (d, J_{C-F} = 4.4 Hz, C23 or C24).

N.B. Signal for C4 not observed, rotamers observed.

MS: *m/z* (ES+) 533.3 (100%, [M+H]$^+$)

R$_t$ (method 1) = 2.08 min

(*E*)-3-(diisopropylamino)-1-(1-fluorocyclopropyl)prop-2-en-1-one (206)
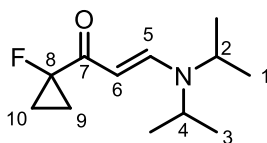
1-Fluorocycloproylcarboxylic acid (**205**) (100 mg, 0.962 mmol, 1.0 eq) and DIPEA (514 μL, 2.89 mmol, 3.0 eq) were dissolved in DMF (3.0 mL) at room temperatre. HATU (730 mg, 1.92 mmol, 2.0 eq) was added and the reaction stirred at room temperature for 1.0 h. The mixture was diluted with EtOAc (10 mL) and H$_2$O (10 mL). The mixture was extracted with EtOAc (5 x 5.0 mL), and the combined organics washed with H$_2$O (3 x 5.0 mL) and brine (5.0 mL). The combined organics were dried over MgSO$_4$, filtered, and concentrated under reduced pressure. The residue was purified by reverse phase flash column chromatography (acidic modifier) to afford the title compound as a colourless oil (27.1 mg, 13%).

^{1}H NMR (500 MHz, CDCl$_3$) δ 7.87 (dd, J = 12.8, 1.4 Hz, 1H, H5), 5.81 (dd, J = 12.8, 4.0 Hz, 1H, H6), 4.00 (hept, J = 6.8 Hz, 1H, H2 or H4), 3.61 (hept, J = 6.8 Hz, 1H, H2 or H4),

1.39 – 1.33 (m, 2H, stack of H9a and H10a), 1.29 – 1.21 (m, 13H, stack of H1, H3, and one of H9b or H10b), 1.22 – 1.16 (m, 1H, one of H9b or H10b).

^{13}C NMR (126 MHz, CDCl$_3$) δ 193.1 (d, J = 20.1 Hz, C7), 148.4 (d, J_{C-F} = 2.3 Hz, C5), 89.8 (C6), 82.0 (d, J = 232.6 Hz, C8), 49.5 (C2 or C4), 48.1 (C2 or C4), 23.6 (C1 or C3), 19.6 (C1 or C3), 15.2 (d, J_{C-F} = 10.6 Hz, stack of C9 and C10).

^{19}F NMR (471 MHz, CDCl$_3$) δ -75.7.

MS: *m/z* (ES+) 214.3 (100%, [M+H]$^+$)

R$_t$ (method 1) = 2.36 min

HRMS calculated for C$_{12}$H$_{21}$ONF [M+H]$^+$ 214.1602, found 214.1596

(*E*)-4-(diethylamino)-1,1-difluoro-1-phenylbut-3-en-2-one (220)

2,2-Difluoro-2-phenylacetic acid (**217**) (100 mg, 0.581 mmol, 1.0 eq) and NEt$_3$ (242 µL, 1.74 mmol, 3.0 eq) were dissolved in DMF (3.0 mL) at room temperatre. HATU (442 mg, 1.16 mmol, 2.0 eq) was added and the reaction stirred at room temperature for 1.0 h. The mixture was diluted with EtOAc (10 mL) and H$_2$O (10 mL). The mixture was extracted with EtOAc (5 x 5.0 mL), and the combined organics washed with H$_2$O (3 x 5.0 mL) and brine (5.0 mL). The combined organics were dried over MgSO$_4$, filtered, and concentrated under reduced pressure. The residue was purified by reverse phase flash column chromatography (acidic modifier) to afford the title compound as a colourless oil (60.2 mg, 41%).
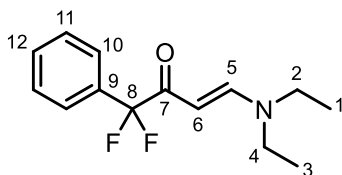
^{1}H NMR (400 MHz, CDCl$_3$) δ 7.77 (d, J = 12.5 Hz, 1H, H6), 7.66 – 7.57 (m, 2H, H10), 7.41 (dd, J = 5.1, 2.0 Hz, 3H, stack of H11 and H12), 5.47 (app. dt, J = 12.5, 1.6 Hz, 1H, H5), 3.33 (q, J = 7.2 Hz, 2H, H2 or H4), 3.26 (q, J = 7.2 Hz, 2H, H2 or H4), 1.25 – 1.16 (m, 6H, stack of H1 and H3).

^{13}**C NMR** (101 MHz, CDCl$_3$) δ 186.0 (C7), 154.1 (C6), 135.0 (C9), 130.0 (C12), 128.3 (C11), 125.6 (t, J_{C-F} = 6.1 Hz, C10), 88.1 (C5), 50.9 (C2 or C4), 43.1 (C2 or C4), 14.6 (C1 or C3), 11.5 (C1 or C3).

N.B. Signal for C8 not observed.

MS: *m/z* (ES+) 254.2 (100%, [M+H]$^+$)

R$_t$ (method 1) = 2.41 min

R$_f$ (2:3 EtOAc:hexane) = 0.22

6-(((*S*)-1-((2*S*,4*R*)-4-Hydroxy-2-((4-(4-methylthiazol-5-yl)benzyl)carbamoyl)pyrrolidin-1-yl)-3,3-dimethyl-1-oxobutan-2-yl)amino)-6-oxohexanoic acid (228)
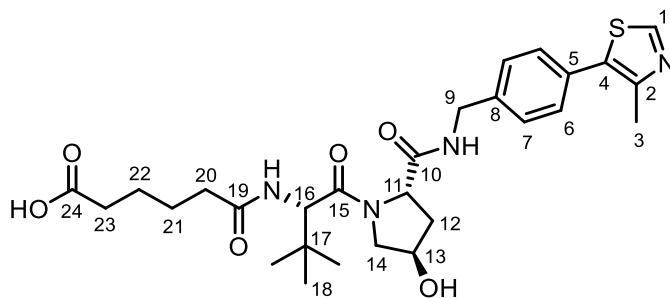
HATU (122 mg, 0.321 mmol, 3.0 eq), methyl adipate (31.7 μL, 0.214 mmol, 2.0 eq), and DIPEA (74.4 μL, 0.428 mmol, 4.0 eq) were dissolved in DMF (1.0 mL) at room temperature and stirred for 40 min. VH032.HCl (**183**) (50.0 mg, 0.107 mmol, 1.0 eq) in DMF (1.0 mL) was added at room temperature, and the mixture stirred overnight. The reaction was then quenched with H$_2$O (5.0 mL) and extracted with Et$_2$O (5 mL x 5). The organics were then washed sequentially with H$_2$O and brine (5.0 ml each), then dried over MgSO$_4$, filtered and concentrated under reduced pressure. The resulting residue was redissolved in MeOH:H$_2$O:THF 1:1:4 (6.0 mL), and LiOH.H$_2$O (85.3 mg, 2.03 mmol, 20 eq) was added at room temperature. The mixture was stirred for 30 min. The reaction was then concentrated under reduced pressure, and the residue purified by reverse phase flash column chromatography (acid modifier) to afford the title compound as a white solid (25.0 mg, 41% over two steps).

¹H NMR (500 MHz, MeOD) δ 8.88 (s, 1H, H1), 7.46 (d, *J* = 8.1 Hz, 2H, H7), 7.41 (d, *J* = 8.2 Hz, 2H, H6), 4.63 (s, 1H, H16), 4.60 – 4.57 (m, 1H, H11), 4.56 – 4.51 (m, 1H, H9a), 4.51 – 4.48 (m, 1H, H13), 4.35 (d, *J* = 15.5 Hz, 1H, H9b), 3.93 – 3.89 (m, 1H, H14a), 3.80 (dd, *J* = 11.0, 3.9 Hz, 1H, H14b), 2.47 (s, 3H, H3), 2.36 – 2.26 (m, 4H, stack of H22 and H23), 2.25 – 2.18 (m, 1H, H12a), 2.08 (ddd, *J* = 13.4, 9.1, 4.5 Hz, 1H, H12b), 1.69 – 1.58 (m, 4H, stack of H20 and H21), 1.04 (s, 9H, H18).

¹³C NMR (126 MHz, MeOD) δ 175.9 (C24), 174.3 (C19), 173.1 (C10), 170.9 (C15), 151.5 (C1), 147.6 (C2), 138.9 (C8), 132.0 (C4), 130.1 (C5), 129.0 (C6), 127.6 (C7), 69.7 (C13), 59.4 (C11), 57.6 (C16), 56.6 (C14), 42.3 (C9), 37.5 (C12), 35.1 (C17), 34.9 (C17), 33.2 (either C22 or C23), 25.6 (either C22 or C23), 25.1 (C18), 24.3 (either C20 or C21), 17.0 (either C20 or C21), 14.4 (C3).

HRMS calculated for $C_{28}H_{38}O_6N_4NaS$ [M+Na]$^+$ 581.2404, found 581.2402

MS: *m/z* (ES+) 557.3 (100%, [M+H]$^+$)

R$_t$ (method 1) = 2.04 min

(*R*)-3-((2*S*,4*R*)-4-Hydroxy-2-((4-(4-methylthiazol-5-yl)benzyl)carbamoyl)pyrrolidine-1-carbonyl)-2,2-dimethyl-5-oxo-7,10,13,16-tetraoxa-4-azanonadecan-19-oic acid (229)
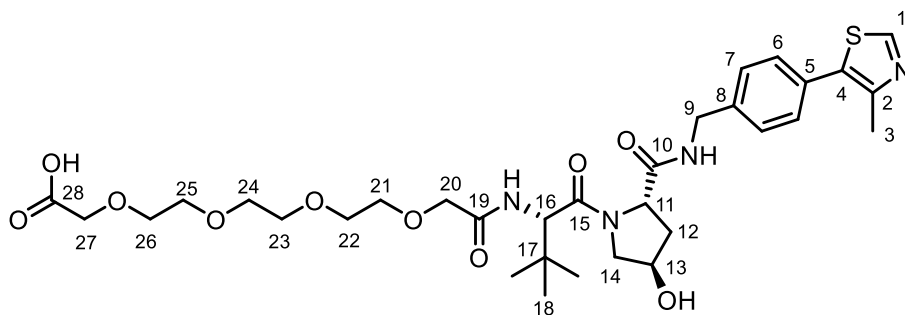
3,6,9,12-Tetraoxatetradecanedioic acid (42.8 mg, 0.161 mmol, 1.5 eq), HATU (81.3 mg, 0.214 mmol, 2.0 eq), and NEt$_3$ (44.7 μL, 0.340 mmol, 3.0 eq) were dissolved in DCM (2.5 mL) at room temperature and stirred for 1.5 h. VH032.HCl (**183**) (50.0 mg, 0.107 mmol, 1.0 eq) was added and the mixture stirred overnight at room temperature. The mixture was concentrated to dryness under reduced pressure, and

the residue purified by reverse phase flash column chromatography (acid modifier) to afford the title compound as a colourless oil (38.0 mg, 52%).

^{1}H NMR (500 MHz, MeOD) δ 8.89 (s, 1H, H1), 7.48 – 7.41 (m, 4H, stack of H6 and H7), 4.70 (s, 1H, H16), 4.60 – 4.52 (m, 2H, stack of H11 and H9a), 4.52 – 4.49 (m, 1H, H13), 4.36 (d, J = 15.5 Hz, 1H, H9b), 4.11 (s, 2H, H27), 4.09 – 4.01 (m, 2H, H20), 3.88 (d, J = 11.0 Hz, 1H, H14a), 3.80 (dd, J = 11.0, 3.8 Hz, 1H, H14b), 3.74 – 3.62 (m, 12H, stack of H21-26), 2.48 (s, 3H, H3), 2.26 – 2.20 (m, 1H, H12a), 2.08 (ddd, J = 13.4, 9.3, 4.4 Hz, 1H, H12b), 1.05 (s, 9H, H18).

^{13}C NMR (126 MHz, MeOD) δ 173.0 (C10), 172.7 (C28), 170.8 (C19), 170.2 (C15), 151.5 (C1), 147.6 (C2), 138.9 (C8), 132.0 (C4), 130.1 (C5), 129.0 (C6), 127.6 (C7), 70.9 (one of C21-26), 70.31 (one of C21-26), 70.21 (one of C21-26), 70.19 (one of C21-26), 70.17 (one of C21-26), 70.1 (one of C21-26), 69.7 (stack of C13 and C20), 67.7 (C27), 59.4 (C11), 56.7 (stack of C14 and C16), 42.3 (C9), 37.6 (C12), 35.7 (C17), 25.6 (C18), 14.5 (C3).

HRMS calculated for $C_{32}H_{46}O_{10}N_4SNa$ [M+Na]$^{+}$ 701.2827, found 701.2847

MS: m/z (ES-) 677.4 (100%, [M-H]$^{-}$)

R$_{t}$ (acid method) = 2.03 min

6-(2-(((2S,4R)-1-((S)-2-(1-Fluorocyclopropane-1-carboxamido)-3,3-dimethylbutanoyl)-4-hydroxypyrrolidine-2-carboxamido)methyl)-5-(4-methylthiazol-5-yl)phenoxy)hexanoic acid (230)
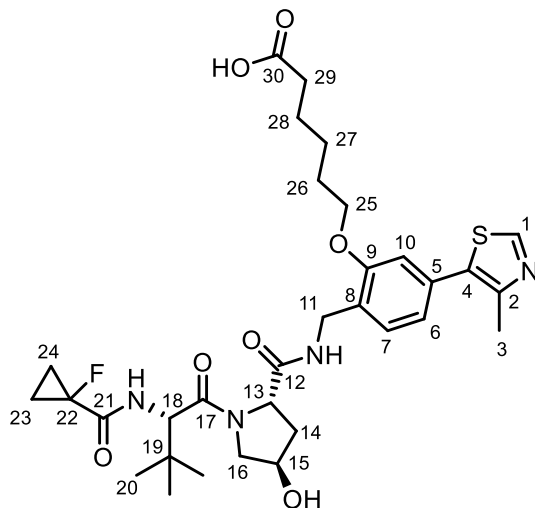
(2S,4R)-1-((S)-2-(1-Fluorocyclopropane-1-carboxamido)-3,3-dimethylbutanoyl)-4-hydroxy-N-(2-hydroxy-4-(4-methylthiazol-5-yl)benzyl)pyrrolidine-2-carboxamide (**184**) (68.0 mg, 0.128 mmol, 1.0 eq), methyl 6-bromohexanoate (40.8 µL, 0.256 mmol, 2.0 eq), K₂CO₃ (53.0 mg, 0.384 mmol, 3.0 eq), and KI (5.31 mg, 0.0320 mmol, 0.25 eq) were dissolved in DMF (3.0 mL) at room temperature. The mixture was heated to 75 ℃ and stirred overnight. The reaction was diluted with H₂O (10.0 mL) and extracted with EtOAc (5 x 6.0 mL). The combined organics were washed with H₂O (5.0 mL) and brine (5.0 mL), then dried over MgSO₄, filtered, and concentrated under reduced pressure. The residue was redissolved in THF/MeOH/H₂O (3:1:1), and LiOH.H₂O (97.2 mg, 2.31 mmol, 18 eq) added at room temperature. The mixture was stirred for 1.5 h then concentrated to dryness under reduced pressure. The residue was purified by reverse phase flash column chromatography (acidic modifier) to afford the title compound (37.0 mg, 45% over two steps).

¹H NMR (500 MHz, MeOD) δ 8.87 (s, 1H, H1), 7.48 (d, *J* = 7.6 Hz, 1H, H7), 7.04 − 6.93 (m, 2H, stack of H6 and H10), 4.75 (s, 1H, H18), 4.64 (t, *J* = 9.1, 7.6 Hz, 1H, H13), 4.53 − 4.49 (m, 1H, H15), 4.49 − 4.37 (m, 2H, H11), 4.07 (t, *J* = 6.3 Hz, 2H, H25), 3.88 − 3.77 (m, 2H, H16), 2.49 (s, 3H, H3), 2.34 (t, *J* = 7.3 Hz, 2H, H29), 2.29 − 2.20 (m, 1H, H14), 2.17 − 2.08 (m, 1H, H14'), 1.87 (app. p, *J* = 6.5 Hz, 2H, H26), 1.70 (app. p, *J* = 7.3 Hz, 2H,

H28), 1.62 – 1.53 (m, 2H, H27), 1.43 – 1.23 (m, 4H, stack of H23 and H24), 1.03 (s, 9H, H20).

^{13}C NMR (126 MHz, MeOD) δ 176.3 (C30), 172.9 (C12), 170.3 (C17), 170.1 (d, J_{C-F} = 20.5 Hz, C21), 156.6 (C9), 151.4 (C1), 147.6 (C2), 132.3 (C4), 131.3 (C5), 128.2 (C7), 126.5 (C8), 121.0 (C6 or C10), 111.6 (C6 or C10), 77.7 (d, J_{C-F} = 231.8 Hz, C22), 69.7 (C15), 67.7 (C25), 59.4 (C13), 57.3 (C18), 56.8 (C16), 37.9 (C11), 37.5 (C14), 35.9 (C19), 33.5 (C29), 28.7 (C26), 25.5 (C20), 25.4 (C27), 24.5 (C28), 14.5 (C3), 12.7 (d, J_{C-F} = 10.4 Hz, C23 or C24), 12.7 (d, J_{C-F} = 10.4 Hz, C23 or C24), 12.5 (d, J_{C-F} = 10.7 Hz, C23 or C24).

HRMS calculated for $C_{32}H_{43}FN_4O_7SNa$ [M+Na]$^+$ 669.2729, found 669.2719

MS: *m/z* (ES-) 645.5 (100%, [M-H]$^-$)

R$_t$ (method 1) = 1.81 min

N^1-((*R*)-1-((2*S*,4*R*)-4-Hydroxy-2-((4-(4-methylthiazol-5-yl)benzyl)carbamoyl)pyrrolidin-1-yl)-3,3-dimethyl-1-oxobutan-2-yl)-N^{15}-(4-(2-(4-(4-((*E*)-3-(pyridin-3-yl)acrylamido)butyl)piperidine-1-carbonyl)phenoxy)butyl)-3,6,9,12-tetraoxapentadecanediamide (231)
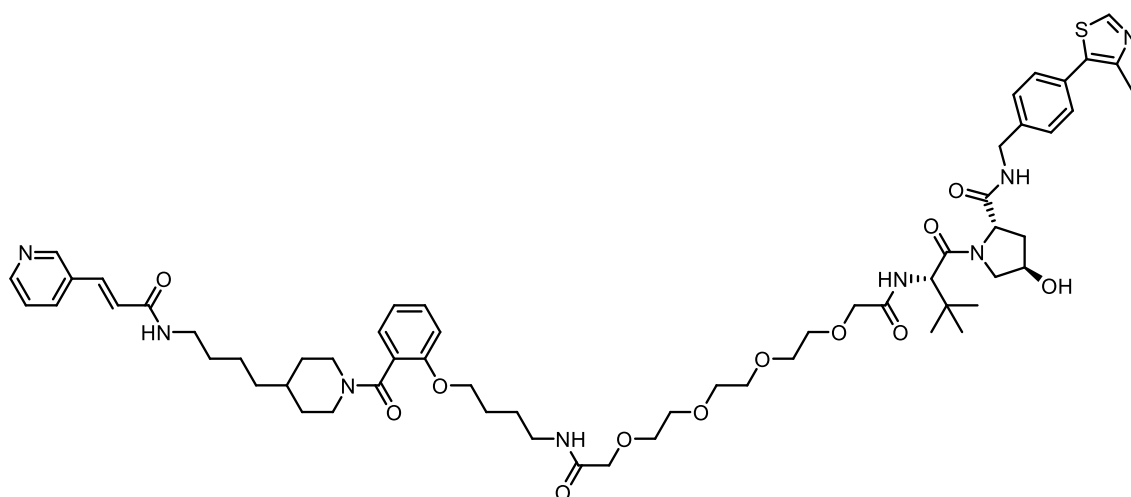
(*R*)-3-((2*S*,4*R*)-4-Hydroxy-2-((4-(4-methylthiazol-5-yl)benzyl)carbamoyl)pyrrolidine-1-carbonyl)-2,2-dimethyl-5-oxo-7,10,13,16-tetraoxa-4-azanonadecan-19-oic acid (**229**) (38.0 mg, 0.0560 mmol, 1.1 eq), HATU (38.7 mg, 0.102 mmol, 2.0 eq), and NEt$_3$ (70.1 μL, 0.509 mmol, 10.0 eq) were dissolved in DMF (1.0 mL) at room temperature and stirred for 3.0 h. (*E*)-*N*-(4-(1-(2-(4-Aminobutoxy)benzoyl)piperidin-4-yl)butyl)-3-

(pyridin-3-yl)acrylamide TFA salt (**167**) (assumed 0.0509 mmol, 1.0 eq) in DMF (0.90 mL) was added, and the reaction stirred at 40 °C The reaction was diluted with H_2O (5.0 mL), and extracted with EtOAc (5 x 5.0 mL). The combined organics were washed sequentially with H_2O and brine (5.0 mL each), dried over $MgSO_4$, filtered, and concentrated under reduced pressure. The residue was purified by reverse phase flash column chromatography (acid modifier) to afford the title compound as a yellow oil (15.0 mg, 26%).

^{1}H NMR (500 MHz, CD_3CN) δ 8.74 (s, 1H), 8.70 (d, *J* = 2.3 Hz, 1H), 8.51 (dd, *J* = 4.8, 1.6 Hz, 1H), 7.89 (dt, *J* = 7.9, 2.0 Hz, 1H), 7.47 (d, *J* = 15.8 Hz, 1H), 7.44 – 7.37 (m, 4H), 7.36 – 7.31 (m, 2H), 7.21 – 7.13 (m, 1H), 7.08 – 7.01 (m, 1H), 6.99 – 6.92 (m, 2H), 6.63 (dd, *J* = 15.8, 5.8 Hz, 1H), 5.34 (t, *J* = 3.5 Hz, 1H), 4.60 (dd, *J* = 9.5, 4.9 Hz, 1H), 4.56 (d, *J* = 9.7 Hz, 1H), 4.52 – 4.44 (m, 2H), 4.42 – 4.38 (m, 1H), 4.32 (dd, *J* = 15.5, 5.7 Hz, 1H), 4.29 – 4.21 (m, 1H), 4.15 (d, *J* = 14.8 Hz, 1H), 4.08 (d, *J* = 19.0 Hz, 1H), 4.04 – 3.93 (m, 3H), 3.85 (d, *J* = 5.0 Hz, 1H), 3.74 (ddd, *J* = 10.2, 7.6, 4.7 Hz, 2H), 3.70 – 3.52 (m, 12H), 3.32 (d, *J* = 13.4 Hz, 1H), 3.28 – 3.18 (m, 2H), 2.99 – 2.81 (m, 1H), 2.73 – 2.62 (m, 1H), 2.47 (s, 3H), 2.39 – 2.26 (m, 2H), 2.13 – 2.01 (m, 2H), 1.77 – 1.66 (m, 2H), 1.64 – 1.42 (m, 4H), 1.38 – 1.20 (m, 3H), 1.19 – 1.02 (m, 2H), 0.96 (s, 9H).

N.B.: Aromatics overintegrate by 1 proton, aliphatics underintegrate by 4 protons.

HRMS calculated for $C_{60}H_{82}N_8O_{12}SNa$ [M+Na]$^+$ 1161.5665, found 1161.5653

MS: *m/z* (ES+) 1139.4 (100%, [M+H]$^+$)

R_t (method 1) = 2.38 min
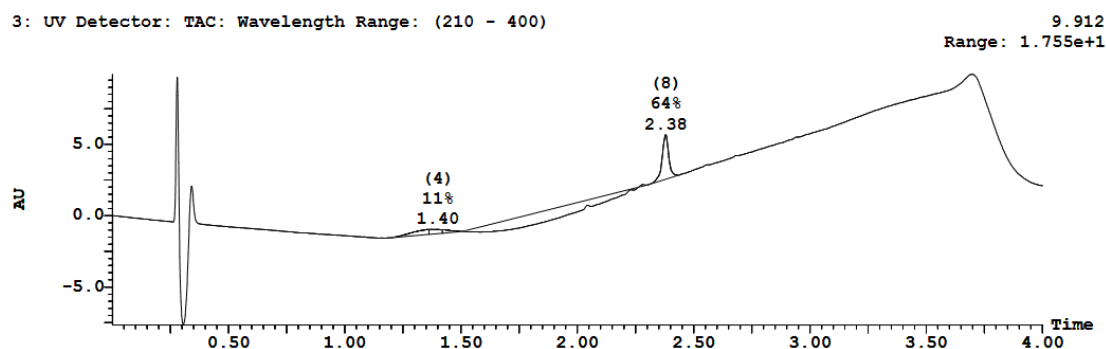
N^1-((*S*)-1-((2*S*,4*R*)-4-Hydroxy-2-((4-(4-methylthiazol-5-yl)benzyl)carbamoyl)pyrrolidin-1-yl)-3,3-dimethyl-1-oxobutan-2-yl)-N^6-(4-(2-(4-(4-((*E*)-3-(pyridin-3-yl)acrylamido)butyl)piperidine-1-carbonyl)phenoxy)butyl)adipamide (232)
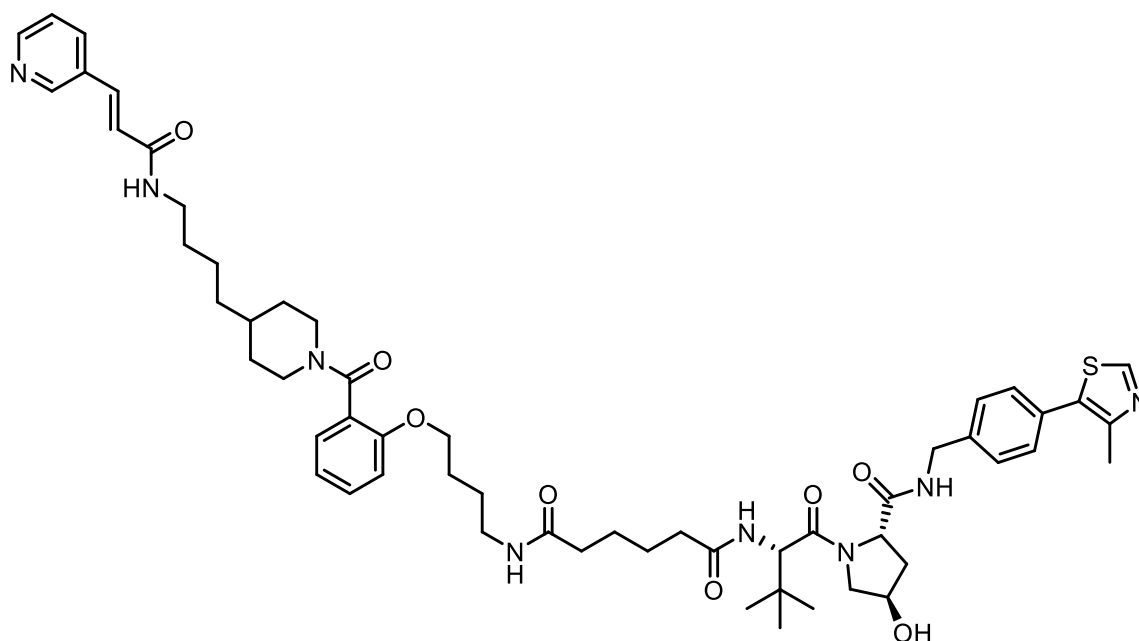
A flask was charged with a solution of 6-(((*S*)-1-((2*S*,4*R*)-4-hydroxy-2-((4-(4-methylthiazol-5-yl)benzyl)carbamoyl)pyrrolidin-1-yl)-3,3-dimethyl-1-oxobutan-2-yl)amino)-6-oxohexanoic acid (**228**) (32.0 mg, 0.0570 mmol, 1.1 eq) in DMF (0.5 mL), HATU (118 mg, 0.312 mmol, 6.0 eq), and DIPEA (90.0 μL, 0.520 mmol, 10 eq). The reation mixture was stirred for 40 min at room temperature before crude (*E*)-*N*-(4-(1-(2-(4-aminobutoxy)benzoyl)piperidin-4-yl)butyl)-3-(pyridin-3-yl)acrylamide TFA salt (**167**) (assumed 0.0520 mmol, 1.0 eq) in DMF (0.5 mL) was added and the mixture stirred overnight at room temperature. The reaction was quenched with water and extracted with EtOAc (5 x 5 mL). The combined organics were washed sequentially with water and brine then dried over MgSO₄, filtered, and concentrated under reduced pressure. The residue was purified by reverse phase flash column chromatography (acid modifier) to yield the title compound (15.0 mg, 28%).

¹H NMR (500 MHz, Acetone-d_6) δ 8.85 (s, 1H), 8.76 (dd, *J* = 7.6, 2.3 Hz, 1H), 8.54 – 8.51 (m, 1H), 7.94 (d, *J* = 8.1 Hz, 1H), 7.55 (dd, *J* = 15.9, 4.7 Hz, 1H), 7.46 (td, *J* = 8.1, 2.9 Hz, 2H), 7.40 (app. q, *J* = 6.7, 6.0 Hz, 3H), 7.33 (app. q, *J* = 7.1 Hz, 1H), 7.19 (d, *J* = 7.4 Hz,

0.5H), 7.11 (d, *J* = 7.1 Hz, 0.5H), 7.02 (dd, *J* = 8.5, 4.5 Hz, 1H), 6.96 (td, *J* = 7.5, 3.2 Hz, 1H), 6.80 (dd, *J* = 15.8, 13.5 Hz, 1H), 4.69 – 4.47 (m, 5H), 4.34 (dd, *J* = 15.5, 4.6 Hz, 1H), 4.12 – 3.87 (m, 3H), 3.78 – 3.71 (m, 1H), 3.41 (t, *J* = 11.1 Hz, 1H), 3.32 (app. q, *J* = 6.7, 6.2 Hz, 2H), 3.27 – 3.16 (m, 2H), 3.06 – 2.81 (m, 3H), 2.76 – 2.63 (m, 1H), 2.33 – 2.20 (m, 3H), 2.19 – 2.11 (m, 2H), 1.83 – 1.72 (m, 3H), 1.69 – 1.48 (m, 9H), 1.44 – 1.36 (m, 2H), 1.35 – 1.25 (m, 4H), 1.18 (d, *J* = 6.7 Hz, 1H), 1.08 – 1.03 (m, 1H), 1.00 (s, 9H), 0.91 – 0.84 (m, 1H).

t$_R$ (method 1) = 2.24 min

MS: *m/z* (ES+) 1019.3 (100%, [M+H]$^+$)

HRMS calculated for C$_{56}$H$_{74}$N$_8$O$_8$SNa [M+Na]$^+$ 1041.5243, found 1041.5232
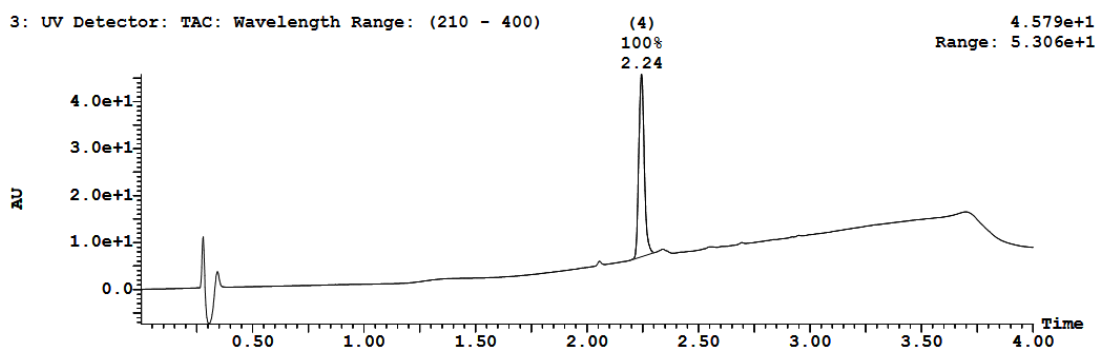
(*E*)-7-(2-(2,6-Dioxopiperidin-3-yl)-1-oxoisoindolin-4-yl)-*N*-(4-(2-(4-(4-(3-(pyridin-3-yl)acrylamido)butyl)piperidine-1-carbonyl)phenoxy)butyl)hept-6-ynamide (233)
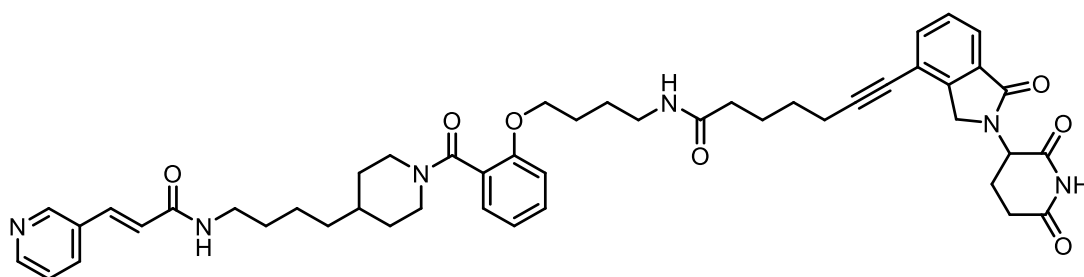
HATU (77.2 mg, 0.203 mmol, 3.0 eq) and DIPEA (118 µL, 0.675 mmol, 10 eq) were added at room temperature to a stirred solution of 7-(2-(2,6-dioxopiperidin-3-yl)-1-oxoisoindolin-4-yl)hept-6-ynoic acid (**188**) (28.1 mg, 0.0763 mmol, 1.13 eq) in DMF (0.5 mL) and the mixture stirred at room temperature for 1 h. (*E*)-*N*-(4-(1-(2-(4-Aminobutoxy)benzoyl)piperidin-4-yl)butyl)-3-(pyridin-3-yl)acrylamide TFA salt (**167**)

(assumed 0.0675 mmol, 1.0 eq) in DMF (0.5 mL) was then added and the mixture stirred overnight. The reaction was quenched with water and extracted with EtOAC (5 x 5 mL), then the combined organics washed sequentially with water and brine (each 10 mL), dried over $MgSO_4$, filtered, and concentrated under reduced pressure. The residue was purified by reverse phase flash column chromatography (acid modifier) to yield the title compound as an orange oil (13.0 mg, 23%).

^{1}H NMR (500 MHz, Acetone-d_6) δ 8.74 (d, J = 2.3 Hz, 1H), 8.53 (dd, J = 4.9, 1.6 Hz, 1H), 7.94 (app. dt, J = 7.9, 2.0 Hz, 1H), 7.70 (dd, J = 7.6, 4.2 Hz, 1H), 7.61 − 7.57 (m, 1H), 7.52 (s, 1H), 7.51 − 7.48 (m, 1H), 7.38 (dd, J = 7.9, 4.8 Hz, 1H), 7.32 (app. td, J = 8.1, 7.3, 2.1 Hz, 1H), 7.19 (d, J = 7.5 Hz, 0.5H), 7.11 (dd, J = 7.4, 1.7 Hz, 0.5H), 7.02 (dd, J = 8.3, 4.2 Hz, 1H), 6.96 (app. td, J = 7.4, 2.5 Hz, 1H), 6.77 (dd, J = 15.8, 4.0 Hz, 1H), 5.24 (dd, J = 13.3, 5.2 Hz, 1H), 4.69 − 4.61 (m, 1H), 4.60 − 4.44 (m, 2H), 4.13 − 3.96 (m, 2H), 3.46 − 3.37 (m, 1H), 3.31 (td, J = 8.2, 5.9 Hz, 2H), 3.28 − 3.18 (m, 2H), 3.06 − 2.87 (m, 3H), 2.81 − 2.64 (m, 3H), 2.48 (app. q, J = 6.4 Hz, 2H), 2.23 − 2.12 (m, 3H), 1.83 − 1.71 (m, 4H), 1.71 − 1.47 (m, 7H), 1.42 − 1.21 (m, 7H), 1.01 − 0.82 (m, 1H).

t_R (method 1) = 2.21

MS: m/z (ES+) 829.3 (100%, [M+H]$^+$)

HRMS calculated for $C_{48}H_{56}N_6O_7Na$ [M+Na]$^+$ 851.4103, found 851.4091
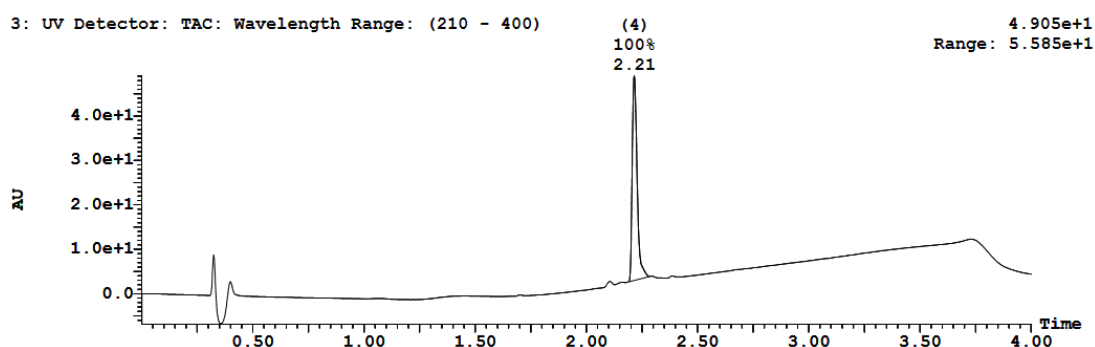
(2S,4R)-1-((S)-2-(1-Fluorocyclopropane-1-carboxamido)-3,3-dimethylbutanoyl)-4-hydroxy-N-(4-(4-methylthiazol-5-yl)-2-((6-oxo-6-((4-(2-(4-(4-((E)-3-(pyridin-3-yl)acrylamido)butyl)piperidine-1-carbonyl)phenoxy)butyl)amino)hexyl)oxy)benzyl)pyrrolidine-2-carboxamide (234)
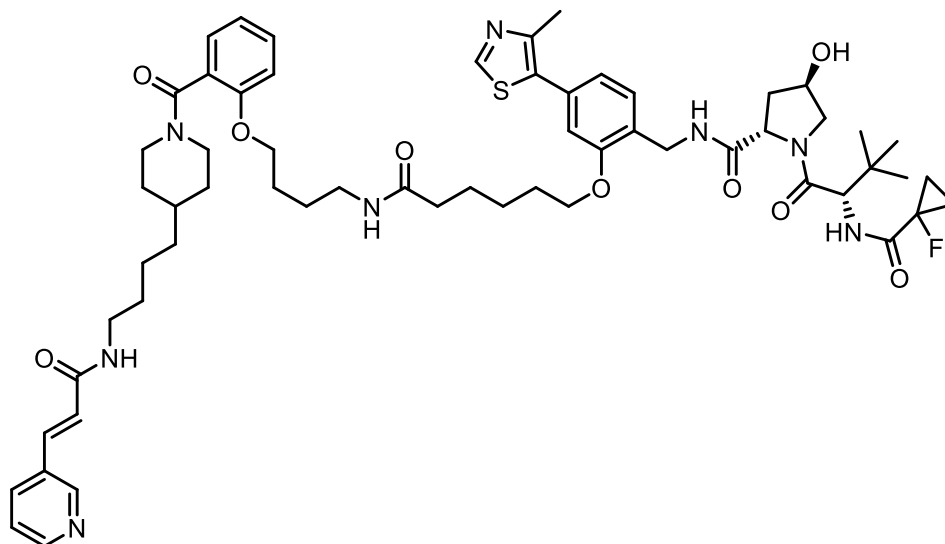
6-(2-(((2S,4R)-1-((S)-2-(1-Fluorocyclopropane-1-carboxamido)-3,3-dimethylbutanoyl)-4-hydroxypyrrolidine-2-carboxamido)methyl)-5-(4-methylthiazol-5-yl)phenoxy)hexanoic acid (**230**) (37.0 mg, 0.0572 mmol, 1.0 eq), (E)-N-(4-(1-(2-(4-aminobutoxy)benzoyl)piperidin-4-yl)butyl)-3-(pyridin-3-yl)acrylamide TFA salt (**167**) (assumed 0.0800 mmol, 1.4 eq), HOBt.H$_2$O (12.0 mg, 0.0801 mmol, 1.4 eq), and DIPEA (40.7 μL, 0.229 mmol, 4.0 eq) were dissolved in DMF (2.5 mL) at room temperature. HATU (33.0 mg, 0.0858 mmol, 1.5 eq) was added at room temperature, and the mixture stirred for 2 h. The reaction was diluted with H$_2$O (7.0 mL), and extracted with EtOAc (5 x 5.0 mL). The combined organics were washed sequentially with H$_2$O (7.0 mL) and brine (7.0 mL), then dried over MgSO$_4$, filtered, and concentrated under reduced pressure. The residue was purified by reverse phase flash column chromatography (acid modifier) to afford the title compound as a yellow gum (31.0 mg, 49%).

^{1}H NMR (400 MHz, MeOD) δ 8.86 (s, 1H), 8.69 (s, 1H), 8.50 (s, 1H), 8.05 – 7.97 (m, 1H), 7.55 (s, 0.5H), 7.51 (s, 0.5H), 7.39 – 7.32 (m, 2H), 7.21 – 7.16 (m, 0.5H), 7.13 – 7.09 (m, 0.5H), 7.04 – 6.94 (m, 4H), 6.73 (s, 0.5H), 6.69 (s, 0.5H), 4.75 (s, 1H), 4.69 – 4.58 (m, 2H), 4.53 – 4.35 (m, 3H), 4.13 – 3.93 (m, 4H), 3.89 – 3.76 (m, 2H), 3.33 – 3.18 (m, 4H),

2.84 – 2.71 (m, 1H), 2.47 (s, 3H), 2.28 – 2.19 (m, 3H), 2.14 – 2.07 (m, 1H), 1.90 – 1.48 (m, 16H), 1.46 – 1.11 (m, 11H), 1.04 (s, 9H).

N.B. Protons underintegrate by 6H in total.

MS: *m/z* (ES+) 1107.6 (100%, [M+H]$^+$)

R$_t$ (method 1) = 2.49 min

HRMS calculated for $C_{60}H_{79}O_9N_8FNaS$ [M+Na]$^+$ 1129.5567, found 1129.5579
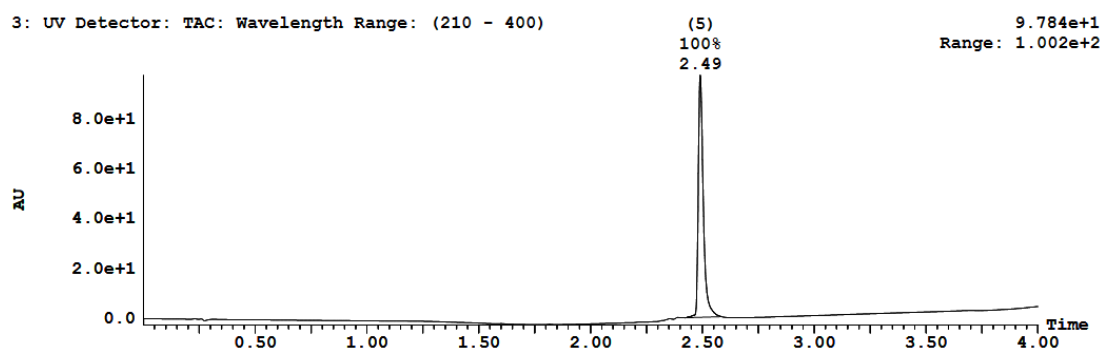
(*E*)-7-(2-(2,6-Dioxopiperidin-3-yl)-1,3-dioxoisoindolin-4-yl)-*N*-(4-(2-(4-(4-(3-(pyridin-3-yl)acrylamido)butyl)piperidine-1-carbonyl)phenoxy)butyl)heptanamide (235)
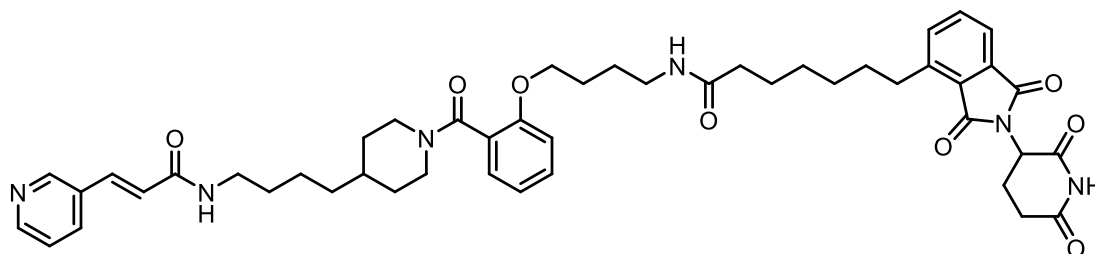
A flask was charged with a solution of 7-(2-(2,6-Dioxopiperidin-3-yl)-1,3-dioxoisoindolin-4-yl)heptanoic acid (**194**) (22.0 mg, 0.0570 mmol, 1.1 eq) in DMF (0.5 mL), HATU (118 mg, 0.312 mmol, 6.0 eq), and DIPEA (90.0 μL, 0.520 mmol, 10 eq). The reation mixture was stirred for 40 min at room temperature before (*E*)-*N*-(4-(1-(2-(4-Aminobutoxy)benzoyl)piperidin-4-yl)butyl)-3-(pyridin-3-yl)acrylamide TFA salt (**167**) (assumed 0.0520 mmol, 1.0 eq) in DMF (0.5 mL) was added and the mixture stirred overnight at room temperature. The reaction was quenched with water (5 mL) and extracted with EtOAc (5 x 5 mL). The combined organics were washed sequentially with water and brine then dried over MgSO$_4$, filtered, and concentrated under reduced

pressure. The residue was purified by reverse phase flash column chromatography (acid modifier) to yield the title compound (8.0 mg, 18%).

¹H NMR (500 MHz, Acetone-d_6) δ 8.74 (s, 1H), 8.53 (d, J = 4.5 Hz, 1H), 7.93 (dd, J = 7.8, 2.0 Hz, 1H), 7.78 – 7.65 (m, 3H), 7.54 (s, 1H), 7.38 (dd, J = 8.0, 4.8 Hz, 1H), 7.32 (app. q, J = 7.4 Hz, 1H), 7.19 (d, J = 7.8 Hz, 0.5H), 7.10 (d, J = 7.5 Hz, 0.5H), 7.02 (dd, J = 8.5, 2.9 Hz, 1H), 6.99 – 6.93 (m, 1H), 6.77 (dd, J = 15.8, 11.5 Hz, 1H), 5.15 (dd, J = 12.7, 5.4 Hz, 1H), 4.65 (d, J = 12.9 Hz, 1H), 4.13 – 3.95 (m, 2H), 3.45 – 3.36 (m, 1H), 3.36 – 3.28 (m, 2H), 3.28 – 3.17 (m, 2H), 3.13 – 3.04 (m, 2H), 3.03 – 2.87 (m, 2H), 2.81 – 2.78 (m, 2H), 2.74 – 2.64 (m, 1H), 2.28 – 2.20 (m, 1H), 1.84 – 1.72 (m, 3H), 1.69 – 1.62 (m, 4H), 1.61 – 1.51 (m, 6H), 1.43 – 1.25 (m, 10H), 1.02 – 0.83 (m, 2H).

t_R (method 1) = 2.42 min

MS: *m/z* (ES+) 847.4 (100%, [M+H]⁺)

HRMS calculated for $C_{48}H_{58}N_6O_8Na$ [M+Na]⁺ 869.4208, found 869.4201

v_{max} (thin film, ATR)/cm⁻¹: 3429, 2999, 2915, 1661, 1437, 1406, 1312, 1018, 952, 899, 700, 669
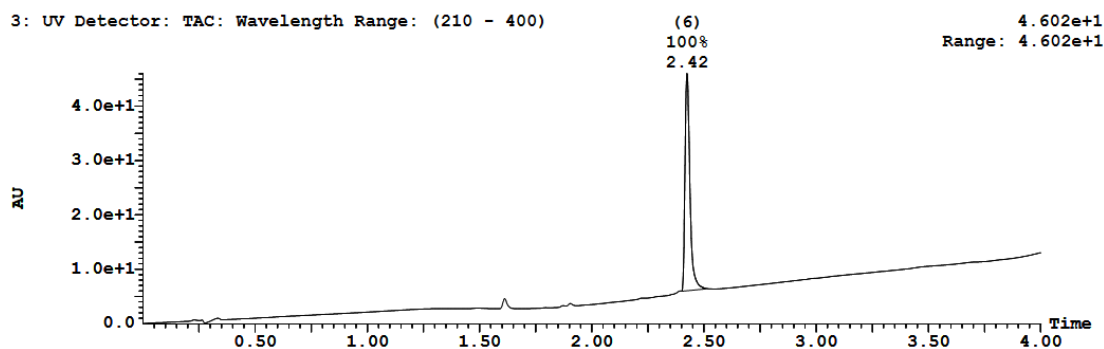
Tert-butyl 4-((4-nitrophenyl)sulfonyl)piperazine-1-carboxylate (257)
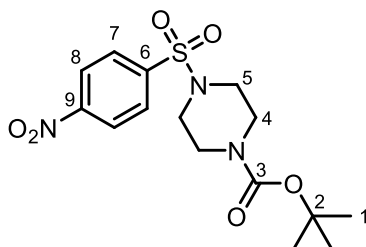
Tert-butyl piperazine-1-carboxylate (**256**) (1.67 g, 9.00 mmol, 2.0 eq), 4-nitrobenzenesulfonyl chloride (**255**) (1.00 g, 4.50 mmol, 1.0 eq), and NEt$_3$ (626 µL, 4.50 mmol, 1.0 eq) were dissolved in DCM (30 mL) at room temperature and stirred for 30 minutes. The reaction mixture was then washed twice with HCl (1.0 M, aq.), once with brine (each 10 mL), dried over MgSO$_4$, filtered, and concentrated under reduced pressure to afford the title compound as a beige powder (1.61 g, 96%) that was used without further purification.

^{1}H NMR (400 MHz, CDCl$_3$) δ 8.43 – 8.35 (m, 2H, H7 or H8), 7.97 – 7.89 (m, 2H, H7 or H8), 3.56 – 3.48 (m, 4H, H4), 3.03 (app. t, *J* = 5.0 Hz, 4H, H5), 1.39 (s, 9H, H1).

^{13}C NMR (101 MHz, CDCl$_3$) δ 154.0 (C3), 150.3 (C9), 141.8 (C6), 128.9 (C7 or C8), 124.5 (C7 or C8), 80.7 (C2), 45.8 (C5), 43.0 (C4, broad, weak), 28.3 (C1).

HRMS calculated for C$_{15}$H$_{21}$N$_3$O$_6$SNa [M+Na]$^+$ 394.1043, found 394.1039

MS: *m/z* (ES+) 272.2 (100%, [M-Boc+H]$^+$)

R$_t$ (method 1) = 2.59 min

v$_{max}$ (thin film, ATR)/cm^{-1}: 3106, 2978, 2929, 2864, 1691, 1607, 1529, 1479, 1455, 1421, 1402, 1349, 1330, 1310, 1283, 1264, 1248, 1222, 1164, 1129, 1107, 1085, 1055, 1013, 993, 933, 855, 830, 751, 741, 707, 687, 601, 586, 538

Analytical data matches that found in the literature.[261]

Tert-butyl 4-((4-aminophenyl)sulfonyl)piperazine-1-carboxylate (258)
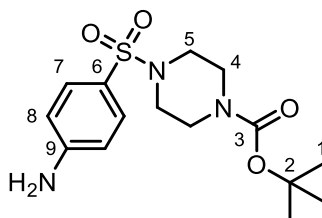
Tert-butyl 4-((4-nitrophenyl)sulfonyl)piperazine-1-carboxylate (**257**) (1.50 g, 4.04 mmol, 1.0 eq) was dissolved in a 1:5 mixture of EtOH and H$_2$O (30 mL) at room temperature. Fe filings (reduced, 588 mg, 10.5 mmol, 2.6 eq) and NH$_4$Cl (sat. aq., 1.0 mL) were added, and the mixture heated at 75 °C for 1 h 40 minutes. The reaction

mixture was then allowed to cool to room temperature, before filtering through celite and the pad washed successively with EtOH (10 mL), and EtOAc (50 mL). The filtrate was concentrated under reduced pressure, and then partitioned between EtOAc and H_2O. The organic layer was washed with brine, and the organics dried over $MgSO_4$, filtered, and concentrated under reduced pressure to afford the title compound (beige powder, 1.28 g, 93%) that was used without further purification.

^{1}H NMR (500 MHz, MeOD) δ 7.47 − 7.40 (m, 2H, H7), 6.76 − 6.69 (m, 2H, H8), 3.47 (app. t, J = 4.7 Hz, 4H, H4), 2.86 (app. t, J = 5.1 Hz, 4H, H5), 1.42 (s, 9H, H1).

^{13}C NMR (126 MHz, MeOD) δ 154.5 (C3), 153.4 (C9), 129.7 (C7), 120.3 (C6), 113.0 (C8), 80.2 (C2), 45.9 (C5 and C5'), 43.4 (C4 or C4'), 42.3 (C4 or C4'), 27.3 (C1).

HRMS calculated for $C_{15}H_{23}O_4N_3NaS$ [M+Na]$^+$ 364.1301, found 364.1302

MS: *m/z* (ES+) 242.2 (100%, [M-Boc+H]$^+$)

R$_t$ (method 1) = 2.32 min

v$_{max}$ (thin film, ATR)/cm^{-1}: 3460, 3359, 2969, 1676, 1632, 1593, 1503, 1480, 1428, 1367, 1345, 1322, 1311, 1284, 1267, 1253, 1220, 1168, 1154, 1127, 1105, 1088, 1056, 1001, 929, 864, 838, 828, 772, 760, 737, 716, 662, 636, 590, 549, 537, 515

Analytical data matches that found in the literature.[279]

***Tert*-butyl 4-((4-isothiocyanatophenyl)sulfonyl)piperazine-1-carboxylate (259)**
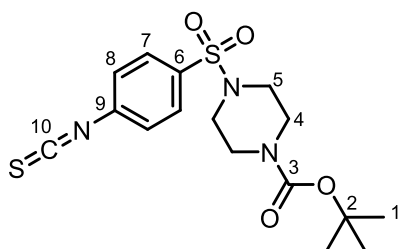
Tert-butyl 4-((4-aminophenyl)sulfonyl)piperazine-1-carboxylate (**258**) (1.50 g, 4.40 mmol, 1.0 eq) and NEt$_3$ (1.22 mL, 8.80 mmol, 2.0 eq) were dissolved in DCM (10 mL) and cooled to 0 °C. 1,1'-Thiocarbonyldiimidazole (2.35 g, 13.2 mmol, 3.0 eq) was added and the reaction mixture allowed to warm to room temperature, then

stirred overnight. The mixture was evaporate to dryness and purified by flash column chromatography (EtOAc: hexane 1:3) to afford the product as a beige solid (915 mg, 54%).

¹H NMR (500 MHz, CDCl₃) δ 7.76 – 7.71 (m, 2H, H7), 7.38 – 7.33 (m, 2H, H8), 3.51 (app. t, *J* = 5.0 Hz, 4H, H4), 2.97 (app. t, *J* = 5.1 Hz, 4H, H5), 1.41 (s, 9H, H1).

¹³C NMR (126 MHz, CDCl₃) δ 154.1 (C3), 139.5 (C6), 136.3 (C10), 134.0 (C9), 129.3 (C7), 126.3 (C8), 80.5 (C2), 45.9 (C4 and C5), 28.3 (C1).

MS: *m/z* (ES+) 284.1 (100%, [M-Boc+H]⁺)

R$_t$ (method 1) = 2.84 min

R$_f$ (1:4 EtOAc:hexane) = 0.34

v$_{max}$ (thin film, ATR)/cm⁻¹: 2976, 1699, 1593, 1530, 1423, 1352, 1313, 1283, 1250, 1164, 1141, 1054, 933, 839, 735, 590, 572, 541

Tert-butyl 4-((4-(3-(pyridin-3-ylmethyl)thioureido)phenyl)sulfonyl)piperazine-1-carboxylate (260)
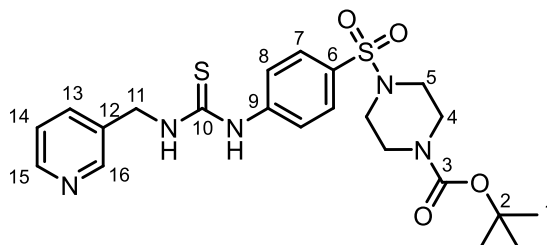
Tert-butyl 4-((4-isothiocyanatophenyl)sulfonyl)piperazine-1-carboxylate (**259**) (895 mg, 2.33 mg, 1.0 eq) and 3-aminomethylpyridine (237 µL, 2.33 mmol, 1.0 eq) were dissolved in DCM (6.0 mL) and the mixture stirred at room temperature overnight. The reaction mixture was evaporated to dryness, and the resulting solid triturated with DCM (10 mL) to afford the title compound as a white solid (902 mg, 79%) that was used without further purification.

¹H NMR (500 MHz, DMSO) δ 10.13 (br. s, 1H, ArN**H**C(S)), 8.64 (br. s, 1H, ArCH₂N**H**C(S)), 8.57 (d, *J* = 2.3 Hz, 1H, H16), 8.47 (dd, *J* = 4.7, 1.7 Hz, 1H, H15), 7.84 – 7.79 (m, 2H, H7),

7.76 (app. dt, *J* = 7.9, 2.0 Hz, 1H, H13), 7.68 – 7.63 (m, 2H, H8), 7.37 (dd, *J* = 4.8, 3.0 Hz, 1H, H14), 4.79 (s, 2H, H11), 3.39 (app. t, *J* = 4.9 Hz, 4H, H4), 2.83 (app. t, *J* = 5.0 Hz, 4H, H5), 1.34 (s, 9H, H1).

^{13}C NMR (126 MHz, DMSO) δ 181.2 (C10), 153.9 (C3), 149.4 (C16), 148.7 (C15), 144.6 (C9), 135.7 (C13), 134.6 (C12), 128.9 (C8), 123.9 (C14), 121.9 (C7), 79.8 (C2), 46.2 (stack of C4 and C5), 45.2 (C11), 28.4 C1).

MS: *m/z* (ES+) 492.3 (100%, [M+H]$^+$)

R$_t$ (method 1) = 2.06 min

1-(4-(Piperazin-1-ylsulfonyl)phenyl)-3-(pyridin-3-ylmethyl)thiourea (261)
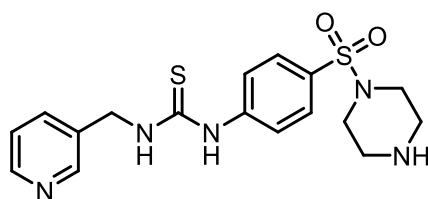
Tert-butyl 4-((4-(3-(pyridin-3-ylmethyl)thioureido)phenyl)sulfonyl)piperazine-1-carboxylate (**260**) (854 mg, 1.73 mmol) was dissolved in DCM (1.6 mL). TFA (1.0 mL) was added at room temperature, and the mixture stirred for 6 h. The mixture was concentrated to dryness under reduced pressure to afford the title compound as a yellowish gum. The crude mixture was dissolved in a solution of NH$_3$ in MeOH (3.0 mL, 3.5 M) at room temperature and stirred for 2 h. The mixture was concentrated to dryness to afford the title compound as a yellow gum that was used without further purification.

Methyl 4-((4-((4-(3-(pyridin-3-ylmethyl)thioureido)phenyl)sulfonyl)piperazin-1-yl)methyl)benzoate (262)
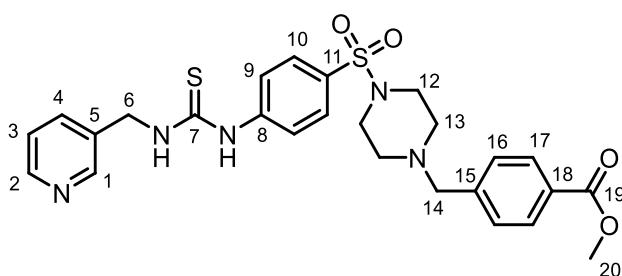
1-(4-(Piperazin-1-ylsulfonyl)phenyl)-3-(pyridin-3-ylmethyl)thiourea (**261**) (assumed 0.662 mmol, 1.0 eq), methyl 4-(bromomethyl)benzoate (380 mg, 1.66 mmol, 2.5 eq), and NEt$_3$ (552 μL, 3.97 mmol, 6.0 eq) were dissolved in DCM (5.0 eq) at room temperature and the reaction shielded from ambient light. The mixture was stirred at room temperature for 2 h. The mixture was concentrated to dryness under reduced pressure and the residue purified by reverse phase flash column chromatography (basic modifier) to afford the title compound as a pale yellow oil (70.0 mg, 20% over two steps).

^{1}H NMR (500 MHz, CDCl$_3$) δ 8.47 (s, 1H, H1), 8.39 (d, J = 4.9 Hz, 1H, H2), 7.91 (d, J = 8.0 Hz, 2H, H17), 7.81 − 7.75 (m, 2H, H3), 7.62 (d, J = 8.4 Hz, 2H, H10), 7.55 (d, J = 8.4 Hz, 2H, H9), 7.31 − 7.24 (m, 3H, stack of H16 and H4), 4.86 (d, J = 5.3 Hz, 2H, H6), 3.86 (s, 3H, H20), 3.51 (s, 2H, H14), 2.95 (app. s, 4H, H12), 2.47 (t, J = 4.9 Hz, 4H, H13).

^{13}C NMR (126 MHz, CDCl$_3$) δ 181.3 (C7), 167.0 (C19), 148.0 (C1), 147.7 (C2), 142.9 (C8 or C15), 142.7 (C8 or C15), 137.0 (C3), 134.3 (C5), 130.6 (C11), 129.7 (C17), 129.2 (C18), 128.92 (C16), 128.90 (C9), 124.1 (C4), 122.6 (C10), 62.0 (C14), 52.2 (C20), 51.9 (C13), 46.0 (C12), 45.7 (C6).

N.B. Signal for H3 over-integrates

HRMS calculated for C$_{26}$H$_{30}$N$_5$O$_4$S$_2$ [M+H]$^+$ 540.1734, found 540.1732

MS: *m/z* (ES+) 540.20 (100%, [M+H]$^+$)

R$_t$ (method 1) = 1.74 min

ν$_{max}$ (thin film, ATR)/cm^{-1}: 2950, 1717, 1595, 1532, 1434, 1328, 1279, 1161, 1112, 948, 735, 620, 557

4-((4-((4-(3-(Pyridin-3-ylmethyl)thioureido)phenyl)sulfonyl)piperazin-1-yl)methyl)benzoic acid (263)
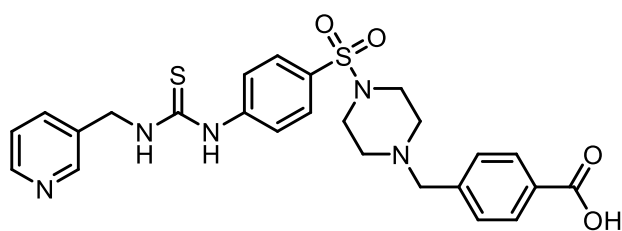
Methyl 4-((4-((4-(3-(pyridin-3-ylmethyl)thioureido)phenyl)sulfonyl)piperazin-1-yl)methyl)benzoate (**262**) (70.0 mg, 0.130 mmol, 1.0 eq) was dissolved in a 1:2:3 mixture of H_2O:MeOH:THF (2.0 mL). LiOH.H_2O (32.7 mg, 0.778 mmol, 6.0 eq) was added at room temperature, and the mixture stirred overnight. The mixture was concentrated to dryness under reduced pressure, and suspended in HCl (2.0 mL, 1.0 M, aq.). The precipitate was collected to afford the title compound as a white solid (42.0 mg, 61%) that was used without further purification.

(2S,4R)-1-((S)-17-Azido-2-(*tert*-butyl)-4-oxo-6,9,12,15-tetraoxa-3-azaheptadecanoyl)-4-hydroxy-*N*-((R)-1-(4-(4-methylthiazol-5-yl)phenyl)ethyl)pyrrolidine-2-carboxamide (265)
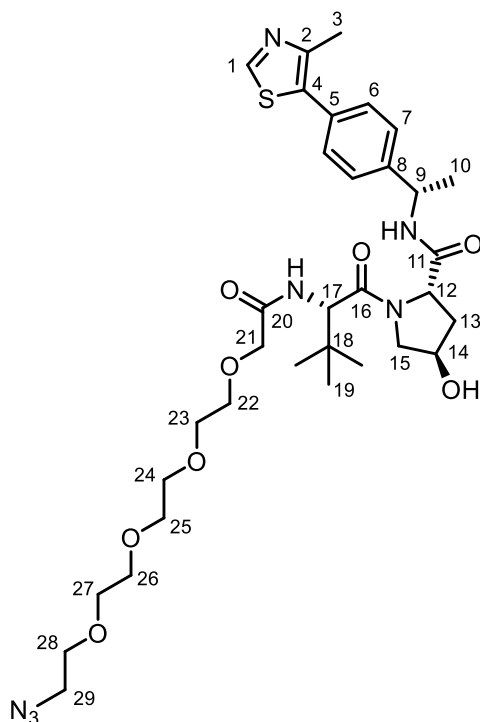
(2*S*,4*R*)-1-((*S*)-2-Amino-3,3-dimethylbutanoyl)-4-hydroxy-*N*-((*R*)-1-(4-(4-methylthiazol-5-yl)phenyl)ethyl)pyrrolidine-2-carboxamide (**264**) (100 mg, 0.225 mmol, 1.0 eq), 14-azido-3,6,9,12-tetraoxatetradecanoic acid (63.0 mg, 0.227 mmol, 1.0 eq), HOBt.H$_2$O (68.9 mg, 0.450 mmol, 2.0 eq), and DIPEA (160 µL, 0.900 mmol, 4.0 eq) were dissolved in DMF (2.5 mL). HATU (171 mg, 0.450 mmol, 2.0 eq) was added at room temperature and the reaction stirred for 2 h. The mixture was diluted with EtOAc (10 mL) and H$_2$O (10 mL) and extracted with EtOAc (5 x 5.0 mL). The combined organics were then washed with brine (3 x 5.0 mL), dried over MgSO$_4$, filtered, and concentrated under reduced pressure. The residue was purified by reverse phase flash column chromatography (acidic modifier) to afford the title compound as a yellow gum (103 mg, 65%).

1H NMR (500 MHz, MeOD) δ 8.87 (d, *J* = 1.8 Hz, 1H, H1), 7.43 (d, *J* = 2.9 Hz, 4H, stack of H6 and H7), 5.01 (q, *J* = 6.3 Hz, 1H, H9), 4.69 – 4.68 (m, 1H, H17), 4.62 – 4.55 (m, 1H, H12), 4.46 – 4.42 (m, 1H, H14), 4.10 – 4.01 (m, 2H, H21), 3.85 (br. d, *J* = 11.6 Hz, 1H, H15), 3.75 (dd, *J* = 11.2, 3.9 Hz, 1H, H15'), 3.73 – 3.63 (m, 14H, stack of H22-H28), 3.37 (t, *J* = 4.9 Hz, 2H, H29), 2.47 (s, 3H, H3), 2.25 – 2.16 (m, 1H, H13), 1.96 (ddd, *J* = 13.4, 9.2, 4.4 Hz, 1H, H13'), 1.51 (d, *J* = 7.0 Hz, 3H, H10), 1.05 (s, 9H, H19).

13C NMR (126 MHz, MeOD) δ 171.7 (C11), 170.7 (C16 or C20), 170.2 (C16 or C20), 151.5 (C1), 147.7 (C2), 144.2 (C8), 132.0 (C4), 130.1 (C5), 129.1 (C6 or C7), 126.3 (C6 or C7), 70.92 (one of C22-28), 70.31 (one of C22-28), 70.29 (one of C22-28), 70.28 (one of C22-28), 70.18 (one of C22-28), 70.16 (one of C22-28), 69.8 (one of C22-28), 69.7 (C21), 69.6 (C14), 59.2 (C12), 56.8 (C17), 56.7 (C15), 50.4 (C29), 48.7 (C9), 37.4 (C13), 35.7 (C18), 25.6 (C19), 21.1 (C10), 14.5 (C3).

HRMS calculated for C$_{33}$H$_{49}$N$_7$O$_8$SNa [M+Na]$^+$ 726.3240, found 726.3241

MS: *m/z* (ES+) 704.52 (100%, [M+H]$^+$)

R$_t$ (method 1) = 2.30 min

ν$_{max}$ (thin film, ATR)/cm^{-1}: 3304, 2872, 2103, 1630, 1525, 1436, 1371, 1344, 1278, 1227, 1108, 1034, 1015, 967, 937, 849, 834, 733, 701, 569

(2*S*,4*R*)-1-((*S*)-17-Amino-2-(*tert*-butyl)-4-oxo-6,9,12,15-tetraoxa-3-azaheptadecanoyl)-4-hydroxy-*N*-((*R*)-1-(4-(4-methylthiazol-5-yl)phenyl)ethyl)pyrrolidine-2-carboxamide (266)
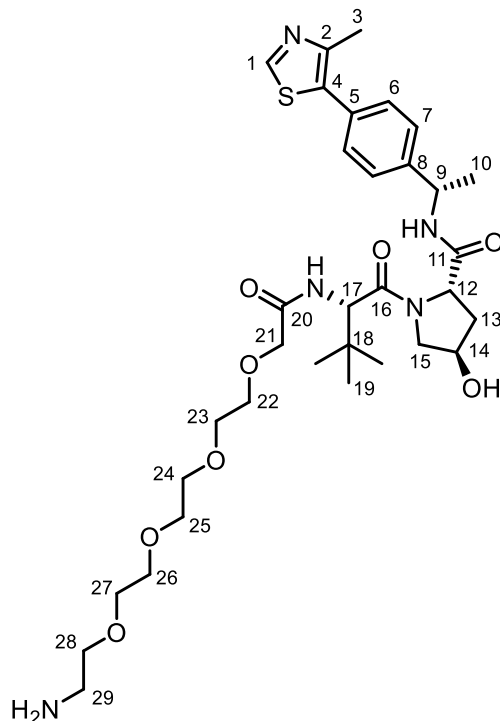
(2*S*,4*R*)-1-((*S*)-17-Azido-2-(*tert*-butyl)-4-oxo-6,9,12,15-tetraoxa-3-azaheptadecanoyl)-4-hydroxy-*N*-((*R*)-1-(4-(4-methylthiazol-5-yl)phenyl)ethyl)pyrrolidine-2-carboxamide (**265**) (100 mg, 0.142 mmol) was dissolved in EtOAc (10 mL) at room temperature and degassed with Ar for 15 min. Pd/C (25.0 mg) was added, and H_2 bubbled through the mixture for 10 min. The reaction was then stirred under an atmosphere of H_2 at room temperature overnight. The mixture was filtered through celite and the pad washed with EtOAc (20 mL). The resulting solution was concentrated to dryness under reduced pressure to afford the title compound as a pale yellow oil (36.0 mg, 37%) that was used without further purification.

^{1}H NMR (500 MHz, MeOD) δ 8.87 (s, 1H, H1), 7.43 (d, *J* = 3.9 Hz, 4H, stack of H6 and H7), 5.01 (q, *J* = 7.0 Hz, 1H, H9), 4.69 (s, 1H, H17), 4.62 − 4.54 (m, 1H, H12), 4.44 (d, *J* = 4.2 Hz, 1H, H14), 4.11 − 4.02 (m, 2H, H21), 3.86 (d, *J* = 11.1 Hz, 1H, H15), 3.75 (dd, *J* = 11.1, 3.8 Hz, 1H, H15'), 3.73 − 3.59 (m, 12H, stack of H22-27), 3.55 (t, *J* = 5.5 Hz, 2H,

H28), 2.86 − 2.78 (m, 1H, H29), 2.48 (s, 3H, H3), 2.22 (dd, *J* = 13.2, 7.7 Hz, 1H, H13), 1.96 (ddd, *J* = 13.4, 9.2, 4.4 Hz, 1H, H13'), 1.51 (d, *J* = 7.0 Hz, 3H, H10), 1.04 (s, 9H, H19).

^{13}**C NMR** (126 MHz, MeOD) δ 171.8 (C11), 170.6 (C16 or C20), 170.3 (C16 or C20), 151.5 (C1), 147.7 (C2), 144.3 (C8), 131.9 (C4), 130.1 (C5), 129.1 (C6 or C7), 126.2 (C6 or C7), 71.7 (C28), 70.6 (one of C22-27), 70.1 (one of C22-27), 70.0 (one of C22-27), 69.9 (one of C22-27), 69.79 (one of C22-27), 69.76 (one of C22-27), 69.5 (stack of C14 and C21), 59.2 (C12), 56.9 (C17), 56.7 (C15), 48.7 (C9), 40.5 (C29), 37.5 (C13), 35.6 (C18), 25.6 (C19), 21.0 (C10), 14.4 (C3).

N.B. Signal for H29 under-integrates.

HRMS calculated for $C_{33}H_{52}N_5O_8S$ [M+H]$^+$ 678.3518, found 678.3518

MS: *m/z* (ES+) 648.41 (100%, [M+H]$^+$)

R$_t$ (method 1) = 1.90 min

ν$_{max}$ (thin film, ATR)/cm^{-1}: 3296, 2923, 1636, 1529, 1437, 1371, 1110, 1033, 850, 572

(2*S*,4*R*)-1-((*S*)-18-(*Tert*-butyl)-1,16-dioxo-1-(4-((4-((4-(3-(pyridin-3-ylmethyl)thioureido)phenyl)sulfonyl)piperazin-1-yl)methyl)phenyl)-5,8,11,14-tetraoxa-2,17-diazanonadecan-19-oyl)-4-hydroxy-*N*-((*R*)-1-(4-(4-methylthiazol-5-yl)phenyl)ethyl)pyrrolidine-2-carboxamide (238)
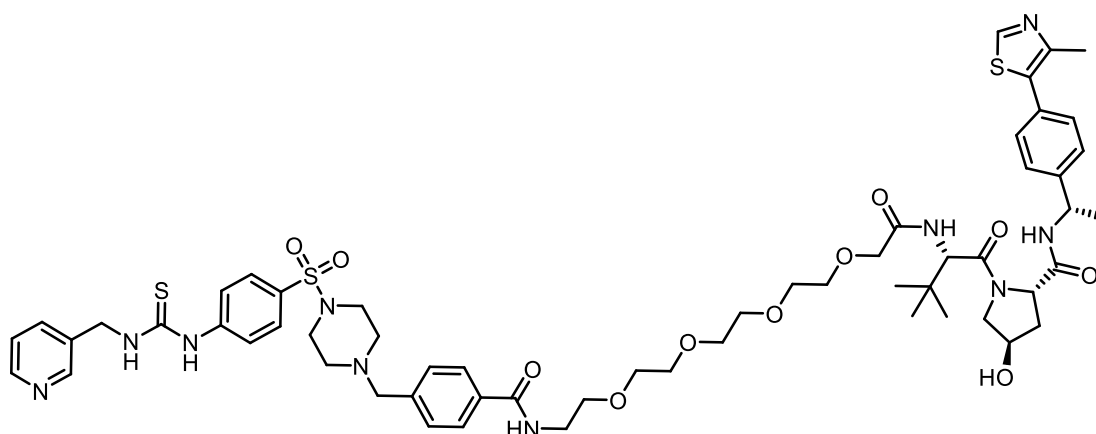
4-((4-((4-(3-(Pyridin-3-ylmethyl)thioureido)phenyl)sulfonyl)piperazin-1-yl)methyl)benzoic acid (**263**) (42.0 mg, 0.0798 mmol, 1.5 eq), (2*S*,4*R*)-1-((*S*)-17-amino-2-(*tert*-butyl)-4-oxo-6,9,12,15-tetraoxa-3-azaheptadecanoyl)-4-hydroxy-*N*-((*R*)-1-(4-

(4-methylthiazol-5-yl)phenyl)ethyl)pyrrolidine-2-carboxamide **(266)** (36.0 mg, 0.0531 mmol, 1.0 eq), HOBt.H$_2$O (16.2 mg, 0.106 mmol, 2.0 eq), and DIPEA (56.7 µL, 0.319 mmol, 6.0 eq) were dissolved in DMF (2.5 mL). HATU (60.4 mg, 0.159 mmol, 3.0 eq) was then added, and the reaction stirred at room temperature overnight. The reaction was diluted with EtOAc (5.0 mL) and water (5.0 mL), and extracted with EtOAc (5.0 mL x 5). The combined organics were then sequentially washed with H$_2$O and brine (10 mL each), dried over MgSO$_4$, filtered, and concentrated under reduced pressure. The residue was purified by reverse phase flash column chromatography (basic modifier) to afford the title compound as a yellow gum (12.0 mg, 19%).

^{1}H NMR (500 MHz, MeOD) δ 8.87 (s, 1H), 8.57 (d, *J* = 2.3 Hz, 1H), 8.46 – 8.42 (m, 1H), 7.89 (dt, *J* = 7.9, 2.0 Hz, 1H), 7.78 – 7.74 (m, 4H), 7.71 – 7.68 (m, 2H), 7.45 – 7.38 (m, 5H), 7.37 – 7.34 (m, 2H), 4.99 (q, *J* = 7.0 Hz, 1H), 4.90 (s, 2H), 4.67 (s, 1H), 4.57 (dd, *J* = 9.0, 7.5 Hz, 1H), 4.45 – 4.40 (m, 1H), 4.06 – 3.96 (m, 2H), 3.85 – 3.81 (m, 1H), 3.73 (dd, *J* = 11.1, 3.8 Hz, 1H), 3.68 – 3.58 (m, 14H), 3.58 – 3.53 (m, 4H), 3.04 – 2.96 (m, 4H), 2.52 – 2.49 (m, 4H), 2.47 (s, 3H), 2.20 (app. ddt, *J* = 13.2, 7.7, 2.0 Hz, 1H), 1.95 (ddd, *J* = 13.4, 9.2, 4.5 Hz, 1H), 1.49 (d, *J* = 7.0 Hz, 3H), 1.18 (t, *J* = 7.1 Hz, 1H), 1.03 (s, 9H).

N.B. Signals over-integrate by 2H.

HRMS calculated for C$_{58}$H$_{76}$N$_{10}$O$_{11}$S$_3$Na [M+Na]$^+$ 1207.4736, found 1207.4732

MS: *m/z* (ES+) 1185.38 (100%, [M+H]$^+$)

R$_t$ (method 1) = 2.36 min

v$_{max}$ (thin film, ATR)/cm^{-1}: 3303, 2924, 1637, 1534, 1454, 1328, 1267, 1163, 1110, 948, 836, 735, 620, 572
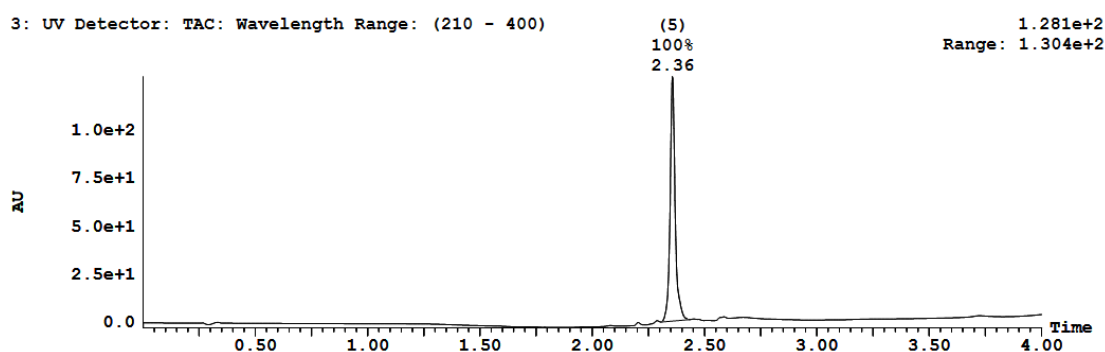
3.3.1 Variable temperature NMR of **182**

25 °C

37 °C

45 °C
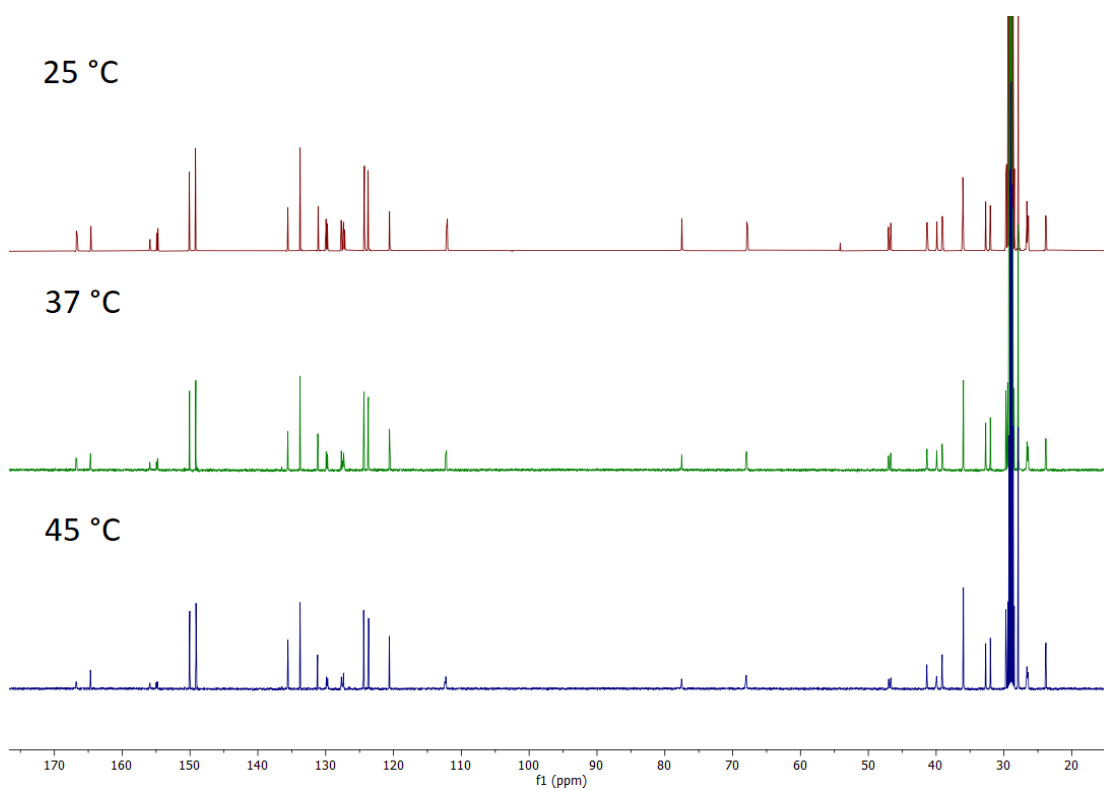
*Figure 3.1 VT NMR of **182** at 25 °C, 37 °C, and 45 °C.*

25 °C

C16 C5 C22

37 °C

45 °C

41.9 41.7 41.5 41.3 41.1 40.9 40.7 40.5 40.3 40.1 39.9 39.7 39.5 39.3 39.1 38.9 38.7 38.5 38.3 38.
f1 (ppm)
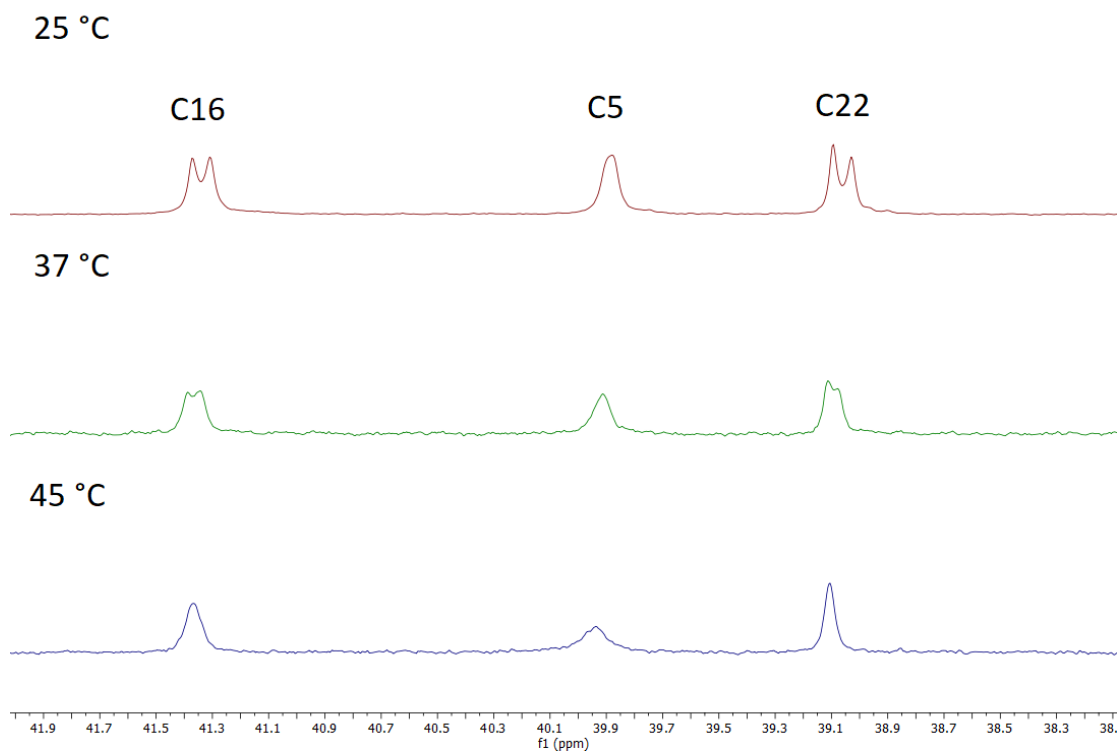
*Figure 3.2 VT NMR of **182** at 25 °C, 37 °C, and 45 °C showing C16, C5, and C22.*
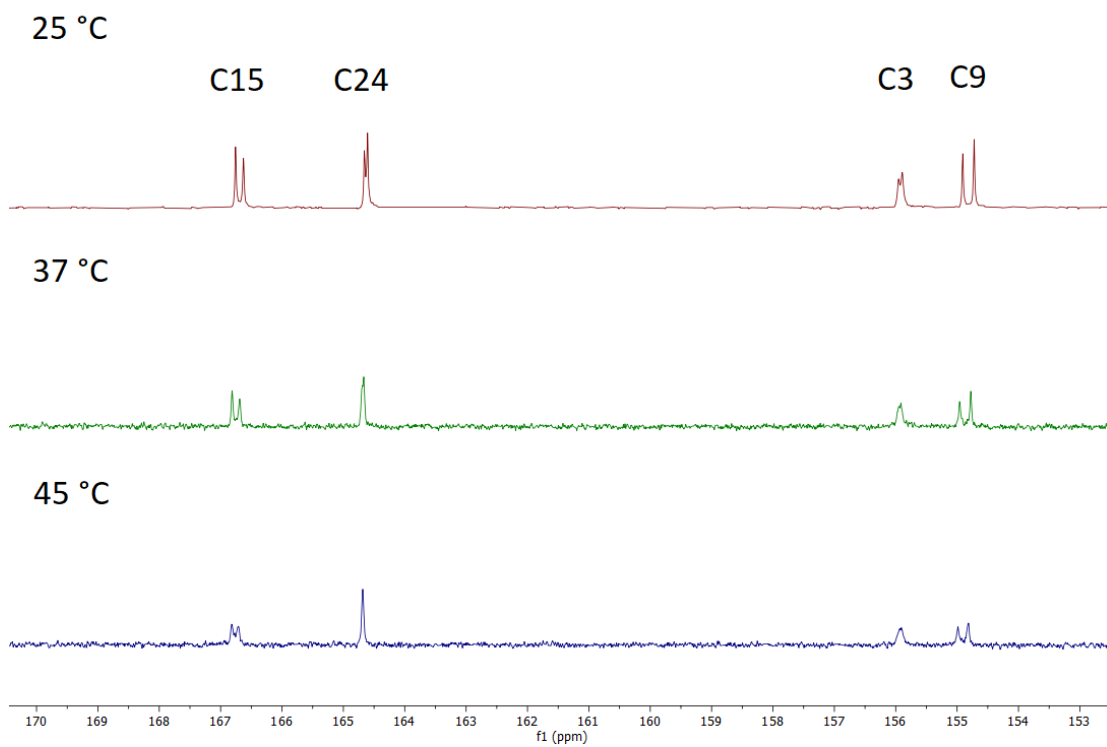
*Figure 3.3 VT NMR of **182** at 25 °C, 37 °C, and 45 °C showing C15, C24, C3, and C9.*

4 References

(1) Sensi, M.; Anichini, A. Unique Tumor Antigens: Evidence for Immune Control of Genome Integrity and Immunogenic Targets for T Cell-Mediated Patient-Specific Immunotherapy. *Clin. Cancer Res. Off. J. Am. Assoc. Cancer Res.* **2006**, *12* (17), 5023–5032. https://doi.org/10.1158/1078-0432.CCR-05-2682.

(2) Ehrlich, P. The Relationship Existing between Chemical Constitution, Distribution and Pharmacological Action. In *Collected Studies on Immunity.*; Wiley & Sons, 1906; pp 441–450.

(3) Ehrlich, P. Chemotherapy. Proceedings of 17th International Congress of Medicine. In *Collected Papers of Paul Ehrlich*; Pergamon Press, 1913; pp 505–518.

(4) Mathé, G.; Lo, T. B.; Bernard, J. Effect on Mouse Leukemia 1210 of a Combination by Diazo-Reaction of Amethopterin and Gamma-Globulins from Hamsters Inoculated with Such Leukemia by Heterografts. *C R Hebd Seances Acad Sci* **1958**, *246*, 1626–1628.

(5) Köhler, G.; Milstein, C. Continuous Cultures of Fused Cells Secreting Antibody of Predefined Specificity. *Nature* **1975**, *256* (5517), 495–497. https://doi.org/10.1038/256495a0.

(6) Perez, H. L.; Cardarelli, P. M.; Deshpande, S.; Gangwar, S.; Schroeder, G. M.; Vite, G. D.; Borzilleri, R. M. Antibody–Drug Conjugates: Current Status and Future Directions. *Drug Discov. Today* **2014**, *19* (7), 869–881. https://doi.org/10.1016/j.drudis.2013.11.004.

(7) Riechmann, L.; Clark, M.; Waldmann, H.; Winter, G. Reshaping Human Antibodies for Therapy. *Nature* **1988**, *332* (6162), 323–327. https://doi.org/10.1038/332323a0.

(8) Egan, P. C.; Reagan, J. L. The Return of Gemtuzumab Ozogamicin: A Humanized Anti-CD33 Monoclonal Antibody–Drug Conjugate for the Treatment of Newly Diagnosed Acute Myeloid Leukemia. *OncoTargets Ther.* **2018**, *11*, 8265–8272. https://doi.org/10.2147/OTT.S150807.

(9) Peters, C.; Brown, S. Antibody–Drug Conjugates as Novel Anti-Cancer Chemotherapeutics. *Biosci. Rep.* **2015**, *35* (4), e00225. https://doi.org/10.1042/BSR20150089.

(10) *Antibody-Drug Conjugate Drug Release*. https://www.biorender.com/template/antibody-drug-conjugate-drug-release (accessed 2023-09-25).

(11) Su, D.; Zhang, D. Linker Design Impacts Antibody-Drug Conjugate Pharmacokinetics and Efficacy via Modulating the Stability and Payload Release Efficiency. *Front. Pharmacol.* **2021**, *12*.

(12) Ritchie, M.; Tchistiakova, L.; Scott, N. Implications of Receptor-Mediated Endocytosis and Intracellular Trafficking Dynamics in the Development of Antibody Drug Conjugates. *mAbs* **2013**, *5* (1), 13–21. https://doi.org/10.4161/mabs.22854.

(13) Janeway, C. *Immunobiology: The Immune System in Health and Disease*; Elsevier España, 2001.

(14) Woof, J. M.; Burton, D. R. Human Antibody-Fc Receptor Interactions Illuminated by Crystal Structures. *Nat. Rev. Immunol.* **2004**, *4* (2), 89–99. https://doi.org/10.1038/nri1266.

(15) Pier, G. B.; Lyczak, J. B.; Wetzler, L. M. *Immunology, Infection, and Immunity*; ASM Press, 2004.

(16) Maverakis, E.; Kim, K.; Shimoda, M.; Gershwin, M. E.; Patel, F.; Wilken, R.; Raychaudhuri, S.; Ruhaak, L. R.; Lebrilla, C. B. Glycans In The Immune System and The Altered Glycan Theory of Autoimmunity: A Critical Review. *J. Autoimmun.* **2015**, *0*, 1–13. https://doi.org/10.1016/j.jaut.2014.12.002.

(17) Cobb, B. A. The History of IgG Glycosylation and Where We Are Now. *Glycobiology* **2019**, *30* (4), 202–213. https://doi.org/10.1093/glycob/cwz065.

(18) *Definition of monoclonal antibody - NCI Dictionary of Cancer Terms - NCI*. https://www.cancer.gov/publications/dictionaries/cancer-terms/def/monoclonal-antibody (accessed 2023-06-14).

(19) Fu, Z.; Li, S.; Han, S.; Shi, C.; Zhang, Y. Antibody Drug Conjugate: The "Biological Missile" for Targeted Cancer Therapy. *Signal Transduct. Target. Ther.* **2022**, *7* (1), 93. https://doi.org/10.1038/s41392-022-00947-7.

(20) Pettinato, M. C. Introduction to Antibody-Drug Conjugates. *Antibodies* **2021**, *10* (4), 42. https://doi.org/10.3390/antib10040042.

(21) Strop, P.; Liu, S.-H.; Dorywalska, M.; Delaria, K.; Dushin, R. G.; Tran, T.-T.; Ho, W.-H.; Farias, S.; Casas, M. G.; Abdiche, Y.; Zhou, D.; Chandrasekaran, R.; Samain, C.; Loo, C.; Rossi, A.; Rickert, M.; Krimm, S.; Wong, T.; Chin, S. M.; Yu, J.; Dilley, J.; Chaparro-Riggers, J.; Filzen, G. F.; O'Donnell, C. J.; Wang, F.; Myers, J. S.; Pons, J.; Shelton, D. L.; Rajpal, A. Location Matters: Site of Conjugation Modulates Stability and Pharmacokinetics of Antibody Drug Conjugates. *Chem. Biol.* **2013**, *20* (2), 161–167. https://doi.org/10.1016/j.chembiol.2013.01.010.

(22) Hollander, I.; Kunz, A.; Hamann, Philip. R. Selection of Reaction Additives Used in the Preparation of Monomeric Antibody–Calicheamicin Conjugates. *Bioconjug. Chem.* **2008**, *19* (1), 358–361. https://doi.org/10.1021/bc700321z.

(23) Chari, R. V. J. Targeted Cancer Therapy: Conferring Specificity to Cytotoxic Drugs. *Acc. Chem. Res.* **2008**, *41* (1), 98–107. https://doi.org/10.1021/ar700108g.

(24) Kim, M. T.; Chen, Y.; Marhoul, J.; Jacobson, F. Statistical Modeling of the Drug Load Distribution on Trastuzumab Emtansine (Kadcyla), a Lysine-Linked Antibody Drug Conjugate. *Bioconjug. Chem.* **2014**, *25* (7), 1223–1232. https://doi.org/10.1021/bc5000109.

(25) Tsuchikama, K.; An, Z. Antibody-Drug Conjugates: Recent Advances in Conjugation and Linker Chemistries. *Protein Cell* **2018**, *9* (1), 33–46. https://doi.org/10.1007/s13238-016-0323-0.

(26) Haque, M.; Forte, N.; R. Baker, J. Site-Selective Lysine Conjugation Methods and Applications towards Antibody–Drug Conjugates. *Chem. Commun.* **2021**, *57* (82), 10689–10702. https://doi.org/10.1039/D1CC03976H.

(27) Schroeder, D. D.; Tankersly, D. L.; Lundblad, J. L. A New Preparation of Modified Immune Serum Globulin (Human) Suitable for Intravenous Administration. *Vox Sang.* **1981**, *40* (6), 373–382. https://doi.org/10.1111/j.1423-0410.1981.tb00725.x.

(28) Renault, K.; Fredy, J. W.; Renard, P.-Y.; Sabot, C. Covalent Modification of Biomolecules through Maleimide-Based Labeling Strategies. *Bioconjug. Chem.* **2018**, *29* (8), 2497–2513. https://doi.org/10.1021/acs.bioconjchem.8b00252.

(29) Shen, B.-Q.; Xu, K.; Liu, L.; Raab, H.; Bhakta, S.; Kenrick, M.; Parsons-Reponte, K. L.; Tien, J.; Yu, S.-F.; Mai, E.; Li, D.; Tibbitts, J.; Baudys, J.; Saad, O. M.; Scales, S. J.; McDonald, P. J.; Hass, P. E.; Eigenbrot, C.; Nguyen, T.; Solis, W. A.; Fuji, R. N.; Flagella, K. M.; Patel, D.; Spencer, S. D.; Khawli, L. A.; Ebens, A.; Wong, W. L.; Vandlen, R.; Kaur, S.; Sliwkowski, M. X.; Scheller, R. H.; Polakis, P.; Junutula, J. R. Conjugation Site Modulates the in Vivo Stability and Therapeutic Activity of Antibody-Drug Conjugates. *Nat. Biotechnol.* **2012**, *30* (2), 184–189. https://doi.org/10.1038/nbt.2108.

(30) Lyon, R. P.; Setter, J. R.; Bovee, T. D.; Doronina, S. O.; Hunter, J. H.; Anderson, M. E.; Balasubramanian, C. L.; Duniho, S. M.; Leiske, C. I.; Li, F.; Senter, P. D. Self-Hydrolyzing Maleimides Improve the Stability and Pharmacological Properties of Antibody-Drug Conjugates. *Nat. Biotechnol.* **2014**, *32* (10), 1059–1062. https://doi.org/10.1038/nbt.2968.

(31) Kolodych, S.; Koniev, O.; Baatarkhuu, Z.; Bonnefoy, J.-Y.; Debaene, F.; Cianférani, S.; Van Dorsselaer, A.; Wagner, A. CBTF: New Amine-to-Thiol Coupling Reagent for Preparation of Antibody Conjugates with Increased Plasma Stability. *Bioconjug. Chem.* **2015**, *26* (2), 197–200. https://doi.org/10.1021/bc500610g.

(32) Behrens, C. R.; Ha, E. H.; Chinn, L. L.; Bowers, S.; Probst, G.; Fitch-Bruhns, M.; Monteon, J.; Valdiosera, A.; Bermudez, A.; Liao-Chan, S.; Wong, T.; Melnick, J.; Theunissen, J.-W.; Flory, M. R.; Houser, D.; Venstrom, K.; Levashova, Z.; Sauer, P.; Migone, T.-S.; van der Horst, E. H.; Halcomb, R. L.; Jackson, D. Y. Antibody-Drug Conjugates (ADCs) Derived from Interchain Cysteine Cross-Linking Demonstrate Improved Homogeneity and Other Pharmacological Properties over Conventional Heterogeneous ADCs. *Mol. Pharm.* **2015**, *12* (11), 3986–3998. https://doi.org/10.1021/acs.molpharmaceut.5b00432.

(33) Maruani, A.; Smith, M. E. B.; Miranda, E.; Chester, K. A.; Chudasama, V.; Caddick, S. A Plug-and-Play Approach to Antibody-Based Therapeutics via a Chemoselective Dual Click Strategy. *Nat. Commun.* **2015**, *6* (1), 6645. https://doi.org/10.1038/ncomms7645.

(34) Bryant, P.; Pabst, M.; Badescu, G.; Bird, M.; McDowell, W.; Jamieson, E.; Swierkosz, J.; Jurlewicz, K.; Tommasi, R.; Henseleit, K.; Sheng, X.; Camper, N.; Manin, A.; Kozakowska, K.; Peciak, K.; Laurine, E.; Grygorash, R.; Kyle, A.; Morris, D.; Parekh, V.; Abhilash, A.; Choi, J.-W.; Edwards, J.; Frigerio, M.; Baker, M. P.; Godwin, A. In Vitro and In Vivo Evaluation of Cysteine Rebridged Trastuzumab-MMAE Antibody Drug Conjugates with Defined Drug-to-Antibody Ratios. *Mol. Pharm.* **2015**, *12* (6), 1872–1879. https://doi.org/10.1021/acs.molpharmaceut.5b00116.

(35) Lee, M. T. W.; Maruani, A.; Baker, J. R.; Caddick, S.; Chudasama, V. Next-Generation Disulfide Stapling: Reduction and Functional Re-Bridging All in One. *Chem. Sci.* **2016**, *7* (1), 799–802. https://doi.org/10.1039/C5SC02666K.

(36) Procopio-Melino, R.; Kotch, F. W.; Prashad, A. S.; Gomes, J. M.; Wang, W.; Arve, B.; Dawdy, A.; Chen, L.; Sperry, J.; Hosselet, C.; He, T.; Kriz, R.; Lin, L.; Marquette, K.; Tchistiakova, L.; Somers, W.; Rouse, J. C.; Zhong, X. Cysteine Metabolic Engineering and Selective Disulfide Reduction Produce Superior Antibody-Drug-

Conjugates. *Sci. Rep.* **2022**, *12* (1), 7262. https://doi.org/10.1038/s41598-022-11344-z.

(37) F. Schumacher, F.; M. Nunes, J. P.; Maruani, A.; Chudasama, V.; B. Smith, M. E.; A. Chester, K.; R. Baker, J.; Caddick, S. Next Generation Maleimides Enable the Controlled Assembly of Antibody–Drug Conjugates via Native Disulfide Bond Bridging. *Org. Biomol. Chem.* **2014**, *12* (37), 7261–7269. https://doi.org/10.1039/C4OB01550A.

(38) M. Dannheim, F.; J. Walsh, S.; T. Orozco, C.; Højgaard Hansen, A.; D. Bargh, J.; E. Jackson, S.; J. Bond, N.; S. Parker, J.; S. Carroll, J.; R. Spring, D. All-in-One Disulfide Bridging Enables the Generation of Antibody Conjugates with Modular Cargo Loading. *Chem. Sci.* **2022**, *13* (30), 8781–8790. https://doi.org/10.1039/D2SC02198F.

(39) Junutula, J. R.; Raab, H.; Clark, S.; Bhakta, S.; Leipold, D. D.; Weir, S.; Chen, Y.; Simpson, M.; Tsai, S. P.; Dennis, M. S.; Lu, Y.; Meng, Y. G.; Ng, C.; Yang, J.; Lee, C. C.; Duenas, E.; Gorrell, J.; Katta, V.; Kim, A.; McDorman, K.; Flagella, K.; Venook, R.; Ross, S.; Spencer, S. D.; Lee Wong, W.; Lowman, H. B.; Vandlen, R.; Sliwkowski, M. X.; Scheller, R. H.; Polakis, P.; Mallet, W. Site-Specific Conjugation of a Cytotoxic Drug to an Antibody Improves the Therapeutic Index. *Nat. Biotechnol.* **2008**, *26* (8), 925–932. https://doi.org/10.1038/nbt.1480.

(40) Adhikari, P.; Zacharias, N.; Ohri, R.; Sadowsky, J. Site-Specific Conjugation to Cys-Engineered THIOMAB^TM Antibodies. In *Antibody-Drug Conjugates: Methods and Protocols*; Tumey, L. N., Ed.; Methods in Molecular Biology; Springer US: New York, NY, 2020; pp 51–69. https://doi.org/10.1007/978-1-4939-9929-3_4.

(41) Li, X.; Nelson, C. G.; Nair, R. R.; Hazlehurst, L.; Moroni, T.; Martinez-Acedo, P.; Nanna, A. R.; Hymel, D.; Burke, T. R.; Rader, C. Stable and Potent Selenomab-Drug Conjugates. *Cell Chem. Biol.* **2017**, *24* (4), 433-442.e6. https://doi.org/10.1016/j.chembiol.2017.02.012.

(42) Carrico, I. S.; Carlson, B. L.; Bertozzi, C. R. Introducing Genetically Encoded Aldehydes into Proteins. *Nat. Chem. Biol.* **2007**, *3* (6), 321–322. https://doi.org/10.1038/nchembio878.

(43) Rabuka, D.; Rush, J. S.; deHart, G. W.; Wu, P.; Bertozzi, C. R. Site-Specific Chemical Protein Conjugation Using Genetically Encoded Aldehyde Tags. *Nat. Protoc.* **2012**, *7* (6), 1052–1067. https://doi.org/10.1038/nprot.2012.045.

(44) Agarwal, P.; van der Weijden, J.; Sletten, E. M.; Rabuka, D.; Bertozzi, C. R. A Pictet-Spengler Ligation for Protein Chemical Modification. *Proc. Natl. Acad. Sci.* **2013**, *110* (1), 46–51. https://doi.org/10.1073/pnas.1213186110.

(45) Antos, J. M.; Truttmann, M. C.; Ploegh, H. L. Recent Advances in Sortase-Catalyzed Ligation Methodology. *Curr. Opin. Struct. Biol.* **2016**, *38*, 111–118. https://doi.org/10.1016/j.sbi.2016.05.021.

(46) Mao, H.; Hart, S. A.; Schink, A.; Pollok, B. A. Sortase-Mediated Protein Ligation: A New Method for Protein Engineering. *J. Am. Chem. Soc.* **2004**, *126* (9), 2670–2671. https://doi.org/10.1021/ja039915e.

(47) Madej, M. P.; Coia, G.; Williams, C. C.; Caine, J. M.; Pearce, L. A.; Attwood, R.; Bartone, N. A.; Dolezal, O.; Nisbet, R. M.; Nuttall, S. D.; Adams, T. E. Engineering of an Anti-Epidermal Growth Factor Receptor Antibody to Single Chain Format and Labeling by Sortase A-Mediated Protein Ligation. *Biotechnol. Bioeng.* **2012**, *109* (6), 1461–1470. https://doi.org/10.1002/bit.24407.

(48) Popp, M. W.-L.; Antos, J. M.; Ploegh, H. L. Site-Specific Protein Labeling via Sortase-Mediated Transpeptidation. *Curr. Protoc. Protein Sci.* **2009**, *56* (1), 15.3.1-15.3.9. https://doi.org/10.1002/0471140864.ps1503s56.

(49) Beerli, R. R.; Hell, T.; Merkel, A. S.; Grawunder, U. Sortase Enzyme-Mediated Generation of Site-Specifically Conjugated Antibody Drug Conjugates with High In Vitro and In Vivo Potency. *PLOS ONE* **2015**, *10* (7), e0131177. https://doi.org/10.1371/journal.pone.0131177.

(50) Witte, M. D.; Theile, C. S.; Wu, T.; Guimaraes, C. P.; Blom, A. E. M.; Ploegh, H. L. Production of Unnaturally Linked Chimeric Proteins Using a Combination of Sortase-Catalyzed Transpeptidation and Click Chemistry. *Nat. Protoc.* **2013**, *8* (9), 1808–1819. https://doi.org/10.1038/nprot.2013.103.

(51) Guimaraes, C. P.; Witte, M. D.; Theile, C. S.; Bozkurt, G.; Kundrat, L.; Blom, A. E. M.; Ploegh, H. L. Site-Specific C-Terminal and Internal Loop Labeling of Proteins Using Sortase-Mediated Reactions. *Nat. Protoc.* **2013**, *8* (9), 1787–1799. https://doi.org/10.1038/nprot.2013.101.

(52) Policarpo, R. L.; Kang, H.; Liao, X.; Rabideau, A. E.; Simon, M. D.; Pentelute, B. L. Flow-Based Enzymatic Ligation by Sortase A. *Angew. Chem.* **2014**, *126* (35), 9357–9362. https://doi.org/10.1002/ange.201403582.

(53) Prota, A. E.; Magiera, M. M.; Kuijpers, M.; Bargsten, K.; Frey, D.; Wieser, M.; Jaussi, R.; Hoogenraad, C. C.; Kammerer, R. A.; Janke, C.; Steinmetz, M. O. Structural Basis of Tubulin Tyrosination by Tubulin Tyrosine Ligase. *J. Cell Biol.* **2013**, *200* (3), 259–270. https://doi.org/10.1083/jcb.201211017.

(54) Schumacher, D.; Hackenberger, C. P. R.; Leonhardt, H.; Helma, J. Current Status: Site-Specific Antibody Drug Conjugates. *J. Clin. Immunol.* **2016**, *36* (1), 100–107. https://doi.org/10.1007/s10875-016-0265-6.

(55) Schumacher, D.; Helma, J.; Mann, F. A.; Pichler, G.; Natale, F.; Krause, E.; Cardoso, M. C.; Hackenberger, C. P. R.; Leonhardt, H. Versatile and Efficient Site-Specific Protein Functionalization by Tubulin Tyrosine Ligase. *Angew. Chem. Int. Ed.* **2015**, *54* (46), 13787–13791. https://doi.org/10.1002/anie.201505456.

(56) Keppler, O. T.; Horstkorte, R.; Pawlita, M.; Schmidt, C.; Reutter, W. Biochemical Engineering of the N-Acyl Side Chain of Sialic Acid: Biological Implications. *Glycobiology* **2001**, *11* (2), 11R-18R. https://doi.org/10.1093/glycob/11.2.11R.

(57) Schmaltz, R. M.; Hanson, S. R.; Wong, C.-H. Enzymes in the Synthesis of Glycoconjugates. *Chem. Rev.* **2011**, *111* (7), 4259–4307. https://doi.org/10.1021/cr200113w.

(58) Li, X.; Fang, T.; Boons, G. Preparation of Well-Defined Antibody–Drug Conjugates through Glycan Remodeling and Strain-Promoted Azide–Alkyne Cycloadditions. *Angew. Chem. Int. Ed.* **2014**, *53* (28), 7179–7182. https://doi.org/10.1002/anie.201402606.

(59) Zhu, Z.; Ramakrishnan, B.; Li, J.; Wang, Y.; Feng, Y.; Prabakaran, P.; Colantonio, S.; Dyba, M. A.; Qasba, P. K.; Dimitrov, D. S. Site-Specific Antibody-Drug Conjugation through an Engineered Glycotransferase and a Chemically Reactive Sugar. *mAbs* **2014**, *6* (5), 1190–1200. https://doi.org/10.4161/mabs.29889.

(60) Clarke, D. D.; Mycek, M. J.; Neidle, A.; Waelsch, H. The Incorporation of Amines into Protein. *Arch. Biochem. Biophys.* **1959**, *79*, 338–354. https://doi.org/10.1016/0003-9861(59)90413-8.

(61) Pisano, J. J.; Finlayson, J. S.; Peyton, M. P. Cross-Link in Fibrin Polymerized by Factor XIII: ε-(γ-Glutamyl)Lysine. *Science* **1968**, *160* (3830), 892–893. https://doi.org/10.1126/science.160.3830.892.

(62) Griffin, M.; Casadio, R.; Bergamini, C. M. Transglutaminases: Nature's Biological Glues. *Biochem. J.* **2002**, *368* (2), 377–396. https://doi.org/10.1042/bj20021234.

(63) Kanaji, T.; Ozaki, H.; Takao, T.; Kawajiri, H.; Ide, H.; Motoki, M.; Shimonishi, Y. Primary Structure of Microbial Transglutaminase from Streptoverticillium Sp. Strain s-8112. *J. Biol. Chem.* **1993**, *268* (16), 11565–11572.

(64) Del Duca, S.; Beninati, S.; Serafini-Fracassini, D. Polyamines in Chloroplasts: Identification of Their Glutamyl and Acetyl Derivatives. *Biochem. J.* **1995**, *305* (Pt 1), 233–237.

(65) Singh, R. N.; Mehta, K. Purification and Characterization of a Novel Transglutaminase from Filarial Nematode Brugia Malayi. *Eur. J. Biochem.* **1994**, *225* (2), 625–634. https://doi.org/10.1111/j.1432-1033.1994.00625.x.

(66) Zhang, J.; Masui, Y. Role of Amphibian Egg Transglutaminase in the Development of Secondary Cytostatic Factor in Vitro. *Mol. Reprod. Dev.* **1997**, *47* (3), 302–311. https://doi.org/10.1002/(SICI)1098-2795(199707)47:3<302::AID-MRD9>3.0.CO;2-P.

(67) Yasueda, H.; Kumazawa, Y.; Motoki, M. Purification and Characterization of a Tissue-Type Transglutaminase from Red Sea Bream (Pagrus Major). *Biosci. Biotechnol. Biochem.* **1994**, *58* (11), 2041–2045. https://doi.org/10.1271/bbb.58.2041.

(68) Puszkin, E. G.; Raghuraman, V. Catalytic Properties of a Calmodulin-Regulated Transglutaminase from Human Platelet and Chicken Gizzard. *J. Biol. Chem.* **1985**, *260* (29), 16012–16020.

(69) Strop, P. Versatility of Microbial Transglutaminase. *Bioconjug. Chem.* **2014**, *25* (5), 855–862. https://doi.org/10.1021/bc500099v.

(70) Kieliszek, M.; Misiewicz, A. Microbial Transglutaminase and Its Application in the Food Industry. A Review. *Folia Microbiol. (Praha)* **2014**, *59* (3), 241–250. https://doi.org/10.1007/s12223-013-0287-x.

(71) *Ramsay helps creates largest beef wellington weighing same as eight-year-old boy*. The Independent. https://www.independent.co.uk/news/uk/gordon-ramsay-tiktok-youtube-twitter-b2355486.html (accessed 2023-06-15).

(72) Kashiwagi, T.; Yokoyama, K.; Ishikawa, K.; Ono, K.; Ejima, D.; Matsui, H.; Suzuki, E. Crystal Structure of Microbial Transglutaminase from Streptoverticillium Mobaraense. *J. Biol. Chem.* **2002**, *277* (46), 44252–44260. https://doi.org/10.1074/jbc.M203933200.

(73) Ohtsuka, T.; Umezawa, Y.; Nio, N.; Kubota, K. Comparison of Deamidation Activity of Transglutaminases. *J. Food Sci.* **2001**, *66* (1), 25–29. https://doi.org/10.1111/j.1365-2621.2001.tb15576.x.

(74) Rachel, N. M.; Toulouse, J. L.; Pelletier, J. N. Transglutaminase-Catalyzed Bioconjugation Using One-Pot Metal- Free Bioorthogonal Chemistry. *Bioconjugate Chem* **2017**, 6.

(75) Ohtsuka, T.; Sawa, A.; Kawabata, R.; Nio, N.; Motoki, M. Substrate Specificities of Microbial Transglutaminase for Primary Amines. *J. Agric. Food Chem.* **2000**, *48* (12), 6230–6233. https://doi.org/10.1021/jf000302k.

(76) Gundersen, M. T.; Keillor, J. W.; Pelletier, J. N. Microbial Transglutaminase Displays Broad Acyl-Acceptor Substrate Specificity. *Appl. Microbiol. Biotechnol.* **2014**, *98* (1), 219–230. https://doi.org/10.1007/s00253-013-4886-x.

(77) Folk, J. E.; Cole, P. W. Transglutaminase: Mechanistic Features of the Active Site as Determined by Kinetic and Inhibitor Studies. *Biochim. Biophys. Acta BBA - Enzymol. Biol. Oxid.* **1966**, *122* (2), 244–264. https://doi.org/10.1016/0926-6593(66)90066-X.

(78) Jeger, S.; Zimmermann, K.; Blanc, A.; Grünberg, J.; Honer, M.; Hunziker, P.; Struthers, H.; Schibli, R. Site-Specific and Stoichiometric Modification of Antibodies by Bacterial Transglutaminase. *Angew. Chem. Int. Ed.* **2010**, *49* (51), 9995–9997. https://doi.org/10.1002/anie.201004243.

(79) Ebenig, A.; Juettner, N. E.; Deweid, L.; Avrutina, O.; Fuchsbauer, H.-L.; Kolmar, H. Efficient Site-Specific Antibody-Drug Conjugation by Engineering a Nature-Derived Recognition Tag for Microbial Transglutaminase. *Chembiochem Eur. J. Chem. Biol.* **2019**, *20* (18), 2411–2419. https://doi.org/10.1002/cbic.201900101.

(80) Jennewein, M. F.; Alter, G. The Immunoregulatory Roles of Antibody Glycosylation. *Trends Immunol.* **2017**, *38* (5), 358–372. https://doi.org/10.1016/j.it.2017.02.004.

(81) Dennler, P.; Chiotellis, A.; Fischer, E.; Brégeon, D.; Belmant, C.; Gauthier, L.; Lhospice, F.; Romagne, F.; Schibli, R. Transglutaminase-Based Chemo-Enzymatic Conjugation Approach Yields Homogeneous Antibody–Drug Conjugates. *Bioconjug. Chem.* **2014**, *25* (3), 569–578. https://doi.org/10.1021/bc400574z.

(82) Lhospice, F.; Brégeon, D.; Belmant, C.; Dennler, P.; Chiotellis, A.; Fischer, E.; Gauthier, L.; Boëdec, A.; Rispaud, H.; Savard-Chambard, S.; Represa, A.; Schneider, N.; Paturel, C.; Sapet, M.; Delcambre, C.; Ingoure, S.; Viaud, N.; Bonnafous, C.; Schibli, R.; Romagné, F. Site-Specific Conjugation of Monomethyl Auristatin E to Anti-CD30 Antibodies Improves Their Pharmacokinetics and Therapeutic Index in Rodent Models. *Mol. Pharm.* **2015**, *12* (6), 1863–1871. https://doi.org/10.1021/mp500666j.

(83) Strop, P.; Delaria, K.; Foletti, D.; Witt, J. M.; Hasa-Moreno, A.; Poulsen, K.; Casas, M. G.; Dorywalska, M.; Farias, S.; Pios, A.; Lui, V.; Dushin, R.; Zhou, D.; Navaratnam, T.; Tran, T.-T.; Sutton, J.; Lindquist, K. C.; Han, B.; Liu, S.-H.; Shelton, D. L.; Pons, J.; Rajpal, A. Site-Specific Conjugation Improves Therapeutic Index of Antibody Drug Conjugates with High Drug Loading. *Nat. Biotechnol.* **2015**, *33* (7), 694–696. https://doi.org/10.1038/nbt.3274.

(84) Rachel, N. M.; Pelletier, J. N. One-Pot Peptide and Protein Conjugation: A Combination of Enzymatic Transamidation and Click Chemistry. *Chem. Commun.* **2016**, *52* (12), 2541–2544. https://doi.org/10.1039/C5CC09163B.

(85) Seguro, K.; Nio, N.; Motoki, M. Some Characteristics of a Microbial Protein Cross-Linking Enzyme: Transglutaminase. In *Macromolecular Interactions in Food Technology*; ACS Symposium Series; American Chemical Society, 1996; Vol. 650, pp 271–280. https://doi.org/10.1021/bk-1996-0650.ch021.

(86) Steffen, W.; Ko, F. C.; Patel, J.; Lyamichev, V.; Albert, T. J.; Benz, J.; Rudolph, M. G.; Bergmann, F.; Streidl, T.; Kratzsch, P.; Boenitz-Dulat, M.; Oelschlaegel, T.; Schraeml, M. Discovery of a Microbial Transglutaminase Enabling Highly Site-Specific Labeling of Proteins. *J. Biol. Chem.* **2017**, *292* (38), 15622–15635. https://doi.org/10.1074/jbc.M117.797811.

(87) Teicher, B. A.; Chari, R. V. J. Antibody Conjugate Therapeutics: Challenges and Potential. *Clin. Cancer Res.* **2011**, *17* (20), 6389–6397. https://doi.org/10.1158/1078-0432.CCR-11-1417.

(88) Shefet-Carasso, L.; Benhar, I. Antibody-Targeted Drugs and Drug Resistance--Challenges and Solutions. *Drug Resist. Updat. Rev. Comment. Antimicrob. Anticancer Chemother.* **2015**, *18*, 36–46. https://doi.org/10.1016/j.drup.2014.11.001.

(89) Dumontet, C.; Jordan, M. A. Microtubule-Binding Agents: A Dynamic Field of Cancer Therapeutics. *Nat. Rev. Drug Discov.* **2010**, *9* (10), 790–803. https://doi.org/10.1038/nrd3253.

(90) Searcey, M. Duocarmycins--Natures Prodrugs? *Curr. Pharm. Des.* **2002**, *8* (15), 1375–1389. https://doi.org/10.2174/1381612023394539.

(91) Hartley, J. A. The Development of Pyrrolobenzodiazepines as Antitumour Agents. *Expert Opin. Investig. Drugs* **2011**, *20* (6), 733–744. https://doi.org/10.1517/13543784.2011.573477.

(92) Smets, L. A. Programmed Cell Death (Apoptosis) and Response to Anti-Cancer Drugs. *Anticancer. Drugs* **1994**, *5* (1), 3–9. https://doi.org/10.1097/00001813-199402000-00001.

(93) Francisco, J. A.; Cerveny, C. G.; Meyer, D. L.; Mixan, B. J.; Klussman, K.; Chace, D. F.; Rejniak, S. X.; Gordon, K. A.; DeBlanc, R.; Toki, B. E.; Law, C.-L.; Doronina, S. O.; Siegall, C. B.; Senter, P. D.; Wahl, A. F. cAC10-vcMMAE, an Anti-CD30-Monomethyl Auristatin E Conjugate with Potent and Selective Antitumor Activity. *Blood* **2003**, *102* (4), 1458–1465. https://doi.org/10.1182/blood-2003-01-0039.

(94) Okeley, N. M.; Miyamoto, J. B.; Zhang, X.; Sanderson, R. J.; Benjamin, D. R.; Sievers, E. L.; Senter, P. D.; Alley, S. C. Intracellular Activation of SGN-35, a Potent Anti-CD30 Antibody-Drug Conjugate. *Clin. Cancer Res. Off. J. Am. Assoc. Cancer Res.* **2010**, *16* (3), 888–897. https://doi.org/10.1158/1078-0432.CCR-09-2069.

(95) Gerber, H.-P.; Kung-Sutherland, M.; Stone, I.; Morris-Tilden, C.; Miyamoto, J.; McCormick, R.; Alley, S. C.; Okeley, N.; Hayes, B.; Hernandez-Ilizaliturri, F. J.; McDonagh, C. F.; Carter, P. J.; Benjamin, D.; Grewal, I. S. Potent Antitumor Activity of the Anti-CD19 Auristatin Antibody Drug Conjugate hBU12-vcMMAE against Rituximab-Sensitive and -Resistant Lymphomas. *Blood* **2009**, *113* (18), 4352–4361. https://doi.org/10.1182/blood-2008-09-179143.

(96) Dornan, D.; Bennett, F.; Chen, Y.; Dennis, M.; Eaton, D.; Elkins, K.; French, D.; Go, M. A. T.; Jack, A.; Junutula, J. R.; Koeppen, H.; Lau, J.; McBride, J.; Rawstron, A.; Shi, X.; Yu, N.; Yu, S.-F.; Yue, P.; Zheng, B.; Ebens, A.; Polson, A. G. Therapeutic Potential of an Anti-CD79b Antibody-Drug Conjugate, Anti-CD79b-vc-MMAE, for the Treatment of Non-Hodgkin Lymphoma. *Blood* **2009**, *114* (13), 2721–2729. https://doi.org/10.1182/blood-2009-02-205500.

(97) Hamblett, K. J. Effects of Drug Loading on the Antitumor Activity of a Monoclonal Antibody Drug Conjugate. *Clin. Cancer Res.* **2004**, *10* (20), 7063–7070. https://doi.org/10.1158/1078-0432.CCR-04-0789.

(98) Oroudjev, E.; Lopus, M.; Wilson, L.; Audette, C.; Provenzano, C.; Erickson, H.; Kovtun, Y.; Chari, R.; Jordan, M. A. Maytansinoid-Antibody Conjugates Induce Mitotic Arrest by Suppressing Microtubule Dynamic Instability. *Mol. Cancer*

Ther. **2010**, *9* (10), 2700–2713. https://doi.org/10.1158/1535-7163.MCT-10-0645.

(99) Poon, K. A.; Flagella, K.; Beyer, J.; Tibbitts, J.; Kaur, S.; Saad, O.; Yi, J.-H.; Girish, S.; Dybdal, N.; Reynolds, T. Preclinical Safety Profile of Trastuzumab Emtansine (T-DM1): Mechanism of Action of Its Cytotoxic Component Retained with Improved Tolerability. *Toxicol. Appl. Pharmacol.* **2013**, *273* (2), 298–313. https://doi.org/10.1016/j.taap.2013.09.003.

(100) Walker, S.; Landovitz, R.; Ding, W. D.; Ellestad, G. A.; Kahne, D. Cleavage Behavior of Calicheamicin Gamma 1 and Calicheamicin T. *Proc. Natl. Acad. Sci. U. S. A.* **1992**, *89* (10), 4608–4612. https://doi.org/10.1073/pnas.89.10.4608.

(101) Lo Coco, F.; Ammatuna, E.; Noguera, N. Treatment of Acute Promyelocytic Leukemia with Gemtuzumab Ozogamicin. *Clin. Adv. Hematol. Oncol. HO* **2006**, *4* (1), 57–62, 76–77.

(102) Tercel, M.; McManaway, S. P.; Leung, E.; Liyanage, H. D. S.; Lu, G.-L.; Pruijn, F. B. The Cytotoxicity of Duocarmycin Analogues Is Mediated through Alkylation of DNA, Not Aldehyde Dehydrogenase 1: A Comment. *Angew. Chem. Int. Ed Engl.* **2013**, *52* (21), 5442–5446. https://doi.org/10.1002/anie.201208373.

(103) Rahman, K. M.; Thompson, A. S.; James, C. H.; Narayanaswamy, M.; Thurston, D. E. The Pyrrolobenzodiazepine Dimer SJG-136 Forms Sequence-Dependent Intrastrand DNA Cross-Links and Monoalkylated Adducts in Addition to Interstrand Cross-Links. *J. Am. Chem. Soc.* **2009**, *131* (38), 13756–13766. https://doi.org/10.1021/ja902986x.

(104) Criscitiello, C.; Morganti, S.; Curigliano, G. Antibody–Drug Conjugates in Solid Tumors: A Look into Novel Targets. *J. Hematol. Oncol.J Hematol Oncol* **2021**, *14* (1), 20. https://doi.org/10.1186/s13045-021-01035-z.

(105) Conilh, L.; Sadilkova, L.; Viricel, W.; Dumontet, C. Payload Diversification: A Key Step in the Development of Antibody–Drug Conjugates. *J. Hematol. Oncol.J Hematol Oncol* **2023**, *16* (1), 1–28. https://doi.org/10.1186/s13045-022-01397-y.

(106) EMA. *Enhertu*. European Medicines Agency. https://www.ema.europa.eu/en/medicines/human/EPAR/enhertu (accessed 2023-07-24).

(107) Pommier, Y. DNA Topoisomerase I Inhibitors: Chemistry, Biology and Interfacial Inhibition. *Chem. Rev.* **2009**, *109* (7), 2894–2902. https://doi.org/10.1021/cr900097c.

(108) Ogitani, Y.; Aida, T.; Hagihara, K.; Yamaguchi, J.; Ishii, C.; Harada, N.; Soma, M.; Okamoto, H.; Oitate, M.; Arakawa, S.; Hirai, T.; Atsumi, R.; Nakada, T.; Hayakawa, I.; Abe, Y.; Agatsuma, T. DS-8201a, A Novel HER2-Targeting ADC with a Novel DNA Topoisomerase I Inhibitor, Demonstrates a Promising Antitumor Efficacy with Differentiation from T-DM1. *Clin. Cancer Res.* **2016**, *22* (20), 5097–5108. https://doi.org/10.1158/1078-0432.CCR-15-2822.

(109) Makhlin, I.; DeMichele, A. Trastuzumab Deruxtecan: An Antibody-Drug Conjugate Embracing Its Destiny in Breast Cancer. *Cell Rep. Med.* **2022**, *3* (6). https://doi.org/10.1016/j.xcrm.2022.100668.

(110) Mckertish, C. M.; Kayser, V. Advances and Limitations of Antibody Drug Conjugates for Cancer. *Biomedicines* **2021**, *9* (8), 872. https://doi.org/10.3390/biomedicines9080872.

(111) *Recombinant microbial (bacterial) transglutaminase - Microbial (Pro)TGase - Microbial Transglutaminase - Products - Zedira GmbH.* https://zedira.com/Microbial-Transglutaminase/Microbial-Pro-TGase/Recombinant-microbial-bacterial-transglutaminase_T001 (accessed 2023-06-19).

(112) *Moo Gloo RM Transglutaminase.* Modernist Pantry, LLC. https://modernistpantry.com/products/moo-gloo-rm-transglutaminase.html (accessed 2023-06-19).

(113) Umezawa, Y.; Ohtsuka, T.; Yokoyama, K.; Nio, N. Comparison of Enzymatic Properties of Microbial Transglutaminase from *Streptomyces* Sp. *Food Sci. Technol. Res.* **2002**, *8* (2), 113–118. https://doi.org/10.3136/fstr.8.113.

(114) Ando, H.; Adachi, M.; Umeda, K.; Matsuura, A.; Nonaka, M.; Uchio, R.; Tanaka, H.; Motoki, M. Purification and Characteristics of a Novel Transglutaminase Derived from Microorganisms. *Agric. Biol. Chem.* **1989**, *53* (10), 2613–2617. https://doi.org/10.1080/00021369.1989.10869735.

(115) Hansen, T.; Vermeeren, P.; Bickelhaupt, M.; Hamlin, T. Origin of the α-Effect in SN2 Reactions. *Angew. Chem. Int. Ed.* **2021**, *60* (38), 20840–20848. https://doi.org/10.1002/anie.202106053.

(116) Nobeli, I.; Price, S. L.; Lommerse, J. P. M.; Taylor, R. Hydrogen Bonding Properties of Oxygen and Nitrogen Acceptors in Aromatic Heterocycles. *J. Comput. Chem.* **1997**, *18* (16), 2060–2074. https://doi.org/10.1002/(SICI)1096-987X(199712)18:16<2060::AID-JCC10>3.0.CO;2-S.

(117) Gnaccarini, C.; Ben-Tahar, W.; Mulani, A.; Roy, I.; Lubell, W. D.; Pelletier, J. N.; Keillor, J. W. Site-Specific Protein Propargylation Using Tissue Transglutaminase. *Org. Biomol. Chem.* **2012**, *10* (27), 5258. https://doi.org/10.1039/c2ob25752a.

(118) Oxidation of Primary Alcohols to Carboxylix Acids With Sodium Chlorite Catalyzed by TEMPO and Bleach: 4-Methoxyphenylacetic Acid. *Org. Synth.* **2005**, *81*, 195. https://doi.org/10.15227/orgsyn.081.0195.

(119) Wang, C.; Huang, K.; Wang, J.; Wang, H.; Liu, L.; Chang, W.; Li, J. Synthesis of Tetrasubstituted Pyrroles from Homopropargylic Amines via a Sonogashira Coupling/Intramolecular Hydroamination/Oxidation Sequence. *Adv. Synth. Catal.* **2015**, *357* (13), 2795–2802. https://doi.org/10.1002/adsc.201500350.

(120) Chang, Z.; Jing, X.; He, C.; Liu, X.; Duan, C. Silver Clusters as Robust Nodes and π–Activation Sites for the Construction of Heterogeneous Catalysts for the Cycloaddition of Propargylamines. *ACS Catal.* **2018**, *8* (2), 1384–1391. https://doi.org/10.1021/acscatal.7b02844.

(121) Green, T.; Wuts, P. Protecting Groups in Organic Synthesis. In *Protecting Groups in Organic Synthesis*; Wiley-Interscience: New York, 1999; p 600.

(122) Green, T.; Wuts, P. Protective Groups in Organic Synthesis. In *Protective Groups in Organic Synthesis*; Wiley-Interscience: New York, 1999; p 1303.

(123) Audrito, V.; Managò, A.; Gaudino, F.; Sorci, L.; Messana, V. G.; Raffaelli, N.; Deaglio, S. NAD-Biosynthetic and Consuming Enzymes as Central Players of Metabolic Regulation of Innate and Adaptive Immune Responses in Cancer. *Front. Immunol.* **2019**, *10*. https://doi.org/10.3389/fimmu.2019.01720.

(124) Ruggieri, S.; Orsomando, G.; Sorci, L.; Raffaelli, N. Regulation of NAD Biosynthetic Enzymes Modulates NAD-Sensing Processes to Shape Mammalian Cell Physiology under Varying Biological Cues. *Biochim. Biophys. Acta - Proteins*

Proteomics **2015**, *1854* (9), 1138–1149. https://doi.org/10.1016/j.bbapap.2015.02.021.

(125) Chiarugi, A.; Dölle, C.; Felici, R.; Ziegler, M. The NAD Metabolome - A Key Determinant of Cancer Cell Biology. *Nat. Rev. Cancer* **2012**, *12* (11), 741–752. https://doi.org/10.1038/nrc3340.

(126) Xie, N.; Zhang, L.; Gao, W.; Huang, C.; Huber, P. E.; Zhou, X.; Li, C.; Shen, G.; Zou, B. NAD+ Metabolism: Pathophysiologic Mechanisms and Therapeutic Potential. *Signal Transduct. Target. Ther.* **2020**, *5* (1). https://doi.org/10.1038/s41392-020-00311-7.

(127) Gasparrini, M.; Audrito, V. NAMPT: A Critical Driver and Therapeutic Target for Cancer. *Int. J. Biochem. Cell Biol.* **2022**, *145*, 106189. https://doi.org/10.1016/j.biocel.2022.106189.

(128) Garten, A.; Schuster, S.; Penke, M.; Gorski, T.; de Giorgis, T.; Kiess, W. Physiological and Pathophysiological Roles of NAMPT and NAD Metabolism. *Nat. Rev. Endocrinol.* **2015**, *11* (9), 535–546. https://doi.org/10.1038/nrendo.2015.117.

(129) Revollo, J. R.; Grimm, A. A.; Imai, S. The Regulation of Nicotinamide Adenine Dinucleotide Biosynthesis by Nampt/PBEF/Visfatin in Mammals: *Curr. Opin. Gastroenterol.* **2007**, *23* (2), 164–170. https://doi.org/10.1097/MOG.0b013e32801b3c8f.

(130) Yoshida, M.; Satoh, A.; Lin, J. B.; Mills, K. F.; Sasaki, Y.; Rensing, N.; Wong, M.; Apte, R. S.; Imai, S.-I. Extracellular Vesicle-Contained eNAMPT Delays Aging and Extends Lifespan in Mice. *Cell Metab.* **2019**, *30* (2), 329-342.e5. https://doi.org/10.1016/j.cmet.2019.05.015.

(131) Yoon, M. J.; Yoshida, M.; Johnson, S.; Takikawa, A.; Usui, I.; Tobe, K.; Nakagawa, T.; Yoshino, J.; Imai, S.-I. SIRT1-Mediated eNAMPT Secretion from Adipose Tissue Regulates Hypothalamic NAD+ and Function in Mice. *Cell Metab.* **2015**, *21* (5), 706–717. https://doi.org/10.1016/j.cmet.2015.04.002.

(132) Hara, N.; Yamada, K.; Shibata, T.; Osago, H.; Tsuchiya, M. Nicotinamide Phosphoribosyltransferase/Visfatin Does Not Catalyze Nicotinamide Mononucleotide Formation in Blood Plasma. *PLoS ONE* **2011**, *6* (8). https://doi.org/10.1371/journal.pone.0022781.

(133) Zamporlini, F.; Ruggieri, S.; Mazzola, F.; Amici, A.; Orsomando, G.; Raffaelli, N. Novel Assay for Simultaneous Measurement of Pyridine Mononucleotides Synthesizing Activities Allows Dissection of the NAD(+) Biosynthetic Machinery in Mammalian Cells. *FEBS J.* **2014**, *281* (22), 5104–5119. https://doi.org/10.1111/febs.13050.

(134) Audrito, V.; Serra, S.; Brusa, D.; Mazzola, F.; Arruga, F.; Vaisitti, T.; Coscia, M.; Maffei, R.; Rossi, D.; Wang, T.; Inghirami, G.; Rizzi, M.; Gaidano, G.; Garcia, J. G. N.; Wolberger, C.; Raffaelli, N.; Deaglio, S. Extracellular Nicotinamide Phosphoribosyltransferase (NAMPT) Promotes M2 Macrophage Polarization in Chronic Lymphocytic Leukemia. *Blood* **2015**, *125* (1), 111–123. https://doi.org/10.1182/blood-2014-07-589069.

(135) Dalamaga, M.; Christodoulatos, G. S.; Mantzoros, C. S. The Role of Extracellular and Intracellular Nicotinamide Phosphoribosyl-Transferase in Cancer: Diagnostic and Therapeutic Perspectives and Challenges. *Metabolism.* **2018**, *82*, 72–87. https://doi.org/10.1016/j.metabol.2018.01.001.

(136) Navas, L. E.; Carnero, A. NAD+ Metabolism, Stemness, the Immune Response, and Cancer. *Signal Transduct. Target. Ther.* **2021**, *6* (1). https://doi.org/10.1038/s41392-020-00354-w.

(137) Vander Heiden, M. G.; Cantley, L. C.; Thompson, C. B. Understanding the Warburg Effect: The Metabolic Requirements of Cell Proliferation. *Science* **2009**, *324* (5930), 1029–1033. https://doi.org/10.1126/science.1160809.

(138) Warburg, O. On Respiratory Impairment in Cancer Cells. *Science* **1956**, *124* (3215), 269–270.

(139) Gatenby, R. A.; Gillies, R. J. Why Do Cancers Have High Aerobic Glycolysis? *Nat. Rev. Cancer* **2004**, *4* (11), 891–899. https://doi.org/10.1038/nrc1478.

(140) Estrella, V.; Chen, T.; Lloyd, M.; Wojtkowiak, J.; Cornnell, H. H.; Ibrahim-Hashim, A.; Bailey, K.; Balagurunathan, Y.; Rothberg, J. M.; Sloane, B. F.; Johnson, J.; Gatenby, R. A.; Gillies, R. J. Acidity Generated by the Tumor Microenvironment Drives Local Invasion. *Cancer Res.* **2013**, *73* (5), 1524–1535. https://doi.org/10.1158/0008-5472.CAN-12-2796.

(141) Colegio, O. R.; Chu, N.-Q.; Szabo, A. L.; Chu, T.; Rhebergen, A. M.; Jairam, V.; Cyrus, N.; Brokowski, C. E.; Eisenbarth, S. C.; Phillips, G. M.; Cline, G. W.; Phillips, A. J.; Medzhitov, R. Functional Polarization of Tumour-Associated Macrophages by Tumour-Derived Lactic Acid. *Nature* **2014**, *513* (7519), 559–563. https://doi.org/10.1038/nature13490.

(142) Batra, S.; Adekola, K. U. A.; Rosen, S. T.; Shanmugam, M. Cancer Metabolism as a Therapeutic Target. *Oncol. Williston Park N* **2013**, *27* (5), 460–467.

(143) Moreira, J. D. V.; Hamraz, M.; Abolhassani, M.; Bigan, E.; Pérès, S.; Paulevé, L.; Nogueira, M. L.; Steyaert, J.-M.; Schwartz, L. The Redox Status of Cancer Cells Supports Mechanisms behind the Warburg Effect. *Metabolites* **2016**, *6* (4), 33. https://doi.org/10.3390/metabo6040033.

(144) DeBerardinis, R. J.; Lum, J. J.; Hatzivassiliou, G.; Thompson, C. B. The Biology of Cancer: Metabolic Reprogramming Fuels Cell Growth and Proliferation. *Cell Metab.* **2008**, *7* (1), 11–20. https://doi.org/10.1016/j.cmet.2007.10.002.

(145) Hong, S. M.; Hwang, S. W.; Wang, T.; Park, C. W.; Ryu, Y.-M.; Jung, J.-H.; Shin, J. H.; Kim, S.-Y.; Lee, J. L.; Kim, C. W.; Yoon, G.; Kim, K. H.; Myung, S.-J.; Choi, K. Y. Increased Nicotinamide Adenine Dinucleotide Pool Promotes Colon Cancer Progression by Suppressing Reactive Oxygen Species Level. *Cancer Sci.* **2019**, *110* (2), 629–638. https://doi.org/10.1111/cas.13886.

(146) Lucena-Cacace, A.; Otero-Albiol, D.; Jiménez-García, M. P.; Muñoz-Galvan, S.; Carnero, A. NAMPT Is a Potent Oncogene in Colon Cancer Progression That Modulates Cancer Stem Cell Properties and Resistance to Therapy through Sirt1 and PARP. *Clin. Cancer Res. Off. J. Am. Assoc. Cancer Res.* **2018**, *24* (5), 1202–1215. https://doi.org/10.1158/1078-0432.CCR-17-2575.

(147) Lucena-Cacace, A.; Otero-Albiol, D.; Jiménez-García, M. P.; Peinado-Serrano, J.; Carnero, A. NAMPT Overexpression Induces Cancer Stemness and Defines a Novel Tumor Signature for Glioma Prognosis. *Oncotarget* **2017**, *8* (59), 99514–99530. https://doi.org/10.18632/oncotarget.20577.

(148) Barraud, M.; Garnier, J.; Loncle, C.; Gayet, O.; Lequeue, C.; Vasseur, S.; Bian, B.; Duconseil, P.; Gilabert, M.; Bigonnet, M.; Maignan, A.; Moutardier, V.; Garcia, S.; Turrini, O.; Delpero, J.-R.; Giovannini, M.; Grandval, P.; Gasmi, M.; Ouaissi, M.; Secq, V.; Poizat, F.; Guibert, N.; Iovanna, J.; Dusetti, N. A Pancreatic Ductal

Adenocarcinoma Subpopulation Is Sensitive to FK866, an Inhibitor of NAMPT. *Oncotarget* **2016**, *7* (33), 53783–53796. https://doi.org/10.18632/oncotarget.10776.

(149) Espindola-Netto, J. M.; Chini, C. C. S.; Tarragó, M.; Wang, E.; Dutta, S.; Pal, K.; Mukhopadhyay, D.; Sola-Penna, M.; Chini, E. N. Preclinical Efficacy of the Novel Competitive NAMPT Inhibitor STF-118804 in Pancreatic Cancer. *Oncotarget* **2017**, *8* (49), 85054–85067. https://doi.org/10.18632/oncotarget.18841.

(150) Sampath, D.; Zabka, T. S.; Misner, D. L.; O'Brien, T.; Dragovich, P. S. Inhibition of Nicotinamide Phosphoribosyltransferase (NAMPT) as a Therapeutic Strategy in Cancer. *Pharmacol. Ther.* **2015**, *151*, 16–31. https://doi.org/10.1016/j.pharmthera.2015.02.004.

(151) Bi, T.; Che, X. Nampt/PBEF/Visfatin and Cancer. *Cancer Biol. Ther.* **2010**, *10* (2), 119–125. https://doi.org/10.4161/cbt.10.2.12581.

(152) Galli, U.; Colombo, G.; Travelli, C.; Tron, G. C.; Genazzani, A. A.; Grolla, A. A. Recent Advances in NAMPT Inhibitors: A Novel Immunotherapic Strategy. *Front. Pharmacol.* **2020**, *11*, 656. https://doi.org/10.3389/fphar.2020.00656.

(153) Wei, Y.; Xiang, H.; Zhang, W. Review of Various NAMPT Inhibitors for the Treatment of Cancer. *Front. Pharmacol.* **2022**, *13*, 970553. https://doi.org/10.3389/fphar.2022.970553.

(154) Hasmann, M.; Schemainda, I. FK866, a Highly Specific Noncompetitive Inhibitor of Nicotinamide Phosphoribosyltransferase, Represents a Novel Mechanism for Induction of Tumor Cell Apoptosis. 8.

(155) Khan, J. A.; Tao, X.; Tong, L. Molecular Basis for the Inhibition of Human NMPRTase, a Novel Target for Anticancer Agents. *Nat. Struct. Mol. Biol.* **2006**, *13* (7), 582–588. https://doi.org/10.1038/nsmb1105.

(156) Oh, A.; Ho, Y.-C.; Zak, M.; Liu, Y.; Chen, X.; Yuen, P.-W.; Zheng, X.; Liu, Y.; Dragovich, P. S.; Wang, W. Structural and Biochemical Analyses of the Catalysis and Potency Impact of Inhibitor Phosphoribosylation by Human Nicotinamide Phosphoribosyltransferase. *Chembiochem Eur. J. Chem. Biol.* **2014**, *15* (8), 1121–1130. https://doi.org/10.1002/cbic.201402023.

(157) Bai, J.; Liao, C.; Liu, Y.; Qin, X.; Chen, J.; Qiu, Y.; Qin, D.; Li, Z.; Tu, Z.-C.; Jiang, S. Structure-Based Design of Potent Nicotinamide Phosphoribosyltransferase Inhibitors with Promising in Vitro and in Vivo Antitumor Activities. *J. Med. Chem.* **2016**, *59* (12), 5766–5779. https://doi.org/10.1021/acs.jmedchem.6b00324.

(158) Zhang, K.; Ni, Y.; Chen, J.; Tu, Z.; Wu, X.; Chen, D.; Yao, H.; Jiang, S. Discovery of Trans-3-(Pyridin-3-Yl)Acrylamide-Derived Sulfamides as Potent Nicotinamide Phosphoribosyltransferase (NAMPT) Inhibitors for the Potential Treatment of Cancer. *Bioorg. Med. Chem. Lett.* **2019**, *29* (12), 1502–1506. https://doi.org/10.1016/j.bmcl.2019.04.013.

(159) Colombano, G.; Travelli, C.; Galli, U.; Caldarelli, A.; Chini, M. G.; Canonico, P. L.; Sorba, G.; Bifulco, G.; Tron, G. C.; Genazzani, A. A. A Novel Potent Nicotinamide Phosphoribosyltransferase Inhibitor Synthesized via Click Chemistry. *J. Med. Chem.* **2010**, *53* (2), 616–623. https://doi.org/10.1021/jm9010669.

(160) Travelli, C.; Aprile, S.; Rahimian, R.; Grolla, A. A.; Rogati, F.; Bertolotti, M.; Malagnino, F.; di Paola, R.; Impellizzeri, D.; Fusco, R.; Mercalli, V.; Massarotti, A.; Stortini, G.; Terrazzino, S.; Del Grosso, E.; Fakhfouri, G.; Troiani, M. P.; Alisi, M. A.; Grosa, G.; Sorba, G.; Canonico, P. L.; Orsomando, G.; Cuzzocrea, S.;

Genazzani, A. A.; Galli, U.; Tron, G. C. Identification of Novel Triazole-Based Nicotinamide Phosphoribosyltransferase (NAMPT) Inhibitors Endowed with Antiproliferative and Antiinflammatory Activity. *J. Med. Chem.* **2017**, *60* (5), 1768–1792. https://doi.org/10.1021/acs.jmedchem.6b01392.

(161) Theeramunkong, S.; Galli, U.; Grolla, A. A.; Caldarelli, A.; Travelli, C.; Massarotti, A.; Troiani, M. P.; Alisi, M. A.; Orsomando, G.; Genazzani, A. A.; Tron, G. C. Identification of a Novel NAMPT Inhibitor by Combinatorial Click Chemistry and Chemical Refinement. *MedChemComm* **2015**, *6* (10), 1891–1897. https://doi.org/10.1039/C5MD00261C.

(162) Zak, M.; Yuen, P.; Liu, X.; Patel, S.; Sampath, D.; Oeh, J.; Liederer, B. M.; Wang, W.; O'Brien, T.; Xiao, Y.; Skelton, N.; Hua, R.; Sodhi, J.; Wang, Y.; Zhang, L.; Zhao, G.; Zheng, X.; Ho, Y.-C.; Bair, K. W.; Dragovich, P. S. Minimizing CYP2C9 Inhibition of Exposed-Pyridine NAMPT (Nicotinamide Phosphoribosyltransferase) Inhibitors. *J. Med. Chem.* **2016**, *59* (18), 8345–8368. https://doi.org/10.1021/acs.jmedchem.6b00697.

(163) Zak, M.; Liederer, B. M.; Sampath, D.; Yuen, P.-W.; Bair, K. W.; Baumeister, T.; Buckmelter, A. J.; Clodfelter, K. H.; Cheng, E.; Crocker, L.; Fu, B.; Han, B.; Li, G.; Ho, Y.-C.; Lin, J.; Liu, X.; Ly, J.; O'Brien, T.; Reynolds, D. J.; Skelton, N.; Smith, C. C.; Tay, S.; Wang, W.; Wang, Z.; Xiao, Y.; Zhang, L.; Zhao, G.; Zheng, X.; Dragovich, P. S. Identification of Nicotinamide Phosphoribosyltransferase (NAMPT) Inhibitors with No Evidence of CYP3A4 Time-Dependent Inhibition and Improved Aqueous Solubility. *Bioorg. Med. Chem. Lett.* **2015**, *25* (3), 529–541. https://doi.org/10.1016/j.bmcl.2014.12.026.

(164) Wilsbacher, J. L.; Cheng, M.; Cheng, D.; Trammell, S. A. J.; Shi, Y.; Guo, J.; Koeniger, S. L.; Kovar, P. J.; He, Y.; Selvaraju, S.; Heyman, H. R.; Sorensen, B. K.; Clark, R. F.; Hansen, T. M.; Longenecker, K. L.; Raich, D.; Korepanova, A. V.; Cepa, S.; Towne, D. L.; Abraham, V. C.; Tang, H.; Richardson, P. L.; McLoughlin, S. M.; Badagnani, I.; Curtin, M. L.; Michaelides, M. R.; Maag, D.; Buchanan, F. G.; Chiang, G. G.; Gao, W.; Rosenberg, S. H.; Brenner, C.; Tse, C. Discovery and Characterization of Novel Nonsubstrate and Substrate NAMPT Inhibitors. *Mol. Cancer Ther.* **2017**, *16* (7), 1236–1245. https://doi.org/10.1158/1535-7163.MCT-16-0819.

(165) Holen, K.; Saltz, L. B.; Hollywood, E.; Burk, K.; Hanauske, A.-R. The Pharmacokinetics, Toxicities, and Biologic Effects of FK866, a Nicotinamide Adenine Dinucleotide Biosynthesis Inhibitor. *Invest. New Drugs* **2008**, *26* (1), 45–51. https://doi.org/10.1007/s10637-007-9083-2.

(166) Goldinger, S. M.; Gobbi Bischof, S.; Fink-Puches, R.; Klemke, C.-D.; Dréno, B.; Bagot, M.; Dummer, R. Efficacy and Safety of APO866 in Patients With Refractory or Relapsed Cutaneous T-Cell Lymphoma: A Phase 2 Clinical Trial. *JAMA Dermatol.* **2016**, *152* (7), 837–839. https://doi.org/10.1001/jamadermatol.2016.0401.

(167) Olesen, U. H.; Thougaard, A. V.; Jensen, P. B.; Sehested, M. A Preclinical Study on the Rescue of Normal Tissue by Nicotinic Acid in High-Dose Treatment with APO866, a Specific Nicotinamide Phosphoribosyltransferase Inhibitor. *Mol. Cancer Ther.* **2010**, *9* (6), 1609–1617. https://doi.org/10.1158/1535-7163.MCT-09-1130.

(168) Ghanem, M. S.; Monacelli, F.; Nencioni, A. Advances in NAD-Lowering Agents for Cancer Treatment. *Nutrients* **2021**, *13* (5), 1665. https://doi.org/10.3390/nu13051665.

(169) Karpov, A. S.; Abrams, T.; Clark, S.; Raikar, A.; D'Alessio, J. A.; Dillon, M. P.; Gesner, T. G.; Jones, D.; Lacaud, M.; Mallet, W.; Martyniuk, P.; Meredith, E.; Mohseni, M.; Nieto-Oberhuber, C. M.; Palacios, D.; Perruccio, F.; Piizzi, G.; Zurini, M.; Bialucha, C. U. Nicotinamide Phosphoribosyltransferase Inhibitor as a Novel Payload for Antibody–Drug Conjugates. *ACS Med. Chem. Lett.* **2018**, *9* (8), 838–842. https://doi.org/10.1021/acsmedchemlett.8b00254.

(170) Neumann, C. S.; Olivas, K. C.; Anderson, M. E.; Cochran, J. H.; Jin, S.; Li, F.; Loftus, L. V.; Meyer, D. W.; Neale, J.; Nix, J. C.; Pittman, P. G.; Simmons, J. K.; Ulrich, M. L.; Waight, A. B.; Wong, A.; Zaval, M. C.; Zeng, W.; Lyon, R. P.; Senter, P. D. Targeted Delivery of Cytotoxic NAMPT Inhibitors Using Antibody–Drug Conjugates. *Mol. Cancer Ther.* **2018**, *17* (12), 2633–2642. https://doi.org/10.1158/1535-7163.MCT-18-0643.

(171) Böhnke, N.; Berger, M.; Griebenow, N.; Rottmann, A.; Erkelenz, M.; Hammer, S.; Berndt, S.; Günther, J.; Wengner, A. M.; Stelte-Ludwig, B.; Mahlert, C.; Greven, S.; Dietz, L.; Jörißen, H.; Barak, N.; Bömer, U.; Hillig, R. C.; Eberspaecher, U.; Weiske, J.; Giese, A.; Mumberg, D.; Nising, C. F.; Weinmann, H.; Sommer, A. A Novel NAMPT Inhibitor-Based Antibody–Drug Conjugate Payload Class for Cancer Therapy. *Bioconjug. Chem.* **2022**, *33* (6), 1210–1221. https://doi.org/10.1021/acs.bioconjchem.2c00178.

(172) Ciechanover, A.; Orian, A.; Schwartz, A. L. Ubiquitin-Mediated Proteolysis: Biological Regulation via Destruction. *BioEssays News Rev. Mol. Cell. Dev. Biol.* **2000**, *22* (5), 442–451. https://doi.org/10.1002/(SICI)1521-1878(200005)22:5<442::AID-BIES6>3.0.CO;2-Q.

(173) Koegl, M.; Hoppe, T.; Schlenker, S.; Ulrich, H. D.; Mayer, T. U.; Jentsch, S. A Novel Ubiquitination Factor, E4, Is Involved in Multiubiquitin Chain Assembly. *Cell* **1999**, *96* (5), 635–644. https://doi.org/10.1016/s0092-8674(00)80574-7.

(174) Pei, H.; Peng, Y.; Zhao, Q.; Chen, Y. Small Molecule PROTACs: An Emerging Technology for Targeted Therapy in Drug Discovery. *RSC Adv.* **2019**, *9* (30), 16967–16976. https://doi.org/10.1039/C9RA03423D.

(175) Zoppi, V.; Hughes, S. J.; Maniaci, C.; Testa, A.; Gmaschitz, T.; Wieshofer, C.; Koegl, M.; Riching, K. M.; Daniels, D. L.; Spallarossa, A.; Ciulli, A. Iterative Design and Optimization of Initially Inactive Proteolysis Targeting Chimeras (PROTACs) Identify VZ185 as a Potent, Fast, and Selective von Hippel–Lindau (VHL) Based Dual Degrader Probe of BRD9 and BRD7. *J. Med. Chem.* **2019**, *62* (2), 699–726. https://doi.org/10.1021/acs.jmedchem.8b01413.

(176) Hopkins, A. L.; Groom, C. R. The Druggable Genome. *Nat. Rev. Drug Discov.* **2002**, *1* (9), 727–730. https://doi.org/10.1038/nrd892.

(177) Lai, A. C.; Crews, C. M. Induced Protein Degradation: An Emerging Drug Discovery Paradigm. *Nat. Rev. Drug Discov.* **2017**, *16* (2), 101–114. https://doi.org/10.1038/nrd.2016.211.

(178) Adjei, A. A. What Is the Right Dose? The Elusive Optimal Biologic Dose in Phase I Clinical Trials. *J. Clin. Oncol. Off. J. Am. Soc. Clin. Oncol.* **2006**, *24* (25), 4054–4055. https://doi.org/10.1200/JCO.2006.07.4658.

(179) Lai, A. C.; Toure, M.; Hellerschmied, D.; Salami, J.; Jaime-Figueroa, S.; Ko, E.; Hines, J.; Crews, C. M. Modular PROTAC Design for the Degradation of Oncogenic BCR-ABL. *Angew. Chem. Int. Ed Engl.* **2016**, *55* (2), 807–810. https://doi.org/10.1002/anie.201507634.

(180) Zengerle, M.; Chan, K.-H.; Ciulli, A. Selective Small Molecule Induced Degradation of the BET Bromodomain Protein BRD4. *ACS Chem. Biol.* **2015**, *10* (8), 1770–1777. https://doi.org/10.1021/acschembio.5b00216.

(181) Visakorpi, T.; Hyytinen, E.; Koivisto, P.; Tanner, M.; Keinänen, R.; Palmberg, C.; Palotie, A.; Tammela, T.; Isola, J.; Kallioniemi, O. P. In Vivo Amplification of the Androgen Receptor Gene and Progression of Human Prostate Cancer. *Nat. Genet.* **1995**, *9* (4), 401–406. https://doi.org/10.1038/ng0495-401.

(182) An, S.; Fu, L. Small-Molecule PROTACs: An Emerging and Promising Approach for the Development of Targeted Therapy Drugs. *EBioMedicine* **2018**, *36*, 553–562. https://doi.org/10.1016/j.ebiom.2018.09.005.

(183) Balbas, M. D.; Evans, M. J.; Hosfield, D. J.; Wongvipat, J.; Arora, V. K.; Watson, P. A.; Chen, Y.; Greene, G. L.; Shen, Y.; Sawyers, C. L. Overcoming Mutation-Based Resistance to Antiandrogens with Rational Drug Design. *eLife* **2013**, *2*, e00499. https://doi.org/10.7554/eLife.00499.

(184) Tsubata, Y.; Tanino, R.; Isobe, T. Current Therapeutic Strategies and Prospects for EGFR Mutation-Positive Lung Cancer Based on the Mechanisms Underlying Drug Resistance. *Cells* **2021**, *10* (11), 3192. https://doi.org/10.3390/cells10113192.

(185) Buhimschi, A. D.; Armstrong, H. A.; Toure, M.; Jaime-Figueroa, S.; Chen, T. L.; Lehman, A. M.; Woyach, J. A.; Johnson, A. J.; Byrd, J. C.; Crews, C. M. Targeting the C481S Ibrutinib-Resistance Mutation in Bruton's Tyrosine Kinase Using PROTAC-Mediated Degradation. *Biochemistry* **2018**, *57* (26), 3564–3575. https://doi.org/10.1021/acs.biochem.8b00391.

(186) Sun, Y.; Zhao, X.; Ding, N.; Gao, H.; Wu, Y.; Yang, Y.; Zhao, M.; Hwang, J.; Song, Y.; Liu, W.; Rao, Y. PROTAC-Induced BTK Degradation as a Novel Therapy for Mutated BTK C481S Induced Ibrutinib-Resistant B-Cell Malignancies. *Cell Res.* **2018**, *28* (7), 779–781. https://doi.org/10.1038/s41422-018-0055-1.

(187) Sun, B.; Fiskus, W.; Qian, Y.; Rajapakshe, K.; Raina, K.; Coleman, K. G.; Crew, A. P.; Shen, A.; Saenz, D. T.; Mill, C. P.; Nowak, A. J.; Jain, N.; Zhang, L.; Wang, M.; Khoury, J. D.; Coarfa, C.; Crews, C. M.; Bhalla, K. N. BET Protein Proteolysis Targeting Chimera (PROTAC) Exerts Potent Lethal Activity against Mantle Cell Lymphoma Cells. *Leukemia* **2018**, *32* (2), 343–352. https://doi.org/10.1038/leu.2017.207.

(188) Burslem, G. M.; Smith, B. E.; Lai, A. C.; Jaime-Figueroa, S.; McQuaid, D. C.; Bondeson, D. P.; Toure, M.; Dong, H.; Qian, Y.; Wang, J.; Crew, A. P.; Hines, J.; Crews, C. M. The Advantages of Targeted Protein Degradation Over Inhibition: An RTK Case Study. *Cell Chem. Biol.* **2018**, *25* (1), 67-77.e3. https://doi.org/10.1016/j.chembiol.2017.09.009.

(189) Sakamoto, K. M.; Kim, K. B.; Kumagai, A.; Mercurio, F.; Crews, C. M.; Deshaies, R. J. Protacs: Chimeric Molecules That Target Proteins to the Skp1–Cullin–F Box Complex for Ubiquitination and Degradation. *Proc. Natl. Acad. Sci.* **2001**, *98* (15), 8554–8559. https://doi.org/10.1073/pnas.141230798.

(190) Li, X.; Chang, Y. H. Amino-Terminal Protein Processing in Saccharomyces Cerevisiae Is an Essential Function That Requires Two Distinct Methionine Aminopeptidases. *Proc. Natl. Acad. Sci. U. S. A.* **1995**, *92* (26), 12357–12361. https://doi.org/10.1073/pnas.92.26.12357.

(191) Ehlers, T.; Furness, S.; Robinson, T. P.; Zhong, H. A.; Goldsmith, D.; Aribser, J.; Bowen, J. P. Methionine AminoPeptidase Type-2 Inhibitors Targeting Angiogenesis. *Curr. Top. Med. Chem.* **2016**, *16* (13), 1478–1488. https://doi.org/10.2174/1568026615666150915121204.

(192) Sin, N.; Meng, L.; Wang, M. Q. W.; Wen, J. J.; Bornmann, W. G.; Crews, C. M. The Anti-Angiogenic Agent Fumagillin Covalently Binds and Inhibits the Methionine Aminopeptidase, MetAP-2. *Proc. Natl. Acad. Sci. U. S. A.* **1997**, *94* (12), 6099–6103.

(193) Griffith, E. C.; Su, Z.; Turk, B. E.; Chen, S.; Chang, Y. H.; Wu, Z.; Biemann, K.; Liu, J. O. Methionine Aminopeptidase (Type 2) Is the Common Target for Angiogenesis Inhibitors AGM-1470 and Ovalicin. *Chem. Biol.* **1997**, *4* (6), 461–471. https://doi.org/10.1016/s1074-5521(97)90198-8.

(194) Ivan, M.; Kondo, K.; Yang, H.; Kim, W.; Valiando, J.; Ohh, M.; Salic, A.; Asara, J. M.; Lane, W. S.; Kaelin Jr., W. G. HIFα Targeted for VHL-Mediated Destruction by Proline Hydroxylation: Implications for O2 Sensing. *Science* **2001**, *292* (5516), 464–468. https://doi.org/10.1126/science.1059817.

(195) Jaakkola, P.; Mole, D. R.; Tian, Y.-M.; Wilson, M. I.; Gielbert, J.; Gaskell, S. J.; Kriegsheim, A. von; Hebestreit, H. F.; Mukherji, M.; Schofield, C. J.; Maxwell, P. H.; Pugh, ‡ Christopher W.; Ratcliffe, ‡ Peter J. Targeting of HIF-α to the von Hippel-Lindau Ubiquitylation Complex by O2-Regulated Prolyl Hydroxylation. *Science* **2001**, *292* (5516), 468–472. https://doi.org/10.1126/science.1059796.

(196) Hon, W.-C.; Wilson, M. I.; Harlos, K.; Claridge, T. D. W.; Schofield, C. J.; Pugh, C. W.; Maxwell, P. H.; Ratcliffe, P. J.; Stuart, D. I.; Jones, E. Y. Structural Basis for the Recognition of Hydroxyproline in HIF-1 Alpha by pVHL. *Nature* **2002**, *417* (6892), 975–978. https://doi.org/10.1038/nature00767.

(197) Min, J.-H.; Yang, H.; Ivan, M.; Gertler, F.; Kaelin, W. G.; Pavletich, N. P. Structure of an HIF-1alpha -pVHL Complex: Hydroxyproline Recognition in Signaling. *Science* **2002**, *296* (5574), 1886–1889. https://doi.org/10.1126/science.1073440.

(198) Schneekloth, J. S. Jr.; Fonseca, F. N.; Koldobskiy, M.; Mandal, A.; Deshaies, R.; Sakamoto, K.; Crews, C. M. Chemical Genetic Control of Protein Levels: Selective in Vivo Targeted Degradation. *J. Am. Chem. Soc.* **2004**, *126* (12), 3748–3754. https://doi.org/10.1021/ja039025z.

(199) Deshayes, S.; Morris, M. C.; Divita, G.; Heitz, F. Cell-Penetrating Peptides: Tools for Intracellular Delivery of Therapeutics. *Cell. Mol. Life Sci. CMLS* **2005**, *62* (16), 1839–1849. https://doi.org/10.1007/s00018-005-5109-0.

(200) Diehl, C. J.; Ciulli, A. Discovery of Small Molecule Ligands for the von Hippel-Lindau (VHL) E3 Ligase and Their Use as Inhibitors and PROTAC Degraders. *Chem. Soc. Rev.* **2022**, *51* (19), 8216–8257. https://doi.org/10.1039/D2CS00387B.

(201) Buckley, D. L.; Van Molle, I.; Gareiss, P. C.; Tae, H. S.; Michel, J.; Noblin, D. J.; Jorgensen, W. L.; Ciulli, A.; Crews, C. M. Targeting the von Hippel–Lindau E3 Ubiquitin Ligase Using Small Molecules To Disrupt the VHL/HIF-1α Interaction.

J. Am. Chem. Soc. **2012**, *134* (10), 4465–4468. https://doi.org/10.1021/ja209924v.

(202) Galdeano, C.; Gadd, M. S.; Soares, P.; Scaffidi, S.; Van Molle, I.; Birced, I.; Hewitt, S.; Dias, D. M.; Ciulli, A. Structure-Guided Design and Optimization of Small Molecules Targeting the Protein-Protein Interaction between the von Hippel-Lindau (VHL) E3 Ubiquitin Ligase and the Hypoxia Inducible Factor (HIF) Alpha Subunit with in Vitro Nanomolar Affinities. *J. Med. Chem.* **2014**, *57* (20), 8657–8663. https://doi.org/10.1021/jm5011258.

(203) Gable, K. *Thalidomide and the Importance of Stereochemistry*. https://sites.science.oregonstate.edu/~gablek/CH334/Chapter5/Thalidomide.htm.

(204) Kim, J. H.; Scialli, A. R. Thalidomide: The Tragedy of Birth Defects and the Effective Treatment of Disease. *Toxicol. Sci. Off. J. Soc. Toxicol.* **2011**, *122* (1), 1–6. https://doi.org/10.1093/toxsci/kfr088.

(205) Ito, T.; Ando, H.; Suzuki, T.; Ogura, T.; Hotta, K.; Imamura, Y.; Yamaguchi, Y.; Handa, H. Identification of a Primary Target of Thalidomide Teratogenicity. *Science* **2010**, *327* (5971), 1345–1350. https://doi.org/10.1126/science.1177319.

(206) Teo, S. K.; Resztak, K. E.; Scheffler, M. A.; Kook, K. A.; Zeldis, J. B.; Stirling, D. I.; Thomas, S. D. Thalidomide in the Treatment of Leprosy. *Microbes Infect.* **2002**, *4* (11), 1193–1202. https://doi.org/10.1016/S1286-4579(02)01645-3.

(207) Vasiliauskas, E. A.; Kam, L. Y.; Abreu-Martin, M. T.; Hassard, P. V.; Papadakis, K. A.; Yang, H.; Zeldis, J. B.; Targan, S. R. An Open-Label Pilot Study of Low-Dose Thalidomide in Chronically Active, Steroid-Dependent Crohn's Disease. *Gastroenterology* **1999**, *117* (6), 1278–1287. https://doi.org/10.1016/S0016-5085(99)70277-5.

(208) Ehrenpreis, E. D.; Kane, S. V.; Cohen, L. B.; Cohen, R. D.; Hanauer, S. B. Thalidomide Therapy for Patients with Refractory Crohn's Disease: An Open-Label Trial. *Gastroenterology* **1999**, *117* (6), 1271–1277. https://doi.org/10.1016/S0016-5085(99)70276-3.

(209) Fife, K.; Phillips, R. H.; Howard, M. R.; Bower, M.; Gracie, F. Activity of Thalidomide in AIDS-Related Kaposi's Sarcoma and Correlation with HHV8 Titre. *Int. J. STD AIDS* **1998**, *9* (12), 751–755. https://doi.org/10.1258/0956462981921512.

(210) Jacobson, J. M.; Greenspan, J. S.; Spritzler, J.; Ketter, N.; Fahey, J. L.; Brooks Jackson, J.; Fox, L.; Chernoff, M.; Wu, W. W. A.; MacPhail, L. A.; Vasquez, G. J.; Wohl, D. A. Thalidomide for the Treatment of Oral Aphthous Ulcers in Patients with Human Immunodeficiency Virus Infection. *N. Engl. J. Med.* **1997**, *336* (21), 1487–1493. https://doi.org/10.1056/NEJM199705223362103.

(211) Rajkumar, S. V.; Fonseca, R.; Dispenzieri, A.; Lacy, M. Q.; Lust, J. A.; Witzig, T. E.; Kyle, R. A.; Gertz, M. A.; Greipp, P. R. Thalidomide in the Treatment of Relapsed Multiple Myeloma. *Mayo Clin. Proc.* **2000**, *75* (9), 897–901. https://doi.org/10.4065/75.9.897.

(212) Figg, W. D.; Dahut, W.; Duray, P.; Hamilton, M.; Tompkins, A.; Steinberg, S. M.; Jones, E.; Premkumar, A.; Linehan, W. M.; Floeter, M. K.; Chen, C. C.; Dixon, S.; Kohler, D. R.; Krüger, E. A.; Gubish, E.; Pluda, J. M.; Reed, E. A Randomized Phase

II Trial of Thalidomide, an Angiogenesis Inhibitor, in Patients with Androgen-Independent Prostate Cancer. *Clin. Cancer Res.* **2001**, *7* (7), 1888–1893.

(213) Drake, M. J.; Robson, W.; Mehta, P.; Schofield, I.; Neal, D. E.; Leung, H. Y. An Open-Label Phase II Study of Low-Dose Thalidomide in Androgen-Independent Prostate Cancer. *Br. J. Cancer* **2003**, *88* (6), 822–827. https://doi.org/10.1038/sj.bjc.6600817.

(214) Eisen, T.; Boshoff, C.; Mak, I.; Sapunar, F.; Vaughan, M. M.; Pyle, L.; Johnston, S. R. D.; Ahern, R.; Smith, I. E.; Gore, M. E. Continuous Low Dose Thalidomide: A Phase II Study in Advanced Melanoma, Renal Cell, Ovarian and Breast Cancer. *Br. J. Cancer* **2000**, *82* (4), 812–817. https://doi.org/10.1054/bjoc.1999.1004.

(215) Govindarajan, R. Irinotecan/Thalidomide in Metastatic Colorectal Cancer. *Oncol. Williston Park N* **2002**, *16* (4 Suppl 3), 23–26.

(216) Hwu, W.-J.; Raizer, J.; Panageas, K. S.; Lis, E. Treatment of Metastatic Melanoma in the Brain with Temozolomide and Thalidomide. *Lancet Oncol.* **2001**, *2* (10), 634–635. https://doi.org/10.1016/S1470-2045(01)00522-8.

(217) Baidas, S. M.; Winer, E. P.; Fleming, G. F.; Harris, L.; Pluda, J. M.; Crawford, J. G.; Yamauchi, H.; Isaacs, C.; Hanfelt, J.; Tefft, M.; Flockhart, D.; Johnson, M. D.; Hawkins, M. J.; Lippman, M. E.; Hayes, D. F. Phase II Evaluation of Thalidomide in Patients with Metastatic Breast Cancer. *J. Clin. Oncol.* **2000**, *18* (14), 2710–2717. https://doi.org/10.1200/JCO.2000.18.14.2710.

(218) Cheng, M.; Yu, X.; Lu, K.; Xie, L.; Wang, L.; Meng, F.; Han, X.; Chen, X.; Liu, J.; Xiong, Y.; Jin, J. Discovery of Potent and Selective Epidermal Growth Factor Receptor (EGFR) Bifunctional Small-Molecule Degraders. *J. Med. Chem.* **2020**, *63* (3), 1216–1232. https://doi.org/10.1021/acs.jmedchem.9b01566.

(219) Mullard, A. First Targeted Protein Degrader Hits the Clinic. *Nat. Rev. Drug Discov.* **2019**, *18* (4), 237–239. https://doi.org/10.1038/d41573-019-00043-6.

(220) Békés, M.; Langley, D. R.; Crews, C. M. PROTAC Targeted Protein Degraders: The Past Is Prologue. *Nat. Rev. Drug Discov.* **2022**, *21* (3), 181–200. https://doi.org/10.1038/s41573-021-00371-6.

(221) Gao, X.; Burris III, H. A.; Vuky, J.; Dreicer, R.; Sartor, A. O.; Sternberg, C. N.; Percent, I. J.; Hussain, M. H. A.; Rezazadeh Kalebasty, A.; Shen, J.; Heath, E. I.; Abesada-Terk, G.; Gandhi, S. G.; McKean, M.; Lu, H.; Berghorn, E.; Gedrich, R.; Chirnomas, S. D.; Vogelzang, N. J.; Petrylak, D. P. Phase 1/2 Study of ARV-110, an Androgen Receptor (AR) PROTAC Degrader, in Metastatic Castration-Resistant Prostate Cancer (mCRPC). *J. Clin. Oncol.* **2022**, *40* (6_suppl), 17–17. https://doi.org/10.1200/JCO.2022.40.6_suppl.017.

(222) Arvinas Androgen Receptor, Inc. *A Phase 1/2, Open-Label, Dose Escalation, and Cohort Expansion Clinical Trial to Evaluate the Safety, Tolerability, Pharmacokinetics, and Pharmacodynamics of ARV-110 in Patients With Metastatic Castration Resistant Prostate Cancer*; Clinical trial registration NCT03888612; clinicaltrials.gov, 2023. https://clinicaltrials.gov/ct2/show/NCT03888612 (accessed 2023-05-21).

(223) Arvinas Estrogen Receptor, Inc. *A Phase 1/2, Open Label, Dose Escalation, and Cohort Expansion Clinical Trial to Evaluate the Safety, Tolerability, and Pharmacokinetics of ARV-471 Alone and in Combination With Palbociclib (IBRANCE®) in Patients With Estrogen Receptor Positive/Human Epidermal Growth Factor Receptor 2 Negative (ER+/HER2-) Locally Advanced or Metastatic*

Breast Cancer, Who Have Received Prior Hormonal Therapy and Chemotherapy in the Locally Advanced/Metastatic Setting; Clinical trial registration NCT04072952; clinicaltrials.gov, 2023. https://clinicaltrials.gov/ct2/show/NCT04072952 (accessed 2023-05-21).

(224) Accutar Biotechnology Inc. *A Phase I Clinical Study to Evaluate the Safety, Tolerability, Pharmacokinetics, Pharmacodynamics, and Preliminary Anti-Tumor Activity of AC682 in Patients With Estrogen Receptor Positive/Human Epidermal Growth Factor Receptor 2 Negative (ER+/HER2-) Locally Advanced or Metastatic Breast Cancer*; Clinical trial registration NCT05080842; clinicaltrials.gov, 2023. https://clinicaltrials.gov/ct2/show/NCT05080842 (accessed 2023-05-21).

(225) Arvinas Androgen Receptor, Inc. *A Phase 1/2 Open-Label, Dose-Escalation and Cohort Expansion Clinical Trial to Evaluate the Safety, Tolerability, Pharmacokinetics, and Pharmacodynamics of ARV-766 in Patients With Metastatic Castration-Resistant Prostate Cancer*; Clinical trial registration NCT05067140; clinicaltrials.gov, 2023. https://clinicaltrials.gov/ct2/show/NCT05067140 (accessed 2023-05-21).

(226) Celgene. *A Phase 1, Multi-Center, Open-Label, Dose Finding Study to Evaluate the Safety, Tolerability, Pharmacokinetics, and Pharmacodynamics of Cc-94676 in Subjects With Metastatic Castration-Resistant Prostate Cancer*; Clinical trial registration NCT04428788; clinicaltrials.gov, 2023. https://clinicaltrials.gov/ct2/show/NCT04428788 (accessed 2023-05-21).

(227) Dialectic Therapeutics, Inc. *A Phase 1, Dose Escalation and Cohort Expansion Study to Evaluate the Safety, Pharmacokinetics and Clinical Activity of DT2216, an Antiapoptotic Protein Targeted Degradation Compound, in Patients With Relapsed/Refractory Malignancies*; Clinical trial registration NCT04886622; clinicaltrials.gov, 2023. https://clinicaltrials.gov/ct2/show/NCT04886622 (accessed 2023-05-21).

(228) Foghorn Therapeutics Inc. *A Phase 1, Multicenter, Open-Label, Dose Escalation and Expansion Study to Assess the Safety, Tolerability, Pharmacokinetics, Pharmacodynamics, and Clinical Activity of Intravenously Administered FHD-609 in Subjects With Advanced Synovial Sarcoma or Advanced SMARCB1-Loss Tumors*; Clinical trial registration NCT04965753; clinicaltrials.gov, 2023. https://clinicaltrials.gov/ct2/show/NCT04965753 (accessed 2023-05-21).

(229) *A Single and Multiple Ascending Dose Trial of KT-474 in Healthy Adult Volunteers and Patients With Atopic Dermatitis (AD) or Hidradenitis Suppurativa (HS) - Full Text View - ClinicalTrials.gov*. https://clinicaltrials.gov/ct2/show/NCT04772885?term=KT-474&draw=2&rank=1 (accessed 2023-05-23).

(230) Kymera Therapeutics, Inc. *A Phase 1, Multicenter, Open-Label, Dose Escalation and Expansion Study to Evaluate the Safety, Tolerability, PK/PD, and Clinical Activity of Intravenously Administered KT-413 in Adult Patients With Relapsed or Refractory B-Cell NHL*; Clinical trial registration NCT05233033; clinicaltrials.gov, 2023. https://clinicaltrials.gov/ct2/show/NCT05233033 (accessed 2023-05-21).

(231) Kymera Therapeutics, Inc. *A Phase 1, Multicenter, Open-Label, Dose-Escalation and Expansion Study to Evaluate Safety, Tolerability, Pharmacokinetics, Pharmacodynamics, and Clinical Activity of Intravenously Administered KT-333*

in Adult Patients With Relapsed or Refractory Lymphomas, Large Granular Lymphocytic Leukemia, and Solid Tumors; Clinical trial registration NCT05225584; clinicaltrials.gov, 2023. https://clinicaltrials.gov/ct2/show/NCT05225584 (accessed 2023-05-21).

(232) Nurix Therapeutics, Inc. *A Phase 1, Dose Escalation, Safety and Tolerability Study of NX-2127, a Bruton's Tyrosine Kinase (BTK) Degrader, in Adults With Relapsed/Refractory B-Cell Malignancies*; Clinical trial registration NCT04830137; clinicaltrials.gov, 2023. https://clinicaltrials.gov/ct2/show/NCT04830137 (accessed 2023-05-21).

(233) Nurix Therapeutics, Inc. *A Phase 1, Dose Escalation, and Cohort Expansion Study Evaluating NX-5948, a Bruton's Tyrosine Kinase (BTK) Degrader, in Adults With Relapsed/Refractory B-Cell Malignancies*; Clinical trial registration NCT05131022; clinicaltrials.gov, 2023. https://clinicaltrials.gov/ct2/show/NCT05131022 (accessed 2023-05-21).

(234) C4 Therapeutics, Inc. *A Phase 1/2 Open-Label, Multicenter Study to Characterize the Safety and Tolerability of CFT8634 in Subjects With Locally Advanced or Metastatic SMARCB1-Perturbed Cancers, Including Synovial Sarcoma and SMARCB1-Null Tumors*; Clinical trial registration NCT05355753; clinicaltrials.gov, 2023. https://clinicaltrials.gov/ct2/show/NCT05355753 (accessed 2023-05-21).

(235) Bulatov, E.; Ciulli, A. Targeting Cullin–RING E3 Ubiquitin Ligases for Drug Discovery: Structure, Assembly and Small-Molecule Modulation. *Biochem. J.* **2015**, *467* (3), 365–386. https://doi.org/10.1042/BJ20141450.

(236) Ishoey, M.; Chorn, S.; Singh, N.; Jaeger, M. G.; Brand, M.; Paulk, J.; Bauer, S.; Erb, M. A.; Parapatics, K.; Müller, A. C.; Bennett, K. L.; Ecker, G. F.; Bradner, J. E.; Winter, G. E. Translation Termination Factor GSPT1 Is a Phenotypically Relevant Off-Target of Heterobifunctional Phthalimide Degraders. *ACS Chem. Biol.* **2018**, *13* (3), 553–560. https://doi.org/10.1021/acschembio.7b00969.

(237) Gadd, M. S.; Testa, A.; Lucas, X.; Chan, K.-H.; Chen, W.; Lamont, D. J.; Zengerle, M.; Ciulli, A. Structural Basis of PROTAC Cooperative Recognition for Selective Protein Degradation. *Nat. Chem. Biol.* **2017**, *13* (5), 514–521. https://doi.org/10.1038/nchembio.2329.

(238) Girardini, M.; Maniaci, C.; Hughes, S. J.; Testa, A.; Ciulli, A. Cereblon versus VHL: Hijacking E3 Ligases against Each Other Using PROTACs. *Bioorg. Med. Chem.* **2019**, *27* (12), 2466–2479. https://doi.org/10.1016/j.bmc.2019.02.048.

(239) Cyrus, K.; Wehenkel, M.; Choi, E.-Y.; Han, H.-J.; Lee, H.; Swanson, H.; Kim, K.-B. Impact of Linker Length on the Activity of PROTACs. *Mol. Biosyst.* **2011**, *7* (2), 359–364. https://doi.org/10.1039/C0MB00074D.

(240) Smith, B. E.; Wang, S. L.; Jaime-Figueroa, S.; Harbin, A.; Wang, J.; Hamman, B. D.; Crews, C. M. Differential PROTAC Substrate Specificity Dictated by Orientation of Recruited E3 Ligase. *Nat. Commun.* **2019**, *10* (1), 131. https://doi.org/10.1038/s41467-018-08027-7.

(241) Maneiro, M.; Forte, N.; Shchepinova, M. M.; Kounde, C. S.; Chudasama, V.; Baker, J. R.; Tate, E. W. Antibody–PROTAC Conjugates Enable HER2-Dependent Targeted Protein Degradation of BRD4. *ACS Chem. Biol.* **2020**, acschembio.0c00285. https://doi.org/10.1021/acschembio.0c00285.

(242) Pillow, T. H.; Adhikari, P.; Blake, R. A.; Chen, J.; Del Rosario, G.; Deshmukh, G.; Figueroa, I.; Gascoigne, K. E.; Kamath, A. V.; Kaufman, S.; Kleinheinz, T.; Kozak, K. R.; Latifi, B.; Leipold, D. D.; Sing Li, C.; Li, R.; Mulvihill, M. M.; O'Donohue, A.; Rowntree, R. K.; Sadowsky, J. D.; Wai, J.; Wang, X.; Wu, C.; Xu, Z.; Yao, H.; Yu, S.; Zhang, D.; Zang, R.; Zhang, H.; Zhou, H.; Zhu, X.; Dragovich, P. S. Antibody Conjugation of a Chimeric BET Degrader Enables *in Vivo* Activity. *ChemMedChem* **2020**, *15* (1), 17–25. https://doi.org/10.1002/cmdc.201900497.

(243) Dragovich, P. S.; Adhikari, P.; Blake, R. A.; Blaquiere, N.; Chen, J.; Cheng, Y.-X.; den Besten, W.; Han, J.; Hartman, S. J.; He, J.; He, M.; Rei Ingalla, E.; Kamath, A. V.; Kleinheinz, T.; Lai, T.; Leipold, D. D.; Li, C. S.; Liu, Q.; Lu, J.; Lu, Y.; Meng, F.; Meng, L.; Ng, C.; Peng, K.; Lewis Phillips, G.; Pillow, T. H.; Rowntree, R. K.; Sadowsky, J. D.; Sampath, D.; Staben, L.; Staben, S. T.; Wai, J.; Wan, K.; Wang, X.; Wei, B.; Wertz, I. E.; Xin, J.; Xu, K.; Yao, H.; Zang, R.; Zhang, D.; Zhou, H.; Zhao, Y. Antibody-Mediated Delivery of Chimeric Protein Degraders Which Target Estrogen Receptor Alpha (ERα). *Bioorg. Med. Chem. Lett.* **2020**, *30* (4), 126907. https://doi.org/10.1016/j.bmcl.2019.126907.

(244) Hasmann, M.; Schemainda, I. FK866, a Highly Specific Noncompetitive Inhibitor of Nicotinamide Phosphoribosyltransferase, Represents a Novel Mechanism for Induction of Tumor Cell Apoptosis. *Cancer Res.* **2003**, *63* (21), 7436–7442.

(245) Carpino, L. A.; Imazumi, H.; El-Faham, A.; Ferrer, F. J.; Zhang, C.; Lee, Y.; Foxman, B. M.; Henklein, P.; Hanay, C.; Mügge, C.; Wenschuh, H.; Klose, J.; Beyermann, M.; Bienert, M. The Uronium/Guanidinium Peptide Coupling Reagents: Finally the True Uronium Salts. *Angew. Chem. Int. Ed.* **2002**, *41* (3), 441–445. https://doi.org/10.1002/1521-3773(20020201)41:3<441::AID-ANIE441>3.0.CO;2-N.

(246) Lai, A. C.; Toure, M.; Hellerschmied, D.; Salami, J.; Jaime-Figueroa, S.; Ko, E.; Hines, J.; Crews, C. M. Modular PROTAC Design for the Degradation of Oncogenic BCR-ABL. *Angew. Chem. Int. Ed.* **2016**, *55* (2), 807–810. https://doi.org/10.1002/anie.201507634.

(247) Chinchilla, R.; Nájera, C. The Sonogashira Reaction: A Booming Methodology in Synthetic Organic Chemistry. *Chem. Rev.* **2007**, *107* (3), 874–922. https://doi.org/10.1021/cr050992x.

(248) Wang, X.; Song, Y.; Qu, J.; Luo, Y. Mechanistic Insights into the Copper-Cocatalyzed Sonogashira Cross-Coupling Reaction: Key Role of an Anion. *Organometallics* **2017**, *36* (5), 1042–1048. https://doi.org/10.1021/acs.organomet.7b00010.

(249) Gazvoda, M.; Virant, M.; Pinter, B.; Košmrlj, J. Mechanism of Copper-Free Sonogashira Reaction Operates through Palladium-Palladium Transmetallation. *Nat. Commun.* **2018**, *9* (1), 4814. https://doi.org/10.1038/s41467-018-07081-5.

(250) Buckley, D. L.; Raina, K.; Darricarrere, N.; Hines, J.; Gustafson, J. L.; Smith, I. E.; Miah, A. H.; Harling, J. D.; Crews, C. M. HaloPROTACS: Use of Small Molecule PROTACs to Induce Degradation of HaloTag Fusion Proteins. *ACS Chem. Biol.* **2015**, *10* (8), 1831–1837. https://doi.org/10.1021/acschembio.5b00442.

(251) Farnaby, W.; Koegl, M.; Roy, M. J.; Whitworth, C.; Diers, E.; Trainor, N.; Zollman, D.; Steurer, S.; Karolyi-Oezguer, J.; Riedmueller, C.; Gmaschitz, T.; Wachter, J.; Dank, C.; Galant, M.; Sharps, B.; Rumpel, K.; Traxler, E.; Gerstberger, T.; Schnitzer, R.; Petermann, O.; Greb, P.; Weinstabl, H.; Bader, G.; Zoephel, A.;

Weiss-Puxbaum, A.; Ehrenhöfer-Wölfer, K.; Wöhrle, S.; Boehmelt, G.; Rinnenthal, J.; Arnhof, H.; Wiechens, N.; Wu, M.-Y.; Owen-Hughes, T.; Ettmayer, P.; Pearson, M.; McConnell, D. B.; Ciulli, A. BAF Complex Vulnerabilities in Cancer Demonstrated via Structure-Based PROTAC Design. *Nat. Chem. Biol.* **2019**, *15* (7), 672–680. https://doi.org/10.1038/s41589-019-0294-6.

(252) de Vries, A. H. M.; Mulders, J. M. C. A.; Mommers, J. H. M.; Henderickx, H. J. W.; de Vries, J. G. Homeopathic Ligand-Free Palladium as a Catalyst in the Heck Reaction. A Comparison with a Palladacycle. *Org. Lett.* **2003**, *5* (18), 3285–3288. https://doi.org/10.1021/ol035184b.

(253) Požgan, F.; Roger, J.; Doucet, H. Ligand-Free Palladium-Catalysed Direct Arylation of Heteroaromatics Using Low Catalyst Loadings. *ChemSusChem* **2008**, *1* (5), 404–407. https://doi.org/10.1002/cssc.200700166.

(254) Pivsa-Art, S.; Satoh, T.; Kawamura, Y.; Miura, M.; Nomura, M. Palladium-Catalyzed Arylation of Azole Compounds with Aryl Halides in the Presence of Alkali Metal Carbonates and the Use of Copper Iodide in the Reaction. *Chem. Soc. Jpn.* **1998**, *71*, 467–473.

(255) Amberchan, G.; Snelling, R. A.; Moya, E.; Landi, M.; Lutz, K.; Gatihi, R.; Singaram, B. Reaction of Diisobutylaluminum Borohydride, a Binary Hydride, with Selected Organic Compounds Containing Representative Functional Groups. *J. Org. Chem.* **2021**, *86* (9), 6207–6227. https://doi.org/10.1021/acs.joc.0c03062.

(256) Schreiber, S. L. Hydrogen Transfer from Tertiary Amines to Trifluoroacetic Anhydride. *Tetrahedron Lett.* **1980**, *21* (11), 1027–1030. https://doi.org/10.1016/S0040-4039(00)78830-7.

(257) Bernett, W. A. A Unified Theory of Bonding for Cyclopropanes. *J. Chem. Educ.* **1967**, *44* (1), 17. https://doi.org/10.1021/ed044p17.

(258) Leggio, A.; Comandè, A.; Belsito, E. L.; Greco, M.; Lo Feudo, L.; Liguori, A. Alternative Formation of Amides and β-Enaminones from Aroyl Chlorides Using the TiCl$_4$-Trialkylamine Reagent System. *Org. Biomol. Chem.* **2018**, *16* (31), 5677–5683. https://doi.org/10.1039/C8OB01536H.

(259) Foster, M. P.; McElroy, C. A.; Amero, C. D. Solution NMR of Large Molecules and Assemblies. *Biochemistry* **2007**, *46* (2), 331–340. https://doi.org/10.1021/bi0621314.

(260) *Protocol Guide: WST-1 Assay for Cell Proliferation and Viability*. https://www.sigmaaldrich.com/GB/en/technical-documents/protocol/cell-culture-and-cell-culture-analysis/cell-counting-and-health-analysis/cell-proliferation-reagent-wst-1 (accessed 2023-08-02).

(261) Wu, Y.; Pu, C.; Fu, Y.; Dong, G.; Huang, M.; Sheng, C. NAMPT-Targeting PROTAC Promotes Antitumor Immunity via Suppressing Myeloid-Derived Suppressor Cell Expansion. *Acta Pharm. Sin. B* **2022**, *12* (6), 2859–2868. https://doi.org/10.1016/j.apsb.2021.12.017.

(262) Bi, K.; Cheng, J.; He, S.; Fang, Y.; Huang, M.; Sheng, C.; Dong, G. Discovery of Highly Potent Nicotinamide Phosphoribosyltransferase Degraders for Efficient Treatment of Ovarian Cancer. *J. Med. Chem.* **2023**, *66* (1), 1048–1062. https://doi.org/10.1021/acs.jmedchem.2c01990.

(263) Cheng, J.; He, S.; Xu, J.; Huang, M.; Dong, G.; Sheng, C. Making Protein Degradation Visible: Discovery of Theranostic PROTACs for Detecting and

Degrading NAMPT. *J. Med. Chem.* **2022**, *65* (23), 15725–15737. https://doi.org/10.1021/acs.jmedchem.2c01243.

(264) Zhang, P.; Wang, W.; Guo, M.; Zhou, L.; Dong, G.; Xu, D.; Sheng, C. Discovery of Potent NAMPT-Targeting PROTACs Using FK866 as the Warhead. *Bioorg. Med. Chem. Lett.* **2023**, *92*, 129393. https://doi.org/10.1016/j.bmcl.2023.129393.

(265) Zhu, X.; Liu, H.; Chen, L.; Wu, C.; Liu, X.; Cang, Y.; Jiang, B.; Yang, X.; Fan, G. Addressing the Enzyme-Independent Tumor-Promoting Function of NAMPT via PROTAC-Mediated Degradation. *Cell Chem. Biol.* **2022**, *29* (11), 1616-1629.e12. https://doi.org/10.1016/j.chembiol.2022.10.007.

(266) Dekamin, M. G.; Moghaddam, F. M.; Saeidian, H.; Mallakpour, S. The Performance of Phthalimide-N-Oxyl Anion. *Monatshefte Für Chem. Chem. Mon.* **2006**, *137* (12), 1591–1595. https://doi.org/10.1007/s00706-006-0553-6.

(267) Wolfe, S.; Wilson, M.-C.; Cheng, M.-H.; Shustov, G. V.; Akuche, C. I. Cyclic Hydroxamates, Especially Multiply Substituted [1,2]Oxazinan-3-Ones. *Can. J. Chem.* **2003**, *81* (8), 937–960.

(268) Trost, B. M.; Rudd, M. T. Ruthenium-Catalyzed Alkyne–Propargyl Alcohol Addition. An Asymmetric Total Synthesis of (+)-α-Kainic Acid. *Org. Lett.* **2003**, *5* (9), 1467–1470. https://doi.org/10.1021/ol034241y.

(269) Nguyen, H. H.; Palazzo, T. A.; Kurth, M. J. Facile One-Pot Assembly of Imidazotriazolobenzodiazepines via Indium(III)-Catalyzed Multicomponent Reactions. *Org. Lett.* **2013**, *15* (17), 4492–4495. https://doi.org/10.1021/ol402045h.

(270) Sasmal, P. K.; Chandrasekhar, A.; Sridhar, S.; Iqbal, J. Novel One-Step Method for the Conversion of Isothiocyanates to 2-Alkyl(Aryl)Aminothiazoles. *Tetrahedron* **2008**, *64* (49), 11074–11080. https://doi.org/10.1016/j.tet.2008.09.074.

(271) Clausen, D. J.; Wan, S.; Floreancig, P. E. Total Synthesis of the Protein Phosphatase 2A Inhibitor Lactodehydrothyrsiferol. *Angew. Chem. Int. Ed.* **2011**, *50* (22), 5178–5181. https://doi.org/10.1002/anie.201007757.

(272) Kervefors, G.; Kersting, L.; Olofsson, B. Transition Metal-Free *N-* Arylation of Amino Acid Esters with Diaryliodonium Salts. *Chem. – Eur. J.* **2021**, *27* (18), 5790–5795. https://doi.org/10.1002/chem.202005351.

(273) Dekker, F. J.; Ghizzoni, M.; van der Meer, N.; Wisastra, R.; Haisma, H. J. Inhibition of the PCAF Histone Acetyl Transferase and Cell Proliferation by Isothiazolones. *Bioorg. Med. Chem.* **2009**, *17* (2), 460–466. https://doi.org/10.1016/j.bmc.2008.12.008.

(274) Pinto, A.; Wang, M.; Horsman, M.; Boddy, C. N. 6-Deoxyerythronolide B Synthase Thioesterase-Catalyzed Macrocyclization Is Highly Stereoselective. *Org. Lett.* **2012**, *14* (9), 2278–2281. https://doi.org/10.1021/ol300707j.

(275) McCarthy, B. G.; MacArthur, N. S.; Jakobsche, C. E. A Simple Synthesis of 6-Hydroxynorleucine Based on the Rearrangement of an N-Nitrosodichloroacetamide. *Tetrahedron Lett.* **2016**, *57* (4), 502–504. https://doi.org/10.1016/j.tetlet.2015.12.070.

(276) Heilmann, M.; Knezevic, M.; Piccini, G.; Tiefenbacher, K. Understanding the Binding Properties of Phosphorylated Glycoluril-Derived Molecular Tweezers and Selective Nanomolar Binding of Natural Polyamines in Aqueous Solution.

    Org. Biomol. Chem. **2021**, *19* (16), 3628–3633. https://doi.org/10.1039/D1OB00379H.

(277) Delor, M.; Dai, J.; Roberts, T. D.; Rogers, J. R.; Hamed, S. M.; Neaton, J. B.; Geissler, P. L.; Francis, M. B.; Ginsberg, N. S. Exploiting Chromophore–Protein Interactions through Linker Engineering To Tune Photoinduced Dynamics in a Biomimetic Light-Harvesting Platform. *J. Am. Chem. Soc.* **2018**, *140* (20), 6278–6287. https://doi.org/10.1021/jacs.7b13598.

(278) Zhang, N.; Jiang, J.; Liu, M.; Taniguchi, M.; Mandal, A. K.; Evans-Storms, R. B.; Pitner, J. B.; Bocian, D. F.; Holten, D.; Lindsey, J. S. Bioconjugatable, PEGylated Hydroporphyrins for Photochemistry and Photomedicine. Narrow-Band, near-Infrared-Emitting Bacteriochlorins. *New J. Chem.* **2016**, *40* (9), 7750–7767. https://doi.org/10.1039/C6NJ01155A.

(279) Prime, M. E.; Andersen, O. A.; Barker, J. J.; Brooks, M. A.; Cheng, R. K. Y.; Toogood-Johnson, I.; Courtney, S. M.; Brookfield, F. A.; Yarnold, C. J.; Marston, R. W.; Johnson, P. D.; Johnsen, S. F.; Palfrey, J. J.; Vaidya, D.; Erfan, S.; Ichihara, O.; Felicetti, B.; Palan, S.; Pedret-Dunn, A.; Schaertl, S.; Sternberger, I.; Ebneth, A.; Scheel, A.; Winkler, D.; Toledo-Sherman, L.; Beconi, M.; Macdonald, D.; Muñoz-Sanjuan, I.; Dominguez, C.; Wityak, J. Discovery and Structure–Activity Relationship of Potent and Selective Covalent Inhibitors of Transglutaminase 2 for Huntington's Disease. *J. Med. Chem.* **2012**, *55* (3), 1021–1046. https://doi.org/10.1021/jm201310y.